Baryon resonances in pion- and photon-induced hadronic reactions

Dissertation

zur

Erlangung des Doktorgrades (Dr. rer. nat.)

der

Mathematisch-Naturwissenschaftlichen Fakultät
der
Rheinischen Friedrich-Wilhelms-Universität Bonn

vorgelegt von

Deborah Rönchen
aus
Gummersbach

Bonn 2014

Angefertigt mit Genehmigung der Mathematisch-Naturwissenschaftlichen Fakultät der Rheinischen Friedrich-Wilhelms-Universität Bonn

1. Gutachter:	Prof. Dr. Siegfried Krewald
2. Gutachter:	Prof. Dr. Ulf-G. Meißner
Tag der Promotion:	26.03.2014
Erscheinungsjahr:	2014

Summary

The aim of the present work is the analysis of the baryon spectrum in the medium-energy regime. At those energies, a perturbative treatment of Quantum Chromodynamics, that is feasible in the high-energy regime, is not possible. Chiral perturbation theory, the low-energy effective theory of the strong interaction, is limited to the lowest excited states and does not allow to analyze the complete resonance region. For the latter purpose, dynamical coupled-channel approaches provide an especially suited framework. In the present study, we apply the Jülich model, a dynamical coupled-channel model developed over the years, to analyze pion- and photon-induced hadronic reactions in a combined approach.

In the Jülich model, the interaction of the mesons and baryons is built of t- and u-channel exchange diagrams based on an effective Lagrangian. Genuine resonances are included as s-channel states. The scattering potential is unitarized in a Lippmann-Schwinger-type equation. Analyticity is preserved, which is a prerequisite for a reliable extraction of resonance parameters in terms of pole positions and residues in the complex energy plane. Upon giving an introduction to the subject in Chap. 1 and showing selected results in Chap. 2, we will describe the simultaneous analysis of elastic πN scattering and the reactions $\pi^- p \to \eta n$, $K^0\Lambda$, $K^+\Sigma^-$, $K^0\Sigma^0$ and $\pi^+ p \to K^+\Sigma^+$ within the Jülich framework in Chap. 3. The free parameters of the model are adjusted to the GWU/SAID analysis of elastic πN scattering and, in case of the inelastic reactions, to experimental data. Partial waves up to $J = 9/2$ are included and we consider the world data set from threshold up to $E \sim 2.3$ GeV. We show our fit results compared to differential and total cross sections, to polarizations and to measurements of the spin-rotation parameter. Finally, we present the results of a pole search in the complex energy plane of the scattering amplitude and discuss the extracted resonance spectrum in the isospin $I = 1/2$ and $I = 3/2$ sector.

The approach will be extended to pion photoproduction in Chap. 4. Here, the reactions $\gamma p \to \pi^0 p$ and $\gamma p \to \pi^+ n$ are analyzed using the Jülich model as final-state interaction. In a flexible and easy-to-implement parameterization, the γN interaction is approximated by energy-dependent polynomials. We analyze over 22,000 data points of single- and double-polarization observables. In order to estimate the impact of the high-precision double-polarization measurements, we perform two fits excluding those data from the first one. We discuss our fit results and present the photocouplings at the poles of the resonances determined in the Jülich model of the hadronic interactions.

Conclusions and an outlook to future developments planned within the present framework are given in Chap. 5.

Contents

[1] The content of this section has been published in Ref. [1].
[2] The content of this section can be found in Ref. [2].

Chapter 1

Introduction

1.1 Strong interactions and the spectrum of excited hadrons

The experimental discovery of the Higgs boson at CERN in 2012 has closed one of the last missing gaps of the standard model: the Higgs mechanism gives a finite mass to the elementary fermions and bosons of the standard model. Now a unified theory of the three fundamental forces, the electromagnetic, strong and weak interactions, has been achieved. The elementary particles can be classified according to the forces they experience. Leptons are subject to the electromagnetic and weak interactions, while the quarks experience the strong force in addition. The so-called gauge bosons mediate the fundamental forces. Large effort has been put in experiments designed to confirm the existence of particles predicted by the standard model.

The manifestations of the electromagnetic force can be described in the formalism of quantum electrodynamics (QED), a perturbative theory with a small coupling constant, that provides very accurate predictions of fundamental quantities and is applicable at all energies of the standard model. A unified theory of the electromagnetic and the weak interaction, hence called electroweak interaction, was developed by Glashow, Weinberg, and Salam.

The strong interaction, on the other hand, proved to be less accessible in terms of a perturbative approach. This is due to certain properties intrinsic to the strong force. In contrast to the other fundamental particles, quarks are not observed as isolated particles, a phenomenon known as confinement. The observable particles are mesons which contain a quark-antiquark pair, and baryons that are built of three quarks or of three antiquarks. Hadrons requiring more complex quark structures such as dibaryons, are called "exotic". Recently, two new charged Z_b states, which contain at least four quarks, were discovered by the Bell experiment, the $Z_b(10610)$ and $Z_b(10650)$ [3, 4, 5]. A review of the search for exotic states can be found, e.g., in Ref. [6].

Due to confinement, the existence and the properties of quarks could only be deduced from the experimentally observable particles, i.e. from mesons and baryons, collectively called hadrons. In the 1960's and 70's, experiments at SLAC on deep inelastic scattering

of electrons on protons [7, 9, 8] confirmed the Bjorken scaling [10], which implies that in a scattering process with very high energy the constituents of a proton behave like almost free, non-interacting particles. At low and medium energies, however, they are confined in hadrons. This observation is known as asymptotic freedom: at large momentum transfer or short distances, the coupling of the quarks inside the hadron is weak, whereas it is strong at small momenta or long distances. A class of theories that incorporates the phenomenon of asymptotic freedom is given by the non-Abelian gauge theories, developed by t'Hooft, Politzer, Gross and Wilczek in the 1970's. Quantum Chromodynamics (QCD) is a non-Abelian gauge theory with gauge group $SU(3)_c$ that allows a perturbative treatment of the strong interactions at high energies. A new quantum number is introduced: color [11], the "charge" of the strong interaction. A quark carries one of three color states, red, green or blue, an antiquark can be anti-red, anti-green or anti-blue. The observed hadrons, however, are color-neutral objects. The gauge bosons of QCD are called gluons, they also carry color charge and mediate the strong force.
Despite all these successes of the standard model, there remains one important terra incognita: "strong QCD", the non-perturbative regime of the strong interaction. To make progress in this field, there is a large experimental effort to study the production and decay of baryon resonances.
Elastic πN scattering provides a well suited possibility to access the baryon spectrum. Besides its large cross section, the comparable simple kinematical structure and the fact that there are only four polarization observables, facilitate the theoretical as well as the experimental analysis. Moreover, over 90 % of the mass in the visible universe is composed of protons and neutrons. Accordingly, the first experimental studies of the elastic πN scattering process date back several decades. The bigger part of the existing data on elastic and inelastic πN scattering was taken in the 1960's and 70's. More recent data are available only for the reaction $\pi^- p \to \eta n$ from Refs. [12, 13, 14]. In the last years, the study of pion-induced reactions started at the EPECUR experiment at ITEP [15] and at the E19 experiment at J-PARC [16]. Data are expected soon.
The photoproduction of pseudoscalar mesons provides another access to the baryon spectrum. The data situation of photon-induced hadronic reactions differs in quantity and quality from the major part of the inelastic pion-induced reactions. At several experimental facilities, such as ELSA, JLab, MAMI, Spring-8 or GRAAL, the photo- and electroproduction of different final states like πN, ηN and KY is studied and a considerable amount of high-precision data is available. A complete experiment, i.e. a set of measurements that suffice to fully determine the photoproduction amplitude, has to contain single- as well as double-polarization observables and will be available soon. A recent review of baryon spectroscopy discussing experimental and theoretical approaches can be found in Ref. [17].

1.1.1 Theoretical approaches in the non-perturbative regime

Due to the large coupling, a perturbative treatment of QCD is not feasible at low or medium energies —the expansion in a perturbation series does not converge. In the following we briefly discuss selected theoretical approaches to describe the strong interactions and the

spectrum of excited hadrons in the non-perturbative regime.

A. Quark models

In the early 60's, Gell-Mann and Zweig developed a model built on SU(3) symmetry that provides a pattern of how to compose the different hadrons of quarks [18, 19]. They introduced a flavor quantum number to characterize different species of quarks. The light baryons are built of three quark flavors: u (up), d (down) and s (strange). They can be arranged into different multiplets, a meson octet, a baryon octet and a baryon decuplet, with respect to their isospin I_z and hypercharge Y. This is known as the eight-fold way. Based on this approach, Gell-Mann predicted the existence of the Ω^- baryon, that was observed experimentally shortly after [20]. Since then, additional hadrons were discovered whose properties could not be explained in terms of the three light quarks u, d, and s. Their observation supplemented by certain standard model constraints suggested three more, heavy quarks flavors: c (charm), b (bottom) and t (top). The existence of those heavy quarks was confirmed in experiments on high energy collision. The perception that hadrons are formed of valence quarks is very successful in explaining and predicting the quantum numbers of hadrons, but it cannot account for the fact that the mass of a hadron is much larger than the summed masses of its valence quarks. The greater part of the mass is associated with the gluon-field energy inside a hadron.

Besides the ground state hadrons, there is a large number of excited states. Those resonances are produced in scattering processes and decay back into their ground states very quickly. An excited state can become visible in experimental observables, e.g., the Δ resonance shows up as a very prominent peak in the πN total cross section. However, such a clear identification of a resonance is most seldom possible. In the medium energy regime from about 1 GeV up to 2 GeV, a rich spectrum of excited states is observed, whose formation and characteristics have been the subject of many experimental and theoretical programs. With regard to a universal description of the strong interaction, understanding the excitation spectrum of hadrons is essential.

In the 1960's, quark models have been developed to describe the spectrum of excited hadrons. Constituent quark models aim at a systematic organization of hadron properties in terms of $SU(6) \times O(3)$ supermultiplets [21]. In more advanced approaches, relativistic kinematics are introduced as, e.g., in Ref. [22] and in relativistic quark models a covariant formulation is developed, see, e.g., Refs. [23, 24, 25].

The predictions of quark models for the low-lying resonances are in good agreement with experimental results, while evidence for other predicted states at higher energy is missing. This is frequently called the "missing resonance problem" [26]. A highly controversial resonance state is given by the first excitation of the nucleon with positive parity, the Roper resonance $N(1440)\ 1/2^+$. In quark model calculations such as the harmonic oscillator model, the mass of the Roper resonance was usually predicted to lie above the first negative-parity states. The experimental spectrum, however, reveals a Roper mass below the latter. This observation gave rise to the interpretation of the Roper resonance as a state generated dynamically from the meson-baryon interaction without any genuine three-quark structure.

Concerning the decay widths of the hadronic resonances, there are hardly any quark model studies. At present, quark models are superseded by more fundamental approaches.

B. Fundamental theories

B.1 Effective field theory

One very powerful tool to describe the strong interactions in the non-perturbative regime of QCD is provided by effective field theories (EFTs). The concept of an EFT is built on the assumption that the details of the high-energy dynamics should not affect the low-energy dynamics very strongly. Identifying the relevant degrees of freedom in the considered energy regime often allows for a perturbative solution of the problem. The influence of the underlying theory is absorbed in the strength of the coupling constant. Furthermore, the low-energy theory should be consistent with the symmetries of the underlying high-energy theory. As Weinberg stated in Ref. [27], the task is to find the most general possible Lagrangian including all terms consistent with those symmetries. The complexity of calculating cross sections or other observable quantities is strongly reduced in effective theories.
As an example, consider light by light scattering at energies much lower than the electron mass. An effective Lagrangian can be constructed where the photons are the only dynamical degrees of freedom. However, electrons, that are the dynamical degrees of freedom in the underlying theory (QED), contribute to the scattering of the two photons, e.g., via a box diagram. The explicit evaluation of those diagrams in the framework of QED gives the values of the coupling constants in the effective theory. The effective theory for light by light scattering is given by the Euler-Heisenberg effective Lagrangian [28].
In case of the strong interaction, the underlying high-energy theory is QCD, while the relevant degrees of freedom at low energies are the color-neutral hadrons.
Considering only the three light quark flavors u, d, and s, the QCD Lagrangian reads

$$\mathcal{L}_{QCD} = \bar{q}(i\not{D} - \mathcal{M}_q)q - \frac{1}{4}G^{\alpha}_{\mu\nu}G^{\alpha\mu\nu} \tag{1.1}$$

where q denotes the quark field $q^T = (u, d, s)$, D_μ is the covariant derivative, $G^{\alpha}_{\mu\nu}$ the gluon field strength tensor and $\mathcal{M}_q = \mathrm{diag}(m_u, m_d, m_s)$. Decomposing the quark fields q into left-handed and right-handed components,

$$q_L = \frac{1}{2}(1 - \gamma_5)q \qquad \text{and} \qquad q_R = \frac{1}{2}(1 + \gamma_5)q\,, \tag{1.2}$$

Eq.(1.1) can be written as

$$\mathcal{L}_{QCD} = \bar{q}_L i\not{D} q_L + \bar{q}_R i\not{D} q_R - \bar{q}_L \mathcal{M}_q q_R - \bar{q}_R \mathcal{M}_q^{\dagger} q_L - \frac{1}{4}G^{\alpha}_{\mu\nu}G^{\alpha\mu\nu}\,. \tag{1.3}$$

Compared to the typical hadronic mass scale of about 1 GeV, the masses of the light quarks can be neglected, i.e. $\mathcal{M}_q = 0$. In this limit, the QCD Lagrangian Eq. (1.3) exhibits a global symmetry

$$SU(3)_L \times SU(3)_R \times U(1)_V \times U(1)_A\,, \tag{1.4}$$

besides other symmetries like Lorentz invariance, $SU(3)_c$ gauge invariance and P, C, T invariance. The left- and right-handed quark fields transform independently under the chiral symmetry $SU(3)_L \times SU(3)_R$

$$(q_L, q_R) \to (Lq_L, Rq_R) \qquad \text{with} \quad L, R \in SU(3)_{L,R}\,. \tag{1.5}$$

The limit of vanishing light quark masses is hence called the "chiral limit". The subscripts V and A in Eq.(1.4) denote vector ($V = L + R$) and axial vector ($A = L - R$) transformations. While the symmetry $U(1)_V$ is realized as the conservation of the baryon number in the standard model, there is no conserved current in quantum theory that corresponds to the $U(1)_A$ symmetry ($U(1)_A$ anomaly).
The chiral symmetry is realized in nature in the Goldstone mode, which implicates a spontaneous breakdown of the symmetry: the ground state is not invariant under the full $SU(3)_L \times SU(3)_R$ symmetry, but the vector subgroup $SU(3)_V$ remains unbroken (c.f. Vafa-Witten theorem [29]). Goldstone's theorem implies that a spontaneously broken continuous symmetry leads to the appearance of a massless particle with spin 0 [30, 31]. Such particles are called Goldstone bosons. In case of the spontaneous breaking of the chiral symmetry to the vector subgroup $SU(3)_V$, the number of Goldstone bosons is 8 and an identification with the 8 lightest pseudoscalar mesons of the known hadronic spectrum ($\pi^{\pm}$, π^0, $K^{\pm}$, K^0, $\bar{K}^0$) stands to reason.

B.2 Chiral perturbation theory

At energies well below 1 GeV, the Goldstone bosons are the only relevant degrees of freedom. A general formalism to construct the most general Lagrangian consistent with a spontaneously broken symmetry was presented in Refs. [32, 33]. In reality, chiral symmetry is explicitly broken by the non-vanishing quark masses, which has to be taken into account when constructing the effective Lagrangian for the Goldstone bosons. The same applies to electromagnetic effects. A systematic low-energy expansion of the Lagrangian is given in the framework of chiral perturbation theory (ChPT), which represents the EFT for the low-energy strong interactions. Fundamental developments of ChPT have been done, e.g, in Refs. [27, 34, 35], see also Refs. [36, 37, 38] for reviews.
Expanding the theory to higher orders of momentum requires the inclusion of loop diagrams in order to preserve unitarity and analyticity. Weinberg established a power counting scheme to determine the number of terms needed to evaluate the Lagrangian to a fixed order in momentum [27]. In this way, the effective theory, that is in general not renormalizable, behaves like a renormalizable field theory. Beside the power counting in momentum, other schemes have been developed.
Unknown coupling constants of the chiral Lagrangian, called low-energy constants (LEC), incorporate effects of heavy degrees of freedom or higher mass states. The LECs cannot be calculated directly from the underlying theory (QCD), but have to be determined from experimental data or phenomenology. Other possibilities are provided, e.g., by lattice gauge theory.

Compared to the masses of the Goldstone bosons, baryon masses constitute a heavier mass scale. The ground state baryons can be included in the formalism of ChPT in form of matter fields and one constructs the most general chiral Lagrangian in terms of the Goldstone bosons and those matter fields. Due to the new mass scale, the power counting scheme cannot be applied in the same way as in the Goldstone boson sector [39]. Tools to resolve this problem are given by heavy-baryon chiral perturbation theory (HBChPT) [40, 41, 42] or the method of infrared regularizations [43]. A review of ChPT involving one or more nucleons can be found in Refs. [44, 45].
In a variety of different approaches, the concepts of ChPT have been developed further to tackle many of the problems in the low-energy regime of strong interactions. Here, we would like to mention unitarized chiral perturbation theory. In this approach, a scattering kernel derived from the chiral Lagrangian is iterated in a Bethe-Salpeter equation and baryon resonances restricted to a few partial waves can be described. Coupled-channels calculation are possible as well as the dynamical generation of resonances. See, e.g., Refs. [46, 47, 48] or, for more recent developments, Refs. [49, 50, 51].
In πN scattering, the low-energy regime is completely understood in terms of ChPT [52, 53]. However, a combined description of the resonance spectrum at low and medium energies requires model assumptions from other approaches.

B.3 Lattice QCD

Lattice gauge calculations [54] provide a promising approach to extend QCD into the non-perturbative regime of hadrons. Instead of a continuum gauge theory, a discrete statistical mechanical system is applied on a four-dimensional Euclidean lattice. Exact gauge invariance is preserved. Wilson showed in Ref. [54] that in the computable strong-coupling limit the asymptotic states of the theory are $SU(3)$ color singlets, which is equivalent to the assumption that QCD exhibits confinement of quarks.
In Ref. [55], properties of different ground state hadrons have been determined using lattice calculations and in Refs. [56, 57, 58] also excited states were studied. Recent progress in the determination of the resonance spectrum can be found in Refs. [59, 60, 61, 62, 63].
Despite this obvious success of lattice gauge simulations, the pion mass that enters the calculations is still unphysically large and the numerical treatment entails a high computational effort. The analysis is, thus, usually restricted to the ground states or at most to the first excited states.

C. Phenomenological analyses

C.1 Partial-wave analyses and K-matrix approaches

In the past to present day, partial-wave analyses have played an essential role in the determination of resonance properties. The classic analyses by Cutkosky, Höhler or Arndt [64, 65, 66, 67, 68] were mainly limited to elastic πN scattering . More recent partial-wave analyses are provided by the SAID analysis of the GWU/DAC group [69, 70, 71], by

the Bonn-Gatchina group [72, 73, 74, 75] or by the unitary isobar model of the MAID group [76, 77]. Large data sets of the pion- and photon-induced production of pions, etas, kaons or multiple particles like $\pi\pi N$ are analyzed and the considered energy range covers the complete resonance region.
In order to derive resonance parameters from partial-wave amplitudes, a frequently applied tool is given by K-matrix approaches. Here, the scattering kernel of a Bethe-Salpeter equation is usually approximated by on-shell intermediate states in addition to explicit resonance graphs. While unitarity is preserved, the omission of the real dispersive parts of the intermediate two-body states leads to the violation of analyticity. In this way, the strength of multiple scattering contributions is truncated and bound states cannot be generated. Due to the above mentioned approximations, the K-matrix approach offers a practical tool to analyze large amounts of data in different channels. However, for the extraction of resonance parameters in terms of poles and residues, analyticity is crucial. Moreover, the dynamical generation of a resonance state is, in general, not possible in K-matrix approaches.
In the K-matrix approach of the Gießen group [78, 79, 80, 81], the resonance and background diagrams are constructed based on an effective Lagrangian. Many reaction channels are analyzed simultaneously.
The K-matrix in the GWU/SAID partial-wave analysis is built of energy-dependent, purely phenomenological polynomials. With the exception of the $\Delta(1232)3/2^+$, no explicit resonance states are included. In this sense, the extraction of the baryon spectrum is model-independent. Of course, information on the microscopic reaction dynamics cannot be obtained from such a phenomenological approach. In Ref. [82] a review of the GWU/SAID analysis can be found.

C.2 Dynamical coupled-channel models

At higher energies, the coupling of the different reaction channels becomes important. Overlapping, broad resonances and the superposition of resonances and background complicate the disentangling of the individual states. To approach those problems, dynamical coupled-channel (DCC) models provide a particularly suited tool. Based on effective Lagrangians, they preserve essential QCD symmetries at tree level. Unitarity of the scattering amplitude is ensured by an iteration in a Lippmann-Schwinger equation, which is also the origin of the linking of different reaction channels and partial waves.
A systematic, microscopic description of the background is provided by meson- and baryon-exchange potentials in form of t- and u-channel diagrams. In contrast to many K-matrix approaches, the real dispersive parts of the intermediate states are included in the calculation of the scattering amplitude and analyticity is, thus, preserved. This enables a reliable determination of the resonance spectrum in the form of pole positions and residues in the complex energy plane. Explicit resonance states are included as s-channel graphs, but the dynamical generation of resonances caused by the interplay of the meson and baryon exchanges is also possible. This allows for a systematic test of the nature of certain states as, e.g., the Roper resonance.

Furthermore, a simultaneous analysis of different reactions in a coupled-channel approach provides the possibility to shed light on the "missing resonance problem", since states not seen in experiments on elastic πN scattering might couple predominantly to inelastic channels like ηN or KY.
Dynamical coupled-channel models have been applied to the analysis of pion- and photon-induced reactions considering energies over the whole resonance region from threshold up to and beyond 2 GeV. Recent examples can be found in Refs. [83, 84, 85, 86, 87, 88, 89, 90, 91, 92].
In this study, we apply the DCC approach of the Jülich2012 model [1] described in more detail in the following section.

1.2 The Jülich model of πN scattering

The Jülich model is a dynamical coupled-channel model originally constructed to describe elastic pion-nucleon scattering in the threshold region. In Refs. [93, 94, 95, 96, 97, 98] the $\pi\pi N$ channel was introduced parameterized as effective ρN, σN and $\pi\Delta$ channels, as well as the ηN channel, and the model was extended to higher energies. It was found that the Roper resonance $N(1440)1/2^+$ can be generated dynamically from the σN channel [96]. A first step towards the extension to the strangeness sector was achieved in Ref. [99], where the reactions $\pi N \to \pi N$ and $\pi^+ p \to K^+\Sigma^+$ were analyzed and the isospin 3/2 resonance spectrum was extracted.
In the Jülich model, analyticity is respected and the correct structure of branch points is included [100, 101], which allows for a reliable determination of the resonance spectrum in terms of pole positions and residues in the complex scattering plane. The scattering amplitude is unitarized in a Lippmann-Schwinger equation and two-body unitarity is guaranteed. Due to the large inelasticity caused by the $\pi\pi N$ channel, three-body unitarity is also important. In the current approach, three-body unitarity is only approximate as described in Sec. 3.2 of Chap. 3.
In the most recent version of the Jülich model (*Jülich2012*) [1], the resonance analysis is extended to the isospin 1/2 sector. In a simultaneous analysis, elastic πN scattering and the reactions $\pi^- p \to \eta n$, $K^0\Lambda$, $K^+\Sigma^-$, $K^0\Sigma^0$ and $\pi^+ p \to K^+\Sigma^+$ are studied. An overview of the channels included in the Jülich approach and their threshold energies can be found in Fig. 1.1. Pole positions and residues of nucleon and Delta resonances are extracted.
The Jülich2012 model is one of the subjects of the present study. The foundations of the approach will be explained in the following sections, while the results of the fit to experimental data and the resonance analysis can be found in Chap. 3.

1.2.1 The scattering equation

The scattering of two relativistic particles can be described by the covariant Bethe-Salpeter equation

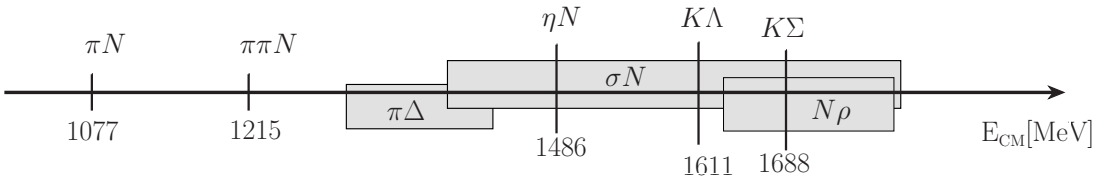

Figure 1.1: Channels included in the Jülich model and their threshold energies. The effective $\pi\pi N$ channels ($\pi\Delta$, σN, ρN) are not depicted with a fixed threshold energy since they are matched to the phase shifts of the Δ, ρ and σ resonances and therefore come with a finite width.

$$T = K + KGT \; . \tag{1.6}$$

Here, T is the scattering matrix from which all observables can be calculated and G is the relativistic two-body propagator. The scattering kernel K includes all irreducible diagrams, which results in an infinite series of diagrams that has to be truncated for practical calculations. This approximated scattering kernel will be called V in the following. In momentum space the scattering equation reads

$$T(p'', p', E) \;\; = \;\; V(p'', p', E) - \frac{i}{(2\pi)^4} \int d^4p \, V(p'', p, E) \, G(p, E) \, T(p, p', E) \, , \tag{1.7}$$

where p' (p, p'') is the incoming (intermediate, outgoing) momentum and E is the total energy of the scattering process. The solution of this four dimensional integral equation can be achieved by applying the method of Blankenbecler and Sugar [102]. The integral is reduced to three dimensions by approximating the propagator G. Yet, this approximation is not unique and leads to an ambiguous off-shell behavior. Since the correct off-shell behavior is a prerequisite for the description of inelastic scattering and the extraction of resonance pole positions and residues in the complex energy plane, we solve the four dimensional integral in the framework of time-ordered perturbation theory (TOPT) [103, 104, 105, 106]. This non-covariant approach provides a distinct prescription for the construction of the off-shell potentials and the explicit time-ordering allows to carry out the integration over the energy component in Eq. (1.7) explicitly. In this way, it reduces the scattering equation to three dimensions.

In principle, the scattering equation stated above can be derived starting with the Hamiltonian H of the system:

$$H = H_0 + \mathcal{V} \; , \tag{1.8}$$

where H_0 and $\mathcal{V}$ describe the non-interacting and interacting parts of the system, respectively. A Green's function $\mathcal{G}$ can be defined that solves the inhomogeneous problem

$$(E - H_0)\mathcal{G} = \mathcal{V}\mathcal{G} \; , \tag{1.9}$$

while the free Green's function $\mathcal{G}_0$ solves the homogenous problem

$$(E - H_0)\mathcal{G}_0 = \mathbb{1} \ . \tag{1.10}$$

The Green's function $\mathcal{G}$ can be expressed in terms of the free Green's function $\mathcal{G}_0$ and the interaction potential $\mathcal{V}$:

$$\mathcal{G} = \mathcal{G}_0 + \mathcal{G}_0\mathcal{V}\mathcal{G} = \mathcal{G}_0 + \mathcal{G}_0\mathcal{V}\mathcal{G}_0 + \mathcal{G}_0\mathcal{V}\mathcal{G}_0\mathcal{V}\mathcal{G}_0 + \ldots = \mathcal{G}_0 + \mathcal{G}_0 T \mathcal{G}_0 \ , \tag{1.11}$$

where we have written the scattering matrix T as

$$T = \mathcal{V} + \mathcal{V}\mathcal{G}_0\mathcal{V} + \mathcal{V}\mathcal{G}_0\mathcal{V}\mathcal{G}_0 V + \ldots = \mathcal{V} + \mathcal{V}\mathcal{G}_0 T \ . \tag{1.12}$$

The free Green's function of the system is given by

$$\mathcal{G}_0 = \sum_n \frac{|n\rangle\langle n|}{E - E_n + i\epsilon} \ . \tag{1.13}$$

Here, the sum over n contains all possible multi-particle states, which results in an infinite series. Furthermore, Eq. (1.13) implies the integration over the continuum and the summation over discrete variables. For an actual calculation, the series in Eq. (1.13) has to be truncated. To this purpose, we divide $\mathcal{G}_0$ into a part $\mathcal{G}_0^{(2)}$ which includes all two-body intermediate states and a part $\tilde{\mathcal{G}}_0$ which comprises the rest:

$$\begin{aligned} \mathcal{G}_0 &= \tilde{\mathcal{G}}_0 + \mathcal{G}_0^{(2)} \\ &= \sum_{\tilde{n}} \frac{|\tilde{n}\rangle\langle\tilde{n}|}{E - E_{\tilde{n}} + i\epsilon} + \sum_{n^{(2)}} \frac{|n^{(2)}\rangle\langle n^{(2)}|}{E - E_{n^{(2)}} + i\epsilon} \ . \end{aligned} \tag{1.14}$$

In a last step, we write Eq. (1.12) in terms of the two Green's functions defined in Eq. (1.14) and arrive at an equation of the same form as Eq. (1.7)

$$T = V + V\mathcal{G}_0^{(2)} T \ , \tag{1.15}$$

Here, we defined the effective two-body potential $V = \mathcal{V}/1 - \tilde{\mathcal{G}}_0$. It can be expanded as

$$V = \mathcal{V} \sum_{k=0}^{\infty} \left(\sum_{\tilde{n}} \frac{|\tilde{n}\rangle\langle\tilde{n}|}{E - E_{\tilde{n}} + i\epsilon} \mathcal{V} \right)^k \ . \tag{1.16}$$

The sum in Eq. (1.16) results in a set of all two-body irreducible diagrams with an arbitrary number of particle in the intermediate state. The construction and truncation of the effective potential V will be described in Sec. 1.2.2. Eq. (1.15) denotes a scattering equation for two particles in the initial and final state.
We now define a basis where the initial (intermediate, final) state is characterized by its helicity λ' (λ, λ'') and isospin I. The scattering equation takes the form

$$T^I_{\mu\nu}(\vec{p}\,'', \lambda'', \vec{p}\,', \lambda', E) = V^I_{\mu\nu}(\vec{p}\,'', \lambda'', \vec{p}\,', \lambda', E) + \sum_{\kappa,\lambda} \int d^3p V^I_{\mu\kappa}(\vec{p}\,'', \lambda'', \vec{p}, \lambda, E)\, G_\kappa(p, E) T^I_{\kappa\nu}(\vec{p}, \lambda, \vec{p}\,', \lambda', E)\,. \tag{1.17}$$

The additional index μ (ν) denotes the initial (final) state of the scattering process and we sum over all intermediate channels κ. In this way, we account for the coupling of the different channels, which is important for an energy regime where inelastic processes play a dominant role.
Despite the reduction to three dimensions, the numerical solution of the integral in Eq. (1.17) is still very costly and further simplifications are required. Taking advantage of the rotational invariance of strong interactions, one performs a partial wave decomposition of the helicity states in Eq. (1.17), thus, reducing the integral to one dimension. In addition, we switch from helicity to JLS basis, the conventional basis of partial-wave amplitudes. Here, J denotes the total angular momentum, L is the orbital angular momentum and S the total spin of the state. Details of those transformations can be found in Appendix B.
Explicitly, a matrix element T, describing the transition form channel μ with momentum p', spin S' and orbital angular momentum L' to channel ν with momentum p'', spin S'' and orbital angular momentum L'' for a given scattering energy E (suppressed in Eq. (1.18)) is given by

$$\langle L''S''p''|T^{IJ}_{\mu\nu}|L'S'p'\rangle = \langle L''S''p''|V^{IJ}_{\mu\nu}|L'S'p'\rangle + \sum_{\kappa,L,S} \int dp\, p^2 \langle L''S''p''|V^{IJ}_{\mu\kappa}|LSp\rangle G_\kappa(p) \langle LSp|T^{IJ}_{\kappa\nu}|L'S'p'\rangle. \tag{1.18}$$

The two-body propagator G for channels with the stable particles πN, ηN, $K\Lambda$ and $K\Sigma$ has the form

$$G_\kappa(p, E) \;=\; \frac{1}{E - E_a(p) - E_b(p) + i\epsilon}\,, \tag{1.19}$$

where $E_a = \sqrt{m_a^2 + p^2}$ and $E_b = \sqrt{m_b^2 + p^2}$ are the energies of the intermediate particles a and b in channel κ. In case of the effective $\pi\pi N$ channels parameterized as $\pi\Delta$, σN, and ρN, the unstable subsystems are boosted to the quasi-particle center-of-mass frame and the σ, ρ, and Δ phase shifts are matched. The corresponding propagators take a more complex form than Eq. (1.19) [96, 100].
In a shortened notation the scattering equation can be written as

$$T_{\mu\nu}(p'', p', E) = V_{\mu\nu}(p'', p', E) + \sum_\kappa \int_0^\infty dp\, p^2\, \frac{V_{\mu\kappa}(p'', p, E)\, T_{\kappa\nu}(p, p', E)}{E - E_a(p) - E_b(p) + i\epsilon}\,. \tag{1.20}$$

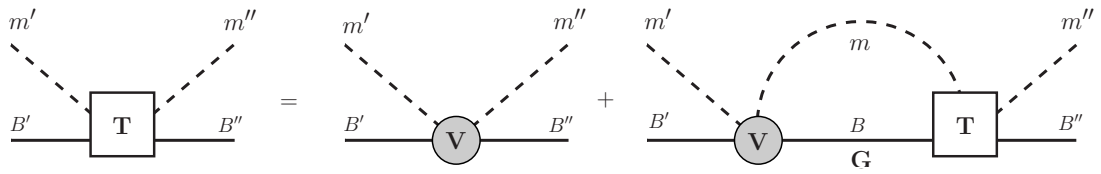

Figure 1.2: Schematic representation of the scattering equation Eq. (1.20).

A schematic representation of Eq. (1.20) for an incoming (intermediate, outgoing) meson m' (m, m'') and an incoming (intermediate, outgoing) baryon B' (B, B'') can be found in Fig. 1.2.
The scattering equation is solved using the Haftel-Tabakin scheme [107].

Decomposition of the amplitude

In the present study, we use the two-potential formalism to decompose the scattering amplitude into a pole and a non-pole part

$$T \;=\; T^P + T^{NP} \,. \tag{1.21}$$

The non-pole part T^{NP} is evaluated from the non-pole potential V^{NP}. The latter is the sum of the t- and u-channel exchange diagrams. Their construction based on effective Lagrangians is described below in Sec. 1.2.2.
The pole or resonance part, T^P is generated by V^P which is built of s-channel resonance graphs. T^P can be calculated via

$$T^P_{\mu\nu}(p'', p', E) = \frac{\Gamma^a_\mu(p'')\Gamma^c_\nu(p')}{E - m^b - \Sigma(E)} \,, \tag{1.22}$$

where m^b is the bare mass of the resonance and Γ^c_μ (Γ^a_μ) is the dressed resonance creation (annihilation) vertex with

$$\begin{aligned} \Gamma^c_\mu(p') \;&=\; \gamma^c_\mu(p') + \sum_\nu \int_0^\infty dp\, p^2\, \gamma^c_\nu(p)\, G_\nu(p, E)\, T^{NP}_{\nu\mu}(p, p', E) \\ \text{and} \quad \Gamma^a_\mu(p'') \;&=\; \gamma^a_\mu(p'') + \sum_\nu \int_0^\infty dp\, p^2\, T^{NP}_{\nu\mu}(p'', p, E)\, G_\nu(p, E)\, \gamma^a_\nu(p) \end{aligned} \tag{1.23}$$

with the bare resonance creation (annihilation) vertices γ^c_μ (γ^a_μ). The explicit form of γ^c_μ and γ^a_μ can be found in Ref. [99] or in Appendix C of this work. The self-energy Σ in Eq. (1.22) is given by

$$\Sigma(E) = \sum_\mu \int_0^\infty dp\, p^2\, \gamma^c_\mu(p') G_\mu(p, E) \Gamma^a_\mu(p') \,. \tag{1.24}$$

The resonances obtain their width from the rescattering in Eq. (1.20). The formalism can be expanded to the case of two resonance in one partial wave [108], and is presented in Eqs. (4) and (5) in Sec. 3.2 of Chap. 3.
The decomposition of the amplitude into a pole and a non-pole part is of advantage in the numerical solution of the scattering equation and in the fitting procedure, since the evaluation of T^P is considerably faster than the evaluation of T^{NP}. As Eqs. (1.22) and (1.23) show, the free parameters in T^P can be varied without recalculating T^{NP}. Numerical details and the free parameters of our model are described in Sec. 3.2 of Chap. 3 on page 33.
T^{NP} is often referred to as *background*, although the dynamical generation of resonances via the interplay of the t- and u-channel diagrams is possible. The separation into T^P and T^{NP} is model-dependent and we do not associate any physical meaning to this decomposition of the amplitude. A clean separation is given by a singularity-free part that constitutes the background, while resonances are defined in terms of pole positions and residues of the full scattering amplitude in the complex energy plane [101, 100]. The determination of pole positions and residues will be described in Sec. 1.2.3.

1.2.2 The scattering potential

The effective Lagrangian

At low and medium energies the description of the strong interaction in terms of quarks and gluons fails because QCD is non-perturbative due to its large coupling constant. As described in Sec. 1.1.1, the concept of an effective field theory addresses this problem by adopting the symmetries of QCD, but formulates the interaction in terms of the relevant hadronic degrees of freedom, i.e. mesons and baryons.
In this study, the non-pole part of the scattering kernel $V_{\mu\nu}$ iterated in Eq. (1.20) is constructed based on effective Lagrangians [109], see also Ref. [110]. Earlier, less general studies of effective chiral Lagrangians involving vector mesons have also been done by Wess and Zumino [111]. This Lagrangian is consistent with the approximate (broken) chiral $SU(2) \times SU(2)$ symmetry of QCD. It describes the interaction of nucleons, pions, and vector mesons like the ρ meson or the pseudovector meson a_1. The Lagrangian can be directly generalized to $SU(3) \times SU(3)$.
In Ref. [111], starting from the nonlinear σ model with the pion field π and the nucleon field ψ, a new pion field ξ and a new nucleon field N are introduced. N is related to ξ and ψ via

$$N = \left(\frac{1 - i\gamma_5\xi}{1 + i\gamma_5\xi}\right)^{1/2} \psi = \frac{1 - i\gamma_5\xi}{(1 + \xi^2)^{1/2}}\psi \; . \tag{1.25}$$

Under chiral symmetry the fields transform like

$$\begin{aligned} \frac{1 - i\gamma_5\xi}{1 + i\gamma_5\xi} &\rightarrow e^{-i\alpha\gamma_5} \frac{1 - i\gamma_5\xi}{1 + i\gamma_5\xi} e^{-i\alpha\gamma_5} \\ N &\rightarrow e^{i\beta} N \end{aligned} \tag{1.26}$$

with $\alpha = \vec{\alpha}\vec{\tau}$ and $\beta = \vec{\beta}\vec{\tau}$. α and β are the group parameters of the axial and vector $SU(2)$ group, respectively. The goal is to find a Lagrangian having invariance properties consistent with the above symmetry transformations.
Performing a gauge transformation, i.e. allowing the parameters α and β to be coordinate dependent, one has to introduce two additional gauge fields to restore the invariance of the Lagrangian. The vector gauge field $\rho_\mu = \vec{\rho}_\mu\vec{\tau}$ is associated with the ρ meson and the axial gauge field $a_\mu = \vec{a}_\mu\vec{\tau}$ with the a_1 meson.
An infinitesimal vector gauge transformation can be written as

$$\delta\rho_\mu = i[\beta, \rho_\mu] + \frac{2}{g}\partial_\mu\beta \qquad \text{and} \qquad \delta a_\mu = i[\beta, a_\mu] \; , \tag{1.27}$$

while an infinitesimal axial gauge transformation can take the form

$$\delta\rho_\mu = i[\alpha, a_\mu] \qquad \text{and} \qquad \delta a_\mu = i[\alpha, \rho_\mu] + \frac{2}{g}\partial_\mu\alpha \; . \tag{1.28}$$

In Eqs. (1.27) and (1.28) g is a coupling constant.
The Lagrangian constructed for the fields ξ, N, ρ_μ and a_μ in Ref. [111] consists of three parts. The first part, $\mathcal{L}_1$, is invariant under the gauge transformation. $\mathcal{L}_2$ has only global $SU(2) \times SU(2)$ invariance and therefore breaks gauge invariance, whereas $\mathcal{L}_3$ is invariant under isospin transformation only. $\mathcal{L}_1$ is built of all functions of ξ, N, ρ_μ and a_μ which preserve $SU(2) \times SU(2)$ gauge invariance. Those invariants are constructed in the usual way, i.e. by defining covariant derivatives and field strength tensors.
In Table 12 in Appendix B of Sec. 3.2 we list the parts of the effective Lagrangian that are applied in the present study. Note that we use a notation slightly different from Ref. [111]. Details on additional terms [96, 98] not included in the Wess-Zumino Lagrangian, like the Δ isobar, the ω, a_0, η meson and the σ, can also be found in this section.

Exchange diagrams

As mentioned at the beginning of this section, we apply time-ordered (or non-covariant, old fashioned) perturbation theory (TOPT) to solve the scattering equation. The method is explained in detail in Ref. [103] and in Refs. [104, 105] its application within the framework of a meson exchange model is presented.
In TOPT, the S-matrix is expanded in terms of the matrix elements of the Hamiltonian $\mathcal{H}$

$$S_{fi} = \delta_{fi} + \sum_{n=1}^{\infty}(-i)^n \int_{-\infty}^{\infty} dt^{(1)} \ldots \int_{-\infty}^{t^{(n-1)}} dt^{(n)} H_I(t^{(1)}) \ldots H_I(t^{(n)}) \tag{1.29}$$

with the interaction part of the Hamiltonian operator $H_I(t)$. The Lagrangian $\mathcal{L}$ is transformed to the Hamiltonian density $\mathcal{H}$ using a Legendre transformation. If the Lagrangian $\mathcal{L}$ includes a time derivative of the exchanged meson, this procedure causes the appearance of additional diagrams, so-called contact graphs, in order to restore the on-shell equivalence between time-ordered and covariant perturbation theory.

Due to the explicit time ordering, an exchange diagram in covariant perturbation theory corresponds to a pair of diagrams in TOPT (plus a possible contact term). Those are called the first and second time ordering and imply the exchange of a particle and its anti-particle, c.f. Fig. 1.3.

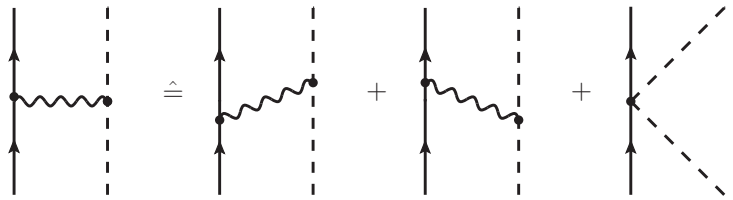

Figure 1.3: Exchange diagram in covariant perturbation theory (left) and TOPT (right).

As can be seen in Eq. (1.16), in principle, the scattering potential corresponds to a set of all two-particle irreducible diagrams with an arbitrary number of virtual particles in the intermediate state. This infinite series has to be truncated. In the present approach, we keep all diagrams with three or less intermediate particles. All t-channel meson exchange and u-channel baryon exchange diagrams, as well as the contact graphs, that constitute V^{NP} can be found in Fig. 2 of Sec. 3.2 on pages 3 and 4. Explicit expressions for the non-pole potentials are given in Appendix B.1. of Sec. 3.2. In Appendix B.2, we explain how the coupling constants of several exchange diagrams are related to each other by $SU(3)$ flavor symmetry.

The effective $\pi\pi N$ channels: ρN, σN and $\pi\Delta$

The intermediate $\pi\pi N$ channel is parameterized as effective ρN, σN and $\pi\Delta$ channels [96, 98]. The diagrams for this interaction are constructed in a different way than the one described above because no stable particles are exchanged. Instead, they are included as correlated $\pi\pi$ and πN pairs. The decay of the ρ and the σ meson into the $\pi\pi$ system and of the Δ into the πN system is accounted for and the properties of the unstable particles are determined from the corresponding phase shifts. The interactions with the ρ and σ were constructed by means of dispersion relation techniques and crossing symmetry using analytically continued $\bar{N}N \to \pi\pi$ data (c.f. Fig. 3 in Sec. 3.2).
To maintain the correct analytic structure of the scattering amplitude the branch points of unstable particles have to move away from the physical axis and into the complex plane [100].

1.2.3 Pole positions and residues

The goal of the present study is the extraction of the baryon spectrum in the second and third resonance region. Here, due to overlapping resonances or the superposition of resonances and background, the characterization of an excited state in terms of a Breit-Wigner

mass and width becomes questionable, especially when different reactions are analyzed simultaneously. In contrast, a reliable characterization of a resonance that is much less model-dependent is given in terms of pole positions and residues in the complex energy plane. The "mass" of a resonance corresponds to the real part of the pole position E_0, while the "width" is associated with the imaginary part via $\Gamma = -2\mathrm{Im}E_0$.
The extraction of pole positions requires full analyticity of the scattering amplitude T and a thorough understanding of the singularity structure of the S-matrix. Every channel opening induces a branch point and a new Riemann sheet and cut. Branch points of channels with stable particles are located on the physical axis and the first (physical) Riemann sheet. Branch points of the channels with unstable particles, in our case ρN, σN and $\pi\Delta$, move into the complex energy plane. Besides those, the only other singularities allowed on the first sheet are bound states, i.e. poles on the real axis below the lowest threshold.
A resonance is defined as a pole on the second, unphysical Riemann sheet with its real part located above the lowest threshold. Poles on the second sheet with the real part below the threshold are called virtual states. In Ref. [112] it was shown that the correct inclusion of branch points in the complex plane is crucial for a reliable extraction of resonance parameters. The absence of those branch points might lead to false pole signals. In Sec. 4 of Sec. 3.2, the singularity structure of the present approach is described in detail and in Fig. 35 of Sec. 3.2 the complex energy plane with all branch points and resonances is shown. The latter figure can also be found in Chap. 2 of the present work.
To determine the pole positions on the second sheet, we apply the method of analytic continuation following Ref. [100]. The partial-wave amplitude on the second Riemann sheet $T^{(2)}$ is accessed via a contour deformation of the momentum integration. In case of two stable particles in the intermediate state, the scattering equation Eq. (1.20) is of the form

$$T^{(2)}_{\mu\nu}(p'',p',E) - V_{\mu\nu}(p'',p',E) = \delta G + \int dp p^2 \frac{V_{\mu\kappa}(p'',p,E)T^{(2)}_{\kappa\nu}(p,p',E)}{E - E_a(p) - E_b(p) + i\epsilon} \; . \tag{1.30}$$

The additional term δG is given by

$$\delta G = \frac{2\pi i p^{>}_{on} E^{on}_a E^{on}_b}{E} V_{\mu\kappa}(p'',p_{on},E)T^{(2)}_{\kappa\nu}(p_{on},p',E) \tag{1.31}$$

with the on-shell energies of the stable particle $E^{on}_{a(b)}$ and the on-shell three-momentum in the c.m. frame of the two stable particles a and b

$$p_{on} = \frac{1}{E}\sqrt{(E^2-(m_a-m_b)^2)(E^2-(m_a+m_b)^2)} \; . \tag{1.32}$$

The on-shell momentum p_{on} is two-valued itself, thus, one has to distinguish the two Riemann sheets of p_{on}:

$$p^{>}_{on} = \begin{cases} -p_{on} & \text{if Im } p_{on} < 0 \\ p_{on} & \text{else} \end{cases} \qquad \text{and} \qquad p^{<}_{on} = -p^{>}_{on} \; . \tag{1.33}$$

In case of unstable particles, the propagator and its analytic continuation is more complicated, because the unstable particle induces two additional branch points in the complex energy plane. This means that instead of two Riemann sheets, there are four sheets. As in the case of a stable particle propagator, the key to access the unphysical sheets is a deformation of the integration contour [100]. Because poles can be located on all these sheets, on has to apply certain selection criteria to define the sheets where the pole search is performed. Those criteria are also given in Ref. [100].
Beside the pole position, the relevant quantities to characterize a resonance are the pole residue $|r|$ and its phase θ. To determine those, in a first step the scattering amplitude $T^{(2)}$ on the second sheet is expanded in a Laurent series around the pole position E_0

$$T^{(2)}_{\mu\nu} = \frac{a_{-1,\mu\nu}}{E-E_0} + a_{0,\mu\nu} + \mathcal{O}(E-E_0)\,, \tag{1.34}$$

and the residue a_{-1} is obtained by a closed contour integration along the path $\Gamma(E)$ around the pole:

$$a_n = \frac{1}{2\pi i}\oint_{\Gamma(E)} \frac{T^{(2)}(E)\,dE}{(E-E_0)^{n+1}}\,. \tag{1.35}$$

An alternative way to determine a_{-1}, that is advantageous in numerical calculation, is given by an iterative procedure [99]

$$\begin{aligned}
\left.\frac{\partial}{\partial E}\right|_{E=E_0} \frac{1}{T^{(2)}(E)} &= \frac{1}{a_{-1}} \\
\left.\frac{\partial^2}{\partial E^2}\right|_{E=E_0} \frac{1}{T^{(2)}(E)} &= -\frac{2a_0}{a_{-1}^2} \\
\left.\frac{\partial^3}{\partial E^3}\right|_{E=E_0} \frac{1}{T^{(2)}(E)} &= \frac{6(a_0^2 - a_{-1}a_1)}{a_{-1}^3}\,.
\end{aligned} \tag{1.36}$$

This procedure is faster than the one in Eq. (1.35) because no integration is required. Although it is numerically stable, it is slightly less accurate than Eq. (1.35).
The pole residue $r = |r|e^{i\theta}$ as quoted by the PDG [113] is defined as

$$\tau = \tau_B + \frac{|r|\,e^{i\theta}}{M - E - i\Gamma/2}. \tag{1.37}$$

Here, the partial-wave amplitude τ can be related to the T-matrix via

$$\tau_{\mu\nu} = -\pi\sqrt{\rho_\mu\,\rho_\nu}\,T_{\mu\nu}, \quad \rho_\mu = \frac{p_\mu\,E_\mu\,\omega_\mu}{E} \tag{1.38}$$

where $p_\mu\,(E_\mu, \omega_\mu)$ are the on-shell three-momentum (baryon, meson energies) of the initial (i) or final (f) meson-baryon system. Γ in Eq. (1.37) denotes the widths of a resonance on top of a background τ_B.

Combining Eqs. (1.34), (1.37) and (1.38) we obtain

$$|r| = |a_{-1}\,\rho_\mu|, \qquad \theta = -\pi + \arctan\left[\frac{\mathrm{Im}\,(a_{-1}\,\rho_\mu)}{\mathrm{Re}\,(a_{-1}\,\rho_\mu)}\right] \ . \tag{1.39}$$

In Tables 3 to 8 of Sec. 3.2 (page 49 and the following), the results of the resonance properties extracted in the present study can be found. In addition to pole positions we show the transition branching ratios defined in terms of the normalized residues. The normalized residue (NR) is given by

$$(NR)_{\pi N\to\mu\nu} = \frac{\pi\sqrt{\rho_{\pi N}\rho_\mu}g_{\pi N}g_\mu}{\Gamma_{\rm tot}/2} \ , \tag{1.40}$$

where g_μ can be obtained from $a_{-1,\pi N\mu} = g_{\pi N}g_\mu$ and $\Gamma_{\rm tot} = -2{\rm Im}E_0$ is the resonance width. The transition branching ration from πN into channel μ is defined by the modulus of the normalized residue:

$$\frac{\Gamma_{\pi N}^{1/2}\Gamma_\mu^{1/2}}{\Gamma_{\rm tot}} = |(NR)_{\pi N\to\mu\nu}| \ . \tag{1.41}$$

1.3 Connection to Photoproduction

The analysis of hadronic reactions and photoproduction in a combined approach is an important step towards a reliable description of the baryon spectrum. A large amount of high-precision photoproduction data is available these days and awaits a theoretical analysis. Because of the high accuracy, it is expected that more information than just the photocoupling of the resonances can be gained from those measurements. An analysis of the data could, e.g., help to resolve the nature of questionable resonances or even lead to the observation of new states.

The connection of pion photoproduction to the hadronic Jülich model was achieved recently [114]. Here, the photon-nucleon interaction is described in a field-theoretical framework [115, 116, 117] that ensures full gauge invariance as dictated by the generalized off-shell Ward-Takahashi identity. The hadronic final state interaction is provided by the Jülich approach. In Ref. [114], an older version of the Jülich model [98] was applied which includes, besides the πN and ηN channel, the three effective $\pi\pi N$ channels ρN, σN and $\pi\Delta$. An analysis incorporating also the photoproduction of kaons and η mesons is in preparation, employing the Jülich2012 analysis described in Chap. 3 as the final state interaction.

A field theoretical implementation of the photoproduction process, as the one described above, constitutes a very complex and technically involved task. Thus, in the present study we follow a different, semi-phenomenological approach. The hadronic final-state interaction is provided by the full Jülich2012 dynamical coupled-channel model, while the γN interaction vertex is approximated by polynomials. This flexible and easy to implement approach allows to consider a much larger data base. On the other hand, it means that no direct information on the microscopic reaction dynamics of the photo-interaction can be obtained. Since the parameters of the Jülich2012 model are not altered, no additional states apart from the resonances included in the hadronic analysis can be found in the present approach. Therefore, this semi-phenomenological study constitutes an intermediate step towards a combined dynamical coupled-channel analysis of pion- and photon-induced reactions.

So far, our analysis is restricted to pion-photoproduction off the proton, i.e. we consider the reactions $\gamma p \to \pi^0 p$ and $\pi^+ n$. The extension to other final states like ηN, $K\Lambda$ or $K\Sigma$ is straightforward.

1.3.1 The phenomenological photoproduction amplitude

Regarding the construction of the most general form of a photoproduction amplitude, it was shown in Ref. [118] that basic symmetry considerations of 4-momentum conservation, Lorentz invariance and gauge invariance allow only four independent functions of the nucleon Dirac operator γ and the photon polarization vector ϵ. Exploiting additionally isospin and crossing symmetry, as well as the basic principle that the S-matrix should be unitary, the photoproduction amplitude J of pseudoscalar mesons can be written in terms

of four amplitudes J_i,

$$J = iJ_1\vec{\sigma}\cdot\vec{\epsilon} + J_2\vec{\sigma}\cdot\hat{q}\vec{\sigma}\cdot(\hat{k}\times\vec{\epsilon}) + iJ_3\vec{\sigma}\cdot\hat{k}\hat{q}\cdot\vec{\epsilon} + iJ_4\vec{\sigma}\cdot\hat{q}\hat{q}\cdot\vec{\epsilon}\,, \tag{1.42}$$

with the meson and photon momentum $\vec{q}$ and $\vec{k}$, and the photon polarization vector $\vec{\epsilon}$. The $J_i(i = 1-4)$ are complex functions of the scattering angle θ and of the total energy E. The scattering angle θ is defined as $\cos\theta = \hat{q}\cdot\hat{k}$, where $\hat{q}$ ($\hat{k}$) denotes the unit vector $\hat{q} = \vec{q}/|\vec{q}|$ ($\hat{k} = \vec{k}/|\vec{k}|$). In the literature, the photoproduction amplitude is also expressed in terms of helicity amplitudes H_i, transversity amplitudes b_i or invariant amplitudes A_i. In the present study, we use the photoproduction amplitude in the formulation of Ref. [119]

$$\hat{\mathcal{M}} = -iJ = F_1\vec{\sigma}\cdot\vec{\epsilon} + iF_2\vec{\epsilon}\cdot(\hat{k}\times\hat{q}) + F_3\vec{\sigma}\cdot\hat{k}\hat{q}\cdot\vec{\epsilon} + F_4\vec{\sigma}\cdot\hat{q}\hat{q}\cdot\vec{\epsilon}\,. \tag{1.43}$$

Eqs. (1.42) and (1.43) apply to the case of real photons, for virtual photons two more independent spin operators can be found because $\hat{\epsilon}\cdot\hat{k} \neq 0$ (see, e.g., Ref. [119]). The coefficients F_i can be decomposed into multipole amplitudes $M_{\mu\gamma}$, as demonstrated in Appendix A of Sec 4.2. The construction of $M_{\mu\gamma}$ is described in detail in Sec. II.B. of Sec. 4.2 and the scattering equation takes a similar form as the hadronic Lippmann-Schwinger equation:

$$M_{\mu\gamma}(q,E) = V_{\mu\gamma}(q,E) + \sum_{\kappa}\int_0^\infty dp\, p^2\, T_{\mu\kappa}(q,p,E)G_\kappa(p,E)V_{\kappa\gamma}(p,E)\ . \tag{1.44}$$

The hadronic scattering matrix $T_{\mu\kappa}$ is provided by the Jülich2012 analysis and their parameters are not alerted in the present study. A schematic representation of Eq. (1.44) is given in Fig. 1.4. The sum in the second part of Eq. (1.44) runs over all possible intermediate channels with a baryon B' and a meson m'.

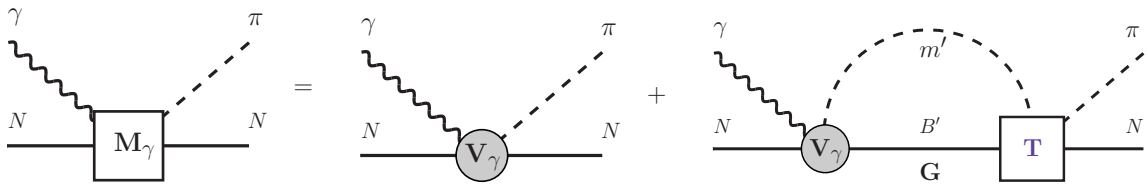

Figure 1.4: Schematic representation of the photoproduction amplitude $M_\gamma = M_{\pi N\,\gamma N}$.

The photoproduction kernel $V_{\mu\gamma}$ is approximated by polynomials. As in case of the purely hadronic interactions, we use the two-potential formalism and divide $V_{\mu\gamma}$ into a pole part, where the photon couples to the resonances, and a non-pole part that simulates the coupling of the photon to t- and u-channels, see Fig. 1.5.

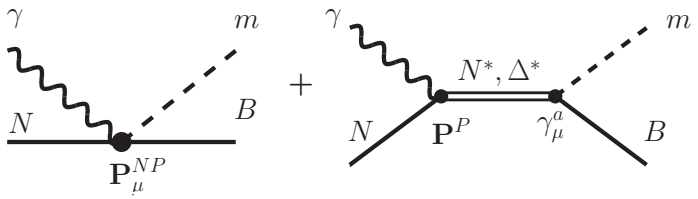

Figure 1.5: Schematic representation of the phenomenological photoproduction potential $V_{\mu\gamma}$. Non-pole part (left), photo-interaction approximated by a polynomial P_μ^{NP} and pole part (right), photo-interaction approximated by a polynomial P^{P}.

1.3.2 Towards a complete experiment

In the photoproduction of pseudoscalar meson π, η, K, 16 polarization observables can be measured. An overview of the different polarization states can be found in Tab. 1.1. Further information and definitions in terms of the coefficients F_i are given in Appendices A and B of Sec. 4.2.

The question of how many of those observables are needed to fully determine the photoproduction amplitude has been addressed in several studies [120, 121]. In Ref. [122] it was shown that the mathematical solution of the problem results in the angular distribution measurement of eight carefully selected observables, that resolve all discrete ambiguities up to an overall phase. A large number of combinations are possible, but each set requires a polarized beam and target, as well as the measurement of the polarization of the recoil particle. It is obvious that this poses a big experimental challenge. The recent development of transversely polarized targets at different facilities rendered the measurement of a complete set of observables possible. A complete experiment is easier to realize for kaon photoproduction, since the self-analyzing decay of hyperons facilitates the measurement of the recoil polarization. In contrast, for pion and eta photoproduction, the measurement of the recoil polarization requires an additional elastic scattering of the outgoing nucleon on a spin 0 nucleus. This puts limits on the number of detected particles. A first large-acceptance measurement of the observable $C_{x'}$, which is defined as the polarization transfer from a polarized photon beam to the recoil nucleon, has been achieved recently [123].

The assumption that eight carefully chosen observables suffice only holds if the measurements would be free of uncertainties. In reality, the number of observables required to remove all ambiguities is larger, as has been shown in Refs. [124, 125, 126, 127]. Moreover, the amplitude can only be determined up to an overall phase ambiguity. A truncated partial wave analysis [128, 129] provides a method to circumvent those problems.

Moving towards the goal of a complete experiment in pseudoscalar meson photoproduction, the last years have brought major advancements. Several experimental facilities all around the world provide the possibility to study the relevant reactions. With the development of (un)polarized photon beams and targets the measurement of single- and double-polarization observables is feasible.

Table 1.1: Overview of the directions of polarization in the definitions of the different observables (Eqs. (B.5) to (B.10) in Appendix B.1 of Sec. 4.2). For each observable, the first (second) line contains the first (second) measurement of which the asymmetry is composed. The reaction plane is $\hat{x} - \hat{z}$, the coordinate system of the final state is denoted by a prime. The polarization of the photon is denoted by $\perp$ or $\parallel$ for linear and by ± 1 for circular polarization. A linear photon polarization with $\perp'$ or $\parallel'$ corresponds to $\phi = \pi/4$ in Eq. (B.3) in Appendix B.1 of Sec. 4.2. "0" stands for unpolarized. Note that some observables differ in sign compared to the definition of other groups, c.f. Ref. [130] for an overview of the sign conventions used in the literature.

Type	Polarization of			Type	Polarization of		
of polarization	Beam	Target	Recoil	of polarization	Beam	Target	Recoil
single				beam-recoil			
$d\sigma/d\Omega$	0	0	0	$C_{x'}$	$+1$	0	$-x'$
					-1	0	$-x'$
Σ	$\perp$	0	0	$C_{z'}$	$+1$	0	$-z'$
	$\parallel$	0	0		-1	0	$-z'$
T	0	$+y$	0	$O_{x'}$	$\perp'$	0	$-x'$
	0	$-y$	0		$\parallel'$	0	$-x'$
P	0	0	$+y'$	$O_{z'}$	$\perp'$	0	$-z'$
	0	0	$-y'$		$\parallel'$	0	$-z'$
beam-target				target-recoil			
E	$+1$	$-z$	0	$L_{x'}$	0	$-z$	x'
	-1	$-z$	0		0	$+z$	x'
F	$+1$	$+x$	0	$L_{z'}$	0	$+z$	z'
	-1	$+x$	0		0	$-z$	z'
G	$\perp'$	$-z$	0	$T_{x'}$	0	$+x$	$+x'$
	$\parallel'$	$-z$	0		0	$-x$	$+x'$
H	$\perp'$	$+x$	0	$T_{z'}$	0	$+x$	$+z'$
	$\parallel'$	$+x$	0		0	$-x$	$+z'$

At the electron stretcher facility ELSA in Bonn the photoproduction of mesons is studied using polarized or unpolarized electrons with an energy of up to 3.5 MeV. Here, until the year 1998 the SPAHIR-Collaborations has been taking data on pion, eta and kaon photoproduction, as well as for multi-pion, omega and phi photoproduction. In 2000, experiments with the Crystal Barrel detector started at ELSA. The installation of the TAPS detector in 2001 allows the production of linear or circular polarized photons and, thus, the measurement of a variety of polarization observables. At the Jefferson Lab in Virginia, USA, the Continuous Electron Beam Accelerator Facility (CEBAF) provides an electron beam with energies up to 6 GeV that is currently upgraded to 12 GeV. Of the four experimental halls, the program of Hall B engages in the measurement of the spectrum of exited nucleon states with the CLAS detector. At the Mainz microtron MAMI a polarized electron beam can be accelerated up to 1.5 GeV. Here, the A2 collaboration focuses on real photons and studies the production of pions and other mesons. The GRAAL experiment at the European Synchrotron Radiation Facility (ESRF) in Grenoble measured several polarization observables for different final states. At the synchrotron radiation facility SPring-8 in Japan, the LEPS experiment provides a high-energy photon beam to study meson photoproduction.
An analysis of the high-precision data measured at those facilities might contribute essentially to the understanding of the resonance spectrum.

Chapter 2

Selected highlights

In this chapter we show selected results of the analyses of pion and photon-induced reactions outlined in Secs. 1.2 and 1.3. The complete analyses will be presented in Chaps. 3 and 4, respectively.

- In Fig. 2.1 selected fit results of the hadronic analysis within the Jülich dynamical coupled-channel framework (Jülich2012) are shown. Two different fits were performed in order to estimate the sensitivity of the results on the starting conditions in the fit parameter space. The approach has been demonstrated to work quantitatively up to a center of mass energy of $E \sim 2.3$ GeV.

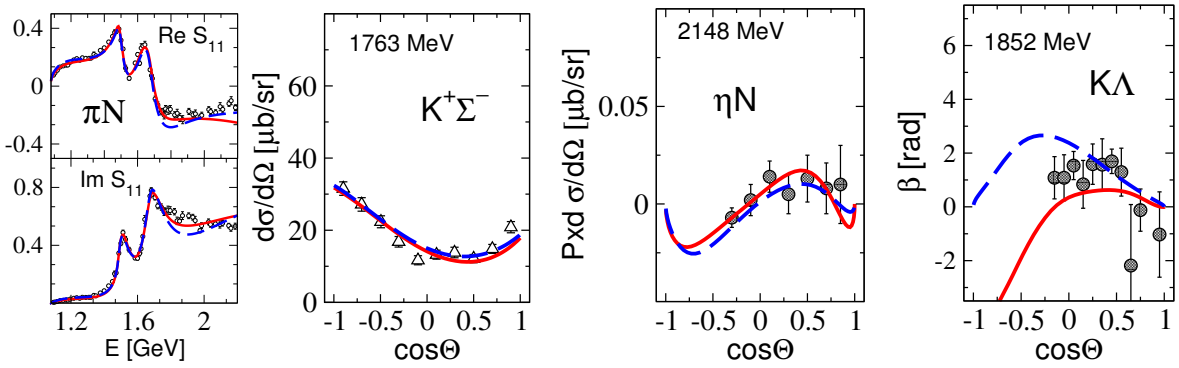

Figure 2.1: Selected results of the Jülich2012 analysis. Solid (red) lines: fit A. Dashed (blue) lines: fit B. Left: S_{11} partial wave in the elastic πN channel, points: GWU/SAID analysis [69]. Second from left: differential cross section of $\pi^- p \to K^+\Sigma^-$, data: Ref. [132]. Third from left: polarization of $\pi^- p \to \eta n$, data: Ref. [133]. Right: spin rotation parameter of $\pi^- p \to K^0\Lambda$, data: Ref. [134]. E is the center of mass energy and θ the scattering angle.

- In Fig. 2.2 the resonance positions in the complex energy plane extracted in the Jülich2012 analysis are shown together with the branch points induced by the opening of the reaction channels.

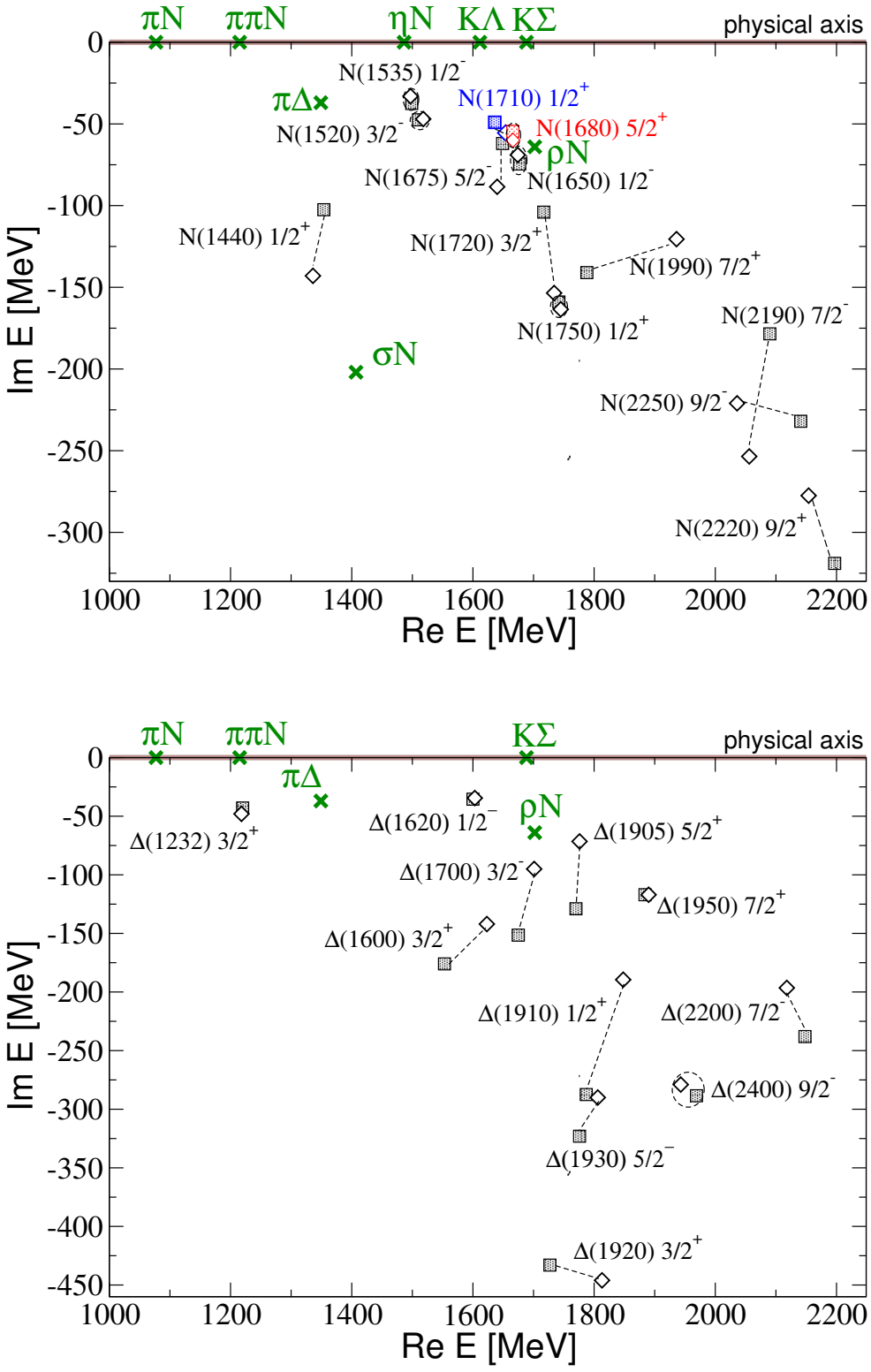

Figure 2.2: Pole positions of the isospin $I = 1/2$ (left) and $I = 3/2$ (right) resonances extracted in the Jülich2012 analysis. Squares: fit A. Diamonds: fit B. The branch points of the amplitude are shown as (green) crosses.

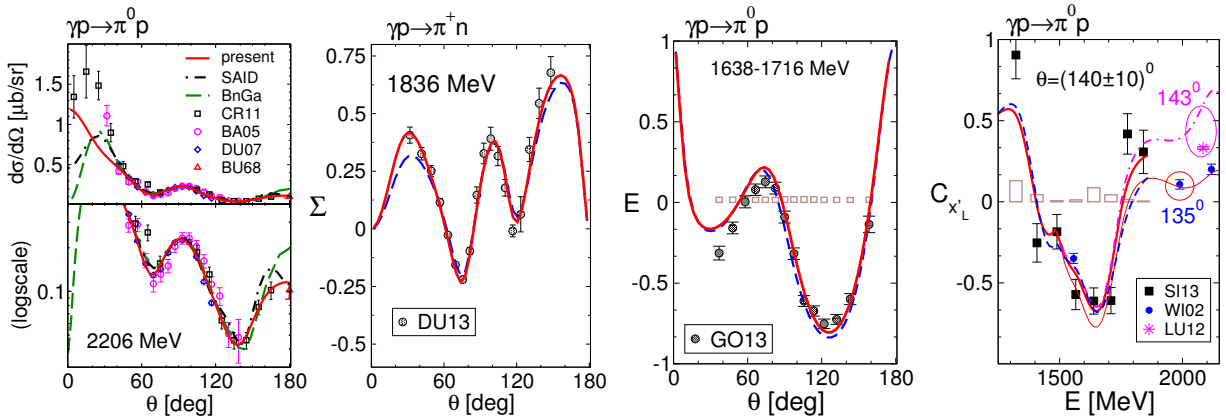

Figure 2.3: Selected results of the semi-phenomenological study of pion photoproduction. Left: differential cross section of $\gamma p \to \pi^0 p$. Solid (red) line: fit 2. Results from other groups: Dash-dotted (black) line: GWU/SAID CM12 [71]. Dashed (green) line: Bonn-Gatchina [72]. Data: CR11 [135], BA05 [136], DU07 [137], BU68 [138]. Second from left: Beam asymmetry Σ of $\gamma p \to \pi^+ n$. Dashed (blue) line: prediction based on fit 1. Solid (red) line: fit 2. Data: DU13 [139]. Third from left: Double polarization E of $\gamma p \to \pi^0 p$. Dashed (blue) line: prediction based on fit 1. Solid (red) line: prediction based on fit 2. Data: GO13 [140]. Systematic errors are separately shown as brown bars. Right: Polarization transfer $C_{x'_L}$ of $\gamma p \to \pi^0 p$. Dashed (blue) line: prediction based on fit 1, angle-averaged. Solid (red) line: prediction based on fit 2, angle-averaged. Thin (red) line: prediction based on fit 2 at $\theta = 135°$. Dash-dotted (magenta) line: prediction based on fit 2 at $\theta = 143°$. Data: SI13 [123], WI02 [141] and LU12 [142]. Systematic errors are separately shown as brown bars.

- Selected fit results of the semi-phenomenological study of the reactions $\gamma p \to \pi^0 p$ and $\pi^+ n$ are presented in Fig. 2.3. We performed two different fits based on different data bases. In fit 1, only measurements of single-polarization data are included. In this way, the impact of recent double-polarization measurements can be seen.

Chapter 3

Pion-induced reactions

In this chapter we present the simultaneous analysis of elastic πN scattering and the reactions $\pi^- p \to \eta N$, $K^0\Lambda$, $K^0\Sigma^0$, $K^+\Sigma^-$ and $\pi^+ p \to K^+\Sigma^+$ in a dynamical coupled-channel approach. This work is published in Ref. [1].

Based on an effective Lagrangian, the effective potential that describes the meson-baryon interaction is included in form of t- and u-channel exchange diagrams. Here, SU(3) flavor symmetry is used to relate the different reaction channels. Explicit resonance states are represented by s-channel diagrams, but the dynamical generation of resonances is also possible.

The scattering potential is iterated in a Lippmann-Schwinger-type equation. Two-body and, to some extend, three-body unitarity is satisfied. The latter is of importance for the analysis of the resonance spectrum because of the large inelasticity of the $\pi\pi N$ channel. In the present approach this channel is parameterized as effective ρN, σN and $\pi\Delta$ channels. The scattering equation is solved in the framework of time-ordered perturbation theory.

Since the dispersive parts of the scattering amplitude and the correct structure of branch points are included, analyticity is respected. This is a prerequisite for the reliable extraction of resonance parameters in the form of poles and residues in the complex energy plane.

In case of the inelastic reactions, we adjust the free parameters of the model to the available data on differential and total cross sections, polarizations and the spin-rotation parameter. As input for the elastic πN channel we use the partial-wave analysis of the GWU/DAC group. We include partial waves up to a total angular momentum of $J = 9/2$ and the considered energy range is extended beyond 2 GeV.

The free parameters of our model are given by the bare masses and couplings of the s-channel resonance states and by the cut-off parameters of the t- and u-channel diagrams. In order to get an estimate of the sensitivity of our results to the starting conditions, we perform two fits starting from different scenarios in the parameter space.

The aim of the present study is the analysis of the resonance spectrum in the isospin $I = 1/2$ and $I = 3/2$ sector. We extract the poles and residues of the nucleon and Delta resonances and calculate branching ratios.

3.1 Summary of the results

We performed two fits adjusting the free parameters of the model simultaneously to the $\pi N \to \pi N$ partial-wave amplitudes of the GWU/SAID analysis with a total angular momentum $J \leq 9/2$ and to experimental data for the reactions $\pi^- p \to \eta N$, $K^0\Lambda$, $K^0\Sigma^0$, $K^+\Sigma^-$ and $\pi^+ p \to K^+\Sigma^+$ up to energies around 2.3 GeV. On the whole, we achieved a good description of the data and the SAID partial-wave amplitudes in both fits. However, the data situation in the individual reaction channels is quite different in quantity and quality, which complicates a combined description. For example, in $K\Lambda$ data on total and differential cross section, on polarization and spin-rotation parameter measurements are available and the data show no severe inconsistencies. In contrast, the data in the ηN channel are much more often incompatible with other experiments or suffer from an underestimation of the systematic errors. In case of the $K^+\Sigma^-$ channel no polarization data is available at all. This is especially unfortunate because due to its u-channel sensitivity this channel is important to disentangle the partial-wave content of the $K\Sigma$ final states.

We calculated scattering lengths and volumes and compared our results to ChPT calculations. We find fair agreement in most cases. Especially, in case of the isoscalar scattering length a^+_{0+} we achieve a very small value, although we cannot match the ChPT value.

In order to analyze the baryon spectrum, a thorough understanding of the analytic structure of the scattering amplitude is essential. In the present study, we included the correct structure of cuts and branch points and determined the pole positions in the complex energy plane. We found all well-established four-star resonances and discussed their pole positions and residues, as well as the branching ratios into the inelastic channels. We included and discussed also some less prominent resonance states. For the most part, the results of the two fits show only small variations.

We looked in detail into the analytic structure of the P_{11} partial wave and its poles. Besides the nucleon pole, that is renormalized to have the physical value of 939 MeV, there is the Roper pole, which is dynamically generated, and the $N(1710)\ 1/2^+$ resonance. The latter was included as explicit s-channel state to improve the fit to $K^0\Lambda$. It shows a considerable branching ratio into the ηN and $K\Lambda$ channels. In one fit, we find an additional dynamically generated pole in P_{11} far in the complex plane.

In the F_{15} partial wave, beside the $N(1680)\ 5/2^+$ the SAID analysis features a second resonance state that is not included in our approach. As a test, we performed a refit of the entire data base including a second genuine resonance in F_{15} but see no need for it since the date description of the inelastic channels is not improved substantially.

In the P_{33} partial wave, apart from the $\Delta(1232)\ 3/2^+$ we included a second genuine resonance called $\Delta(1920)\ 3/2^+$ which has a large coupling into the $K\Sigma$ channel. However, it is located very far in the complex energy plane and the characterization as a resonance is questionable. In addition to those two genuine resonances we find a dynamically generated pole identified with the $\Delta(1600)\ 3/2^+$.

By means of the $\Delta(1620)\ 1/2^-$ we illustrated that the values of bare parameters are often highly correlated. Changing one bare parameter can easily be compensated by altering

the value of another bare parameter whereat the pole position of the resonance does not change. We conclude that no physical meaning should be associated with bare parameters. This is confirmed by the observation that the extracted resonance parameters in our two fits are quite similar although the parameterization is very different.

Eur. Phys. J. A (2013) **49**: 44
DOI 10.1140/epja/i2013-13044-5

THE EUROPEAN PHYSICAL JOURNAL A

Regular Article – Theoretical Physics

Coupled-channel dynamics in the reactions $\pi N \to \pi N, \eta N, K\Lambda, K\Sigma$

D. Rönchen[1,a], M. Döring[2,b], F. Huang[3], H. Haberzettl[4], J. Haidenbauer[1,5], C. Hanhart[1,5], S. Krewald[1,5], U.-G. Meißner[1,2,5], and K. Nakayama[1,3]

[1] Institut für Kernphysik and Jülich Center for Hadron Physics, Forschungszentrum Jülich, D-52425 Jülich, Germany
[2] Helmholtz-Institut für Strahlen- und Kernphysik (Theorie) and Bethe Center for Theoretical Physics, Universität Bonn, Nußallee 14-16, D-53115 Bonn, Germany
[3] Department of Physics and Astronomy, University of Georgia, Athens, Georgia 30602, USA
[4] Institute for Nuclear Studies and Department of Physics, The George Washington University, Washington, DC 20052, USA
[5] Institute for Advanced Simulation, Forschungszentrum Jülich, D-52425 Jülich, Germany

Received: 20 December 2012 / Revised: 5 March 2013
Published online: 12 April 2013 –
Communicated by A. Ramos

Abstract. Elastic πN scattering and the world data of the family of reactions $\pi^- p \to \eta n$, $K^0\Lambda$, $K^0\Sigma^0$, $K^+\Sigma^-$, and $\pi^+ p \to K^+\Sigma^+$ are described simultaneously in an analytic, unitary, coupled-channel approach. SU(3) flavor symmetry is used to relate both the t- and the u- channel exchanges that drive the meson-baryon interaction in the different channels. Angular distributions, polarizations, and spin-rotation parameters are compared with available experimental data. Partial-wave amplitudes are determined and the resonance content is extracted from the analytic continuation, including resonance positions and branching ratios, and possible sources of uncertainties are discussed. The results provide the final-state interactions for the ongoing analysis of photo- and electroproduction data.

[a] e-mail: d.roenchen@fz-juelich.de
[b] e-mail: doering@hiskp.uni-bonn.de

Chapter 4

Photon-induced reactions

In this chapter we present the analysis of the two reactions $\gamma p \to \pi^0 p$ and $\gamma p \to \pi^+ n$ using the Jülich2012 model (Chap. 3) as final-state interaction. This study can be found in Ref. [2].

To describe the photon-nucleon interaction, we apply a phenomenological parameterization of the amplitude. The $\gamma N N^*$ and $\gamma N \Delta^*$ resonance vertices and the couplings of the γN channel to the non-pole part are approximated by energy-dependent polynomials. The interaction in the final state is determined by the hadronic T-matrix of the Jülich model and the corresponding parameters are not altered in the present photoproduction study. This semi-phenomenological analysis should be regarded as an intermediate step towards a combined description of pion- and photon-induced reactions in a microscopic dynamical coupled-channel approach.

The free parameters of the polynomials are fitted to differential cross sections and single- and double-polarization observables. All in all we include more than 22 000 data points up to an energy of $E \sim 2.3$ GeV. We present predictions of beam-target and beam-recoil observables and, if available, compare our predictions to data. We perform two fits based on different data bases. In the first fit, we consider only single-polarization observables, while the data base of the second fit is extended to double-polarization observables and includes also very recent measurements of single-polarization observables. In this way, the impact of the new high-precision data can be assessed.

In case of the single-polarization observables, $d\sigma/d\Omega$, Σ, T and P, we show only the comparison to selected data sets in the following. A comparison to the full data base can be found in Appendix A.

The resonance positions and residues have been determined in the hadronic Jülich2012 analysis. In the present study, we extract the photocouplings at the pole and compare our results to other groups.

4.1 Summary of the results

The parameters of the phenomenologically approximated γN resonance and background vertices were adjusted to experimental data of the reactions $\gamma p \to \pi^0 p$ and $\gamma p \to \pi^+ n$. The data base of fit 1 comprised measurements of $d\sigma/d\Omega$, Σ, T and P. In fit 2, we included additionally data on $\Delta\sigma_{31}$, G, H and a new data set for Σ obtained in a recent CLAS measurement at JLab. All in all, we achieve a good description of the data. Since the hadronic T-matrix of the Jülich2012 analysis is not altered in the present approach, we describe the hadronic reactions $\pi N \to \pi N$, ηN and KY at the same time.

The predictions from the first fit compared to data sets only included in fit 2 turned out to be surprisingly good. However, the influence of the additional data is noticeable.

We present predictions from both fits for the double-polarization observables E, F, $C_{x'_L}$, $C_{z'_L}$ and the cross-section difference $\Delta\sigma$. In case of E and $\Delta\sigma$ for $\gamma p \to \pi^0 p$, we compared our results to the very recent CBELSA/TAPS data. Although in the fitting procedure of fit 2 we included data on $\Delta\sigma_{31}$, which is directly related to E, the predictions show evident deviations from the data. The same applies to fit 1 and suggests that those new data on E will have major impact on the extracted resonance parameters.

For the beam-recoil observable $C_{x'_L}$ we compare our predictions to very recent MAMI data, to one data point from a recent JLab measurement and to older JLab data. We achieved similar results for the two fits and fair agreement with the data. A strong angular-dependence for large angles and high energies can be observed. In case of $C_{z'_L}$, we show our results together with JLab data and one data point from a more recent JLab measurement. The deviations between the two fits are larger than for $C_{x'_L}$ and a strong angular dependence can be seen as well. A fit to those beam-recoil observables will contribute to a more precise determination of resonance parameters.

Other than for the hadronic reactions, for photoproduction there are data at very low energies. In order to achieve a good description of the threshold region, we included some isospin breaking effects in the construction of the photoproduction amplitude. We discussed in detail the $E_{0+}(\pi^0 p)$ multipole and found good agreement for fit 2 with data and other theoretical analyses. The other (isospin averaged) multipoles are compared to the SAID CM12 solution. While the lower multipoles are often quite similar to the latter analysis, in case of the higher multipoles large deviation can be observed between our two fits and between the CM12 solution and our results.

In the Jülich2012 analysis, the pole positions and residues of the resonances in the isosopin 1/2 and 3/2 sector were determined in a coupled-channel analysis of hadronic reactions. In the present study, we extracted the photocouplings at the poles

$$\tilde{A}^h_{pole} = A^h_{pole} e^{i\vartheta^h} \tag{4.1}$$

and found qualitative agreement with the results of other groups. The angles ϑ^h usually differ more than the couplings A^h_{pole}. For some resonances we obtain very different values in fit 1 and 2. This is predominantly the case for less well established states and reflects the impact of the recent high-precision data.

Photocouplings at the Pole from Pion Photoproduction

D. Rönchen,[1,*] M. Döring,[2,3,†] F. Huang,[4,5] H. Haberzettl,[3] J. Haidenbauer,[1,6]
C. Hanhart,[1,6] S. Krewald,[1,6] U.-G. Meißner,[1,2,6] and K. Nakayama[1,5]

[1]*Institut für Kernphysik and Jülich Center for Hadron Physics, Forschungszentrum Jülich, 52425 Jülich, Germany*
[2]*Helmholtz-Institut für Strahlen- und Kernphysik (Theorie) and Bethe Center for Theoretical Physics, Universität Bonn, Nußallee 14-16, 53115 Bonn, Germany*
[3]*Institute for Nuclear Studies and Department of Physics, The George Washington University, Washington, DC 20052, USA*
[4]*School of Physics, University of Chinese Academy of Sciences, Huairou District, Beijing 101408, China*
[5]*Department of Physics and Astronomy, University of Georgia, Athens, Georgia 30602, USA*
[6]*Institute for Advanced Simulation, Forschungszentrum Jülich, 52425 Jülich, Germany*

The reactions $\gamma p \to \pi^0 p$ and $\gamma p \to \pi^+ n$ are analyzed in a semi-phenomenological approach up to $E \sim 2.3$ GeV. Fits to differential cross section and single and double polarization observables are performed. A good overall reproduction of the available photoproduction data is achieved. The Jülich2012 dynamical coupled-channel model —which describes elastic πN scattering and the world data base of the reactions $\pi N \to \eta N$, $K\Lambda$, and $K\Sigma$ at the same time — is employed as the hadronic interaction in the final state. The framework guarantees analyticity and, thus, allows for a reliable extraction of resonance parameters in terms of poles and residues. In particular, the photocouplings at the pole can be extracted and are presented.

PACS numbers: 11.80.Gw, 13.60.Le, 13.75.Gx.

I. INTRODUCTION

Quantum Chromodynamics (QCD) manifests itself in a rich spectrum of excited baryons in the region between the perturbative regime and the ground state hadrons. Most of the available information on the resonance spectrum was obtained by partial-wave analyses of elastic πN scattering [1–3]. However, it is important to include other channels like ηN, $K\Lambda$ or $K\Sigma$ that couple to the πN system into such analyses. It is expected that data obtained for those other meson-baryon channels could help to shed light on the so called "missing resonances" predicted in quark models and related approaches [4–12] or lattice calculations [13] and assumed to couple only weakly to πN.

Since the amount of data on transition reactions like $\pi N \to \eta N$, $K\Lambda$, $K\Sigma$, etc. is somewhat limited, one should take advantage of the wealth and precision of the corresponding photoproduction data supplied over the past few years by experimental facilities like ELSA, GRAAL, JLab, MAMI, and SPring-8. Clearly, also in the case of photoproduction so far, certain assumptions have to be made in partial-wave analyses because the data are not yet accurate enough to allow for a model-independent extraction of the amplitude. However, the latter will become possible once more precise and more complete experiments become available [14–17]. It should be said that for pion photoproduction, in principle, a complete set of observables $\{\sigma, \Sigma, T, P, E, G, C_x, C_z\}$ – which would allow a full determination of the reaction amplitude [18] – has became available quite recently. However, the observables in question have not yet been measured at the same energies – which would be required, at least formally, for a complete experiment. Actually, due to the self-analyzing nature of hyperons, the aim of providing a complete set of experiments is easier to realize in kaon photoproduction than in pion photoproduction. Finally, we want to mention that a smaller number of polarization observables is sufficient for an analysis within a truncated multipole expansion, see the arguments in Refs. [19, 20].

To analyze pion- as well as photon-induced data theoretically, different approaches have been applied. The πN threshold region is well understood in terms of chiral perturbation theory (ChPT) [21–35], while extensions in form of unitarized chiral approaches [36–53] allow one to study the resonance region but also to consider the coupling to other channels like ηN, $K\Lambda$ or $K\Sigma$.

K-matrix [54–65] or unitary isobar models [66, 67] provide practical and flexible tools to analyze large amounts of data. By omitting the real parts of the self-energies the complexity of the calculation is strongly reduced and only on-shell intermediate states are included. While unitarity is preserved, dispersive parts are often neglected; this introduces systematic uncertainties into the extraction of resonance positions and residues.

For the task of a simultaneous analysis of different reactions, dynamical coupled-channel (DCC) models [68–78] are particularly well suited as they obey theoretical constraints of the S-matrix such as analyticity and unitarity. This allows for a reliable extraction of resonance parameters in terms of poles and residues in the complex energy plane. A simultaneous description of the reactions $\pi N \to \pi N$, ηN and KY ($K\Lambda$, $K\Sigma$) has

*Electronic address: d.roenchen@fz-juelich.de
†Electronic address: doering@hiskp.uni-bonn.de

been accomplished within the DCC framework of the Jülich2012 model [79]. See also the supplementary material and tables of hadronic transitions among the channels $\pi N, \eta N, K\Lambda$, and $K\Sigma$ which are available online [80]. In this approach [79, 81–85], the inclusion of the dispersive contributions of intermediate states and the correct structure of branch points [86] guarantee analyticity. The scattering amplitude is obtained as solution of a Lippmann-Schwinger-type equation, formulated in time-ordered perturbation theory (TOPT), which automatically ensures two-body unitarity. The three-body channel $\pi\pi N$ is important because it is the source of large inelasticities. Its effect is included in the model via effective $\pi\Delta$, σN and ρN channels. In the Jülich2012 model, the t-channel exchanges are complemented by u-channel baryon exchanges to approximate the left-hand cut. Together, they constitute the non-resonant part of the interaction, referred to as "background". Bare resonances are introduced as s-channel processes. The explicit treatment of the background in terms of t- and u-channel diagrams imposes strong correlations amongst the different partial waves and generates a non-trivial energy and angular dependence of the observables. Interestingly, the $\pi N \to KY$ amplitudes found in Ref. [79] are quite similar to those of a later analysis performed by the Bonn-Gatchina group [87].

The adaptation of DCC models to finite volumes, to allow for the prediction of lattice levels and the calculation of finite volume corrections, was pioneered in Ref. [88]. In principle, such extensions of hadronic approaches allow for the analysis of experimental and "data" from lattice QCD simulations [13, 89–91] on the same footing [92–95]. Chiral extrapolations are non-trivial due to the intricate coupled-channel structure in meson-baryon scattering [96].

Recently, it was shown how the Jülich coupled-channels approach can be extended to pion photoproduction [97] within a gauge-invariant framework that respects the generalized off-shell Ward-Takahashi identity [98–100] . Such a field-theoretical description of the photoproduction process is, however, technically rather involved. Therefore, in the present work we follow a more phenomenological approach in which we use a flexible and easy-to-implement parametrization of the photo-excitation vertices at the multipole-amplitude level. This approach is inspired by the GWU/DAC CM12 parameterization of Ref. [3], that complements earlier parameterizations [16, 101–104]. In this way, we will be able to consider a far larger and more comprehensive set of pion photoproduction data than before [97], although at the expensive of giving up any direct connection with the microscopic reaction dynamics of the photo-interaction. For the hadronic interaction part, all microscopic features from our full DCC approach [79] are preserved (i.e. the elastic πN and $\pi N \to \eta N$, KY data are described). We view this semi-phenomenological approach as an intermediate step towards building a more microscopic DCC description not only of photoproduction, but also of electroproduction processes along the lines of Ref. [97].

The paper is organized as follows: in Sec. II, we give an overview of the formalism of the hadronic coupled-channel model and the phenomenological parameterization of the photo-excitation vertices. The data base and the fitting strategy are described in Sec. III A. In Sec. III B, the fit results are compared to data and discussed in detail. The extracted photocouplings at the pole can be found in Sec. III D. In the appendices, details of the multipole decomposition of the photoproduction amplitude and the definition of the observables and the photocouplings are given.

II. FORMALISM

A. Two-potential formalism for the hadronic interaction

Both the hadronic scattering matrix and the photoproduction amplitude can be decomposed into a pole and a non-pole part as outlined in this and the following section. This decomposition is not required by the photoproduction formalism because the photoproduction amplitude can be formulated in terms of the full half-offshell T-matrix as shown in the next section. However, the decomposition in pole and non-pole parts simplifies numerics significantly as outlined in Sec. III A.

The partial-wave T-matrix in the Jülich2012 formulation [79] is given by the integral equation,

$$T_{\mu\nu}(q,p',E) = V_{\mu\nu}(q,p',E) + \sum_{\kappa} \int_0^\infty dp\, p^2\, V_{\mu\kappa}(q,p,E) G_\kappa(p,E)\, T_{\kappa\nu}(p,p',E)\ . \quad (1)$$

where $q \equiv |\vec{q}|$ ($p' \equiv |\vec{p}\,'|$) is the modulus of the outgoing (incoming) three-momentum that may be on- or off-shell, E is the scattering energy, and μ, ν, κ are channel indices. In Eq. (1), the propagator G_κ has the form

$$G_\kappa(p,E) = \frac{1}{E - E_a(p) - E_b(p) + i\epsilon}\ , \quad (2)$$

where $E_a = \sqrt{m_a^2 + p^2}$ and $E_b = \sqrt{m_b^2 + p^2}$ are the on-mass-shell energies of the intermediate particles a and b in channel κ with respective masses m_a and m_b. Equation (1) is formulated in the partial-wave basis, i.e. the amplitude only depends on the modulus of the incoming, outgoing, and intermediate particle momenta. This implies a partial-wave decomposition of the exchange potentials [84, 85]. The denominator in Eq. (1) corresponds to the channels with stable particles, πN, ηN, $K\Lambda$, and $K\Sigma$; for the effective $\pi\pi N$ channels ($\pi\Delta$, σN, ρN), the propagator is more involved [83, 85].

The sum of the u- and t-channel diagrams is labeled as $V^{\rm NP}$ in the following. The full set is shown in Figs. 1

and 2 of Ref. [79]. Together with the (bare) s-channel exchanges $V^{\rm P}$, they constitute the interaction V in Eq. (1),

$$V_{\mu\nu} = V_{\mu\nu}^{\rm NP} + V_{\mu\nu}^{\rm P} \equiv V_{\mu\nu}^{\rm NP} + \sum_{i=0}^{n} \frac{\gamma_{\mu;i}^{a}\,\gamma_{\nu;i}^{c}}{E - m_i^b} \,, \qquad (3)$$

with n being the number of bare s-channel states in a given partial wave. The $\gamma_{\mu;i}^{c}$ ($\gamma_{\nu;i}^{a}$) are the bare creation (annihilation) vertices of resonance i with bare mass m_i^b. The notation is chosen to be consistent with earlier work; confusions with the photon (γ) should be excluded by the context. The explicit form of the resonance vertex functions can be found in Appendix B of Ref. [81] and in Appendix A of Ref. [79]. In the following we make use of the two-potential formalism and apply it to the decomposition defined in Eq. (3). Inserting $V^{\rm NP}$ into a Lippmann-Schwinger-type equation,

$$T_{\mu\nu}^{\rm NP} = V_{\mu\nu}^{\rm NP} + \sum_{\kappa} V_{\mu\kappa}^{\rm NP} G_\kappa T_{\kappa\nu}^{\rm NP} \,, \qquad (4)$$

leads to the so-called *non-pole* part of the full T-matrix (projected to a partial wave). For simplicity, in Eq. (4) and the following, the integration over the momentum of the intermediate state p, cf. Eq. (1), is not written explicitly. The s-channel exchanges that constitute $V^{\rm P}$ generate the pole part of the T-matrix, $T^{\rm P}$. The latter involves the non-pole part $T^{\rm NP}$ given in Eq. (4) and can be expressed in terms of the quantities

$$\begin{aligned}
\Gamma_{\mu;i}^{c} &= \gamma_{\mu;i}^{c} + \sum_{\nu} \gamma_{\nu;i}^{c}\, G_\nu\, T_{\nu\mu}^{\rm NP} \,, \\
\Gamma_{\mu;i}^{a} &= \gamma_{\mu;i}^{a} + \sum_{\nu} T_{\mu\nu}^{\rm NP}\, G_\nu\, \gamma_{\nu;i}^{a} \,, \\
\Sigma_{ij} &= \sum_{\mu} \gamma_{\mu;i}^{c}\, G_\mu\, \Gamma_{j;\mu}^{a} \,, \qquad (5)
\end{aligned}$$

where Γ^c (Γ^a) are the so-called dressed resonance creation (annihilation) vertices and Σ is the self-energy. The indices i, j label the s-channel state in the case of multiple resonances. The order of terms in Eq. (5) and all following equations corresponds to the convention that time flows from the right to the left. For the case of two resonances in a partial wave, the pole part reads explicitly [105]

$$\begin{aligned}
T_{\mu\nu}^{\rm P} &= \Gamma_{\mu}^{a}\, D^{-1}\, \Gamma_{\nu}^{c} \,, \text{where} \\
\Gamma_{\mu}^{a} &= (\Gamma_{\mu;1}^{a}, \Gamma_{\mu;2}^{a}), \quad \Gamma_{\mu}^{c} = \begin{pmatrix} \Gamma_{\mu;1}^{c} \\ \Gamma_{\mu;2}^{c} \end{pmatrix}, \\
D &= \begin{pmatrix} E - m_1^b - \Sigma_{11} & -\Sigma_{12} \\ -\Sigma_{21} & E - m_2^b - \Sigma_{22} \end{pmatrix} \,, \qquad (6)
\end{aligned}$$

from which the single-resonance case follows immediately. It is easy to show that the full scattering T-matrix of Eq. (1) is given by the sum of pole and non-pole parts,

$$T_{\mu\nu} = T_{\mu\nu}^{\rm P} + T_{\mu\nu}^{\rm NP} \,. \qquad (7)$$

B. Two-potential formalism for photoproduction

The photoproduction multipole amplitude in terms of a photoproduction kernel $V_{\mu\gamma}$ is given by

$$\begin{aligned}
M_{\mu\gamma}(q, E) &= V_{\mu\gamma}(q, E) \\
&\quad + \sum_{\kappa} \int_0^\infty dp\, p^2\, T_{\mu\kappa}(q, p, E) G_\kappa(p, E) V_{\kappa\gamma}(p, E) \,. \qquad (8)
\end{aligned}$$

Here and in the following the index γ is used exclusively for the γN channel. Note that in the second term the photoproduction kernel produces a meson-baryon pair in channel κ with off-shell momentum p that rescatters via the hadronic half-offshell T-matrix, producing the final πN state (more generally, channel μ) with momentum q. The formalism allows for off-shell external q but we will consider only the production of real pions in the following. Similarly, $V_{\mu\gamma}$ can also depend on the virtuality of the photon, but we will consider only real photons with $Q^2 = 0$. With the choice of $V_{\mu\gamma}$ as specified below, the photoproduction amplitude of Eq. (8) satisfies Watson's theorem by construction.

The photoproduction kernel can be written as

$$V_{\mu\gamma}(p, E) = \alpha_{\mu\gamma}^{\rm NP}(p, E) + \sum_i \frac{\gamma_{\mu;i}^{a}(p)\, \gamma_{\gamma;i}^{c}(E)}{E - m_i^b} \,. \qquad (9)$$

Here, $\alpha_{\mu\gamma}^{\rm NP}$ represents the photon coupling to t- and u-channel diagrams and to contact diagrams. These diagrams together form the non-pole part of the full photoproduction kernel as can bee seen from field-theoretical considerations [100]. The summation in Eq. (9) is over the resonances i in a multipole, and the $\gamma_{\gamma;i}^{c}$ are the real tree-level $\gamma N N_i^*$ and $\gamma N \Delta_i^*$ photon couplings that only depend on the energy E but not on the momentum p. It is crucial that the resonance annihilation vertex γ^a in Eq. (9) is precisely the same as in the hadronic part of Eq. (3) so that the explicit singularity at $E = m_i^b$ cancels.

The two-potential formalism allows one to rewrite the photoproduction amplitude M as

$$\begin{aligned}
M_{\mu\gamma} &= \alpha_{\mu\gamma}^{\rm NP} + \sum_{\kappa} T_{\mu\kappa}^{\rm NP} G_\kappa \alpha_{\kappa\gamma}^{\rm NP} + \Gamma_{\mu;i}^{a}\, (D^{-1})_{ij}\, \Gamma_{\gamma;j}^{c} \\
\Gamma_{\gamma;j}^{c} &= \gamma_{\gamma;j}^{c} + \sum_{\kappa} \Gamma_{\kappa;j}^{c} G_\kappa \alpha_{\kappa\gamma}^{\rm NP} \qquad (10)
\end{aligned}$$

with the dressed resonance-creation photon-vertex $\Gamma_{\gamma;j}^{c}$ which is a vector in resonance space, like the strong dressed vertex $\Gamma_{\mu;i}^{c}$ in Eq. (6). This standard result has been derived, e.g., in Ref. [105]. In the form of Eq. (10) it becomes apparent that in $M_{\mu\gamma}$ all singularities due to the bare resonances of Eq. (9) have canceled.

Alternatively, one can write the amplitude simply in terms of the full hadronic T-matrix as

$$M_{\mu\gamma} = \sum_{\kappa} (1 - VG)^{-1}_{\mu\kappa}\, V_{\kappa\gamma} \,. \qquad (11)$$

In principle, any of the forms (8), (10), or (11) can be used in practical calculations. In the form of Eq. (11), which resembles the one of Ref. [106], the similarity with the CM12 Chew-Mandelstam parameterization of the CNS/DAC group [3] becomes apparent, in which the hadronic kernel $\bar{K}_{\kappa\nu}$ of the hadronic T-matrix,

$$T_{\mu\nu} = \sum_{\kappa} (1 - \bar{K}C)^{-1}_{\mu\kappa} \, \bar{K}_{\kappa\nu} \; , \tag{12}$$

is replaced by a photoproduction kernel, $\bar{K}_{\kappa\gamma}$,

$$M_{\mu\gamma} = \sum_{\kappa} (1 - \bar{K}C)^{-1}_{\mu\kappa} \, \bar{K}_{\kappa\gamma} \; . \tag{13}$$

Here, C is the complex Chew-Mandelstam function that guarantees unitarity. While Eq. (13) is formally identical to Eq. (11), there is a practical difference: Eq. (11) implies an integration over intermediate off-shell momenta, while the quantities $\bar{K}$ and C in Eq. (13) factorize. In both approaches the dispersive parts of the intermediate loops G and C are maintained.

In the present approach, the terms $\alpha^{\rm NP}_{\mu\gamma}$ and $\gamma^{c}_{\gamma;i}$ in Eq. (9) are approximated by polynomials P,

$$\begin{aligned} \alpha^{\rm NP}_{\mu\gamma}(p,E) &= \frac{\tilde{\gamma}^{a}_{\mu}(p)}{\sqrt{m_N}} P^{\rm NP}_{\mu}(E) \\ \gamma^{c}_{\gamma;i}(E) &= \sqrt{m_N} P^{\rm P}_{i}(E) \end{aligned} \tag{14}$$

where $\tilde{\gamma}^{a}_{\mu}$ is a vertex function equal to $\gamma^{a}_{\mu;i}$ but stripped of any dependence on the resonance number i. Equation (14) means that we have $n + m$ polynomials per multipole with n resonances i and m hadronic channels μ. With this parameterization, non-analyticities from left-hand cuts, like the one from the pion-pole term, are approximated by polynomials. As the distance to the physical region is quite large, such an approximation can be justified. Note in this context that even for the $\gamma\gamma \to \pi\pi$ reaction that has a very close-by left-hand cut, the Born contributions can be effectively parameterized by a linear polynomial [107].

The photoproduction kernel $V_{\mu\gamma}$ should have the correct threshold structure, $V_{\mu\gamma} \sim q^{L}$ where q is the center-of-mass momentum in channel μ and L is the orbital angular momentum. The L dependence of the different channels with a given J^P can be found, e.g., in Table XI of Ref. [79]. The correct L dependence is automatically provided by the bare resonance vertices $\gamma^{a}_{\mu;i}$ and, thus, already fulfilled for the pole part of Eq. (14). The same applies to the vertex function $\tilde{\gamma}^{a}_{\mu}$ in the non-pole part of Eq. (14).

The final choice for the polynomials P, for a given multipole, is then:

$$\begin{aligned} P^{\rm P}_{i}(E) &= \sum_{j=1}^{\ell_i} g^{\rm P}_{i,j} \left(\frac{E - E_s}{m_N} \right)^{j} e^{-\lambda^{\rm P}_{i}(E-E_s)} \\ P^{\rm NP}_{\mu}(E) &= \sum_{j=0}^{\ell_\mu} g^{\rm NP}_{\mu,j} \left(\frac{E - E_s}{m_N} \right)^{j} e^{-\lambda^{\rm NP}_{\mu}(E-E_s)} \end{aligned} \tag{15}$$

with E_s being a suitable expansion point close to the πN threshold, $E_s = 1077$ MeV. The appearance of the nucleon mass m_N in Eqs. (14) and (15) ensures that the g's are dimensionless quantities. The g and the $\lambda > 0$ are multipole-dependent free parameters that are fitted to data. Furthermore, to fulfill the decoupling theorem, that resonance contributions are parametrically suppressed at threshold, the sum for $P^{\rm P}$ starts with $j = 1$ and not with $j = 0$ (hence, the expansion is chosen at threshold). In the fitting procedure, ℓ_i and ℓ_μ are chosen as demanded by data but always $\ell_i, \ell_\mu \leq 3$. The factor $e^{-\lambda\,(E-E_s)}$ ensures that the multipole amplitudes are well-behaved in the high-energy limit, and, at the same time, absorbs the potentially strong energy dependence induced by the γN threshold that is close to the πN threshold. In any case, it is clear that this effective parameterization cannot be used for sub-threshold extrapolations.

In the present approach, the photon is allowed to couple to the πN, ηN and $\pi\Delta$ channels. The latter accounts for the inelasticity into the $\pi\pi N$ channels. As long as the analysis is restricted to one-pion photoproduction, as in this study, there is no need to include additional couplings of the photon to σN and ρN. As for the $\pi\Delta$ channels, there are usually two independent couplings for a given multipole; we only couple the photon to the $\pi\Delta$ channel with the lower L (c.f. also Table XI of Ref. [79]). The extension to ηN, $K\Lambda$ and $K\Sigma$ photoproduction is planned for the future and will require direct photon couplings to these states. As for photoproduction on the neutron, the JLab FROST and HD-ICE experiments are currently being analyzed [108, 109] and theoretical methods are being developed to disentangle the neutron amplitudes [101, 110, 111]

For completeness, a multipole decomposition of the pseudoscalar meson photoproduction amplitude is given in Appendix A.

C. Isospin breaking

In the Jülich model, in general, isospin-averaged masses are used, which has little effect at energies that are not very close to the threshold, as it is the case for the hadronic data used in the analysis of Ref. [79]. For pion photoproduction, however, there are data at very low energies and we have to take into account the different threshold energies for the $\pi^0 p$ and the $\pi^+ n$ channels.

In the particle basis, the amplitudes for the processes $\gamma p \to \pi^0 p$ and $\gamma p \to \pi^+ n$ are shown in Fig. 1 and read

$$\begin{aligned} M_{\pi^0 p\,\gamma p} = V_{\pi^0 p\,\gamma p} &+ T_{\pi^0 p\,\pi^0 p}\, G_{\pi^0 p}\, V_{\pi^0 p\,\gamma p} \\ &+ T_{\pi^0 p\,\pi^+ n}\, G_{\pi^+ n}\, V_{\pi^+ n\,\gamma p} \\ &+ \sum_{\kappa \neq \pi N} \Big(T_{\frac{1}{2}\,(\pi N\,\kappa)}\, G_{\kappa}\, V_{\frac{1}{2}\,\kappa\,\gamma p} \\ &\quad + \frac{2}{3}\, T_{\frac{3}{2}\,(\pi N\,\kappa)}\, G_{\kappa}\, V_{\frac{3}{2}\,\kappa\,\gamma p} \Big) \; , \end{aligned} \tag{16}$$

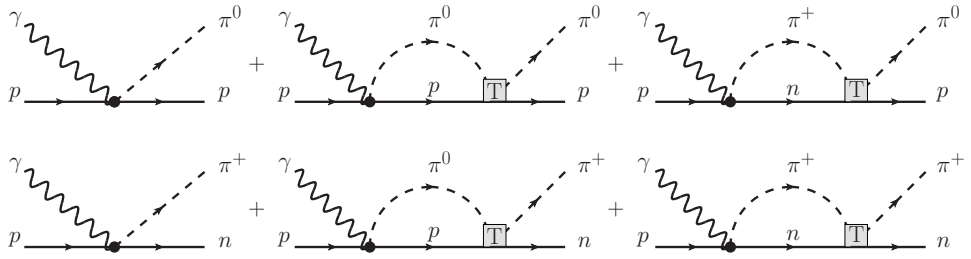

FIG. 1: Schematic representation of the reactions $\gamma p \to \pi^0 p$ (upper row) and $\gamma p \to \pi^+ n$ (lower row), cf. Eqs. (16) and (17). The small black dots represent the potentials $V_{\frac{1}{2}(\pi N\,\gamma p)}$ and $V_{\frac{3}{2}(\pi N\,\gamma p)}$, while T is the hadronic T-matrix. Not shown are the excitations of intermediate $\pi\Delta$ and ηN channels that are treated isospin-symmetrically.

$$\begin{aligned} M_{\pi^+ n\,\gamma p} = V_{\pi^+ n\,\gamma p} \;&+\; T_{\pi^+ n\,\pi^0 p}\, G_{\pi^0 p}\, V_{\pi^0 p\,\gamma p} \\ &+\; T_{\pi^+ n\,\pi^+ n}\, G_{\pi^+ n}\, V_{\pi^+ n\,\gamma p} \\ &+\; \sum_{\kappa\neq\pi N} \Big(\sqrt{2}\, T_{\frac{1}{2}\,(\pi N\,\kappa)}\, G_\kappa\, V_{\frac{1}{2}\,\kappa\,\gamma p} \\ &\quad - \frac{\sqrt{2}}{3}\, T_{\frac{3}{2}\,(\pi N\,\kappa)}\, G_\kappa\, V_{\frac{3}{2}\,\kappa\,\gamma p} \Big) \end{aligned} \tag{17}$$

where $\kappa \neq \pi N$ stands for the sum over the intermediate states $\pi\Delta$ and ηN that are assumed to fulfill isospin symmetry as indicated with isospin indices $I = \frac{1}{2}, \frac{3}{2}$. Furthermore, note that $T_{\pi^0 p\,\pi^0 p}$ is a pure isoscalar transition and, thus, very small near threshold [28–30, 112–115]. As a consequence, $E_0^+(\pi^0 p)$ develops only a very small imaginary part below the $\pi^+ n$ threshold.

For the hadronic final-state interaction $T_{\mu\nu}$, and for $V_{\mu\gamma}$ in Eqs. (16) and (17) we neglect the small mass differences within the isospin multiplets, i.e.

$$\begin{aligned} V_{\pi^0 p\,\gamma p} &= V_{\frac{1}{2}(\pi N\,\gamma p)} + \frac{2}{3} V_{\frac{3}{2}(\pi N\,\gamma p)} \,, \\ V_{\pi^+ n\,\gamma p} &= \sqrt{2} V_{\frac{1}{2}(\pi N\,\gamma p)} - \frac{\sqrt{2}}{3} V_{\frac{3}{2}(\pi N\,\gamma p)} \,, \\ T_{\pi^0 p\,\pi^0 p} &= \frac{1}{3} T_{\frac{1}{2}(\pi N\,\pi N)} + \frac{2}{3} T_{\frac{3}{2}(\pi N\,\pi N)} \,, \\ T_{\pi^0 p\,\pi^+ n} &= \frac{\sqrt{2}}{3} T_{\frac{1}{2}(\pi N\,\pi N)} - \frac{\sqrt{2}}{3} T_{\frac{3}{2}(\pi N\,\pi N)} \,, \\ T_{\pi^+ n\,\pi^+ n} &= \frac{2}{3} T_{\frac{1}{2}(\pi N\,\pi N)} + \frac{1}{3} T_{\frac{3}{2}(\pi N\,\pi N)} \,. \end{aligned} \tag{18}$$

The $\pi^0 p$ and $\pi^+ n$ propagators $G_{\pi^0 p}$, $G_{\pi^+ n}$ have the same form as the isospin-symmetric πN propagator but incorporate the exact proton (neutron) and π^0 (π^+) masses,

$$G_{\pi^0 p} = \frac{1}{E - \sqrt{m_p^2 + p^2} - \sqrt{M_{\pi^0}^2 + p^2} + i\epsilon} \tag{19}$$

$$G_{\pi^+ n} = \frac{1}{E - \sqrt{m_n^2 + p^2} - \sqrt{M_{\pi^+}^2 + p^2} + i\epsilon} \,. \tag{20}$$

Accordingly, to calculate the differential cross section close to threshold in Eq. (B13) instead of the averaged m_N we use m_p and m_n for calculating $|\vec{q}|$. The same applies to m_N appearing in Eq. (A6).

III. RESULTS

Before we start discussing the present results, a remark on the observables discussed in this work is in order. There are many different conventions used in the literature to define the spin polarization observables. Our convention is given explicitly in Appendix B and agrees with that used by the SAID group [104].

A. Data base and fit parameters

The free parameters g and λ of Eq. (15) are determined by MINUIT fits on the JUROPA supercomputer at the Forschungszentrum Jülich. In a first step, the parameters are fitted to the multipole amplitudes of the GWU/SAID CM12 solution [3] which guarantees a good starting point for the second step that involves fitting only to the data. The two reactions $\gamma p \to \pi^0 p$ and $\gamma p \to \pi^+ n$ are studied simultaneously. For the connection of the present formalism to observables see Appendix B. The hadronic T-matrix in Eq. (8) is taken from the Jülich2012 fit A [79]. This interaction describes elastic πN scattering and the world data base of $\pi N \to \eta N$ and KY. Simultaneous fits to pion- and photon-induced reactions in the spirit of Refs. [116, 117] are planned for the future.

In the fitting procedure we consider two scenarios. In fit 1, only differential cross sections, beam and target asymmetries, and recoil polarizations are taken into account. In a second fit (fit 2), also recent CLAS data on the beam asymmetry [118] and data on the double-polarization observables G, H and $\Delta\sigma_{31}$ are included. We expect that a comparison of the two fits allows one to see the impact of the recent high-precision data from ELSA, JLab, MAMI, and Spring-8 on the extracted resonance parameters. An overview of the two fits performed in this study can be found in Table I. The observables E, F, $C_{x'_L}$, and $C_{z'_L}$ are predicted.

The photoproduction data are taken from the GWU/SAID data base [2, 3] where we consider data up to $E = 2330$ MeV for $\gamma p \to \pi^0 p$ and up to $E = 2260$ MeV for $\gamma p \to \pi^+ n$. (The CNS/DAC group at GWU in-

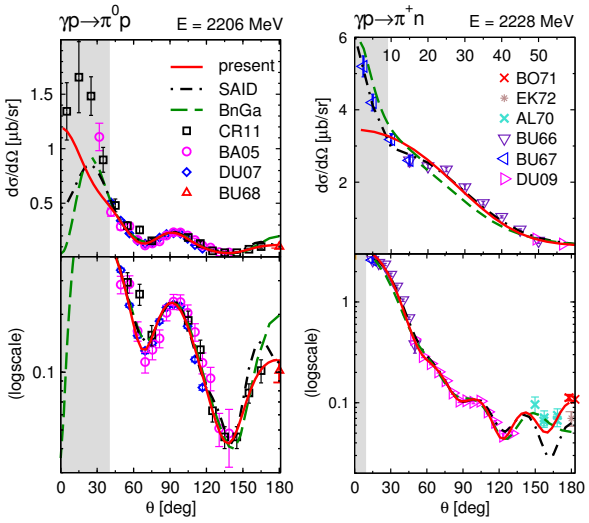

FIG. 2: High energy behavior in the reaction $\gamma p \to \pi^0 p$ (left) and $\gamma p \to \pi^+ n$ (right). Solid (red) line: fit 2; dash-dotted (black) line: GWU/SAID CM12 [3]; dashed (green) line: Bonn-Gatchina [119]. Data $\pi^0 p$: CR11[120], BA05[126], DU07[127], BU68[128]. Data $\pi^+ n$: BO71[129], EK72[130], AL70[131], BU66[132], BU67[133], DU09[134]. The regions excluded in our fit are shown as shaded areas.

cludes data up to higher energies.) For the reaction with final state $\pi^0 p$ ($\pi^+ n$) and for energies $E > 2050$ MeV ($E > 1600$), we exclude data with forward angles $\theta < 40°$ ($\theta < 9°$) because in the present approach we do not include partial waves with total angular momentum $J \geq 11/2$. A detailed look at the two data sets in question is provided in Fig. 2, where results of our fit 2 are shown together with those of the GWU/SAID analysis [3] and the Bonn-Gatchina analysis [119]. As can be seen, for $\pi^0 p$ none of the approaches is able to describe the forward peak (an experimental confirmation of the data CR11 [120] is needed). In case of $\pi^+ n$, on the other hand, the forward peak is well described by the GWU/SAID analysis. Note that the GWU/SAID and the Bonn-Gatchina analyses use prescriptions for partial waves with $J \geq 11/2$ in terms of Born amplitudes and reggeized exchanges, respectively. We plan to improve the matching to the high energy/low t region where Regge trajectories provide an economic parameterization of the amplitude [121–125].

No special weights are assigned to any data in both fit 1 and 2. However, some data sets are contradictory to each other as can be seen, e.g., in Fig. 3 at the energies 1170 MeV and 1268 MeV. The deviations go beyond an overall normalization, i.e. they concern also the angular dependence. To account for such discrepancies we apply an additional systematic error of 5% to all data. Of course, this effectively gives more weight to data with larger errors, such as polarization observables.

TABLE I: Characteristics of fits 1 and 2. The difference between the fits shows the impact of recent high-precision measurements of Σ, $\Delta\sigma_{31}$, G and H from ELSA, JLab and MAMI.

	Fit 1	Fit 2
Line style	- - - -	———
# of data	21,627	23,518
Excluded data	$\pi^0 p$: $E > 2.33$ GeV and $\theta < 40°$ for $E > 2.05$ GeV	
	$\pi^+ n$: $E > 2.26$ GeV and $\theta < 9°$ for $E > 1.60$ GeV	
$ds/d\Omega$, P, T	included	included
Σ	included (CLAS [118] predicted)	included
$\Delta\sigma_{31}$, G, H	predicted	included
E, F, $C_{x'L}$, $C_{z'L}$	predicted	predicted
Sys. Error	5%	5%
χ^2	20,095	22,880
χ^2/d.o.f.	0.95	0.99

In any case, as next step, one would allow for a certain freedom in the normalization of individual data sets as practiced by the CNS/DAC group [2, 3]. We plan to improve our analysis along these lines in the future.

In total, we use 417 free parameters for fit 1 and 388 for fit 2. The parameters are the photon couplings $g^{\rm P}$ and $\lambda^{\rm P}$ to 11 isospin $I = 1/2$ resonance states and 10 isospin $I = 3/2$ resonance states in addition to the non-pole photon couplings $g_\mu^{\rm NP}$ and $\lambda_\mu^{\rm NP}$ with $\mu = \pi N, \eta N, \pi\Delta$ for $I = 1/2$ and $\mu = \pi N, \pi\Delta$ for $I = 3/2$, c.f. Eq. (15).

It is obvious from Eq. (6) that the pole-part can be evaluated from the non-pole part, meaning that for every fit step of parameters tied to the non-pole part, it is most economic to perform a full fit of the parameters tied to the pole part. This was the strategy followed in Ref. [79]. Similarly, the photoproduction amplitude M in Eq. (8) is evaluated from the hadronic T-matrix, that is not altered in the study, and the calculation can be optimized. This is the motivation to perform the decompositions outlined in Sec. II. The photo-excitation of both bare resonances and background is possible as can be seen in Eq. (9). We find that for some less prominent resonances it is possible to set the bare resonance excitation $\gamma_\gamma^c = 0$. However, for the more prominent ones, we need $\gamma_\gamma^c \neq 0$ for a good description of the data. In any case, we do not attribute any physical meaning to the individual components of the decompositions into pole and non-pole part.

B. Fit results

In Figs. 3 to 21, we show selected results of the fits to observables. The results compared to the full data base will be made available online [80]. Data sets that differ by less than 10 MeV in scattering energy are depicted in one

graph if necessary. If more than one data set from the same experiment lies in the same energy bin, we show only the one closest to the quoted energy. Older data with larger error bars are not displayed in many cases but enter the fitting procedure.

The differential cross section for $\gamma p \to \pi^0 p$ is shown in Figs. 3 and 4 from threshold up to 2350 MeV. Due to the inclusion of isospin breaking as explained in Sec. (II C), we achieve a satisfactory description of the data even at energies close to threshold. At very high energies ($E > 2$ GeV) and backward angles, the agreement between data and fit is good, while the fit does not reproduce the forward peak at extreme angles (c.f. Fig. 2). As explained in the previous section, those data points were excluded from the fits (shaded areas in the figures) because the current approach is limited to partial waves with a total angular momentum of $J \leq 9/2$. Higher partial waves would be needed to describe this aspect of the data distribution. The region of forward angles at high energies is then also the only place where differences between fit 1 and fit 2 show up.

By contrast, in case of the differential cross section for $\gamma p \to \pi^+ n$, shown in Figs. 5 and 6, small differences between fit 1 and fit 2 are visible at very low energies $E \leq 1130$ MeV. Small deviations from data, as can be seen, e.g., at $E = 1131$ or 1240 MeV, are due to inconsistencies among the different data sets.

The beam asymmetry Σ is presented in Fig. 7 for the reaction $\gamma p \to \pi^0 p$ and in Fig. 9 for the $\pi^+ n$ final state. In Figs. 8 and 10 results for the new CLAS data [118] on Σ can be found. These data were not included in fit 1 but only in fit 2. At higher energies $E \geq 1970$ MeV (Fig. 8), fit 2 is clearly better than the prediction of fit 1. The medium-energy regime is predicted/described equally well in both fits. For $\gamma p \to \pi^+ n$ (Fig. 10), on the other hand, the influence of the new CLAS data is visible at medium energies $E \sim 1700$ MeV. Here, the description of the forward and backward angles in fit 2 is improved compared to the prediction of fit 1. The same applies to higher energies. Overall, the new CLAS data have a major impact.

The results of the fits to the target asymmetry T can be found in Figs. 11 and 12. Compared to differential cross sections and beam asymmetries, much less data is available for this observable. Although this reduces the influence in the χ^2 minimization, the agreement of fit and data distribution is good, especially at high energies. Differences between fits 1 and 2 show up predominantly at high energies and in $\gamma p \to \pi^+ n$.

For the recoil polarization P (see Figs. 13 and 14), the data situation is similar to the one of the target asymmetry. For the reaction $\gamma p \to \pi^0 p$, contradicting data sets complicate the task of describing this observable as visible, e.g., at $E = 1602$ MeV in Fig. 13. In regions, where the data is without ambiguity, we achieve a nice description in both fits. At backward angles and higher energies, fit 1 and 2 differ from each other, in $\pi^+ n$ more than in $\pi^0 p$. Additional data could resolve the ambiguity.

In Figs. 15 to 17, we display the results for the double polarization observable G. This observable was excluded from fit 1. As Figs. 15 and 17 show, differences between fit 1 and 2 become larger at higher energies and backward angles, where no data are available. The recent high-precision measurement from CB/ELSA-TAPS [222] is presented in Fig. 16. At medium energies, the new CB-ELSA/TAPS data cover almost the whole angular range and the inclusion of G data in fit 2 has a noticeable impact. In case of $\gamma p \to \pi^+ n$, distinguishable differences between the predictions of fit 1 and the results of fit 2 are confined to angles $60° < \theta < 90°$. Note that, compared to $d\sigma/d\Omega$ or Σ, the number of data points available for this observable is very small for both reactions. It is, thus, not possible to improve the fit if one wants to maintain the same weight for all data points (see, e.g. the set at $E = 1910$ MeV in Fig. 17).

Similar considerations apply to the data on the double polarization H in Figs. 18 and 19, that is only included in fit 2. In any case, the agreement between fit and data is acceptable. Again, fit 1 and 2 differ most evidently at backward angles and high energies in $\pi^0 p$.

The inclusion of the data for the helicity cross-section difference $\Delta\sigma_{31}$ which is related to the helicity asymmetry E (cf. Eq.(B23)) for $\gamma p \to \pi^0 p$ (Fig. 20) in fit 2, results in a major improvement at energies $E > 1415$ MeV compared to the prediction of fit 1. This is not the case for $\gamma p \to \pi^+ n$ as can be seen in Fig. 21. Here, the prediction of fit 1 is good and fit 2 shows only minor improvements.

In Figs. 22 and 23, we present predictions for the double polarization observables E and F. At low energies, the results from fit 1 and 2 are quite similar. With increasing energy, the deviation between the two fits becomes larger, which is an indication for the sensitivity of these observables to small variations of the amplitude. Very recently, data on the double polarization observable E for $\gamma p \to \pi^0 p$ became available from the CBELSA/TAPS collaboration [230]. Those data, which were neither included in fit 1 nor in fit 2, are shown in Fig. 24 together with our predictions. As said above E is related to $\Delta\sigma_{31}$, and low-energy data on the latter observable are included in fit 2. This explains why the results for that fit are somewhat better than those for fit 1, at least at lower energies. The evident discrepancies at high energies suggest that the inclusion of the CBELSA/TAPS data [230] in a future fit will certainly yield a modification of the amplitudes and, therefore, have an impact on the resulting resonance parameters. Results for this observable from measurements at JLab are expected soon, as well. In Fig. 25 the total cross section from Ref. [231] and the angle-integrated helicity cross-section difference, $\Delta\sigma = \sigma_{3/2} - \sigma_{1/2}$, from Ref. [230] are shown. As expected from the good description of the unpolarized differential cross section by both fits 1 and 2, the total cross section σ and our results are in excellent agreement. In contrast, the predictions for $\Delta\sigma$ deviate

8

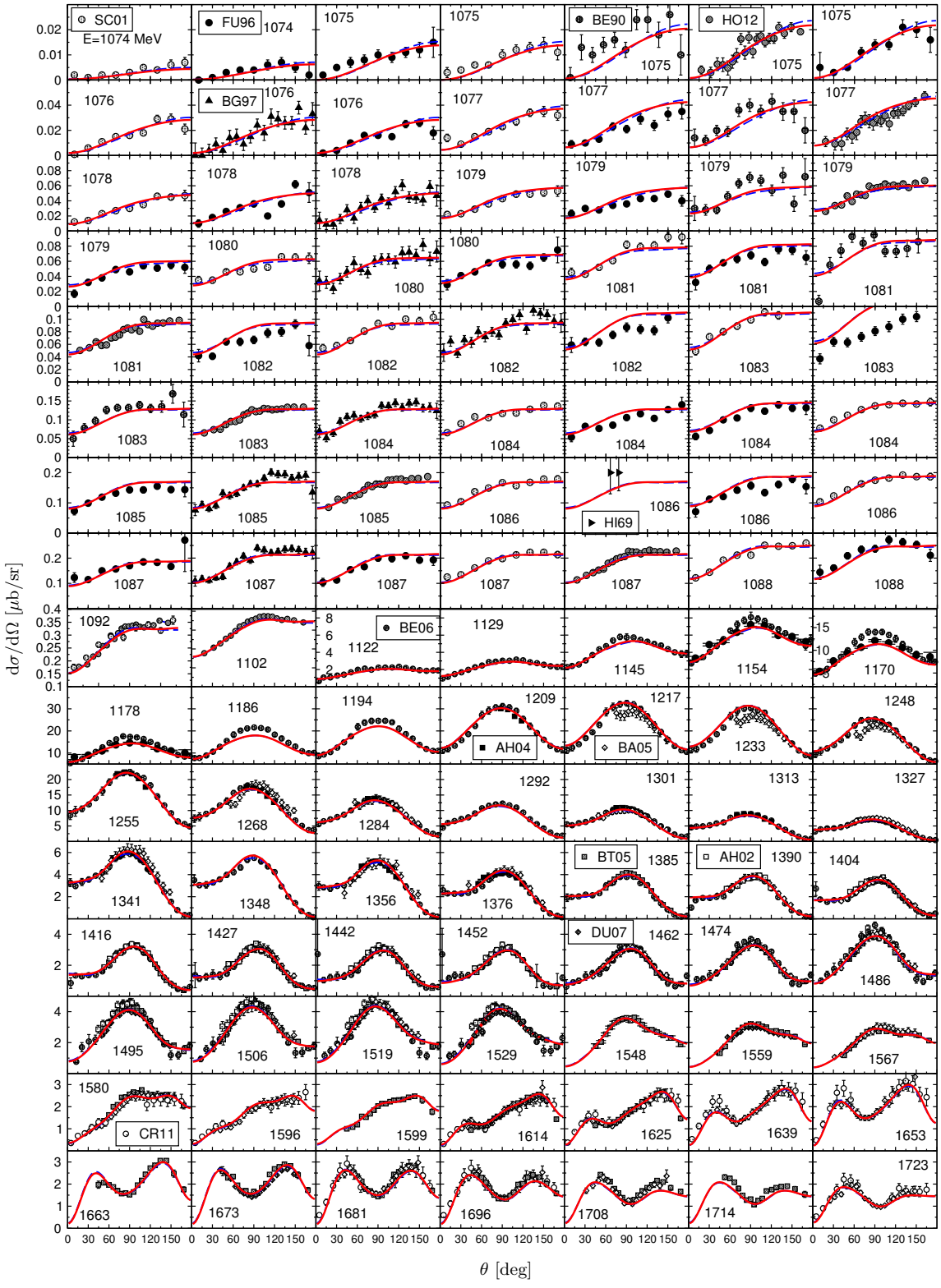

FIG. 3: Differential cross section of the reaction $\gamma p \to \pi^0 p$. Dashed (blue) line: fit 1; solid (red) line: fit 2; data: SC01[135] (MAMI), FU96[136], BE90[137], HO12[138] (MAMI), BG97[139], HI69[140], BE06[141], AH04[142] (MAMI), BA05[126] (ELSA), BT05[143] (GRAAL), AH02[144] (MAMI), DU07[127] (JLab), CR11[120] (ELSA).

9

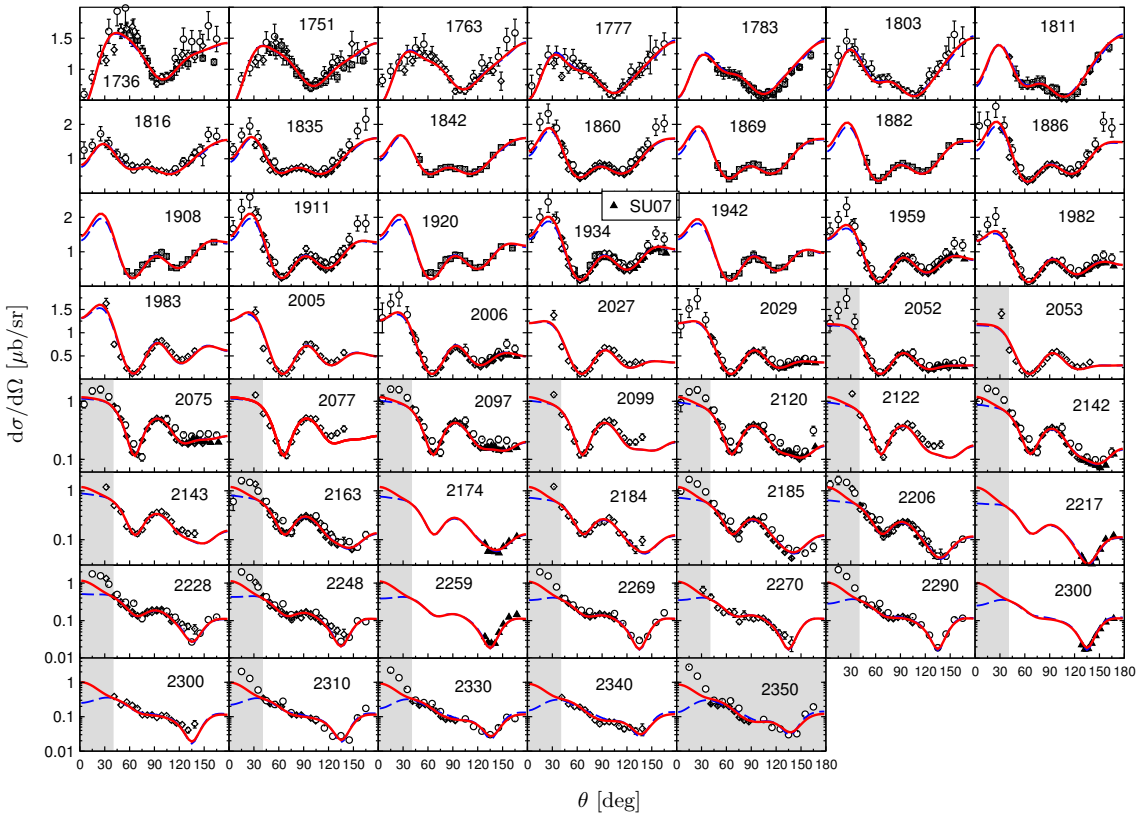

FIG. 4: Differential cross section of the reaction $\gamma p \to \pi^0 p$. Dashed (blue) line: fit 1; solid (red) line: fit 2; grey background: data points excluded from the fit; data: c.f. Fig. 3 and SU07[145] (SPring-8/LEPS).

at lower energies and reflect the differences in the predictions for E. Here, fit 2 gives a much better result, while at higher energies, fit 1 is slightly better. The peak at $E \sim 1700$ MeV is well described by both fits. The broad structure at $E \sim 1900$ MeV, however, is underestimated by both fits.

Predictions of the beam-recoil polarizations $C_{x'_L}$ and $C_{z'_L}$ can be found in Figs. 26 and 27 along with recent data from MAMI [232] and JLab [218], and an earlier measurement, also from JLab [217]. Calculations of these observables have been made, e.g., within a quark model [233] or perturbative QCD [234]. Fit 1 and 2 give similar results for $C_{x'_L}$, which are also, overall, in fair agreement with the data. For certain details in the data distribution improvements could be achieved by including the data in the fit. The predictions are averaged over the indicated angular bin for the MAMI measurement. For the JLab measurement, however, the observable has been evaluated at the exact angle without averaging, displayed in the plots with thin (red) lines. We observe a strong angular dependence for angles $\theta > 110°$ and at high energies. With regard to $C_{z'_L}$, fit 1 and 2 show larger deviations than for $C_{x'_L}$, especially at higher energies. In this case fit 1 seems to be slightly better. Here, the results were not angle-averaged. The rather large difference in the results of fit 2 at $\theta = 135°$ and at $\theta = 143°$ (cf. the solid and the dash-dotted lines in Fig. 27) illustrates that $C_{z'_L}$ exhibits a strong angular dependence, as well.

In general, we observe that fit 1 quite well predicts the data, in particular the new CLAS data on Σ and the double polarization observables G, H, and $\Delta\sigma_{31}$. Still, at the quantitative level, those data have an impact on the resonance properties, once they are included in our fit, as discussed in Sec. III D. Similar effects can be expected from the inclusion of double polarizations, like E, or the polarization transfer $C_{x'_L}$ and $C_{z'_L}$ in future analyses. Although our predictions of those observables do not deviate strongly from data in most cases, a fit to those data will lead to a more precise determination of the resonance parameters.

10

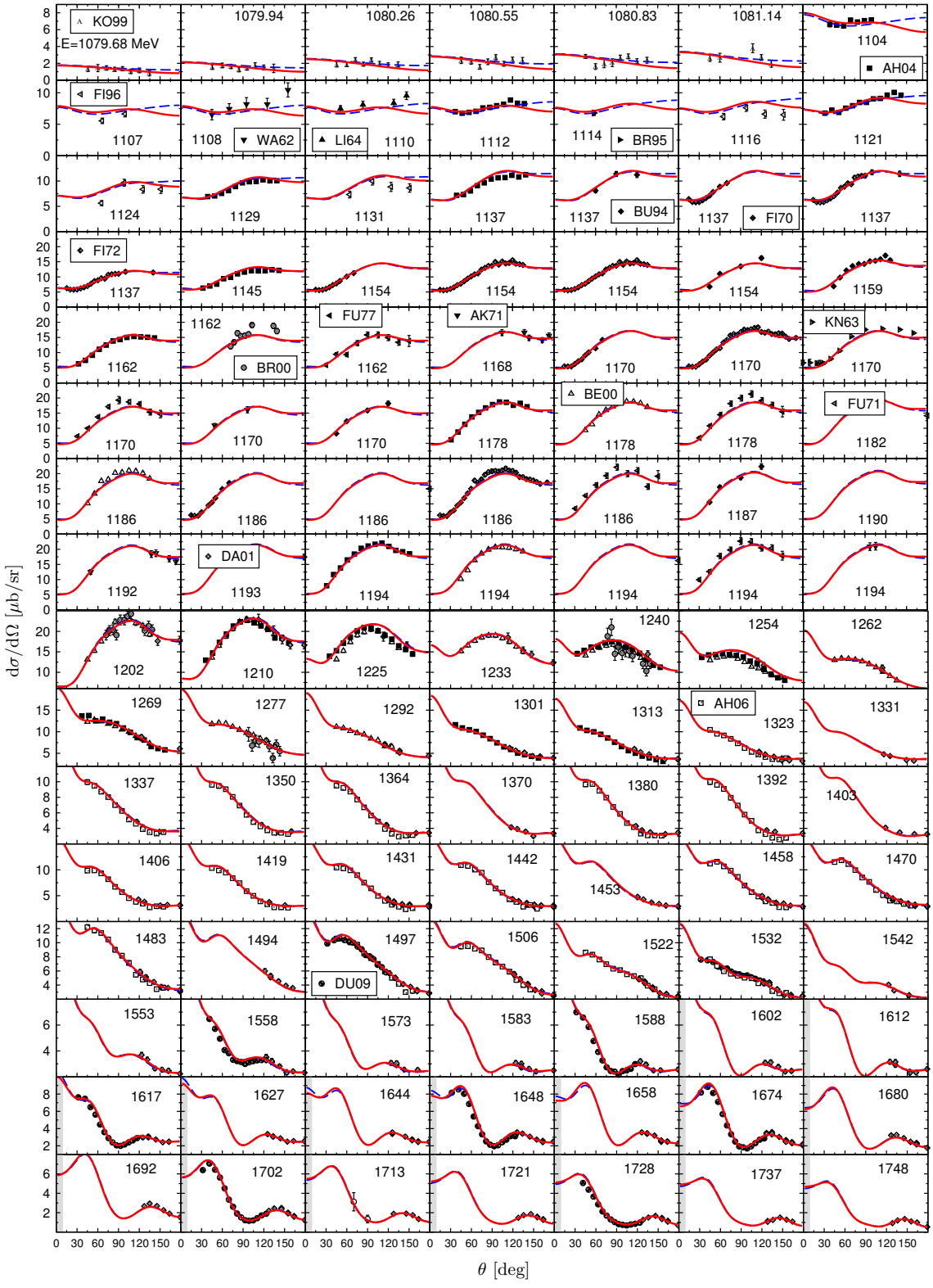

FIG. 5: Differential cross section of the reaction $\gamma p \to \pi^+ n$. Dashed (blue) line: fit 1; solid (red) line: fit 2; grey background: data points excluded from the fit; data: KO99[146], AH04[142] (MAMI), FI96[147], WA62[148], LI64[149], BR95[150], BU94[151], FI70[152], FI72[153], BR00[154] (MAMI), FU77[155], KN63[156], BE00[157] (MAMI), FU71[158], DA01[159], AH06[160] (MAMI), DU09[134] (JLab).

11

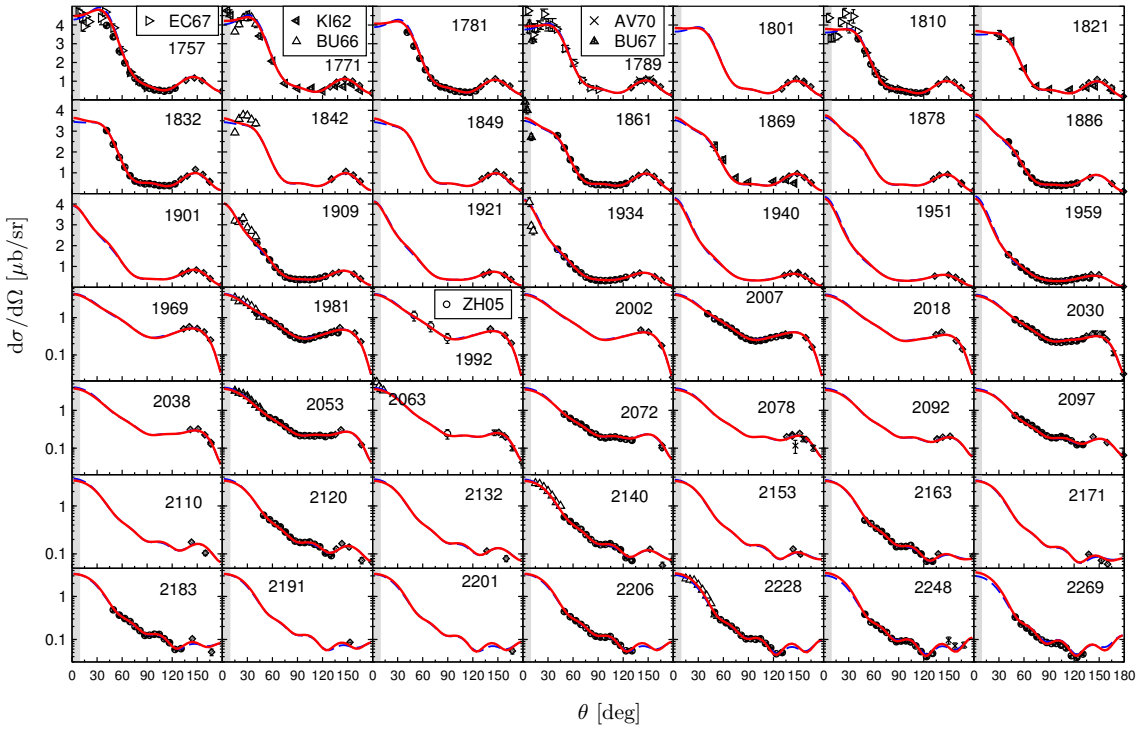

FIG. 6: Differential cross section of the reaction $\gamma p \to \pi^+ n$. Dashed (blue) line: fit 1; solid (red) line: fit 2; grey background: data points excluded from the fit; data: c.f. Fig. 5 and EC67 [161], BU66[132], KI62[162], AV70[163], BU66[132], ZH05[164] (JLab).

12

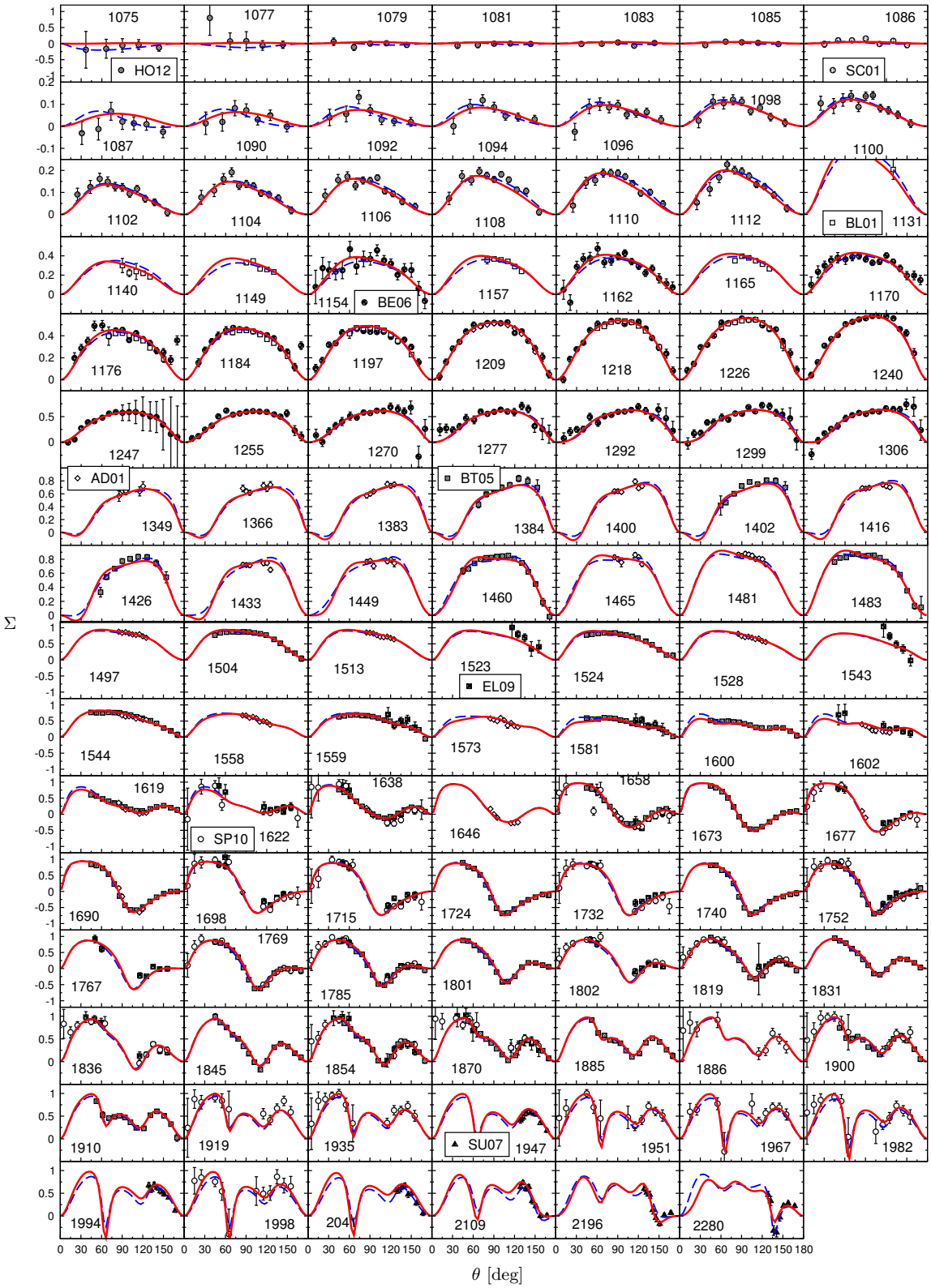

FIG. 7: Beam asymmetry of the reaction $\gamma p \to \pi^0 p$. Dashed (blue) line: fit 1; solid (red) line: fit 2; data: HO12[138] (MAMI), SC01[135], BL01[165] (LEGS), BE06[141] (MAMI), AD01[166], BT05[143] (GRAAL), EL09[167] (ELSA), SP10[168] (ELSA), SU07[145] (SPring-8/LEPS).

13

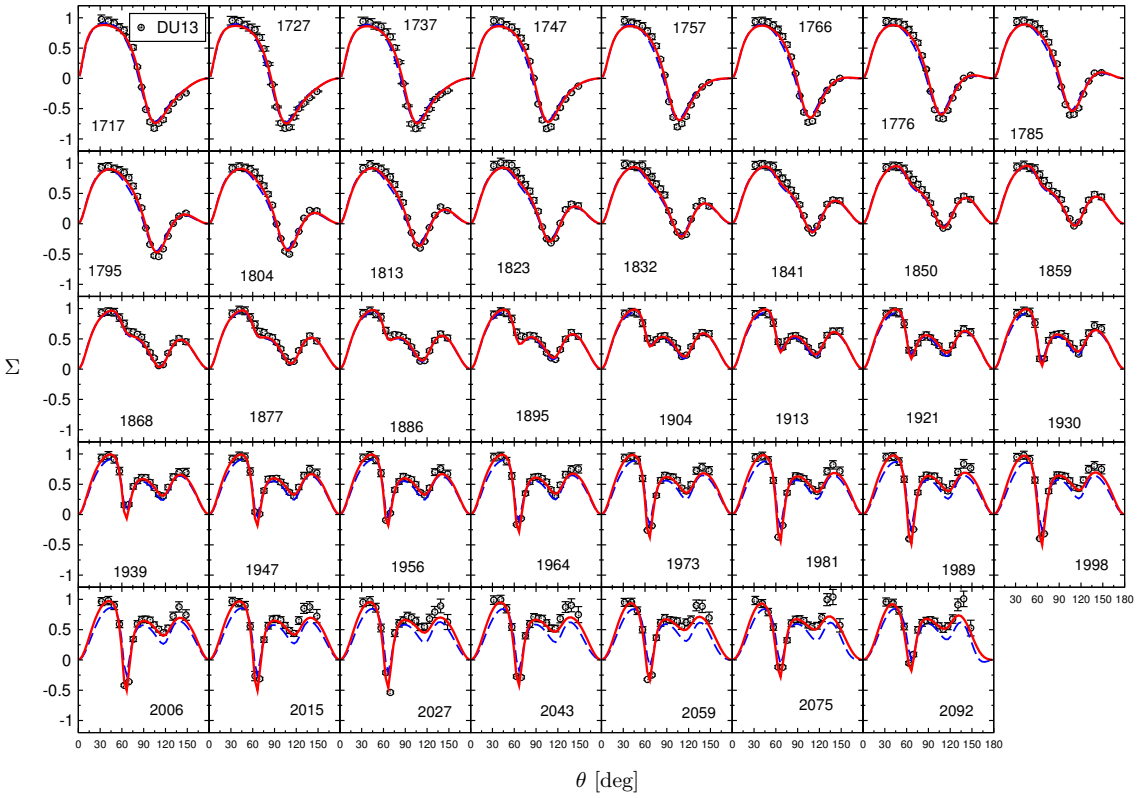

FIG. 8: Beam asymmetry of the reaction $\gamma p \to \pi^0 p$. Dashed (blue) line: fit 1 (prediction); solid (red) line: fit 2; data: DU13[118] (CLAS).

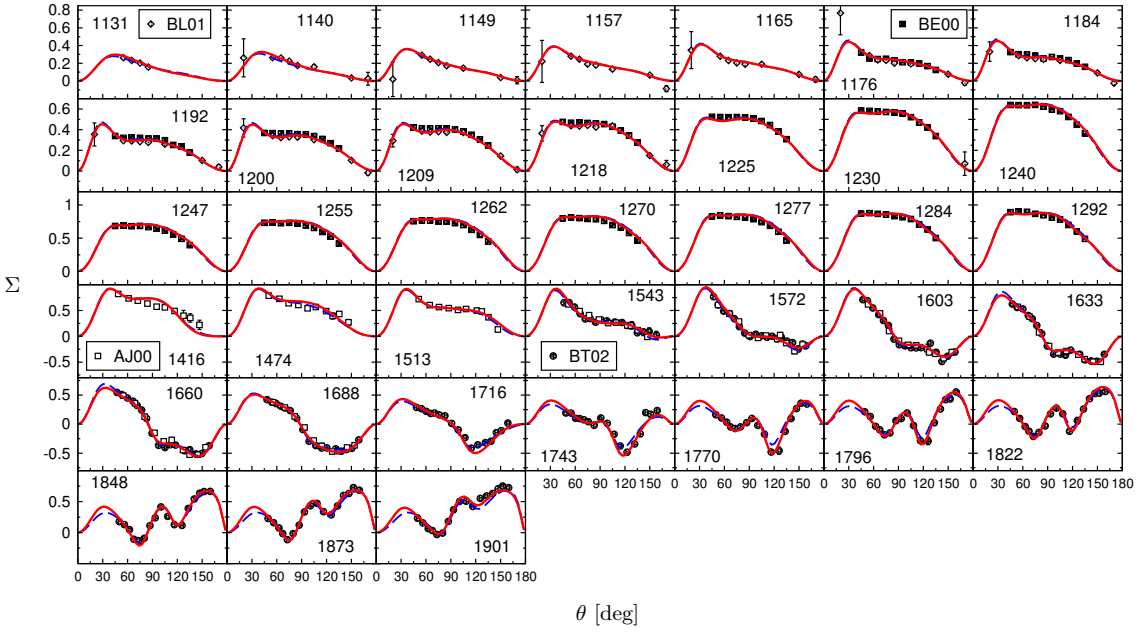

FIG. 9: Beam asymmetry of the reaction $\gamma p \to \pi^+ n$. Dashed (blue) line: fit 1; solid (red) line: fit 2; data: BL01[165] (LEGS), BE00[157] (MAMI), AJ00[169] (GRAAL), BT02[170] (GRAAL).

14

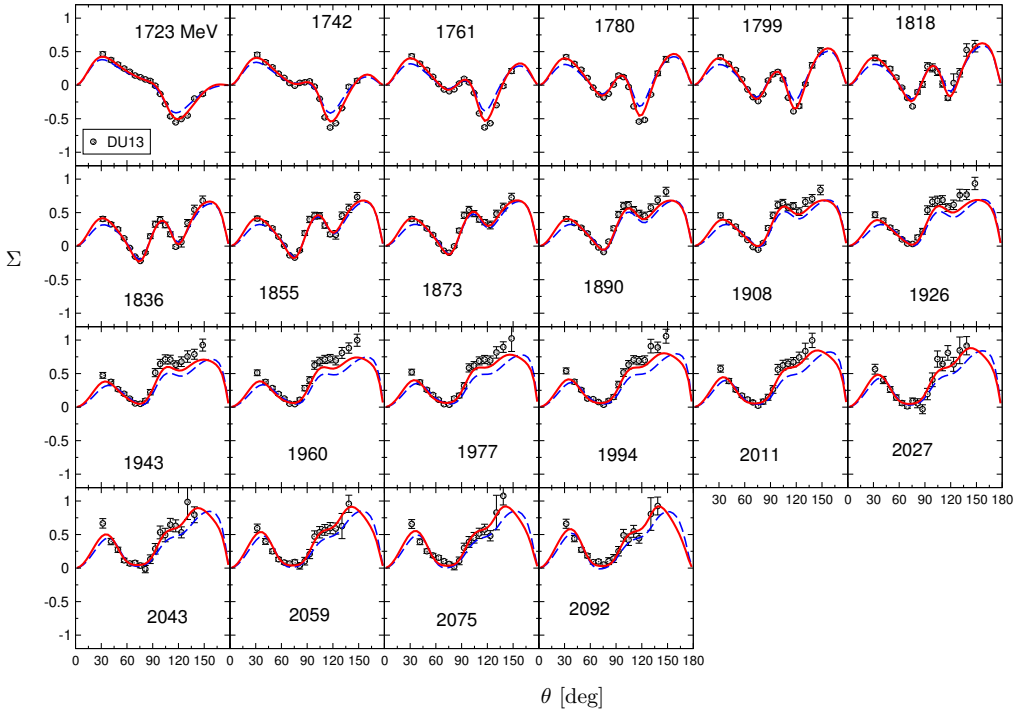

FIG. 10: Beam asymmetry of the reaction $\gamma p \to \pi^+ n$. Dashed (blue) line: fit 1 (prediction); solid (red) line: fit 2; data: DU13[118] (CLAS).

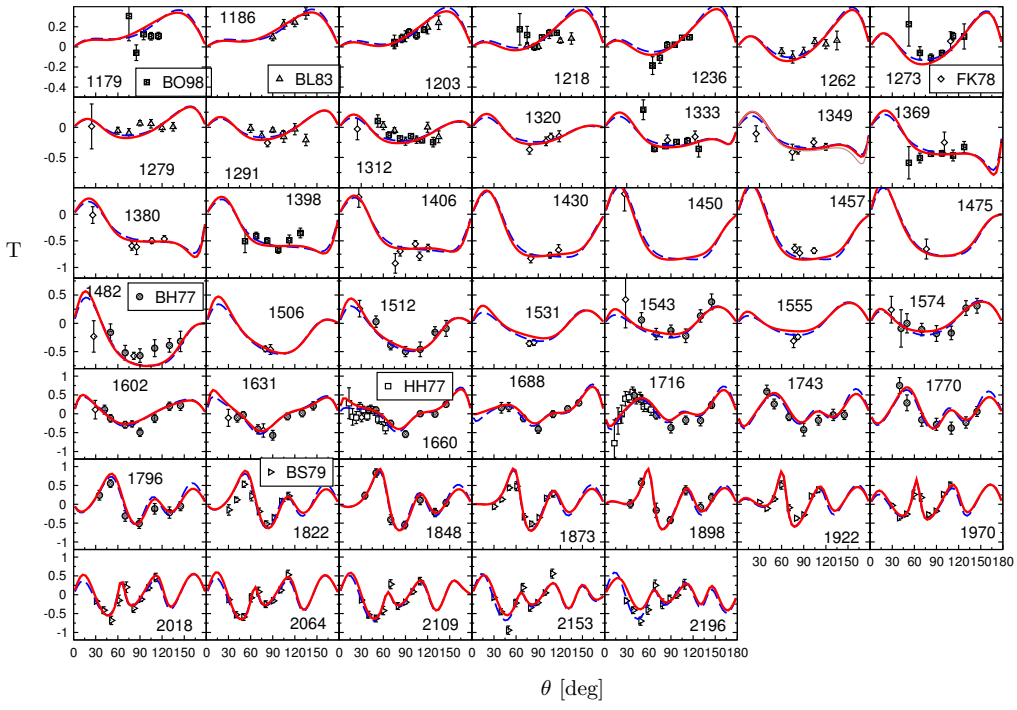

FIG. 11: Target asymmetry of the reaction $\gamma p \to \pi^0 p$. Dashed (blue) line: fit 1; solid (red) line: fit 2; data: BO98[171], BL83[172], FK78[173], BH77[174], HH77[175], BS79[176].

15

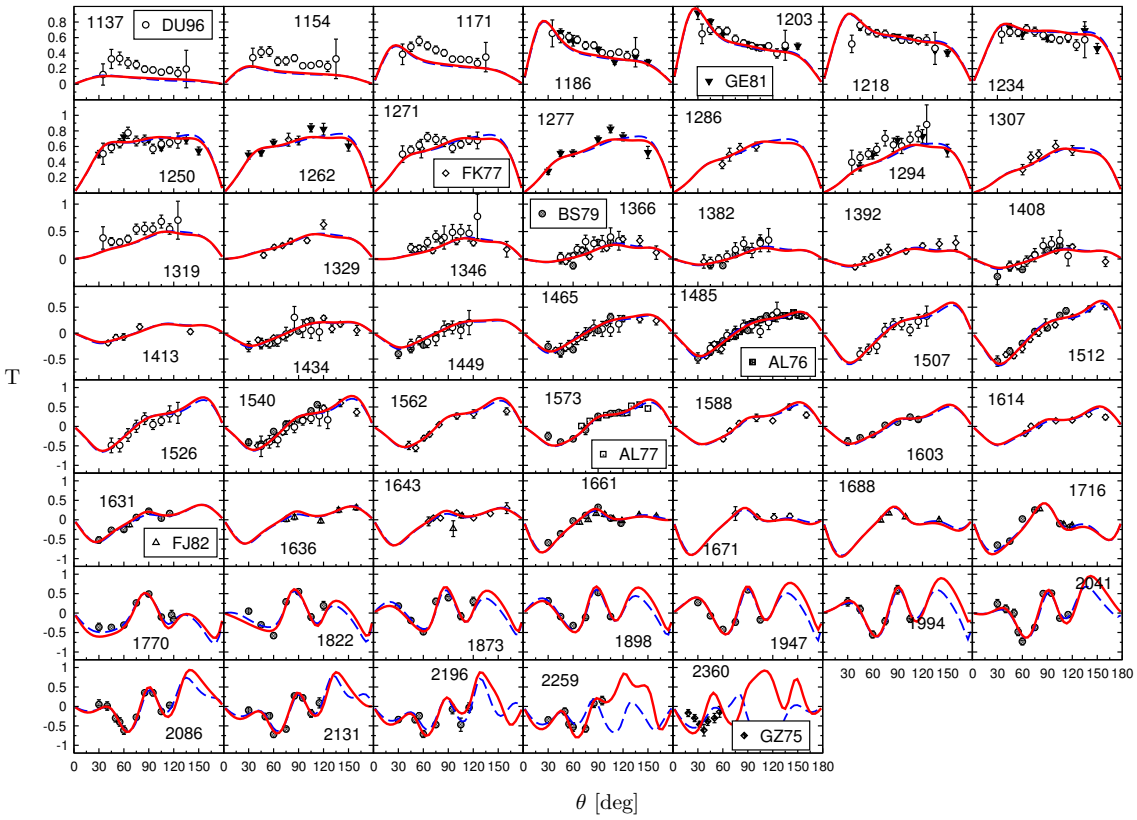

FIG. 12: Target asymmetry of the reaction $\gamma p \to \pi^+ n$. Dashed (blue) line: fit 1; solid (red) line: fit 2; data: DU96[177], GE81[178], FK77[179], BS79[180], AL76[181], AL77[182], FJ82[183].

16

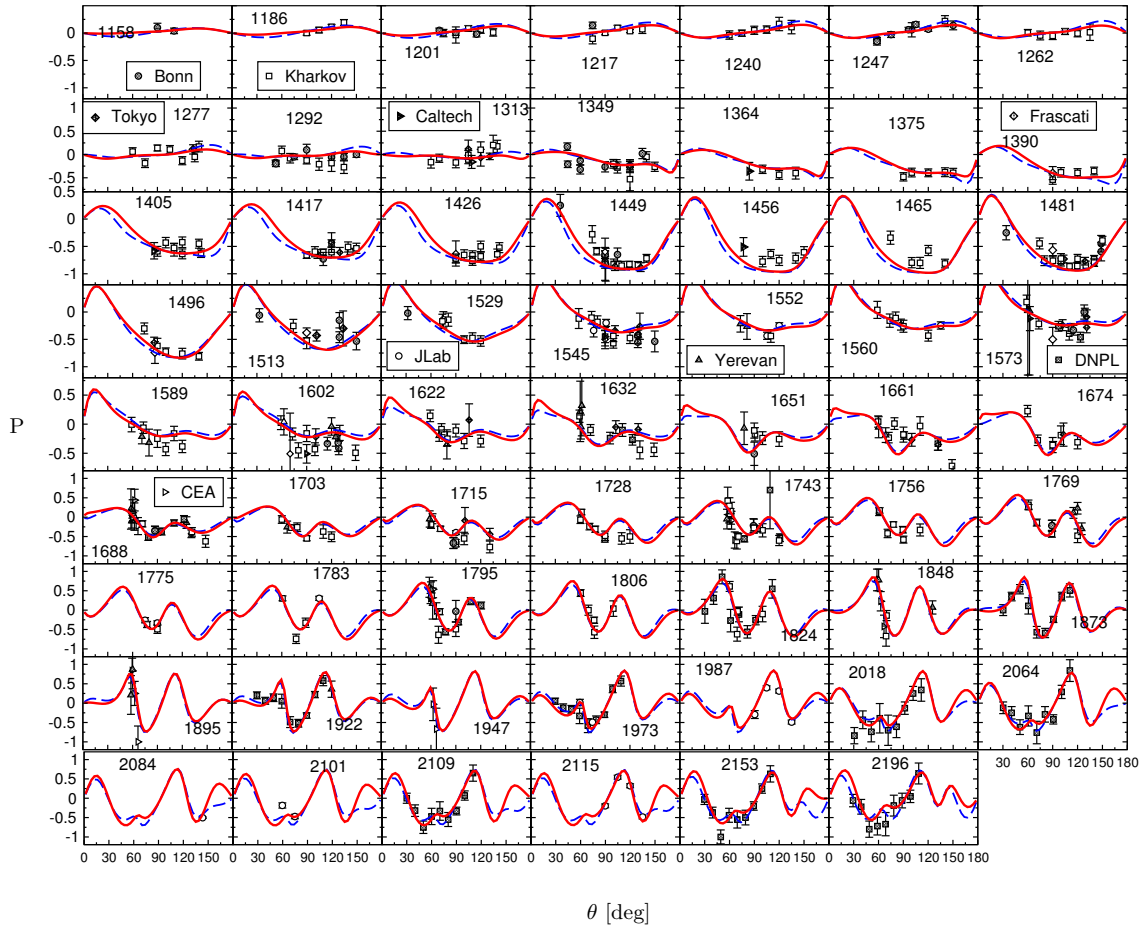

FIG. 13: Recoil polarization of the reaction $\gamma p \to \pi^0 p$. Dashed (blue) line: fit 1; solid (red) line: fit 2; data from Bonn [184–188], Kharkov [172, 189–203], Tokyo [204–206], Caltech [207, 208], Frascati [209, 210], Yerevan [211–216], JLab [217, 218], DNPL [176, 219], and CEA [220].

17

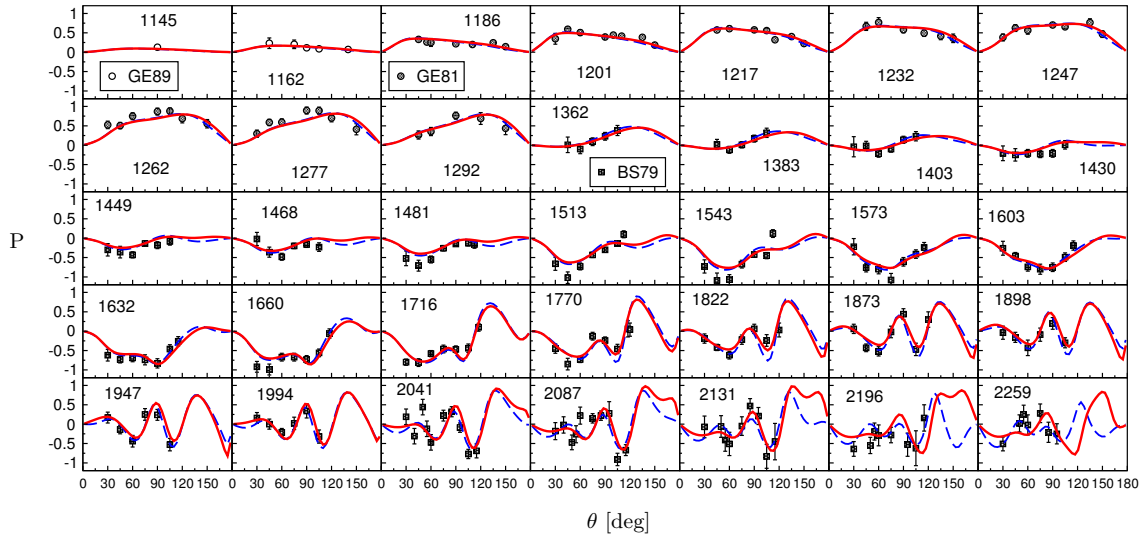

FIG. 14: Recoil polarization of the reaction $\gamma p \to \pi^+ n$. Dashed (blue) line: fit 1; solid (red) line: fit 2; data: GE81[178], GE89 [221], BS79[180].

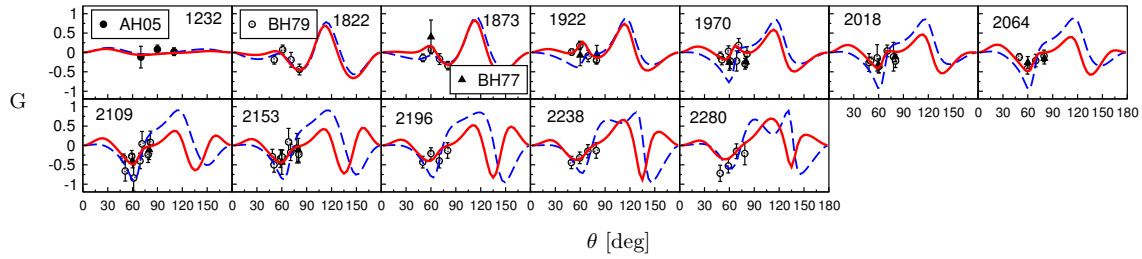

FIG. 15: Double polarization G of the reaction $\gamma p \to \pi^0 p$. Dashed (blue) line: prediction based on fit 1; solid (red) line: fit 2; data: AH05[223] (MAMI), BH79[224], BH77 [225].

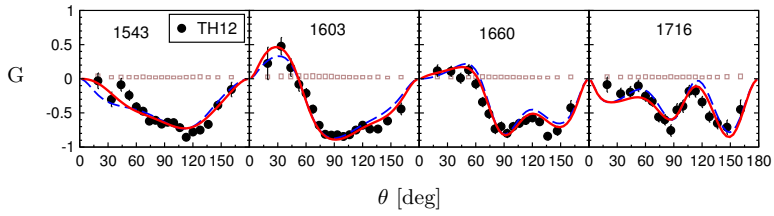

FIG. 16: Double polarization G of the reaction $\gamma p \to \pi^0 p$. Dashed (blue) line: prediction based on fit 1; solid (red) line: fit 2; data: TH12[222] (ELSA). Systematic errors are separately shown as brown bars.

18

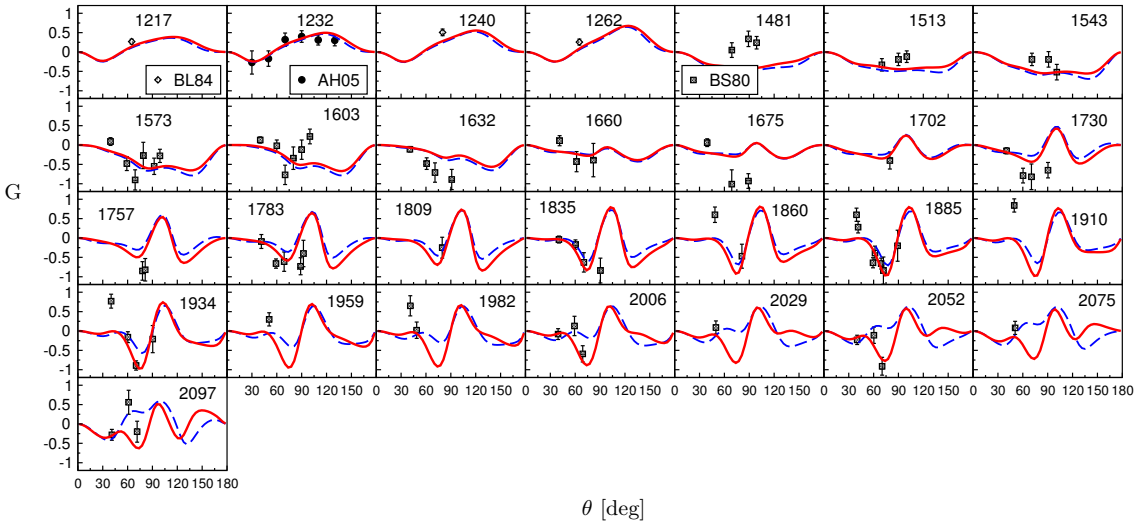

FIG. 17: Double polarization G of the reaction $\gamma p \to \pi^+ n$. Dashed (blue) line: prediction based on fit 1; solid (red) line: fit 2; data: BL84[226], AH05[223] (MAMI), BS80[227].

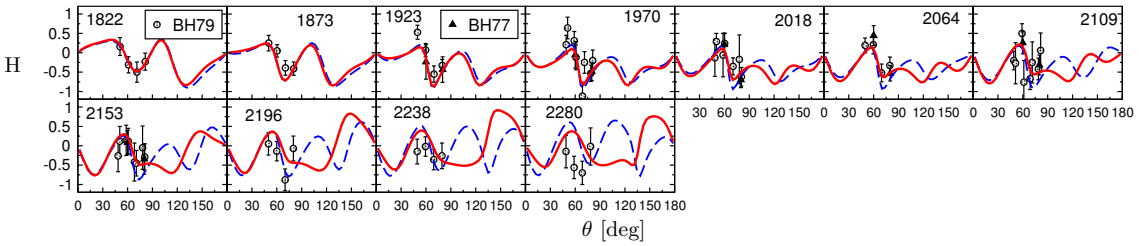

FIG. 18: Double polarization H of the reaction $\gamma p \to \pi^0 p$. Dashed (blue) line: prediction based on fit 1; solid (red) line: fit 2; data: BH77 [225], BH79[224].

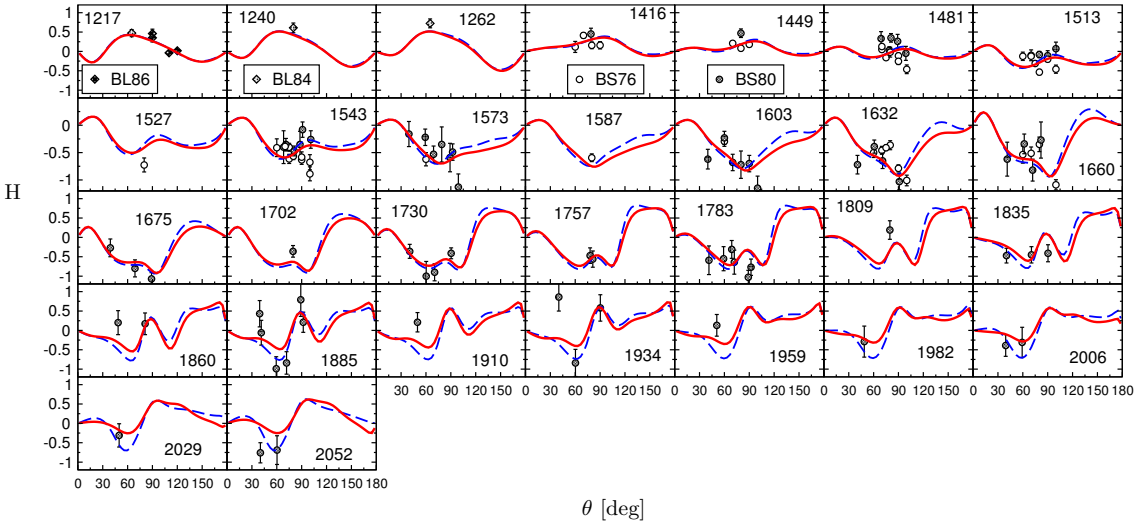

FIG. 19: Double polarization H of the reaction $\gamma p \to \pi^+ n$. Dashed (blue) line: prediction based on fit 1; solid (red) line: fit 2; data: BL86[228], BL84[226], BS76 [229], BS80[227].

19

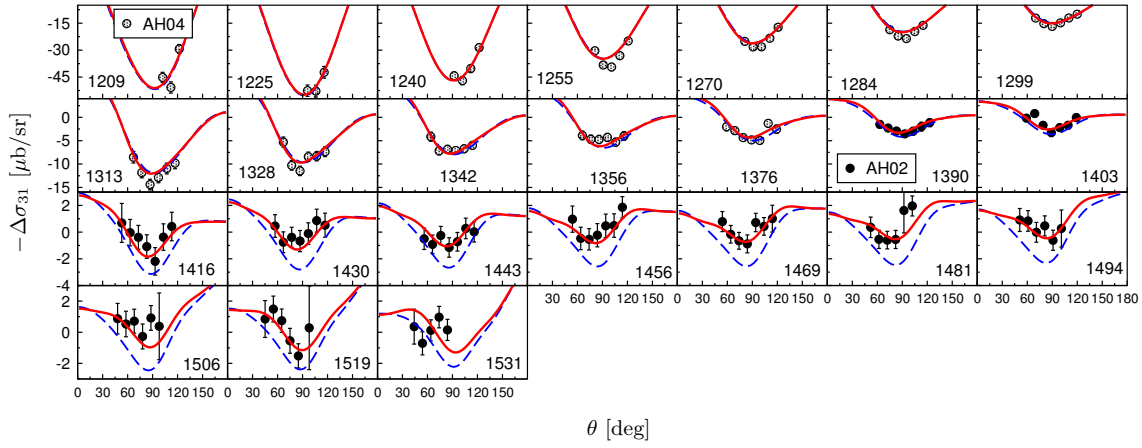

FIG. 20: $\Delta\sigma_{31}$ of the reaction $\gamma p \to \pi^0 p$. Dashed (blue) line: prediction based on fit 1; solid (red) line: fit 2; data: AH04[142], AH02[144] (MAMI) (MAMI).

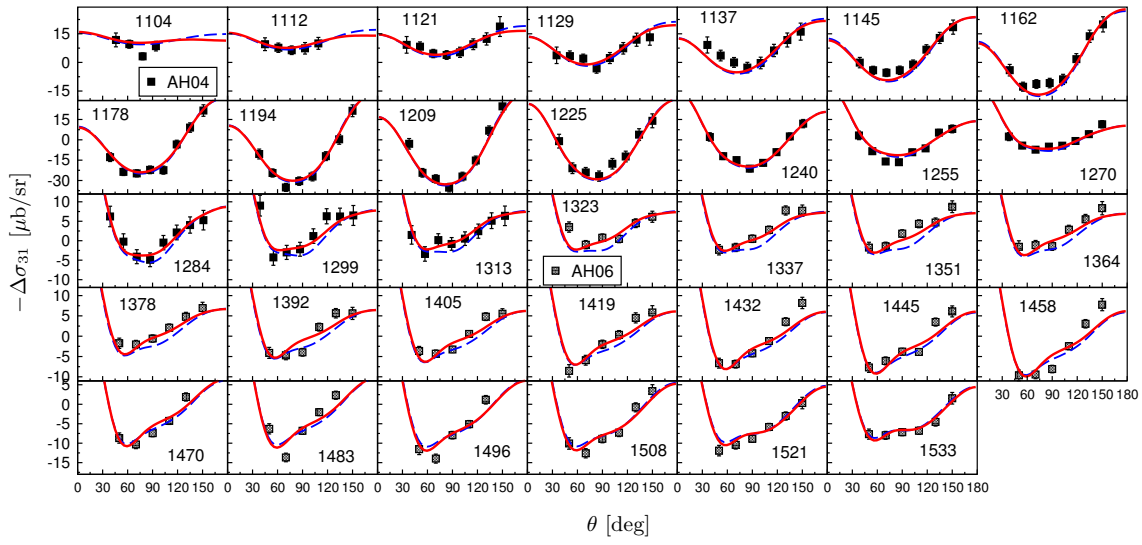

FIG. 21: $\Delta\sigma_{31}$ of the reaction $\gamma p \to \pi^+ n$. Dashed (blue) line: prediction based on fit 1; solid (red) line: fit 2; data: AH04[142] (MAMI), AH06[160] (MAMI).

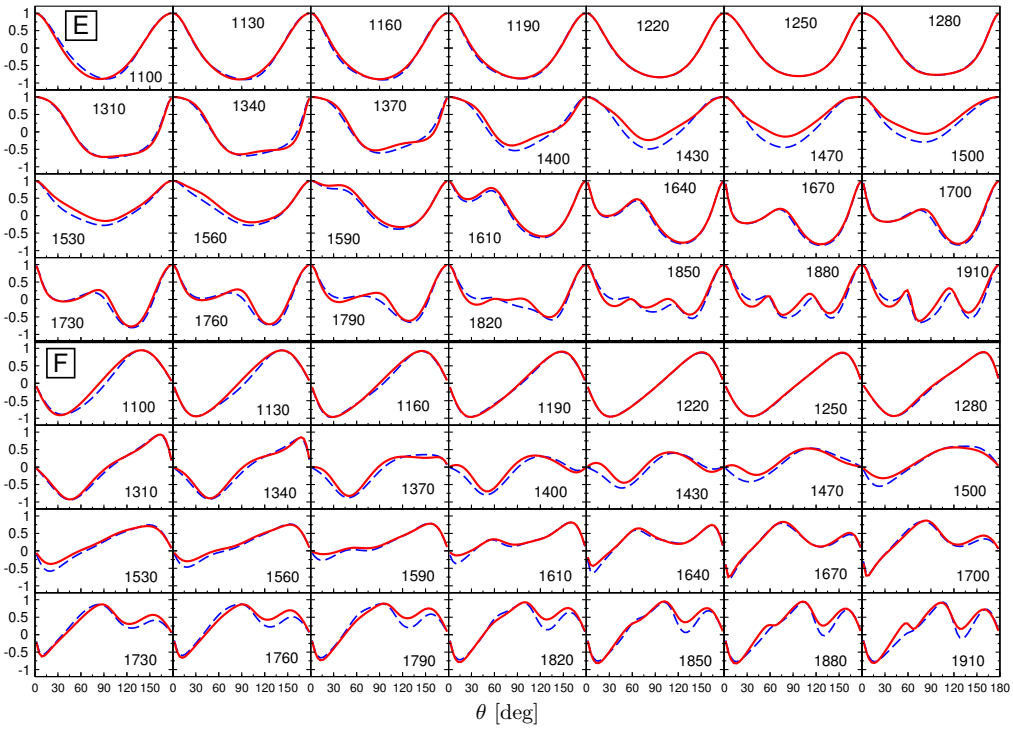

FIG. 22: Double polarizations E (upper 4 rows) and F (lower 4 rows) of the reaction $\gamma p \to \pi^0 p$. Dashed (blue) line: prediction based on fit 1; solid (red) line: prediction based on fit 2.

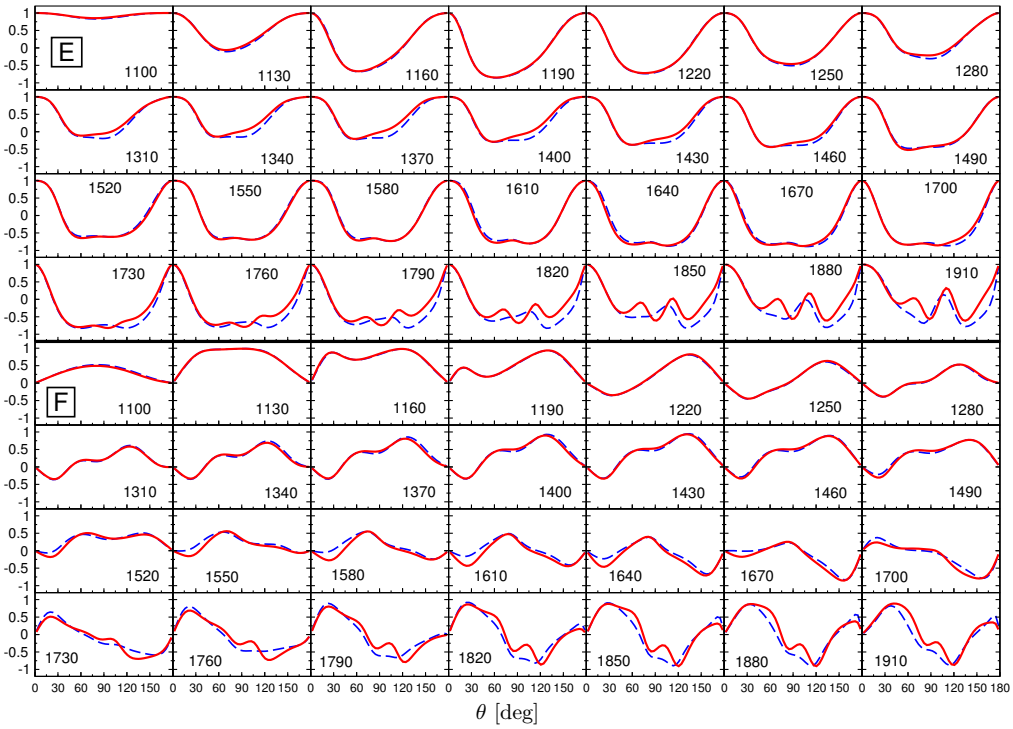

FIG. 23: Double polarizations E (upper 4 rows) and F (lower 4 rows) of the reaction $\gamma p \to \pi^+ n$. Dashed (blue) line: prediction based on fit 1; solid (red) line: prediction based on fit 2.

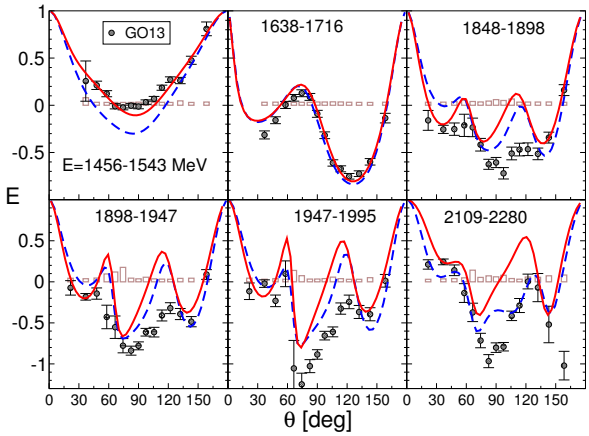

FIG. 24: Double polarization E of the reaction $\gamma p \to \pi^0 p$. Dashed (blue) line: prediction based on fit 1; solid (red) line: prediction based on fit 2; data: GO13 [230] (ELSA). Systematic errors are separately shown as brown bars.

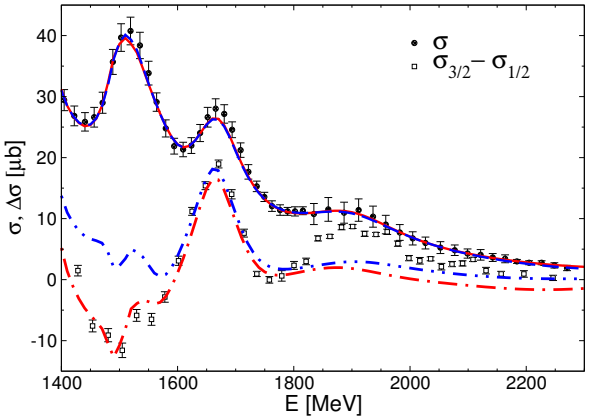

FIG. 25: Total cross section σ and the cross-section difference $\Delta\sigma = \sigma_{3/2} - \sigma_{1/2}$ of the reaction $\gamma p \to \pi^0 p$. Dashed and dash-dot-dotted (blue) line: prediction based on fit 1; solid and dash-dotted (red) line: prediction based on fit 2; data: σ [231], $\Delta\sigma$ [230] (ELSA).

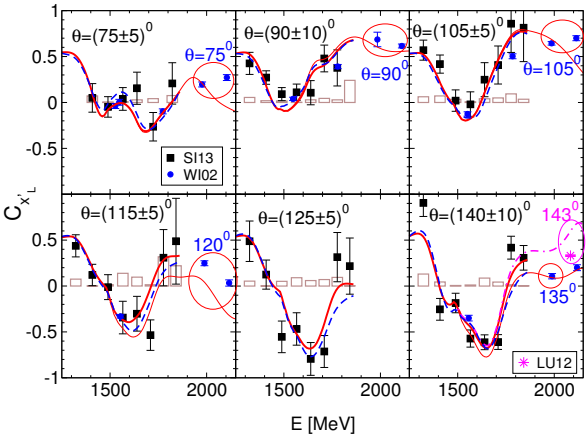

FIG. 26: Polarization transfer $C_{x'_L}$ of the reaction $\gamma p \to \pi^0 p$. Note that this observable is defined with respect to the lab frame but shown for different values of the c.m. scattering angle θ. Dashed (blue) lines: prediction based on fit 1; solid thick (red) lines: prediction based on fit 2. For both fits, the predictions are angle-averaged as indicated, corresponding to the MAMI angular bins (black squares, SI13 [232]). The thin red lines show the predictions of fit 2 for the JLab 2002 measurements (blue circles, WI02 [217]). The magenta line shows the prediction of fit 2 at $\theta = 143°$ of the JLab 2012 data point (magenta star, LU12 [218]). Note that the JLab data WI02 [217] are shown here with a reversed sign due to different conventions (cf. Appendix B). Systematic errors of the MAMI data SI13 [232] are separately shown as brown bars.

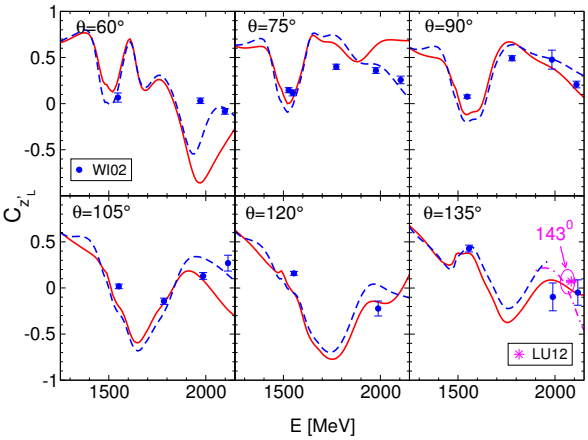

FIG. 27: Polarization transfer $C_{z'_L}$ of the reaction $\gamma p \to \pi^0 p$. Note that this observable is defined with respect to the lab frame but shown for different values of the c.m. scattering angle θ. Dashed (blue) lines: prediction based on fit 1; solid (red) lines: prediction based on fit 2. Both curves show the prediction for the JLab 2002 data (blue circles, WI02 [217]). The magenta line shows the prediction of fit 2 at $\theta = 143°$ of the JLab 2012 data point (magenta star, LU12 [218]).

C. Multipoles

In Figs. 28 and 29, we show our results for the isospin $I = 1/2$ and $3/2$ multipoles together with those of the GWU/SAID CM12 analysis [3]. Single-energy solutions of the latter are available for the lower partial waves. For lower multipoles our solution is similar to the CM12 solution. The most striking example is the dominant $M_{1+}(3/2)$ multipole. In the electric P_{33} multipole $E_{1+}(3/2)$, however, we observe a structure around 1.65 GeV in both fits that does not show up in the SAID analysis. This structure has its origin in the $\Delta(1600)$ $3/2^+$, a resonance which is dynamically generated in the Jülich2012 coupled-channels model [79]. Since this resonance couples predominantly to the $\pi\Delta$ channel, no effect of it was seen in the elastic πN P_{33} partial wave, as discussed in the analysis of Ref. [79] where only hadronic channels were considered. However, the $\gamma N \to \pi\Delta$ transition is large, making the resonance structure visible in photoproduction. Preliminary results of a new parameterization of the MAID approach suggest a similar structure [235]. In case of the electric and magnetic D_{15} multipoles $E_{2+}(1/2)$ and $M_{2+}(1/2)$ the solutions of fit 1 and 2 deviate at $E \sim$1.3 GeV in the real part of the amplitude. At such —comparably low— energies a full dynamical coupled-channels analysis would probably give a result, that is more constrained due to the explicit inclusion of Born terms that can account for a large part of the low-energy dynamics [97]. Further deviations from the SAID solution can be found, e.g., in $M_{1+}(1/2)$ or in $E_{2+}(3/2)$ and $M_{2+}(3/2)$. Here, fit 1 and 2 also give different results. Note that the relatively sharp spike in the real part of the $M_{1+}(1/2)$ multipole is an artifact of the isospin-symmetric representation of the multipoles in the plot. The physical P-waves are all smooth and well-behaved close to the thresholds, as Fig. 31 demonstrates.

The higher multipoles starting with E_{3+} are less well determined. With the exception of $M_{3+}(3/2)$, larger deviations between our fits on the one hand and between our fits and the SAID solution on the other hand can be observed, as well as a strong energy dependence. The scale, especially for the imaginary parts, is much smaller than the scale of the lower multipoles, though.

The threshold region of the $E_{0+}(\pi^0 p)$ multipole in the particle basis is presented in Fig. 30. Note that we only adjust to experimental observables and not to any of the extracted points from analyses shown in the figure (the same applies to Fig. 31). Due to its smallness, the $E_{0+}(\pi^0 p)$ multipole enables very sensitive tests of the photoproduction amplitude and has been addressed in several experimental and theoretical analyses. Precise experimental data are available from MAMI [138], for earlier measurements see Refs. [135, 139]. Within the framework of chiral perturbation theory, $E_{0+}(\pi^0 p)$ close to threshold has been calculated in the fundamental works of Refs. [21–27, 236]. More recent ChPT calculations can be found in Ref. [32–34]. The role of D-waves has been discussed in Refs. [35, 53]. ChPT calculations including isospin breaking have been performed in Refs. [28–30] and relativistic chiral perturbation theory has been applied in Ref. [32]. The new ChiralMAID approach [33] includes also electroproduction of charged pions. ChPT in two-pion photoproduction has been pioneered in Refs. [24, 26] and nowadays ChPT calculations for photoproduction even on the tri-nucleon system have become possible [237].

Predictions of E_{0+} from a dispersion-relation calculation can be found in Ref. [238] and in Ref. [239] the threshold region has been described within a dynamical model for π^0 photo- and electroproduction.

As visible in Fig. 30, the opening of the $\pi^+ n$ channel produces a kink in the $\pi^0 p$ multipole amplitude. For the real part of E_{0+}, we note strong correlations between the value at the $\pi^+ n$ threshold and the slope: A small value in combination with a small slope (fit 1) leads to a very similar χ^2 as a rather large negative value and slope (fit 2), adjusting the higher multipoles at the same time, of course.

The imaginary part of E_{0+} in fit 2 is in good agreement with the high-precision determination of Refs. [28, 30] although it has to be stressed that in the latter works isospin breaking effects beyond those considered here are included. The small imaginary part below the $\pi^+ n$ threshold originates from a non-vanishing $\pi^0 p \to \pi^0 p$ transition, cf. Fig. 1. In this context let us mention that the isoscalar scattering length of the Jülich2012 model [79] which enters into this calculation is with $a^+_{0+} = -16.6 \cdot 10^{-3}\, M^{-1}_{\pi^+}$ very small, but it is still twice as large as the recent high-precision ChPT result [29] of $a^+_{0+} = (7.6 \pm 3.1) \cdot 10^{-3}\, M^{-1}_{\pi^+}$.

In Fig. 31, the P-wave combinations P_1 to P_3 are shown, divided by the π^0 c.m. momentum q. The P_i are defined as

$$\begin{aligned} P_1 &= 3E_{1+} + M_{1+} - M_{1-} \\ P_2 &= 3E_{1+} - M_{1+} + M_{1-} \\ P_3 &= 2M_{1+} + M_{1-}\,. \end{aligned} \tag{21}$$

The data points represent a single-energy analysis of the recent MAMI measurement performed in Ref. [138]. Part of the discrepancy between that analysis and our fits certainly comes from employing a different data base. For our analysis, in addition to the data of Ref. [138], we also use all data shown in Figs. 3 and 7.

Predictions of the P-wave slopes from low-energy theorems have been pioneered in Ref. [25] up to $\mathcal{O}(q^3)$ and in Ref. [240] up to $\mathcal{O}(q^4)$. The $\mathcal{O}(q^3)$ threshold prediction of Ref. [240] is shown in Fig. 31. For P_1, the prediction is in agreement with our fits. The deviation in P_2 is presumably due to too small errors of the experimental analysis. In principle one could fit the differences as LECs appear in P_1 and P_2 in the fourth order. For the reason just mentioned we refrain from fitting these LECs here.

One can use the value of P_3 from our fit 2, extrapolated to threshold ($P_3/q = 11.8 \cdot 10^{-3}/M^2_\pi$), to determine the

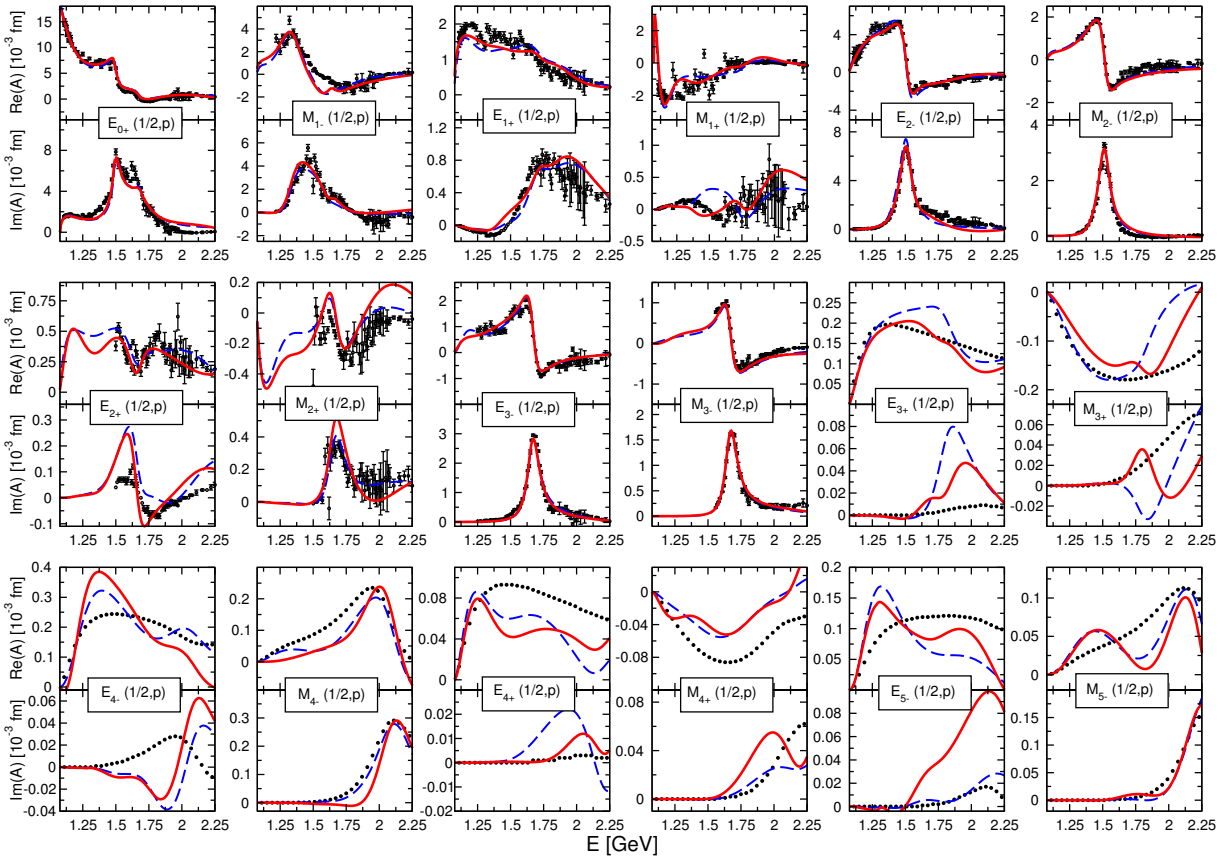

FIG. 28: Isospin $I = 1/2$ multipoles. Points: GWU/SAID CM12 solution [3] (single-energy solution for E_{0+} to M_{3-}, energy-dependent solution for E_{3+} to M_{5-}). Dashed (blue) line: fit 1; solid (red) line: fit 2.

counter term b_P [240]. We obtain $b_P = 14.5$ GeV^{-3} to order $\mathcal{O}(q^3)$ and $b_P = 18.0$ GeV^{-3} to order $\mathcal{O}(q^4)$. The latter value should be compared to the ones of the $\mathcal{O}(q^4)$ fits of Ref. [240] to older data: $b_P = 14.9$ GeV^{-3} (Schmidt *et al.* [135]) and $b_P = 13.0$ GeV^{-3} (Fuchs *et al.* [136]).

D. Photocouplings

The photocouplings $\tilde{A}^h_{pole}$ (cf. the definition in Appendix C) are complex quantities that specify the γN coupling to a resonance. They are well defined because they can be expressed in terms of pole positions and residues of pion photoproduction multipoles and elastic πN scattering amplitudes. The $\tilde{A}^h_{pole}$ play the same role as the complex hadronic couplings g at the pole discussed in Ref. [79]. In particular, residues of multipole amplitude $M_{\mu\gamma}$ have the same factorizing property as the residues of a multi-channel scattering amplitude and can be expressed as the product of the photocoupling $g_{\gamma N}$ and the resonance coupling to the final state πN, i.e. Res $M_{\pi N\,\gamma N} = g_{\pi N}\, g_{\gamma N}$. This means that the photocoupling at the pole is entirely independent of the final state of the studied photoproduction reaction.

Photocouplings at the pole are also the quantities to which, e.g., chiral unitary approaches to radiative baryon decays can compare [43, 241–244].

In contrast, the real-valued helicity amplitudes A^h traditionally quoted [245] depend on the parameterization of the amplitude used in a particular approach. As shown in Ref. [246], $\tilde{A}^h_{pole}$ becomes real only in case of a pure Breit-Wigner amplitude in the absence of background. In that case, $\tilde{A}^h_{pole} = A^h$ [246]. As a side remark, sometimes helicity amplitudes calculated in quark models, real by construction, are compared to the A^h quoted by the PDG [245]; in view of the unclear physical meaning of the A^h one should be very cautious when doing that kind of comparison.

In this context, note also that the bare, real couplings γ^c_γ in our parameterization of Eq. (9) do not have any physical meaning; in particular, they cannot have the meaning of helicity amplitudes of bare resonance states

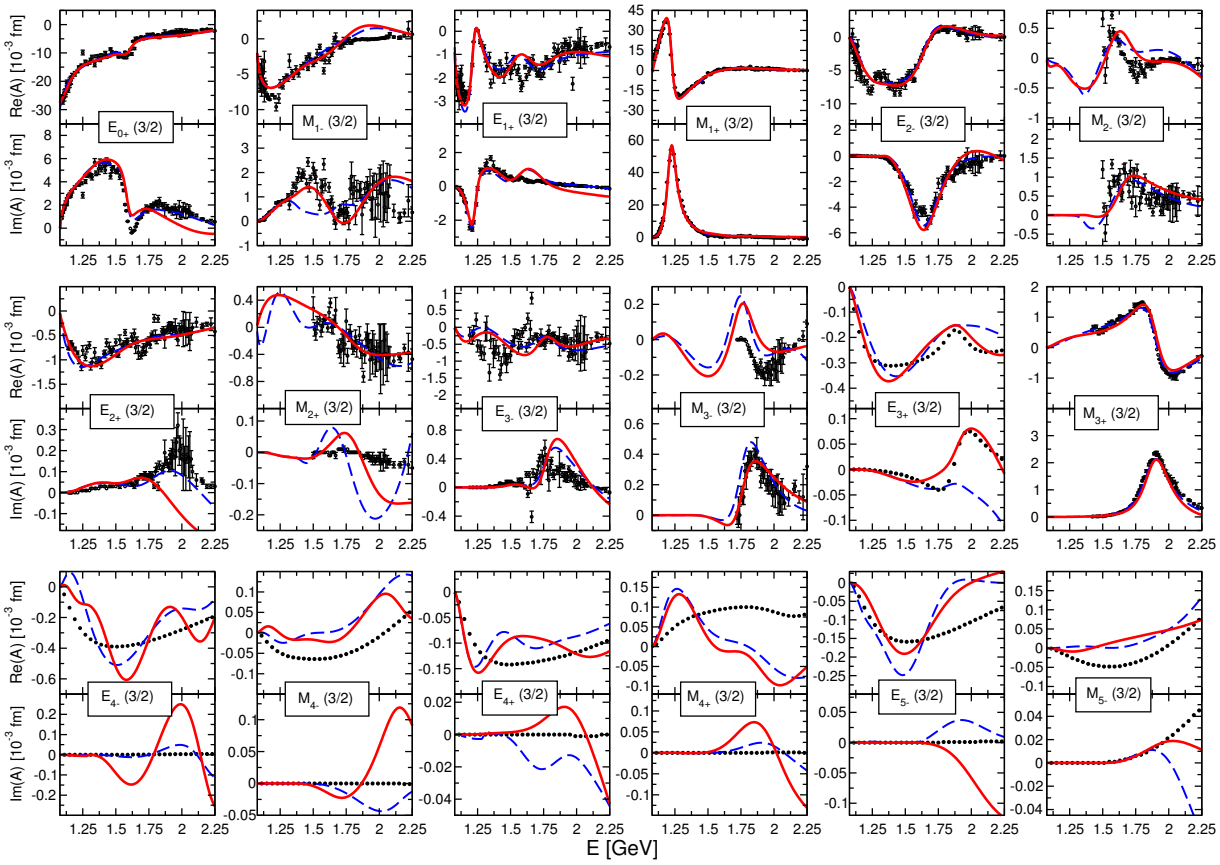

FIG. 29: Isospin $I = 3/2$ multipoles. Points: GWU/SAID CM12 solution [3] (single-energy solution for E_{0+} to M_{3-} and for M_{3+}, energy-dependent solution for E_{3+} and for E_{4-} to M_{5-}). Dashed (blue) line: fit 1; solid (red) line: fit 2.

as sometimes claimed in quark model calculations. The bare parameters γ_γ^c suffer from the same dependencies on the renormalization scheme and channel space as the bare hadronic couplings $\gamma_{\mu;i}$. See Sec. 4.5 and 4.6 of Ref. [79] for a comprehensive discussion of this issue.

In Tables II and III, we list the results for the photocouplings at the pole ($A^h_{pole} \in \mathbb{R}$),

$$\tilde{A}^h_{pole} = A^h_{pole} e^{i\vartheta^h} \tag{22}$$

of the isospin 1/2 and 3/2 resonances calculated in this study together with the pole positions extracted in the Jülich2012 analysis [79]. The analytic continuation is performed with the methods derived in Ref. [83]. Additionally, we compare our results to the ones of the Bonn-Gatchina group [55], the recent ANL-Osaka analysis [68] and parameters extracted [246] from an older version of the GWU/SAID multipole analysis [247, 248]. Our conventions for the photocouplings are identical to those of Ref. [246] and can be found in Appendix C.

In Tables II and III, the photocouplings are quoted for both fit 1 and fit 2. For prominent resonances such as the $N(1535)1/2^-$, the moduli of the photocoupling are similar in both fits, in contrast to some of the angles, that can differ by more than 20°. Angles are in general less well determined than the magnitude of photocouplings. For less prominent resonances, like the $N(1710)1/2^+$ or $\Delta(1930)5/2^+$, the modulus can change by up to a factor of two. This demonstrates that the recent data from ELSA, JLab, MAMI, Spring-8, and GRAAL, included in fit 2 but not in fit 1, have a major impact on the quantitative determination of resonance properties.

We find small to moderate angles ϑ^h for several resonances, among them the $\Delta(1232)3/2^-$, $N(1650)1/2^-$, $N(1440)1/2^+$, $N(1520)3/2^-$, in fair agreement with Ref. [246]. This has led to speculations [246] that the difference between the (real) A^h quoted in the Particle Data Book [245] and the photocouplings at the pole is possibly not large. However, an inspection of Tables II and III reveals that the complex phases are, in general, not really small.

As can be seen in Table II, the real part of the pole position of the N(1535)1/2$^-$ resonance is similar

TABLE II: Properties of the $I = 1/2$ resonances: Pole positions E_p ($\Gamma_{\rm tot}$ defined as -2ImE_p), photocouplings at the pole (A^h_{pole}, ϑ^h) according to Eq. (22). (*): not identified with PDG name; (a): dynamically generated.

	Re E_p	-2Im E_p	$\mathbf{A^{1/2}_{pole}}$		$\vartheta^{1/2}$		$\mathbf{A^{3/2}_{pole}}$		$\vartheta^{3/2}$	
	[MeV]	[MeV]	[10^{-3} GeV$^{-1/2}$]		[deg]		[10^{-3} GeV$^{-1/2}$]		[deg]	
fit→			1	**2**	1	**2**	1	**2**	1	**2**
$\boldsymbol{N(1535)\,1/2^-}$	**1498**	**74**	57	**50**	−51	**−45**				
BnGa [55]	1501 ± 4	134 ± 11		116 ± 10		7 ± 6				
ANL-Osaka [68]	1482	196		161		9				
SAID [246]	1502	95		77 ± 5		4				
$\boldsymbol{N(1650)\,1/2^-}$	**1677**	**146**	27	**23**	−14	**−29**				
BnGa [55]	1647 ± 6	103 ± 8		33 ± 7		−9 ± 15				
ANL-Osaka [68]	1656	170		40		−44				
SAID [246]	1648	80		35 ± 3		−16				
$\boldsymbol{N(1440)\,1/2^+_{(a)}}$	**1353**	**212**	−58	**−54**	−44	**−43**				
BnGa [55]	1370 ± 4	190 ± 7		−44 ± 7		−38 ± 5				
ANL-Osaka [68]	1374	152		49		−10				
SAID [246]	1359	162		−66 ± 5		−38				
$\boldsymbol{N(1710)\,1/2^+}$	**1637**	**97**	15	**28**	13	**77**				
BnGa [55]	1687 ± 17	200 ± 25		55 ± 18		−10 ± 65				
ANL-Osaka [68]	1746	354		86		106				
$\boldsymbol{N(1750)\,1/2^+_{(*,a)}}$	**1742**	**318**	−2	**−10**	8	**32**				
$\boldsymbol{N(1720)\,3/2^+}$	**1717**	**208**	39	**51**	31	**−8**	17	**14**	118	**37**
BnGa [55]	1660 ± 30	450 ± 100		110 ± 45		0 ± 40		150 ± 35		65 ± 35
ANL-Osaka [68]	1703	140		234		2		70		173
$\boldsymbol{N(1520)\,3/2^-}$	**1519**	**110**	−27	**−24**	−18	**−24**	114	**117**	19	**19**
BnGa [55]	1507 ± 3	111 ± 5		−21 ± 4		0 ± 5		132 ± 9		2 ± 4
ANL-Osaka [68]	1501	78		38		2		94		−173
SAID [246]	1515	113		−24 ± 3		−7		157 ± 6		10
$\boldsymbol{N(1675)\,5/2^-}$	**1650**	**126**	22	**22**	24	**38**	21	**36**	−71	**−41**
BnGa [55]	1654 ± 4	151 ± 5		24 ± 3		−16 ± 5		26 ± 8		−19 ± 6
ANL-Osaka [68]	1650	150		5		−22		33		−23
$\boldsymbol{N(1680)\,5/2^+}$	**1666**	**108**	−12	**−13**	−46	**−60**	124	**126**	−26	**−24**
BnGa [55]	1676 ± 6	113 ± 4		−13 ± 4		−25 ± 22		134 ± 5		−2 ± 4
ANL-Osaka [68]	1665	98		53		−5		38		−177
$\boldsymbol{N(1990)\,7/2^+}$	**1788**	**282**	19	**10**	−76	**−173**	37	**53**	97	**−34**
BnGa [55]	2030 ± 65	240 ± 60		42 ± 14		−30 ± 20		58 ± 12		−35 ± 25
$\boldsymbol{N(2190)\,7/2^-}$	**2092**	**363**	−48	**−83**	−16	**−28**	70	**95**	−19	**−21**
BnGa [55]	2150 ± 25	330 ± 30		−63 ± 7		10 ± 15		35 ± 20		25 ± 10
$\boldsymbol{N(2250)\,9/2^-}$	**2141**	**465**	−56	**−90**	−91	**−99**	14	**49**	−89	**121**
BnGa [55]	2195 ± 45	470 ± 50		< 10		–		< 10		–
$\boldsymbol{N(2220)\,9/2^+}$	**2196**	**662**	−108	**−232**	−93	**−91**	87	**162**	−76	**−71**
BnGa [55]	2150 ± 35	440 ± 40		< 10		–		< 10		–

in all quoted analyses, while the imaginary part in the present approach is rather small. Our N(1650)$1/2^-$, on the other hand, is wider compared to other analyses. This illustrates the difficulties to extract pole positions in the S_{11} partial wave [83]. As a result of the small width of the $N(1535)1/2^-$ we also obtain a smaller photocoupling $A^{1/2}_{pole}$. The same correlation can be observed for the $\Delta(1620)1/2^-$ in Table III. Likewise, for the $\Delta(1232)3/2^+$, the slightly different pole position in our analysis leads to photocouplings $A^{1/2}_{pole}$ and $A^{3/2}_{pole}$ slightly different from the ones in the other analyses. In case of the Roper resonance N(1440)$1/2^+$ our result is in good agreement with the SAID analysis.

The photocoupling of the $N(1535)1/2^-$ and its Q^2

TABLE III: Properties of the $I = 3/2$ resonances: Pole positions E_p ($\Gamma_{\rm tot}$ defined as -2ImE_p), photocouplings at the pole (A^h_{pole}, ϑ^h) according to Eq. (22). (a): dynamically generated.

	Re E_p	-2Im E_p	$\mathbf{A^{1/2}_{pole}}$		$\vartheta^{1/2}$		$\mathbf{A^{3/2}_{pole}}$		$\vartheta^{3/2}$	
	[MeV]	[MeV]	[10^{-3} GeV$^{-1/2}$]		[deg]		[10^{-3} GeV$^{-1/2}$]		[deg]	
fit→			1	**2**	1	**2**	1	**2**	1	**2**
Δ(1620) 1/2$^-$	**1599**	**71**	−28	**−28**	85	**92**				
BnGa [55]	1597 ± 4	130 ± 9		52 ± 5		−9 ± 9				
ANL-Osaka [68]	1592	136		113		−1				
Δ(1910) 1/2$^+$	**1788**	**575**	−200	**−246**	−87	**47**				
BnGa [55]	1850 ± 40	350 ± 45		23 ± 9		40 ± 90				
ANL-Osaka [68]	1854	368		52		170				
Δ(1232) 3/2$^+$	**1220**	**86**	−116	**−114**	−27	**−27**	−231	**−229**	−15	**−15**
BnGa [55]	1210 ± 1	99 ± 2		−131±3.5		−19 ± 2		−254±4.5		−9 ± 1
ANL-Osaka [68]	1211	102		−133		−15		−257		−3
SAID [246]	1211	99		−136 ± 5		−18		−255 ± 5		−6
Δ(1600) 3/2$^+_{\rm (a)}$	**1553**	**352**	260	**193**	27	**15**	−72	**−254**	−54	**−25**
BnGa [55]	1498 ± 25	230 ± 50		53 ± 10		130 ± 25		41 ± 11		165 ± 17
ANL-Osaka [68]	1734	352		72		−109		136		−98
Δ(1920) 3/2$^+$	**1724**	**863**	46	**190**	8	**−137**	−352	**−398**	−85	**−87**
BnGa [55]	1890 ± 30	300 ± 60		130^{+30}_{-60}		−65 ± 20		115^{+25}_{-50}		−160 ± 20
Δ(1700) 3/2$^-$	**1675**	**303**	106	**109**	10	**−12**	141	**111**	27	**21**
BnGa [55]	1680 ± 10	305 ± 15		170 ± 20		50 ± 15		170 ± 25		45 ± 10
ANL-Osaka [68]	1707	340		59		−70		125		−75
Δ(1930) 5/2$^-$	**1775**	**646**	84	**130**	−55	**−177**	−231	**−56**	82	**42**
ANL-Osaka [68]	1936	210		53		−21		35		−15
Δ(1905) 5/2$^+$	**1770**	**259**	61	**13**	−92	**19**	112	**72**	85	**67**
BnGa [55]	1805 ± 10	300 ± 15		25 ± 5		−23 ± 15		−50 ± 4		0 ± 10
ANL-Osaka [68]	1765	188		8		−97		18		−90
Δ(1950) 7/2$^+$	**1884**	**234**	−68	**−71**	−18	**−29**	−85	**−89**	−16	**−25**
BnGa [55]	1890 ± 4	243 ± 8		−72 ± 4		−7 ± 5		−96 ± 5		−7 ± 5
ANL-Osaka [68]	1872	206		−62		−9		−76		2
Δ(2200) 7/2$^-$	**2147**	**477**	41	**107**	−105	**−72**	−29	**−131**	71	**−102**
Δ(2400) 9/2$^-$	**1969**	**577**	−59	**−128**	39	**63**	−15	**−115**	27	**84**

dependence has been evaluated in the chiral unitary approach of Ref. [242]. The resonance appears as a quasibound KY state generated from coupled-channel scattering in the πN, ηN, and KY channels. The photocoupling at $Q^2 = 0$ was predicted to be around $50 - 75 \cdot 10^{-3}$ GeV$^{-1/2}$ with an angle of around $-35°$ (the values do not change much if evaluated at the pole position, as we have checked). This prediction compares well to the present data analysis, see Table II.

Our value of the photocoupling $A^{1/2}_{pole}$ for the N(1710)1/2$^+$ is rather small. Including kaon photoproduction data into the approach might lead to a different value because in the Jülich2012 analysis [79] a considerable impact of the N(1710)1/2$^+$ on those channels was observed. A fairly good agreement with the SAID and the Bonn-Gatchina results is found in case of the N(1520)3/2$^-$; the corresponding multipoles $E_{2-}(1/2)$ and $M_{2-}(1/2)$ are indeed quite large and seem to be well determined, c.f. Fig. 28. An agreement with the Bonn-Gatchina group is also observed for the N(1675)5/2$^-$ and the N(1680)5/2$^+$. In contrast, the large γN coupling of the $\Delta(1600)3/2^+$ results in photocouplings $A^{1/2}_{pole}$ and $A^{3/2}_{pole}$ much larger than the ones of the other analyses and is reflected in a resonance-like structure around 1600 MeV in the $E_{1+}(3/2)$ multipole, see Fig. 29. A similar structure has been observed in preliminary results of a new parameterization of the MAID approach [235]. In case of the prominent $\Delta(1950)7/2^+$ all analyses obtain similar results.

For some very wide resonances [$N(2220)9/2^+$, $\Delta(1910)1/2^+$, $\Delta(1920)3/2^+$, $\Delta(1930)5/2^-$, $\Delta(2200)7/2^-$, $\Delta(2400)9/2^-$], the photocouplings are sometimes sizable and very different for fit 1 and

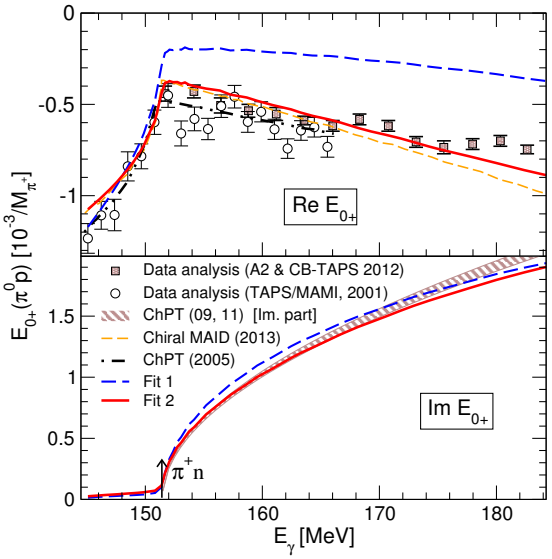

FIG. 30: The $E_{0+}(\pi^0 p)$ multipole close to threshold. The $\pi^+ n$ threshold is indicated with an arrow. Dashed (blue) line: fit 1; solid (red) line: fit 2. Experimental analyses: A2 and CB-TAPS (2012) [138] and TAPS/MAMI (2001) [135]. Theoretical analyses: Chiral MAID (2013) [33] and ChPT (2005) [27]. The imaginary part (dashed area) is provided in Ref. [138] based on the ChPT calculation including isospin breaking of Refs. [28, 30].

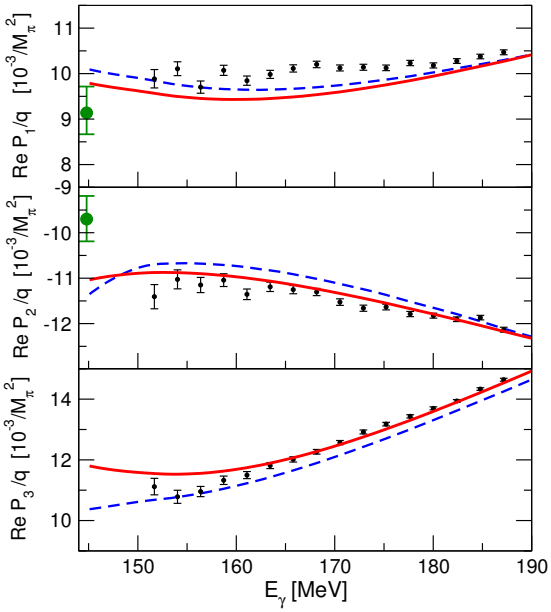

FIG. 31: P-waves for the reaction $\gamma p \to \pi^0 p$ close to threshold. Dashed (blue) lines: fit 1; solid (red) lines: fit 2. The data points at threshold (green circles) show the results of the $\mathcal{O}(q^3)$ calculation of Ref. [240]. Data points beyond threshold (black): Phenomenological analysis of the recent MAMI measurement in Ref. [138].

fit 2. There are very large uncertainties attached to these values, because the higher multipoles themselves are not uniquely determined as seen in the previous section. Second, some of these resonances are not well determined by hadronic data, see the discussion in Ref. [79]. Extreme examples are the $N(1750)1/2^+$ and the $\Delta(1920)3/2^+$. Third, as these resonances are so wide, their contribution to the multipole is difficult to disentangle from background terms; partial cancellations of different contributions to a multipole may occur rendering A_{pole} unnaturally large. We do not assign much significance to the existence or properties of these resonances [79]. The $N(2250)9/2^-$ is also very wide, but the resonance shape is clearly visible in the πN partial wave [2] and its properties can be determined more reliably. We plan to determine uncertainties on photocouplings in the future.

IV. SUMMARY

Photocouplings at the resonance pole are well-defined quantities and, therefore, appropriate to specify the electromagnetic excitations of resonances. They are given as ratios of residues that, together with pole positions, characterize resonances. The corresponding values are necessarily complex. To determine the photocouplings, a reliable analytic continuation to the resonance poles is needed. Here, we rely on the Jülich2012 dynamical coupled-channel model which guarantees unitarity and analyticity, and incorporates general S-matrix principles such as the correct branch points on the real axis and in the complex plane.

In the present study of pion photoproduction, we have chosen a highly flexible, model-independent form of the photo excitation inspired by the GWU/DAC CM12 parameterization. This enables an accurate fit of over 20,000 photoproduction data of the reactions $\gamma p \to \pi^0 p$ and $\gamma p \to \pi^+ n$, for altogether seven observables: $d\sigma/d\Omega$, Σ, T, P, $\Delta\sigma_{31}$, G, and H. The polarization observables E, F, $C_{x'_L}$, and $C_{z'_L}$ are predicted. Minimal chiral constraints and the incorporation of some isospin breaking effects allow for a precise description of the data even very close to threshold.

In order to shed light on the impact of recent high-precision measurements by ELSA, JLab, MAMI, Spring-8 and GRAAL, we have performed another fit where we omitted those recent data and included only data on $d\sigma/d\Omega$, Σ, T, and P. The predictions of $\Delta\sigma_{31}$, G, and H based on such a fit turned out to be surprisingly good. However, the explicit inclusion of actual data on those observables definitely has a significant quantitative influence on the values of the resulting resonance photocouplings.

The resonance positions and residues were determined in the hadronic Jülich2012 analysis. The photocouplings extracted in the present study are found to be in qualitative agreement with other determinations in most cases. Since, in general, the phase angle is not small, the traditionally quoted, real helicity couplings cannot be identified with the photocouplings at the pole.

To complete the analysis, a comprehensive error estimate of extracted multipoles and photocouplings is planned. The extension of the present approach to other photoproduction channels is straightforward.

Acknowledgments

We would like to thank Reinhard Beck, Michael Dugger, César Fernández Ramírez, Manuela Gottschall, Jan Hartmann, Eberhard Klempt, Vincent Mathieu, Paolo Pedroni, Andrei Sarantsev, Toru Sato, Mark Sikora, Igor Strakovsky, Steffen Strauch, Adam Szczepaniak, Annika Thiel, Ulrike Thoma, Lothar Tiator, Daniel Watts, and Ron Workman for many discussions and providing data. The numerical calculations were made possible through the grant jikp07 at the JUROPA supercomputer of the Forschungszentrum Jülich. This work is also supported by the EU Integrated Infrastructure Initiative HadronPhysics3 (contract number 283286) and by the DFG (Deutsche Forschungsgemeinschaft, GZ: DO 1302/1-2 and SFB/TR 16, "Subnuclear Structure of Matter"). The work of F. H. has been partially supported by the FFE Grant No. 41788390 (COSY-058) and by the One Hundred Person Project of the University of Chinese Academy of Sciences.

Appendix A: Multipole decomposition

We start by writing the reaction amplitude for the (pseudoscalar) meson photoproduction process

$$\gamma(k) + N(p) \to M(q) + N(p') \ , \tag{A1}$$

where the arguments k, p, q, and p' stand for the four-momenta of the incident photon, target nucleon, emitted meson, and recoil nucleon, respectively. Following Refs. [249, 250], the photoproduction amplitude of pseudoscalar mesons is written as

$$\begin{aligned} J &= iJ_1\vec{\sigma}\cdot\vec{\epsilon} + J_2\vec{\sigma}\cdot\hat{q}\vec{\sigma}\cdot(\hat{k}\times\vec{\epsilon}) \\ &\quad + iJ_3\vec{\sigma}\cdot\hat{k}\hat{q}\cdot\vec{\epsilon} + iJ_4\vec{\sigma}\cdot\hat{q}\hat{q}\cdot\vec{\epsilon}\,, \end{aligned} \tag{A2}$$

where $\vec{q}$ and $\vec{k}$ denote the meson and photon momentum, respectively; the photon polarization vector is denoted by $\vec{\epsilon}$. For an arbitrary vector $\vec{a}$, the notation $\hat{a}$ stands for the corresponding unit vector. The $J_i\,(i = 1-4)$ are functions of the total energy E and the scattering angle $x \equiv \cos\theta = \hat{q}\cdot\hat{k}$.

For further convenience, we rewrite Eq. (A2) as [251]

$$\begin{aligned} \hat{\mathcal{M}} = -iJ &= F_1\vec{\sigma}\cdot\vec{\epsilon} + iF_2(\hat{k}\times\hat{q})\cdot\vec{\epsilon} \\ &\quad + F_3\vec{\sigma}\cdot\hat{k}\hat{q}\cdot\vec{\epsilon} + F_4\vec{\sigma}\cdot\hat{q}\hat{q}\cdot\vec{\epsilon}\,, \end{aligned} \tag{A3}$$

where

$$F_1 \equiv J_1 - xJ_2 \ , \quad F_2 = J_2 \ , \quad F_3 \equiv J_2 + J_3 \ , \quad F_4 \equiv J_4 \ . \tag{A4}$$

Note that the forms of the amplitudes given by Eqs. (A2,A3) are coordinate-independent.

The multipole decomposition of the photoproduction amplitude J in Eq. (A2) is given by [249, 250]

$$\begin{pmatrix} J_1 \\ J_2 \\ J_3 \\ J_4 \end{pmatrix} = \frac{4\pi E}{m_N}\sum_{L=0}^{\infty}\tilde{D}_L(x)\begin{pmatrix} E_{L+} \\ E_{L-} \\ M_{L+} \\ M_{L-} \end{pmatrix}, \tag{A5}$$

where L stands for the orbital angular momentum of the final nucleon-pion state. The electric and magnetic multipoles $E_{L\pm}$ and $M_{L\pm}$ correspond to our photoproduction amplitude M in Eq. (8) for a given partial wave with $J = L \pm \frac{1}{2}$. The matrix $\tilde{D}_L(x)$ is given by [249]

$$\tilde{D}_L \equiv \begin{pmatrix} P'_{L+1} & P'_{L-1} & LP'_{L+1} & (L+1)P'_{L-1} \\ 0 & 0 & (L+1)P'_L & LP'_L \\ P''_{L+1} & P''_{L-1} & -P''_{L+1} & P''_{L-1} \\ -P''_L & -P''_L & P''_L & -P''_L \end{pmatrix},$$

with $P'_L \equiv P'_L(x)$ and $P''_L \equiv P''_L(x)$ denoting, respectively, the derivative and the double-derivative of the Legendre Polynomial of the first kind, $P_L \equiv P_L(x)$, with respect to x.

Considering partial waves with $J^P \leq 9/2$ corresponding to orbital angular momentum $L \leq 5$ (remember that this excludes E_{5+} and M_{5+}), one obtains from Eqs. (A4) and (A5)

$$\begin{aligned} F_1 &= -i\frac{4\pi E}{m_N}\frac{1}{128}\Big[32\,(4E_{0+} + 9E_{2+} + 4M_{2-} + 9M_{4-}) + 2\cos(\theta)\big(192E_{1+} + 360E_{3+} + 525E_{5+} - 64M_{1-} + 64M_{1+} \\ &\quad + 168M_{3-} + 24M_{3+} + 345M_{5-} + 15M_{5+}\big) + 8\cos(2\theta)\big(60E_{2+} + 105E_{4+} - 48M_{2-} + 48M_{2+} + 40M_{4-} + 20M_{4+}\big) \\ &\quad + 5\cos(3\theta)\big(112E_{3+} + 189E_{5+} - 144M_{3-} + 144M_{3+} + 49M_{5-} + 63M_{5+}\big) + 70\cos(4\theta)\big(9E_{4+} + 16(M_{4+} - M_{4-})\big) \end{aligned}$$

$$
\begin{aligned}
&+450E_{4+}+63\cos(5\theta)(11E_{5+}+25(M_{5+}-M_{5-}))\Big]\ ,\\
F_2 &= -i\,\frac{4\pi E}{m_N}\,\frac{1}{64}\Big[64M_{1-}+128M_{1+}+24\cos(\theta)(16M_{2-}+24M_{2+}+60M_{4-}+75M_{4+})\\
&+60\cos(2\theta)\big(12M_{3-}+16M_{3+}+35M_{5-}+42M_{5+}\big)+9\big(48M_{3-}+64M_{3+}+125M_{5-}+150M_{5+}\big)\\
&+280\cos(3\theta)(4M_{4-}+5M_{4+})+315\cos(4\theta)\big(5M_{5-}+6M_{5+}\big)\Big]\ ,\\
F_3 &= -i\,\frac{4\pi E}{m_N}\,\frac{1}{64}\big[192E_{1+}+24\cos(\theta)\big(40E_{2+}+175E_{4+}+4(4M_{2-}-4M_{2+}+35M_{4-}-25M_{4+})\big)\\
&+60\cos(2\theta)\big(28E_{3+}+105E_{5+}+12M_{3-}-12M_{3+}+91M_{5-}-63M_{5+}\big)+1200E_{3+}\\
&+280\cos(3\theta)\big(9E_{4+}+4M_{4-}-4M_{4+}\big)+315\cos(4\theta)\big(11E_{5+}+5M_{5-}-5M_{5+}\big)+3675E_{5+}+64M_{1-}-64M_{1+}\\
&+816M_{3-}-624M_{3+}+3525M_{5-}-2325M_{5+}\Big]\ ,\\
F_4 &= -i\,\frac{4\pi E}{m_N}\,\frac{3}{8}\Big[-2\big(4E_{2+}+25E_{4+}+8M_{2-}-4M_{2+}+50M_{4-}-25M_{4+}\big)-5\cos(\theta)\big(8E_{3+}+35E_{5+}+16M_{3-}-8M_{3+}\\
&+70M_{5-}-35M_{5+}\big)-70\cos(2\theta)\big(E_{4+}+2M_{4-}-M_{4+}\big)-105\cos(3\theta)\big(E_{5+}+2M_{5-}-M_{5+}\big)\Big]\ . \qquad \text{(A6)}
\end{aligned}
$$

Appendix B: Observables

In order to explain our conventions, we explicitly define the spin-polarization observables first in a coordinate-independent manner. We then provide expressions for the specific coordinate systems relevant for their actual measurements. We will also give some details how these observables are calculated in the present work in terms of the multiple amplitudes introduced in Sec. II B.

1. Definitions of the observables

In the following, we introduce a set of coordinate-independent unit vectors

$$\hat{n}_3=\hat{k}\ ,\quad \hat{n}_2=\frac{\hat{k}\times\hat{q}}{|\hat{k}\times\hat{q}|}\ ,\quad \hat{n}_1=\hat{n}_2\times\hat{n}_3\ . \qquad \text{(B1)}$$

Note that in terms of $\{\hat{n}_1,\hat{n}_2,\hat{n}_3\}$, the center-of-momentum (c.m.) cartesian coordinate system $\{\hat{x},\hat{y},\hat{z}\}$, where $\vec{k}+\vec{p}=\vec{q}+\vec{p}\,'=0$, and the laboratory (lab) cartesian coordinate system $\{\hat{x}_L,\hat{y}_L,\hat{z}_L\}$, where $\vec{p}=0$, are given by

$$
\begin{aligned}
\{\hat{x},\hat{y},\hat{z}\}&=\{\hat{n}_1,\hat{n}_2,\hat{n}_3\}_{(\mathrm{cm})}\ ,\\
\{\hat{x}_L,\hat{y}_L,\hat{z}_L\}&=\{\hat{n}_1,\hat{n}_2,\hat{n}_3\}_{(\mathrm{lab})}\ ,
\end{aligned}
\qquad \text{(B2)}
$$

where the subscript (cm) and (lab) indicate that $\{\hat{n}_1,\hat{n}_2,\hat{n}_3\}$ is to be evaluated in the c.m. and lab frame, respectively.

The reaction plane is defined as the $(\hat{n}_1\hat{n}_3)$-plane. Then, $\hat{n}_2$ is perpendicular to the reaction plane.

A real photon has two independent polarization states. A linearly polarized photon is specified by $\vec{\epsilon}_\parallel$ and $\vec{\epsilon}_\perp$, where $\vec{\epsilon}_\parallel$ ($\vec{\epsilon}_\perp$) stands for the photon polarization vector parallel (perpendicular) to the reaction plane. More generally, we define the linearly polarized photon states $\vec{\epsilon}_{\parallel'}$ and $\vec{\epsilon}_{\perp'}$ obtained by rotating $\vec{\epsilon}_\parallel$ and $\vec{\epsilon}_\perp$ (counterclockwise) by an angle ϕ about the $\hat{n}_3$-axis, i.e.,

$$
\begin{aligned}
\vec{\epsilon}_{\parallel'}&=\cos\phi\,\vec{\epsilon}_\parallel+\sin\phi\,\vec{\epsilon}_\perp\ ,\\
\vec{\epsilon}_{\perp'}&=-\sin\phi\,\vec{\epsilon}_\parallel+\cos\phi\,\vec{\epsilon}_\perp\ .
\end{aligned}
\qquad \text{(B3)}
$$

The circularly polarized photon is specified by

$$\vec{\epsilon}_\pm\equiv\mp\frac{1}{\sqrt{2}}\left(\vec{\epsilon}_\parallel\pm i\vec{\epsilon}_\perp\right)\ . \qquad \text{(B4)}$$

For further convenience, we also introduce the projection operator $\hat{P}_\lambda$ which specifies the state of the photon polarization; namely, $\hat{P}_\lambda\vec{\epsilon}\equiv\vec{\epsilon}_\lambda$. Note that $\hat{P}_{\lambda'}\hat{P}_\lambda=\delta_{\lambda'\lambda}$ and $\sum_\lambda\hat{P}_\lambda=1$. The projection operator $\hat{P}_\lambda$ defined here is associated with the Stokes vector $\vec{P}^S$[252] which specifies the direction and degree of polarization of the photon. For example, $\hat{P}_\pm$ corresponds to $P^S_{z=n_3}=\pm1$, while $\hat{P}_\perp$ ($\hat{P}_\parallel$) corresponds to $P^S_{x=n_1}=+1$ ($P^S_{x=n_1}=-1$). Furthermore, the difference of the appropriate projection operators can be expressed in terms of the usual Pauli spin matrices in photon helicity space, i.e., $\hat{P}_+-\hat{P}_-=\sigma_{n_3}$ and $\hat{P}_\perp-\hat{P}_\parallel=\sigma_{n_1}$.

We now define the coordinate-independent observables. Provided the reaction amplitude $\hat{\mathcal{M}}$ in Eq. (A3) is Lorentz invariant, these observables are also Lorentz invariants. The cross section is defined as

$$\frac{d\sigma}{d\Omega}\equiv\frac{1}{4}Tr[\hat{\mathcal{M}}\hat{\mathcal{M}}^\dagger]\ , \qquad \text{(B5)}$$

where the trace is over both the nucleon spin and photon polarization. The appearance of the factor $\frac{1}{4}$ is due to the averaging over the target-nucleon spin and the photon-beam polarization.

The single polarization observables, namely, the beam, target, and recoil polarization asymmetries, Σ, T, and P,

respectively, are defined as

$$\begin{aligned}\frac{d\sigma}{d\Omega}\Sigma &\equiv \frac{1}{4}Tr[\hat{\mathcal{M}}(\hat{P}_\perp - \hat{P}_\parallel)\hat{\mathcal{M}}^\dagger] ,\\ \frac{d\sigma}{d\Omega}T &\equiv \frac{1}{4}Tr[\hat{\mathcal{M}}\sigma_{n_2}\hat{\mathcal{M}}^\dagger] ,\\ \frac{d\sigma}{d\Omega}P &\equiv \frac{1}{4}Tr[\hat{\mathcal{M}}\hat{\mathcal{M}}^\dagger\sigma_{n_2}] .\end{aligned} \tag{B6}$$

The beam-target asymmetries, E, F, G, and H, are defined as

$$\begin{aligned}\frac{d\sigma}{d\Omega}E &\equiv -\frac{1}{4}Tr[\hat{\mathcal{M}}(\hat{P}_+ - \hat{P}_-)\sigma_{n_3}\hat{\mathcal{M}}^\dagger]\\ &= -2\frac{1}{4}Tr[\hat{\mathcal{M}}\hat{P}_+\sigma_{n_3}\hat{\mathcal{M}}^\dagger] = 2\frac{1}{4}Tr[\hat{\mathcal{M}}\hat{P}_-\sigma_{n_3}\hat{\mathcal{M}}^\dagger] ,\\ \frac{d\sigma}{d\Omega}F &\equiv \frac{1}{4}Tr[\hat{\mathcal{M}}(\hat{P}_+ - \hat{P}_-)\sigma_{n_1}\hat{\mathcal{M}}^\dagger]\\ &= 2\frac{1}{4}Tr[\hat{\mathcal{M}}\hat{P}_+\sigma_{n_1}\hat{\mathcal{M}}^\dagger] = -2\frac{1}{4}Tr[\hat{\mathcal{M}}\hat{P}_-\sigma_{n_1}\hat{\mathcal{M}}^\dagger] ,\\ \frac{d\sigma}{d\Omega}G &\equiv -\frac{1}{4}Tr[\hat{\mathcal{M}}(\hat{P}_{\perp'} - \hat{P}_{\parallel'})\sigma_{n_3}\hat{\mathcal{M}}^\dagger]\\ &= -2\frac{1}{4}Tr[\hat{\mathcal{M}}\hat{P}_{\perp'}\sigma_{n_3}\hat{\mathcal{M}}^\dagger] = 2\frac{1}{4}Tr[\hat{\mathcal{M}}\hat{P}_{\parallel'}\sigma_{n_3}\hat{\mathcal{M}}^\dagger] ,\\ \frac{d\sigma}{d\Omega}H &\equiv \frac{1}{4}Tr[\hat{\mathcal{M}}(\hat{P}_{\perp'} - \hat{P}_{\parallel'})\sigma_{n_1}\hat{\mathcal{M}}^\dagger]\\ &= 2\frac{1}{4}Tr[\hat{\mathcal{M}}\hat{P}_{\perp'}\sigma_{n_1}\hat{\mathcal{M}}^\dagger] = -2\frac{1}{4}Tr[\hat{\mathcal{M}}\hat{P}_{\parallel'}\sigma_{n_1}\hat{\mathcal{M}}^\dagger] .\end{aligned} \tag{B7}$$

Here, in the definitions of G and H, the projection operators $\hat{P}_{\parallel'}$ and $\hat{P}_{\perp'}$ correspond to the photon polarizations given by Eq. (B3) with $\phi = \pi/4$. We note that in the above definition of E and G, we have introduced a minus sign so that our convention matches that of the SAID group [104].

The beam-recoil asymmetries, $C_{n_i'}$ and $O_{n_i'}$ $(i = 1, 3)$, are defined as

$$\begin{aligned}\frac{d\sigma}{d\Omega}C_{n_i'} &\equiv -\frac{1}{4}Tr[\hat{\mathcal{M}}(\hat{P}_+ - \hat{P}_-)\hat{\mathcal{M}}^\dagger\sigma_{n_i'}]\\ &= -2\frac{1}{4}Tr[\hat{\mathcal{M}}\hat{P}_+\hat{\mathcal{M}}^\dagger\sigma_{n_i'}] = 2\frac{1}{4}Tr[\hat{\mathcal{M}}\hat{P}_-\hat{\mathcal{M}}^\dagger\sigma_{n_i'}] ,\\ \frac{d\sigma}{d\Omega}O_{n_i'} &\equiv -\frac{1}{4}Tr[\hat{\mathcal{M}}(\hat{P}_{\perp'} - \hat{P}_{\parallel'})\hat{\mathcal{M}}^\dagger\sigma_{n_i'}]\\ &= -2\frac{1}{4}Tr[\hat{\mathcal{M}}\hat{P}_{\perp'}\hat{\mathcal{M}}^\dagger\sigma_{n_i'}] = 2\frac{1}{4}Tr[\hat{\mathcal{M}}\hat{P}_{\parallel'}\hat{\mathcal{M}}^\dagger\sigma_{n_i'}] ,\end{aligned} \tag{B8}$$

associated with $\{\hat{n}_1', \hat{n}_2', \hat{n}_3'\}$ which is obtained by rotating $\{\hat{n}_1, \hat{n}_2, \hat{n}_3\}$ (counterclockwise) by an angle θ about the $\hat{n}_2$-axis ($\cos\theta \equiv \hat{q}\cdot\hat{n}_3$), such that, $\hat{n}_3'$ is in the direction of the emitted meson momentum $\vec{q}$, i.e., $\hat{n}_3' = \hat{q}$. Explicitly, they are related by

$$\begin{aligned}\hat{n}_1' &= \cos\theta\,\hat{n}_1 - \sin\theta\,\hat{n}_3 ,\\ \hat{n}_3' &= \sin\theta\,\hat{n}_1 + \cos\theta\,\hat{n}_3 ,\\ \hat{n}_2' &= \hat{n}_2 .\end{aligned} \tag{B9}$$

The target-recoil asymmetries, $L_{n_i'}$ and $T_{n_i'}$ $(i = 1, 3)$, are defined as

$$\begin{aligned}\frac{d\sigma}{d\Omega}L_{n_i'} &\equiv \zeta_i\frac{1}{4}Tr[\hat{\mathcal{M}}\sigma_{n_3}\hat{\mathcal{M}}^\dagger\sigma_{n_i'}] ,\\ \frac{d\sigma}{d\Omega}T_{n_i'} &\equiv \frac{1}{4}Tr[\hat{\mathcal{M}}\sigma_{n_1}\hat{\mathcal{M}}^\dagger\sigma_{n_i'}] ,\end{aligned} \tag{B10}$$

where $\zeta_1 = -1$ and $\zeta_3 = +1$. Again, these sign factors have been introduced to match the SAID convention, A list of conventions used by different groups may be found in Ref. [253].

2. Observables in terms of the coefficient amplitudes F_i

Any of the observables defined in the previous subsection may be expressed in terms of the coefficients F_i in Eq. (A3). The photoproduction amplitude given by Eq. (A3) can be put straightforwardly into the form

$$\hat{\mathcal{M}}^\lambda = \sum_{m=0}^{3}\mathcal{M}_m^\lambda\sigma_m \tag{B11}$$

for a given state of photon polarization $\vec{\epsilon}_\lambda$. Here, $\sigma_0 \equiv 1$ [σ_i $(i = 1, 2, 3)$, the usual Pauli spin-matrices]. Note that the form given by the above equation is particularly suited for calculating the observables defined in the previous subsection. Then, following Ref. [251], the differential cross section becomes

$$\begin{aligned}\frac{d\sigma}{d\Omega} &= |F_1|^2 + \frac{1}{2}\Big(|F_2|^2 + |F_3|^2 + |F_4|^2\\ &\quad +2\mathrm{Re}\left[(F_1 + F_3\cos\theta)\,F_4^*\right]\Big)\sin^2\theta .\end{aligned} \tag{B12}$$

In the cross section above, the incident flux and the (final-state) phase-space density factors have been left out for further convenience. Therefore, to get the physical cross section, $\frac{d\sigma_o}{d\Omega}$, one needs to multiply the above defined cross section by these factors, i.e.,

$$\frac{d\sigma_o}{d\Omega} \equiv \left(\frac{m_N}{4\pi E}\right)^2\frac{|\vec{q}|}{|\vec{k}|}\frac{d\sigma}{d\Omega} , \tag{B13}$$

in the c.m. frame.

The single polarization observables become

$$\begin{aligned}\frac{d\sigma}{d\Omega}\Sigma &= \frac{1}{2}\Big(|F_2|^2 - |F_3|^2 - |F_4|^2\\ &\quad -2\mathrm{Re}\left[(F_1 + F_3\cos\theta)\,F_4^*\right]\Big)\sin^2\theta ,\\ \frac{d\sigma}{d\Omega}T &= \mathrm{Im}\Big[\left(-F_2 + F_3 + F_4\cos\theta\right)F_1^*\\ &\quad +\left(F_3 + F_4\cos\theta\right)F_4^*\sin^2\theta\Big]\sin\theta ,\\ \frac{d\sigma}{d\Omega}P &= -\mathrm{Im}\Big[\left(F_2 + F_3 + F_4\cos\theta\right)F_1^*\\ &\quad +\left(F_3 + F_4\cos\theta\right)F_4^*\sin^2\theta\Big]\sin\theta ,\end{aligned} \tag{B14}$$

and the double polarization observables E, F, G and H read

$$\begin{aligned}
\frac{d\sigma}{d\Omega}E &= |F_1|^2 + \mathrm{Re}\left[F_2^*(F_3+F_4\cos\theta)+F_1^*F_4\right]\sin^2\theta,\\
\frac{d\sigma}{d\Omega}F &= -\mathrm{Re}\left[F_2^*(F_1+F_4\sin^2\theta)-F_1^*(F_3+F_4\cos\theta)\right]\sin\theta\\
\frac{d\sigma}{d\Omega}G &= \mathrm{Im}\left[F_2^*(F_3+F_4\cos\theta)+F_1^*F_4\right]\sin^2\theta,\\
\frac{d\sigma}{d\Omega}H &= -\mathrm{Im}[F_2^*(F_1+F_4\sin^2\theta)-\\
&\quad F_1^*(F_3+F_4\cos\theta)\sin\theta]\sin\theta\,. \qquad \text{(B15)}
\end{aligned}$$

The beam-recoil polarizations $C_{n_1'}$ and $C_{n_3'}$ become

$$\begin{aligned}
\frac{d\sigma}{d\Omega}C_{n_1'} &= \left\{|F_1|^2 + Re\left[F_1^*(F_2+F_3)\cos\theta\right.\right.\\
&\quad \left.\left.+(F_1^*F_4 - F_2^*F_3\sin^2\theta)\right]\right\}\sin\theta\,,\\
\frac{d\sigma}{d\Omega}C_{n_3'} &= -|F_1|^2\cos\theta + Re\left[F_1^*(F_2+F_3)\right.\\
&\quad \left.+F_2^*(F_3\cos\theta+F_4)\right]\sin^2\theta\,. \qquad \text{(B16)}
\end{aligned}$$

In the c.m. frame, where the Cartesian coordinate system $\{\hat{x}',\hat{y}',\hat{z}'\}$ is identified with $\{\hat{n}_1',\hat{n}_2',\hat{n}_3'\}_{(cm)}$, we have

$$C_{x'} = C_{n_1'} \qquad \text{and} \qquad C_{z'} = C_{n_3'}\,. \qquad \text{(B17)}$$

where $C_{n_1'}$ and $C_{n_3'}$ given by Eq. (B16) are evaluated in the c.m. frame.

Experimentalists report the beam-target asymmetries in the lab frame. Different groups use different lab coordinate frames. We define the lab frame quantities $C_{x_L'}$ and $C_{z_L'}$ with respect to the coordinate system $\{\hat{x}_L',\hat{y}_L',\hat{z}_L'\}$ which is obtained by a (counterclockwise) rotation of $\{\hat{x}_L,\hat{y}_L,\hat{z}_L\}$ (cf. Eq.(B2)) by an angle $\pi-\theta_{p_L'}$ about the $\hat{y}_L$-axis. Here, $\theta_{p_L'}$ stands for the recoil nucleon scattering angle in the $\{\hat{x}_L,\hat{y}_L,\hat{z}_L\}$ frame, i.e., $\cos\theta_{p_L'}\equiv\hat{p}_L'\cdot\hat{z}_L$ with $\vec{p}_L'$ being the recoil nucleon momentum in the latter frame. Explicitly,

$$\begin{aligned}
\hat{x}_L' &= -\cos\theta_{p_L'}\,\hat{x}_L - \sin\theta_{p_L'}\,\hat{z}_L\,,\\
\hat{z}_L' &= \sin\theta_{p_L'}\,\hat{x}_L - \cos\theta_{p_L'}\,\hat{z}_L\,,\\
\hat{y}_L' &= \hat{y}_L\,. \qquad \text{(B18)}
\end{aligned}$$

Note that $\hat{z}_L'$ points in the direction opposite to the recoil nucleon momentum, i.e., $\hat{z}_L' = -\hat{p}_L'$.

The beam-recoil polarization observables in the lab frame, $C_{x_L'}$ and $C_{z_L'}$, can be obtained from $C_{x'}$ and $C_{z'}$ in the c.m. frame by a combination of Lorentz boosts and rotations. We have [217, 254]

$$\begin{aligned}
C_{x_L'} &= \cos\theta_r\,C_{x'} - \sin\theta_r\,C_{z'}\,,\\
C_{z_L'} &= \sin\theta_r\,C_{x'} + \cos\theta_r\,C_{z'}\,, \qquad \text{(B19)}
\end{aligned}$$

where the rotation angle θ_r is given by

$$\begin{aligned}
\cos\theta_r &= -\cos\theta\cos\theta_{p_L'} - \gamma_3\sin\theta\sin\theta_{p_L'}\,,\\
\sin\theta_r &= \gamma_1[\cos\theta_{p_L'}\sin\theta + \gamma_3\sin\theta_{p_L'}(\beta_1\beta_3-\cos\theta)]\,, \qquad \text{(B20)}
\end{aligned}$$

with the Lorentz boost parameters

$$\beta_1 = \frac{|\vec{q}\,|}{\sqrt{\vec{q}^{\,2}+m_N^2}}\,, \quad \beta_3 = \frac{|\vec{k}_L\,|}{\sqrt{\vec{k}_L^{\,2}+m_N^2}}\,, \qquad \text{(B21)}$$

and $\gamma_i \equiv 1/\sqrt{1-\beta_i^2}$. Here, $\vec{q}$ is the meson momentum in the c.m. frame $\{\hat{x},\hat{y},\hat{z}\}$ and $\vec{k}_L$ is the photon momentum in the lab frame $\{\hat{x}_L,\hat{y}_L,\hat{z}_L\}$.

We note that our choice of the lab frame, $\{\hat{x}_L',\hat{y}_l',\hat{z}_L'\}$, coincides with that of the SAID group [104] ($\{\hat{x}^*,\hat{y}^*,\hat{z}^*\}$), and that, $C_{x_L'} = C_{x^*}$ and $C_{z_L'} = C_{z^*}$.

In Ref. [144], one introduces the cross-section difference of the parallel and anti-parallel helicity states of the photon and target nucleon. Explicitly,

$$\Delta\sigma_{31} = \frac{d\sigma_{3/2}}{d\Omega} - \frac{d\sigma_{1/2}}{d\Omega}\,, \qquad \text{(B22)}$$

where $\sigma_{3/2}$ and $\sigma_{1/2}$ stand for the cross sections with the parallel ($\lambda_N-\lambda_\gamma=\pm 3/2$) and the anti-parallel ($\lambda_N-\lambda_\gamma=\pm 1/2$) initial state helicity, respectively.

$\Delta\sigma_{31}$ is related to the helicity asymmetry E via

$$\Delta\sigma_{31} = -2\frac{d\sigma_o}{d\Omega}E\,, \qquad \text{(B23)}$$

where the factor $1/2$ is due to the fact that $d\sigma_o/d\Omega$ (cf. Eq. (B13) contains the initial spin averaging factor of $1/4$, while $d\sigma_{3/2}/d\Omega$ and $d\sigma_{1/2}/d\Omega$ contain the spin averaging factor of $1/2$.

Appendix C: Definition of the photocouplings

Adopting the convention of Ref. [246] the photocouplings are given as the residue of the helicity multipole $A_{L\pm}^h$ multiplied by a complex factor $\mathcal{N}$:

$$\tilde{A}_{pole}^h = \mathcal{N}\,\mathrm{Res}A_{L\pm}^h\,, \qquad \text{(C1)}$$

where $h = 1/2$ or $3/2$ and

$$\mathcal{N} = I_F\sqrt{\frac{q_p}{k_p}\frac{2\pi\,(2J+1)E_p}{m_N\,r_{\pi N}}}\,. \qquad \text{(C2)}$$

Here, I_F is an isospin factor with $I_{1/2} = -\sqrt{3}$ and $I_{3/2} = \sqrt{2/3}$, q_p (k_p) is the meson (photon) momentum in the c.m. frame evaluated at the pole, J is the total angular momentum, L is the πN orbital angular momentum and m_N the nucleon mass, while E_p and $r_{\pi N}$ represent the pole position and the elastic πN residue of the resonance. Note the convention that $\mathrm{Res}A_{L\pm}^h$ and $r_{\pi N}$ are defined with a minus sign compared to the mathematical residues of the multipole and the elastic πN amplitude, respectively. The cuts of the square root in Eq. (C2) and also the square roots implicitly contained in q_p, k_p, are from the origin to $-\infty$.

In terms of the electric and magnetic multipoles the helicity multipoles read

$$A^{1/2}_{L+} = -\frac{1}{2}\left[(L+2)E_{L+} + L\,M_{L+}\right], \quad \text{(C3)}$$

$$A^{3/2}_{L+} = \frac{1}{2}\sqrt{L(L+2)}\left[E_{L+} - M_{L+}\right], \quad \text{(C4)}$$

with total angular momentum $J = L + 1/2$ and

$$A^{1/2}_{L-} = -\frac{1}{2}\left[(L-1)\,E_{L-} - (L+1)M_{L-}\right], \quad \text{(C5)}$$

$$A^{3/2}_{L-} = -\frac{1}{2}\sqrt{(L-1)(L+1)}\left[E_{L-} + M_{L-}\right], \quad \text{(C6)}$$

with $J = L - 1/2$.

The residues of the electric and magnetic multipoles $E_{L\pm}$ and $M_{L\pm}$ can be determined as explained in Appendix C, Eq. (C.2) of Ref. [81].

[1] G. Höhler, *Pion Nucleon Scattering*, edited by H. Schopper, Landolt Börnstein, New Series, Group 9b, Vol. I (Springer, New York, 1983).
[2] R. A. Arndt, W. J. Briscoe, I. I. Strakovsky and R. L. Workman, Phys. Rev. C **74**, 045205 (2006) [arXiv:nucl-th/0605082].
[3] R. L. Workman, M. W. Paris, W. J. Briscoe and I. I. Strakovsky, Phys. Rev. C **86**, 015202 (2012) [arXiv:1202.0845 [hep-ph]];
webpage: `http://gwdac.phys.gwu.edu/`.
[4] I. G. Aznauryan and V. D. Burkert, Phys. Rev. C **85**, 055202 (2012) [arXiv:1201.5759 [hep-ph]].
[5] M. Ronniger and B. C. Metsch, Eur. Phys. J. A **47**, 162 (2011) [arXiv:1111.3835 [hep-ph]].
[6] B. Golli and S. Širca, Eur. Phys. J. A **49**, 111 (2013) [arXiv:1306.3330 [nucl-th]].
[7] G. Ramalho and M. T. Pena, Phys. Rev. D **84**, 033007 (2011) [arXiv:1105.2223 [hep-ph]].
[8] S. Capstick, Phys. Rev. D **46**, 2864 (1992).
[9] S. Capstick and W. Roberts, Phys. Rev. D **49**, 4570 (1994) [arXiv:9310030[nucl-th]].
[10] C. Jayalath, J. L. Goity, E. González de Urreta and N. N. Scoccola, Phys. Rev. D **84**, 074012 (2011) [arXiv:1108.2042 [nucl-th]].
[11] D. J. Wilson, I. C. Cloët, L. Chang and C. D. Roberts, Phys. Rev. C **85**, 025205 (2012) [arXiv:1112.2212 [nucl-th]].
[12] C. Chen, L. Chang, C. D. Roberts, S. Wan and D. J. Wilson, Few Body Syst. **53**, 293 (2012) [arXiv:1204.2553 [nucl-th]].
[13] R. G. Edwards, N. Mathur, D. G. Richards and S. J. Wallace, Phys. Rev. D **87**, 054506 (2013) [arXiv:1212.5236 [hep-ph]].
[14] I. S. Barker, A. Donnachie and J. K. Storrow, Nucl. Phys. B **95**, 347 (1975).
[15] A. M. Sandorfi, S. Hoblit, H. Kamano and T. -S. H. Lee, J. Phys. G **38**, 053001 (2011) [arXiv:1010.4555 [nucl-th]].
[16] R. L. Workman, M. W. Paris, W. J. Briscoe, L. Tiator, S. Schumann, M. Ostrick and S. S. Kamalov, Eur. Phys. J. A **47**, 143 (2011) [arXiv:1102.4897 [nucl-th]].
[17] T. Vrancx, J. Ryckebusch, T. Van Cuyck and P. Vancraeyveld, Phys. Rev. C **87**, 055205 (2013) [arXiv:1303.2936 [nucl-th]].
[18] W.-T. Chiang and F. Tabakin, Phys. Rev. C **55**, 2054 (1996).
[19] A. S. Omelaenko, Sov. J. Nucl. Phys. **34**, 406 (1981).
[20] Y. Wunderlich, R. Beck and L. Tiator, [arXiv:1312.0245 [nucl-th]].
[21] V. Bernard, N. Kaiser, J. Gasser and U.-G. Meißner, Phys. Lett. B **268**, 291 (1991).
[22] V. Bernard, N. Kaiser and U.-G. Meißner, Nucl. Phys. B **383**, 442 (1992).
[23] V. Bernard, N. Kaiser, T.-S. H. Lee and U.-G. Meißner, Phys. Rept. **246**, 315 (1994) [hep-ph/9310329].
[24] V. Bernard, N. Kaiser, U.-G. Meißner and A. Schmidt, Nucl. Phys. A **580** (1994) 475 [nucl-th/9403013].
[25] V. Bernard, N. Kaiser and U.-G. Meißner, Z. Phys. C **70** (1996) 483 [hep-ph/9411287].
[26] V. Bernard, N. Kaiser and U.-G. Meißner, Phys. Lett. B **382**, 19 (1996) [nucl-th/9604010].
[27] V. Bernard, B. Kubis and U.-G. Meißner, Eur. Phys. J. A **25**, 419 (2005) [nucl-th/0506023].
[28] M. Hoferichter, B. Kubis and U.-G. Meißner, Phys. Lett. B **678**, 65 (2009) [arXiv:0903.3890 [hep-ph]].
[29] V. Baru, C. Hanhart, M. Hoferichter, B. Kubis, A. Nogga and D. R. Phillips, Phys. Lett. B **694**, 473 (2011) [arXiv:1003.4444 [nucl-th]].
[30] V. Baru, C. Hanhart, M. Hoferichter, B. Kubis, A. Nogga and D. R. Phillips, Nucl. Phys. A **872**, 69 (2011) [arXiv:1107.5509 [nucl-th]].
[31] C. Ditsche, M. Hoferichter, B. Kubis and U.-G. Meißner, JHEP **1206**, 043 (2012) [arXiv:1203.4758 [hep-ph]].
[32] M. Hilt, S. Scherer and L. Tiator, Phys. Rev. C **87**, 045204 (2013) [arXiv:1301.5576 [nucl-th]].
[33] M. Hilt, B. C. Lehnhart, S. Scherer and L. Tiator, Phys. Rev. C **88**, 055207 (2013) [arXiv:1309.3385 [nucl-th]].
[34] C. Fernández Ramírez and A. M. Bernstein, Phys. Lett. B **724**, 253 (2013) [arXiv:1212.3237 [nucl-th]].
[35] C. Fernández Ramírez, A. M. Bernstein and T. W. Donnelly, Phys. Rev. C **80**, 065201 (2009) [arXiv:0907.3463 [nucl-th]].
[36] U.-G. Meißner and J. A. Oller, Nucl. Phys. A **673**, 311 (2000) [arXiv:nucl-th/9912026].
[37] M. Mai, P. C. Bruns and U.-G. Meißner, Phys. Rev. D **86**, 094033 (2012) [arXiv:1207.4923 [nucl-th]].
[38] D. Ruic, M. Mai and U.-G. Meißner, Phys. Lett. B **704**, 659 (2011) [arXiv:1108.4825 [nucl-th]].
[39] P. C. Bruns, M. Mai and U.-G. Meißner, Phys. Lett. B **697**, 254 (2011) [arXiv:1012.2233 [nucl-th]].
[40] A. Gasparyan and M. F. M. Lutz, Nucl. Phys. A **848**, 126 (2010) [arXiv:1003.3426 [hep-ph]].
[41] M. Döring, E. Oset and U.-G. Meißner, Eur. Phys. J. A **46**, 315 (2010) [arXiv:1003.0097 [nucl-th]].
[42] M. Döring and K. Nakayama, Phys. Lett. B **683**, 145 (2010) [arXiv:0909.3538 [nucl-th]].

[43] M. Döring, Nucl. Phys. A **786**, 164 (2007) [nucl-th/0701070].

[44] B. Borasoy, P. C. Bruns, U.-G. Meißner and R. Nißler, Eur. Phys. J. A **34**, 161 (2007) [arXiv:0709.3181 [nucl-th]].

[45] B. Borasoy, U.-G. Meißner and R. Nißler, Phys. Rev. C **74**, 055201 (2006) [hep-ph/0606108].

[46] M. Döring, E. Oset and D. Strottman, Phys. Lett. B **639**, 59 (2006) [nucl-th/0602055].

[47] M. Döring, E. Oset and D. Strottman, Phys. Rev. C **73**, 045209 (2006) [nucl-th/0510015].

[48] K. P. Khemchandani, A. Martinez Torres, H. Nagahiro and A. Hosaka, [arXiv:1307.8420 [nucl-th]].

[49] K. P. Khemchandani, A. Martinez Torres, H. Nagahiro and A. Hosaka, [arXiv:1310.0067 [nucl-th]].

[50] E. J. Garzón and E. Oset, Eur. Phys. J. A **48**, 5 (2012) [arXiv:1201.3756 [hep-ph]].

[51] J.-J. Wu, R. Molina, E. Oset and B. S. Zou, Phys. Rev. C **84**, 015202 (2011) [arXiv:1011.2399 [nucl-th]].

[52] E. E. Kolomeitsev and M. F. M. Lutz, Phys. Lett. B **585**, 243 (2004) [nucl-th/0305101].

[53] C. García Recio, M. F. M. Lutz and J. Nieves, Phys. Lett. B **582**, 49 (2004) [nucl-th/0305100].

[54] A. V. Anisovich, R. Beck, E. Klempt, V. A. Nikonov, A. V. Sarantsev and U. Thoma, Eur. Phys. J. A **48**, 88 (2012) [arXiv:1205.2255 [nucl-th]].

[55] A. V. Anisovich, R. Beck, E. Klempt, V. A. Nikonov, A. V. Sarantsev and U. Thoma, Eur. Phys. J. A **48**, 15 (2012) [arXiv:1112.4937 [hep-ph]].

[56] A. V. Anisovich, R. Beck, E. Klempt, V. A. Nikonov, A. V. Sarantsev, U. Thoma and Y. Wunderlich, Eur. Phys. J. A **49**, 121 (2013) [arXiv:1306.5126 [hep-ph]].

[57] X. Cao, V. Shklyar and H. Lenske, Phys. Rev. C **88**, 055204 (2013) [arXiv:1303.2604 [nucl-th]].

[58] V. Shklyar, H. Lenske and U. Mosel, Phys. Rev. C **87**, 015201 (2013) [arXiv:1206.5414 [nucl-th]].

[59] M. Shrestha and D. M. Manley, Phys. Rev. C **86**, 055203 (2012) [arXiv:1208.2710 [hep-ph]].

[60] M. Shrestha and D. M. M. Manley, Phys. Rev. C **86**, 045204 (2012) [arXiv:1205.5294 [hep-ph]].

[61] M. Batinic, S. Ceci, A. Švarc and B. Zauner, Phys. Rev. C **82**, 038203 (2010).

[62] S. Ceci, A. Švarc and B. Zauner, Phys. Rev. Lett. **97**, 062002 (2006) [hep-ph/0603144].

[63] P. F. A. Goudsmit, H. J. Leisi, E. Matsinos, B. L. Birbrair and A. B. Gridnev, Nucl. Phys. A **575**, 673 (1994).

[64] A. B. Gridnev and N. G. Kozlenko, Eur. Phys. J. A **4**, 187 (1999).

[65] A. B. Gridnev, I. Horn, W. J. Briscoe and I. I. Strakovsky, Phys. Atom. Nucl. **69**, 1542 (2006) [hep-ph/0408192].

[66] D. Drechsel, S. S. Kamalov and L. Tiator [MAID2007], Eur. Phys. J. A **34**, 69 (2007) [arXiv:0710.0306 [nucl-th]].

[67] L. Tiator, D. Drechsel, S. S. Kamalov and M. Vanderhaeghen, Eur. Phys. J. ST **198**, 141 (2011) [arXiv:1109.6745 [nucl-th]].

[68] H. Kamano, S. X. Nakamura, T.-S. H. Lee and T. Sato, Phys. Rev. C **88**, 035209 (2013) [arXiv:1305.4351 [nucl-th]].

[69] N. Suzuki, T. Sato and T.-S. H. Lee, Phys. Rev. C **82**, 045206 (2010) [arXiv:1006.2196 [nucl-th]].

[70] M. W. Paris, Phys. Rev. C **79**, 025208 (2009) [arXiv:0802.3383 [nucl-th]].

[71] B. Juliá Díaz, T.-S. H. Lee, A. Matsuyama, T. Sato and L. C. Smith, Phys. Rev. C **77**, 045205 (2008) [arXiv:0712.2283 [nucl-th]].

[72] B. Juliá Díaz, T.-S. H. Lee, A. Matsuyama and T. Sato, Phys. Rev. C **76**, 065201 (2007) [arXiv:0704.1615 [nucl-th]].

[73] A. Matsuyama, T. Sato and T.-S. H. Lee, Phys. Rept. **439**, 193 (2007) [arXiv:nucl-th/0608051].

[74] L. Tiator, S. S. Kamalov, S. Ceci, G. Y. Chen, D. Drechsel, A. Svarc and S. N. Yang, Phys. Rev. C **82**, 055203 (2010) [arXiv:1007.2126 [nucl-th]].

[75] G. Y. Chen, S. S. Kamalov, S. N. Yang, D. Drechsel and L. Tiator, Phys. Rev. C **76**, 035206 (2007) [arXiv:nucl-th/0703096].

[76] C. Fernández-Ramírez, E. Moya de Guerra and J. M. Udías, Annals Phys. **321**, 1408 (2006) [nucl-th/0509020].

[77] V. Pascalutsa and J. A. Tjon, Phys. Rev. C **70**, 035209 (2004) [nucl-th/0407068].

[78] M. G. Fuda and H. Alharbi, Phys. Rev. C **68**, 064002 (2003).

[79] D. Rönchen, M. Döring, F. Huang, H. Haberzettl, J. Haidenbauer, C. Hanhart, S. Krewald, U.-G. Meißner and K. Nakayama, Eur. Phys. J. A **49**, 44 (2013) [arXiv:1211.6998 [nucl-th]].

[80] Figures representing the full solution of this study and tables of hadronic transitions among the channels πN, ηN, $K\Lambda$, and $K\Sigma$ can be downloaded at `http://collaborations.fz-juelich.de/ikp/meson-baryon/main`.

[81] M. Döring, C. Hanhart, F. Huang, S. Krewald, U.-G. Meißner and D. Rönchen, Nucl. Phys. A **851**, 58 (2011) [arXiv:1009.3781 [nucl-th]].

[82] M. Döring, C. Hanhart, F. Huang, S. Krewald and U.-G. Meißner, Phys. Lett. B **681**, 26 (2009) [arXiv:0903.1781 [nucl-th]].

[83] M. Döring, C. Hanhart, F. Huang, S. Krewald and U.-G. Meißner, Nucl. Phys. A **829**, 170 (2009) [arXiv:0903.4337 [nucl-th]].

[84] A. M. Gasparyan, J. Haidenbauer, C. Hanhart and J. Speth, Phys. Rev. C **68**, 045207 (2003) [arXiv:nucl-th/0307072].

[85] O. Krehl, C. Hanhart, S. Krewald and J. Speth, Phys. Rev. C **62**, 025207 (2000) [arXiv:nucl-th/9911080].

[86] S. Ceci, M. Döring, C. Hanhart, S. Krewald, U.-G. Meißner and A. Švarc, Phys. Rev. C **84**, 015205 (2011) [arXiv:1104.3490 [nucl-th]].

[87] A. V. Anisovich, E. Klempt, V. A. Nikonov, A. V. Sarantsev and U. Thoma, [arXiv:1310.3610 [nucl-ex]].

[88] M. Döring, J. Haidenbauer, U.-G. Meißner and A. Rusetsky, Eur. Phys. J. A **47**, 163 (2011) [arXiv:1108.0676 [hep-lat]].

[89] C. B. Lang and V. Verduci, Phys. Rev. D **87**, no. 5, 054502 (2013) [arXiv:1212.5055].

[90] G. P. Engel, C. B. Lang, D. Mohler and A. Schäfer, Phys. Rev. D **87**, 074504 (2013) [arXiv:1301.4318 [hep-lat]].

[91] C. Alexandrou, J. W. Negele, M. Petschlies, A. Strelchenko and A. Tsapalis, Phys. Rev. D **88**, 031501 (2013) [arXiv:1305.6081 [hep-lat]].

[92] M. Lage, U.-G. Meißner and A. Rusetsky, Phys. Lett. B

681, 439 (2009) [arXiv:0905.0069 [hep-lat]].
[93] M. Döring, U.-G. Meißner, E. Oset and A. Rusetsky, Eur. Phys. J. A **48**, 114 (2012) [arXiv:1205.4838 [hep-lat]].
[94] M. Döring and U.-G. Meißner, JHEP **1201**, 009 (2012) [arXiv:1111.0616 [hep-lat]].
[95] M. Döring, U.-G. Meißner, E. Oset and A. Rusetsky, Eur. Phys. J. A **47**, 139 (2011) [arXiv:1107.3988 [hep-lat]].
[96] M. Döring, M. Mai and U.-G. Meißner, Phys. Lett. B **722**, 185 (2013) [arXiv:1302.4065 [hep-lat]].
[97] F. Huang, M. Döring, H. Haberzettl, J. Haidenbauer, C. Hanhart, S. Krewald, U.-G. Meißner and K. Nakayama, Phys. Rev. C **85**, 054003 (2012) [arXiv:1110.3833 [nucl-th]].
[98] H. Haberzettl, F. Huang and K. Nakayama, Phys. Rev. C **83**, 065502 (2011) [arXiv:1103.2065 [nucl-th]].
[99] H. Haberzettl, K. Nakayama, S. Krewald, Phys. Rev. **C74** , 045202 (2006) [nucl-th/0605059].
[100] H. Haberzettl, Phys. Rev. C **56**, 2041 (1997) [nucl-th/9704057].
[101] W. Chen, H. Gao, W. J. Briscoe, D. Dutta, A. E. Kudryavtsev, M. Mirazita, M. W. Paris, P. Rossi *et al.*, Phys. Rev. C **86**, 015206 (2012) [arXiv:1203.4412 [hep-ph]].
[102] R. L. Workman, Phys. Rev. C **83**, 035201 (2011) [arXiv:1007.3041 [nucl-th]].
[103] M. W. Paris and R. L. Workman, Phys. Rev. C **82**, 035202 (2010) [arXiv:1004.0455 [nucl-th]].
[104] R. A. Arndt, W. J. Briscoe, I. I. Strakovsky and R. L. Workman, Phys. Rev. C **66**, 055213 (2002) [nucl-th/0205067].
[105] M. Döring and K. Nakayama, Eur. Phys. J. A **43** 83 (2010) [arXiv:0906.2949 [nucl-th]].
[106] C. Hanhart, Phys. Lett. B **715** 170 (2012) [arXiv:1203.6839 [hep-ph]].
[107] D. Morgan and M. R. Pennington, Z. Phys. C **37**, 431 (1988) [Erratum-ibid. C **39**, 590 (1988)].
[108] W. Chen, T. Mibe, D. Dutta, H. Gao, J. M. Laget, M. Mirazita, P. Rossi and S. Stepanyan *et al.*, Phys. Rev. Lett. **103**, 012301 (2009) [arXiv:0903.1260 [nucl-ex]].
[109] G. Mandaglio *et al.* [Graal Collaboration], Phys. Rev. C **82**, 045209 (2010) [arXiv:1010.1715 [nucl-ex]].
[110] W. J. Briscoe, A. E. Kudryavtsev, P. Pedroni, I. I. Strakovsky, V. E. Tarasov and R. L. Workman, Phys. Rev. C **86**, 065207 (2012) [arXiv:1209.0024 [nucl-th]].
[111] V. E. Tarasov, W. J. Briscoe, H. Gao, A. E. Kudryavtsev and I. I. Strakovsky, Phys. Rev. C **84**, 035203 (2011) [arXiv:1105.0225 [hep-ph]].
[112] S. Weinberg, Phys. Rev. Lett. **17**, 616 (1966).
[113] V. Bernard, N. Kaiser and U.-G. Meißner, Phys. Lett. B **309**, 421 (1993) [hep-ph/9304275].
[114] U.-G. Meißner and S. Steininger, Phys. Lett. B **419**, 403 (1998) [hep-ph/9709453].
[115] A. M. Bernstein, Phys. Lett. B **442**, 20 (1998) [hep-ph/9810376].
[116] F. Huang, H. Haberzettl and K. Nakayama, Phys. Rev. C **87**, 054004 (2013) [arXiv:1208.2279 [nucl-th]].
[117] K. Nakayama, Y. Oh and H. Haberzettl, J. Korean Phys. Soc. **59**, 224 (2011) [arXiv:0803.3169 [hep-ph]].
[118] M. Dugger, B. G. Ritchie, P. Collins, E. Pasyuk, W. J. Briscoe, I. I. Strakovsky, R. L. Workman, Y. Azimov *et al.*, [arXiv:1308.4028 [nucl-ex]].
[119] A. V. Anisovich, E. Klempt, V. A. Nikonov, A. V. Sarantsev and U. Thoma, Eur. Phys. J. A **47**, 153 (2011) [arXiv:1109.0970 [hep-ph]].
[120] V. Crede *et al.* [CBELSA/TAPS Collaboration], Phys. Rev. C **84**, 055203 (2011) [arXiv:1107.2151 [nucl-ex]].
[121] J. P. Ader, M. Capdeville and Ph. Salin Nucl. Phys. B **3**,407 (1967).
[122] J. P. Ader, M. Capdeville and P. Salin, Nucl. Phys. B **17**, 221 (1970).
[123] M. Guidal, J. M. Laget and M. Vanderhaeghen, Nucl. Phys. A **627**, 645 (1997).
[124] A. Sibirtsev, J. Haidenbauer, F. Huang, S. Krewald and U.-G. Meißner, Eur. Phys. J. A **40**, 65 (2009) [arXiv:0903.0535 [hep-ph]].
[125] A. Sibirtsev, J. Haidenbauer, S. Krewald, U.-G. Meißner and A. W. Thomas, Eur. Phys. J. A **41**, 71 (2009) [arXiv:0902.1819 [hep-ph]].
[126] O. Bartholomy *et al.* [CB-ELSA Collaboration], Phys. Rev. Lett. **94**, 012003 (2005) [hep-ex/0407022].
[127] M. Dugger, B. G. Ritchie, J. P. Ball, P. Collins, E. Pasyuk, R. A. Arndt, W. J. Briscoe, I. I. Strakovsky *et al.*, Phys. Rev. C **76**, 025211 (2007) [arXiv:0705.0816 [hep-ex]].
[128] G. Buschhorn, P. Heide, U. Kotz, R. A. Lewis, P. Schmuser and H. J. Skronn, Phys. Rev. Lett. **20**, 230 (1968).
[129] B. Bouquet, B. D' Almagne, P. T. Eschstruth, M. Croissiaux, E. F. Erickson, R. Morand, J. P. Pahin, P. Kitching *et al.*, Phys. Rev. Lett. **27**, 1244 (1971).
[130] K. Ekstrand, A. Browman, L. Hand and M. E. Nordberg, Phys. Rev. D **6**, 1 (1972).
[131] R. A. Alvarez, G. Cooperstein, K. Kalata, R. C. Lanza and D. Luckey, Phys. Rev. D **1**, 1946 (1970).
[132] G. Buschhorn, J. Carroll, R. D. Eandi, P. Heide, R. Hubner, W. Kern, U. Kotz, P. Schmuser *et al.*, Phys. Rev. Lett. **17**, 1027 (1966).
[133] G. Buschhorn, J. Carroll, R. D. Eandi, P. Heide, R. Hubner, W. Kern, U. Kotz, P. Schmuser *et al.*, Phys. Rev. Lett. **18**, 571 (1967).
[134] M. Dugger *et al.* [CLAS Collaboration], Phys. Rev. C **79**, 065206 (2009) [arXiv:0903.1110 [hep-ex]].
[135] A. Schmidt, P. Achenbach, J. Ahrens, H. J. Arends, R. Beck, A. M. Bernstein, V. Hejny, M. Kotulla *et al.*, Phys. Rev. Lett. **87**, 232501 (2001) [Erratum-ibid. **110**, 039903 (2013)] [nucl-ex/0105010].
[136] M. Fuchs, J. Ahrens, G. Anton, R. Averbeck, R. Beck, A. M. Bernstein, A. R. Gabler, F. Härter *et al.*, Phys. Lett. B **368**, 20 (1996).
[137] R. Beck, F. Kalleicher, B. Schoch, J. Vogt, G. Koch, H. Ströher, V. Metag, J. C. McGeorge *et al.*, Phys. Rev. Lett. **65**, 1841 (1990).
[138] D. Hornidge *et al.* [A2 and CB-TAPS Collaboration], Phys. Rev. Lett. **111**, 062004 (2013) [arXiv:1211.5495 [nucl-ex]].
[139] J. C. Bergstrom, R. Igarashi and J. M. Vogt, Phys. Rev. C **55**, 2016 (1997).
[140] W. Hitzeroth, Nuovo Cim. A **60**, 467 (1969).
[141] R. Beck, Eur. Phys. J. A **28S1**, 173 (2006).
[142] J. Ahrens *et al.* [GDH and A2 Collaboration], Eur. Phys. J. A **21**, 323 (2004).
[143] O. Bartalini *et al.* [GRAAL Collaboration], Eur. Phys. J. A **26**, 399 (2005).
[144] J. Ahrens *et al.* [GDH and A2 Collaborations], Phys.

Rev. Lett. **88**, 232002 (2002) [hep-ex/0203006].
[145] M. Sumihama, J. K. Ahn, H. Akimune, Y. Asano, W. C. Chang, S. Date, H. Ejiri, H. Fujimura *et al.*, Phys. Lett. B **657**, 32 (2007) [arXiv:0708.1600 [nucl-ex]].
[146] E. Korkmaz, N. R. Kolb, D. A. Hutcheon, G. V. O'Rielly, J. C. Bergstrom, G. Feldman, D. Jordan, A. K. Opper *et al.*, Phys. Rev. Lett. **83**, 3609 (1999).
[147] K. G. Fissum, H. S. Caplan, E. L. Hallin, D. M. Skopik, J. M. Vogt, M. Frodyma, D. P. Rosenzweig, D. W. Storm *et al.*, Phys. Rev. C **53**, 1278 (1996).
[148] J. K. Walker and J. P. Burq, Phys. Rev. Lett. **8**, 37 (1962).
[149] D. W. G. S. Leith, R. Little and E. M. Lawson, Phys. Lett. **8**, 355 (1964).
[150] H. B. van den Brink, H. P. Blok, H. T. Chung, H. Choi, T. Gresko, E. L. Hallin, W. H. A. Hesselink, T. Kobayashi *et al.*, Nucl. Phys. A **587**, 657 (1995).
[151] K. Büchler, K. H. Althoff, G. Anton, J. Arends, W. Beulertz, M. Breuer, P. Detemple, H. Dutz *et al.*, Nucl. Phys. A **570**, 580 (1994).
[152] G. Fischer, H. Fischer, M. Heuel, G. Von Holtey, G. Knop and J. Stumpfig, Nucl. Phys. B **16**, 119 (1970).
[153] G. Fischer, G. Von Holtey, G. Knop and J. Stuempfig, Z. Phys. **253**, 38 (1972).
[154] D. Branford, J. A. MacKenzie, F. X. Lee, J. Ahrens, J. R. M. Annand, R. Beck, G. E. Cross, T. Davinson *et al.*, Phys. Rev. C **61**, 014603 (2000).
[155] T. Fujii, T. Kondo, F. Takasaki, S. Yamada, S. Homma, K. Huke, S. Kato, H. Okuno *et al.*, Nucl. Phys. B **120**, 395 (1977).
[156] E. A. Knapp, R. W. Kenney and V. Perez-Mendez, Phys. Rev. **114**, 605 (1959).
[157] R. Beck, H. P. Krahn, J. Ahrens, J. R. M. Annand, H. J. Arends, G. Audit, A. Braghieri, N. d'Hose *et al.*, Phys. Rev. C **61**, 035204 (2000) [nucl-ex/9908017].
[158] T. Fujii, H. Okuno, S. Orito, H. Sasaki, T. Nozaki, F. Takasaki, Takikawa, K. Amako *et al.*, Phys. Rev. Lett. **26**, 1672 (1971).
[159] H. W. Dannhausen, E. J. Durwen, H. M. Fischer, M. Leneke, W. Niehaus and F. Takasaki, Eur. Phys. J. A **11**, 441 (2001).
[160] J. Ahrens, S. Altieri, J. R. M. Annand, H. -J. Arends, R. Beck, C. Bradtke, A. Braghieri, N. d'Hose *et al.*, Phys. Rev. C **74**, 045204 (2006).
[161] S. D. Ecklund and R. L. Walker, Phys. Rev. **159**, 1195 (1967).
[162] J. R. Kilner, Ph.D. thesis (1962)
[163] R. A. Alvarez, G. Cooperstein, K. Kalata, R. C. Lanza and D. Luckey, Phys. Rev. D **1**, 1946 (1970).
[164] L. Y. Zhu *et al.* [Jefferson Lab Hall A and Jefferson Lab E94-104 Collaborations], Phys. Rev. C **71**, 044603 (2005) [nucl-ex/0409018].
[165] G. Blanpied, M. Blecher, A. Caracappa, R. Deininger, C. Djalali, G. Giordano, K. Hicks, S. Hoblit *et al.*, Phys. Rev. C **64**, 025203 (2001).
[166] F. V. Adamian, A. Y. Bunyatyan, G. S. Frangulian, P. I. Galumian, V. H. Grabsky, A. V. Airapetian, H. H. Hakopian, V. K. Hoktanian *et al.*, Phys. Rev. C **63**, 054606 (2001) [nucl-ex/0011006].
[167] D. Elsner *et al.* [CBELSA and TAPS Collaborations], Eur. Phys. J. A **39**, 373 (2009) [arXiv:0810.1849 [nucl-ex]].
[168] N. Sparks *et al.* [CBELSA/TAPS Collaboration], Phys. Rev. C **81**, 065210 (2010). [arXiv:1003.1346 [nucl-ex]]
[169] J. Ajaka *et al.* [GRAAL Collaboration], Phys. Lett. B **475**, 372 (2000).
[170] O. Bartalini *et al.* [GRAAL and GW-SAID Group Collaborations], Phys. Lett. B **544**, 113 (2002) [nucl-ex/0207010].
[171] A. Bock, G. Anton, W. Beulertz, C. Bradtke, H. Dutz, R. Gehring, S. Goertz, K. Helbing *et al.*, Phys. Rev. Lett. **81**, 534 (1998).
[172] A. A. Belyaev, V. A. Getman, V. G. Gorbenko, V. A. Gushchin, A. Y. .Derkach, Y. V. Zhebrovsky, I. M. Karnaukhov, L. Y. .Kolesnikov *et al.*, Nucl. Phys. B **213**, 201 (1983).
[173] M. Fukushima, N. Horikawa, R. Kajikawa, H. Kobayakawa, K. Mori, T. Nakanishi, C. O. Pak, S. Suzuki *et al.*, Nucl. Phys. B **136**, 189 (1978).
[174] P. S. L. Booth, L. J. Carroll, G. R. Court, P. R. Daniel, R. Gamet, C. J. Hardwick, P. J. Hayman, J. R. Holt *et al.*, Nucl. Phys. B **121**, 45 (1977).
[175] H. Herr, D. Husmann, W. Jansen, V. Kadansky, B. Lohr, W. Meyer, H. Schilling and T. Yamaki, Nucl. Phys. B **125**, 157 (1977).
[176] P. J. Bussey, C. Raine, J. G. Rutherglen, P. S. L. Booth, L. J. Carroll, G. R. Court, P. R. Daniel, A. W. Edwards *et al.*, Nucl. Phys. B **154**, 492 (1979).
[177] H. Dutz, D. Krämer, B. Zucht, K. H. Althoff, G. Anton, J. Arends, W. Beulertz, A. Bock *et al.*, Nucl. Phys. A **601**, 319 (1996).
[178] V. A. Getman, V. G. Gorbenko, A. Y. Derkach, Y. V. Zhebrovsky, I. M. Karnaukhov, L. Y. Kolesnikov, A. A. Lukhanin, A. L. Rubashkin *et al.*, Nucl. Phys. B **188**, 397 (1981).
[179] M. Fukushima, N. Horikawa, R. Kajikawa, H. Kobayakawa, K. Mori, T. Nakanishi, C. O. Pak, S. Suzuki *et al.*, Nucl. Phys. B **130**, 486 (1977).
[180] P. J. Bussey, C. Raine, J. G. Rutherglen, P. S. L. Booth, L. J. Carroll, G. R. Court, P. R. Daniel, A. W. Edwards *et al.*, Nucl. Phys. B **154**, 205 (1979).
[181] K. H. Althoff, R. Conrad, M. Gies, H. Herr, V. Kadansky, O. Kaul, K. Konigsmann, G. Lenzen *et al.*, Phys. Lett. B **63**, 107 (1976).
[182] K. H. Althoff, M. Gies, H. Herr, V. Kadansky, O. Kaul, K. Königsmann, D. Menze, W. Meyer *et al.*, Nucl. Phys. B **131**, 1 (1977).
[183] K. Fujii, H. Hayashii, S. Iwata, R. Kajikawa, A. Miyamoto, T. Nakanishi, Y. Ohashi, S. Okumi *et al.*, Nucl. Phys. B **197**, 365 (1982).
[184] K. H. Althoff, D. Finken, N. Minatti, H. Piel, D. Trines and M. Unger, Phys. Lett. B **26**, 677 (1968).
[185] K. H. Althoff, K. Kramp, H. Matthay and H. Piel, Z. Phys. **194**, 135 (1966).
[186] K. H. Althoff, K. Kramp, H. Matthay and H. Piel, Z. Phys. **194**, 144 (1966).
[187] P. Blum, P. Brinckmann, R. Brockmann, P. Lutter, W. Mohr and R. Sauerwein, Z. Phys. A **277**, 311 (1976).
[188] P. Blum, R. Brockmann and W. Mohr, Z. Phys. A **278**, 275 (1976).
[189] V. G. Gorbenko, A. I. Derebchinskii, Y. V. Zhebrovskii, A. A. Zybalov, O. G. Konovaloo, V. I. Nikiforov, A. L. Rubashkin, P. V. Sorokin and A. E. Tenishev, Sov. J. Nucl. Phys. **27**, 638 (1978).
[190] A. S. Bratashevsky, V. G. Gorbenko, A. I. Derebchinsky, A. Y. Derkach, Y. V. Zhebrovsky, A. A. Zybalov, I. M. Karnaukhov and L. Y. Kolesnikov *et al.*, Nucl.

Phys. B **166**, 525 (1980).
[191] V. G. Gorbenko *et al.*, JETP Lett. **19**, 340 (1974).
[192] V. G. Gorbenko *et al.*, JETP Lett. **22**, 186 (1975).
[193] V. G. Gorbenko *et al.*, Sov. J. Nucl. Phys. **26**, 167 (1977).
[194] A. I. Derebchinsky *et al.*, JETP **43**, 218 (1976).
[195] A. S. Bratashevsky *et al.*, Sov. J. Nucl. Phys. **42**, 417 (1985).
[196] A. S. Bratashevsky *et al.*, Sov. J. Nucl. Phys. **35**, 33 (1982).
[197] A. A. Zybalov *et al.*, Sov. J. Nucl. Phys. **28**, 52 (1978).
[198] N. V. Goncharov *et al.*, JETP **37**, 205 (1973).
[199] A. S. Bratashevsky *et al.*, Sov. J. Nucl. Phys. **38**, 233 (1983).
[200] A. S. Bratashevsky *et al.*, Sov. J. Nucl. Phys. **46**, 635 (1987).
[201] A. S. Bratashevsky *et al.*, Sov. J. Nucl. Phys. **33**, 538 (1981).
[202] A. S. Bratashevsky *et al.*, Sov. J. Nucl. Phys. **41**, 960 (1985).
[203] A. I. Derebchinsky *et al.*, JETP **39**, 30 (1974).
[204] S. Kato, T. Miyachi, K. Sugano, K. Toshioka, K. Ukai, M. Chiba, K. Egawa, T. Ishii *et al.*, Nucl. Phys. B **168**, 1 (1980).
[205] S. Kayakawa *et al.*, J. Phys. Soc. Jap. **25**, 307 (1968).
[206] S. Kabe, T. Fujii, T. Kamei, R. Yamada, T. Yamagata, S. Kato, I. Kita and T. Kiyoshima, Nucl. Phys. B **50**, 17 (1972).
[207] J. O. Maloy, V. Z. Peterson, G. A. Salandin, F. Waldner, A. Manfredini, J. I. Friedman and H. Kendall, Phys. Rev. **139**, B733 (1965).
[208] E. D. Bloom, C. A. Heusch, C. Y. Prescott and L. S. Rochester, Phys. Rev. Lett. **19**, 671 (1967).
[209] R. Querzoli, G. Salvini and A. Silverman, Nuovo Cim. **19**, no. 1, 53 (1961).
[210] L. Bertanza, I. Mannelli, S. Santucci, G. V. Silvestrini and V. Z. Peterson, Nuovo Cim. **24**, no. 4, 734 (1962).
[211] R. O. Avakyan *et al.*, Sov. J. Nucl. Phys. **37**, 199 (1983).
[212] R. O. Avakyan *et al.*, Sov. J. Nucl. Phys. **46**, 853 (1987).
[213] R. O. Avakyan *et al.*, Sov. J. Nucl. Phys. **48**, 1030 (1988).
[214] N. M. Agababyan *et al.*, Sov. J. Nucl. Phys. **50**, 834 (1989).
[215] M. M. Asaturyan *et al.*, JETP Lett. **44**, 341 (1986).
[216] R. O. Avakyan *et al.*, Sov. J. Nucl. Phys. **53**, 448 (1991).
[217] K. Wijesooriya, A. Afanasev, M. Amarian, K. Aniol, S. Becher, K. Benslama, L. Bimbot, P. Bosted *et al.*, Phys. Rev. C **66**, 034614 (2002).
[218] W. Luo *et al.* [GEp-III and GEp2γ Collaborations], Phys. Rev. Lett. **108**, 222004 (2012) [arXiv:1109.4650 [nucl-ex]].
[219] M. N. Prentice, R. Railton, J. G. Rutherglen, K. M. Smith, G. R. Brookes, P. J. Bussey, F. H. Combley, G. H. Eaton *et al.*, Nucl. Phys. B **41**, 353 (1972).
[220] N. Tanaka, M. M. Castro, R. H. Milburn, W. B. Richards, J. P. Rutherfoord, B. F. Stearns, M. Deutsch, P. M. Patel *et al.*, Phys. Rev. D **8**, 1 (1973).
[221] V. A. Getman *et al.*, Journal of Kharkov Physical Technical Institute, Voprosu Atomnoi Nauki i Techniki **8**, 3 (1989).
[222] A. Thiel, A. V. Anisovich, D. Bayadilov, B. Bantes, R. Beck, Y. Beloglazov, M. Bichow, S. Bose *et al.*, Phys. Rev. Lett. **109**, 102001 (2012) [arXiv:1207.2686 [nucl-ex]].
[223] J. Ahrens, S. Altieri, J. R. Annand, H. J. Arends, R. Beck, A. Braghieri, N. d'Hose, H. Dutz *et al.*, Eur. Phys. J. A **26**, 135 (2005).
[224] P. J. Bussey, J. G. Rutherglen, P. S. L. Booth, L. J. Carroll, G. R. Court, A. W. Edwards, R. Gamet, P. J. Hayman *et al.*, Nucl. Phys. B **159**, 383 (1979).
[225] P. S. L. Booth, Bonn University Annual Report, 1977.
[226] A. A. Belyaev *et al.*, Sov. J. Nucl. Phys. **40**, 83 (1984).
[227] P. J. Bussey, J. G. Rutherglen, P. S. L. Booth, L. J. Carroll, G. R. Court, P. R. Daniel, A. W. Edwards and R. Gamet *et al.*, Nucl. Phys. B **169**, 403 (1980).
[228] A. A. Belyaev *et al.*, Sov. J. Nucl. Phys. **43**, 947 (1983).
[229] P. J. Bussey, *Physik Daten*, 1977 (unpublished).
[230] M. Gottschall *et al.* [CBELSA/TAPS Collaboration], [arXiv:1312.2187 [nucl-ex]]
[231] H. van Pee *et al.* [CB-ELSA Collaboration], Eur. Phys. J. A **31**, 61 (2007) [arXiv:0704.1776 [nucl-ex]].
[232] M. H. Sikora, D. P. Watts, D. I. Glazier, P. Aguar-Bartolome, L. K. Akasoy, J. R. M. Annand, H. J. Arends, K. Bantawa *et al.*, arXiv:1309.7897 [nucl-ex].
[233] A. Afanasev, C. E. Carlson and C. Wahlquist, Phys. Lett. B **398**, 393 (1997) [[hep-ph/9701215]].
[234] G. R. Farrar, K. Huleihel and H. -y. Zhang, Nucl. Phys. B **349**, 655 (1991).
[235] L. Tiator, PWA7 workshop, 09/24/2013, Camogli, Italy.
[236] V. Bernard, N. Kaiser and U.-G. Meißner, Phys. Lett. B **378**, 337 (1996) [hep-ph/9512234].
[237] M. Lenkewitz, E. Epelbaum, H. W. Hammer and U.-G. Meißner, Eur. Phys. J. A **49**, 20 (2013) [arXiv:1209.2661 [nucl-th]].
[238] O. Hanstein, D. Drechsel and L. Tiator, Phys. Lett. B **399**, 13 (1997) [nucl-th/9612057].
[239] S. S. Kamalov, G.-Y. Chen, S.-N. Yang, D. Drechsel and L. Tiator, Phys. Lett. B **522**, 27 (2001) [nucl-th/0107017].
[240] V. Bernard, N. Kaiser and U.-G. Meißner, Eur. Phys. J. A **11** (2001) 209 [hep-ph/0102066].
[241] M. Döring, D. Jido and E. Oset, Eur. Phys. J. A **45**, 319 (2010) [arXiv:1002.3688 [nucl-th]].
[242] D. Jido, M. Döring and E. Oset, Phys. Rev. C **77**, 065207 (2008) [arXiv:0712.0038 [nucl-th]].
[243] L. S. Geng, E. Oset and M. Döring, Eur. Phys. J. A **32**, 201 (2007) [hep-ph/0702093].
[244] M. Döring, E. Oset and S. Sarkar, Phys. Rev. C **74**, 065204 (2006) [nucl-th/0601027].
[245] J. Beringer *et al.* [Particle Data Group Collaboration], Phys. Rev. D **86**, 010001 (2012).
[246] R. L. Workman, L. Tiator and A. Sarantsev, Phys. Rev. C **87**, 068201 (2013) [arXiv:1304.4029 [nucl-th]].
[247] R. A. Arndt, R. L. Workman, Z. Li and L. D. Roper, Phys. Rev. C **42**, 1853 (1990).
[248] R. A. Arndt, R. L. Workman, Z. Li and L. D. Roper, Phys. Rev. C **42**, 1864 (1990).
[249] G. F. Chew, M. L. Goldberger, F. E. Low and Y. Nambu, Phys. Rev. **106**, 1345 (1957).
[250] F. A. Berends, A. Donnachie and D. L. Weaver, Nucl. Phys. B **4**, 1 (1967).
[251] K. Nakayama and W. G. Love, Phys. Rev. C **72**, 034603 (2005).
[252] C. G. Fasano, F. Tabakin, and B. Saghai, Phys. Rev. C **46**, 2430 (1992).
[253] A. M. Sandorfi, B. Dey, A. Sarantsev, L. Tiator, and

37

R. Workmann, AIP Conf. Proc. **1432**, 219 (2012); (see, arXiv:1108.5411v2 for a revised version).

[254] L. Tiator, private communication.

Chapter 5

Conclusion and Outlook

We performed a simultaneous analyses of the reactions $\pi N \to \pi N$, ηN and KY within a dynamical coupled-channel framework and achieved an overall good description of the data. The relevant resonances have been identified and the baryon spectrum in the isospin $I = 1/2$ and $I = 3/2$ sector could be extracted.
Based on this hadronic analysis, we studied the photon-induced reactions $\gamma p \to \pi^0 p$ and $\gamma p \to \pi^+ n$. We were able to obtain a good fit to the data without altering the parameters of the hadronic scattering amplitude, i.e. it was not necessary to include additional genuine resonance states. We determined the photocouplings at the resonance poles.
In the present study, the systematic uncertainties of the extracted resonance parameters have been roughly estimated by performing two different fits. However, a statistical error analysis remains to be done. In principle, this can be achieved by applying the $\chi^2 + 1$ criterion as demonstrated in Ref. [99] in an earlier analyses within the Jülich framework. The uncertainty of a free parameter is given by the range of its value for which the best χ^2_{min} rises by less than $\Delta\chi^2 = 1$, optimizing all other free parameters of the framework at the same time. From those errors the uncertainties of the resonance parameters can be derived. As an example, in Fig. 5.1 we show the pole positions and branching ratios of the $\Delta(1905)5/2^+$ consistent with the $\chi^2 + 1$ criterion determined in Ref. [99]. Such an error analysis entails a considerable numerical effort and is only meaningful if the free parameters are fitted to actual data only. In the present study, however, we used the GWU/SAID partial-wave analysis as input for the elastic πN channel. We therefore postpone the determination of the statistical uncertainties of the resonance parameters to future work.
The extension of the present approach to kaon and eta photoproduction is straightforward and already in progress. Since there is a significant difference in the quality of the data for the pion-induced production of ηN and KY and the high-precision photoproduction data of those final states, an interesting question is wether a refit of the hadronic data will be required. In the hadronic analysis we observed rather strong couplings of some less well-established resonances to the ηN and KY channels. The study of the corresponding photon-induced reactions will help to clarify the nature of those states.
The simultaneous analysis of pion- and photon-induced reactions in one combined micro-

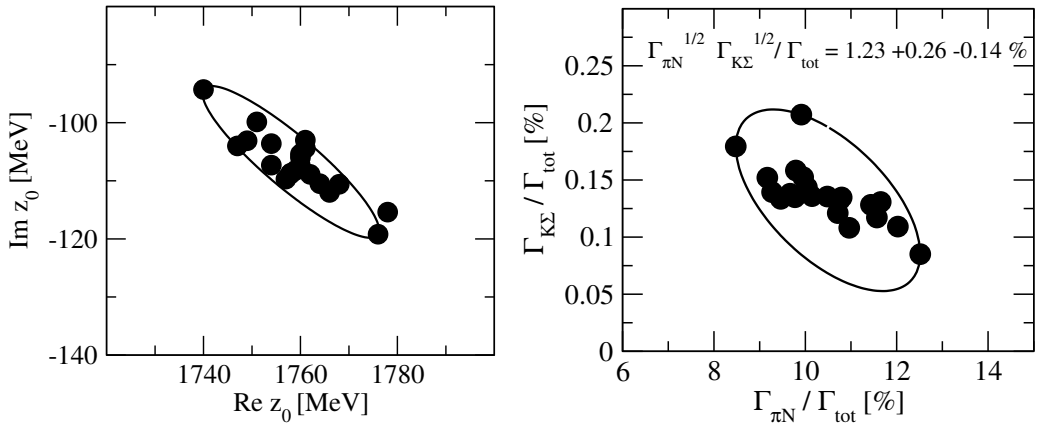

Figure 5.1: Pole positions (left) and branching ratios (right) of the $\Delta(1905)5/2^+$ resonance compatible with the $\chi^2 + 1$ criterion as determined in Ref. [99]. The error of the resonance parameters is given by the maximal range of these solutions. (Figure from Ref. [99])

scopic dynamical coupled-channel framework, employing the gauge invariant approach used in Ref. [114] and the Jülich model is planned for the future. This "complete" calculation will complement the "complete" experiment. Such an analysis is, however, technically and computationally very involved.

In Ref. [143], it has been shown how dynamical coupled-channel approaches can be discretized and evaluated on a momentum lattice. In principle, this enables an analysis of experimental and lattice data on the same footing [144, 145, 146].

Appendix A

Fit results for pion photoproduction

In the following sections we compare the fit results obtained in the study of pion photoproduction as described in Chap. 4 to all single-polarization data included in the analysis. In case of double-polarization observables, all data included are presented in Chap. 4.
In the figures of this appendix, the dashed (blue) lines denote fit 1 and the solid (red) lines represent fit 2.

A.1 Differential cross section

A.1.1 $\gamma p \to \pi^0 p$

Data shown in the figures of this section can be found under the following references:

AB74 [147], AB76 [148], AG75 [149], AH02 [150], AH04 [151], AK77 [152], AK78 [153], AL79 [154], ALBO [155], AM73 [156], AR77 [157], BA05 [136], BaGr [158], BC73 [159], BE90 [160], BE97 [161], BE06 [162], BG68 [163], BG70 [164], BG97 [165], BH71 [166], BH75 [167],BN75 [168], BF75 [169], BO67 [170], BU68 [138], CR11 [135], DE69 [171], DO75 [172], DO77 [173], DU07 [137], FL74 [174], FU96 [175], GZ74 [176], GO68 [177], HA96 [178], HE73 [179], HI69 [180], HO12 [181], HEY73 [182], HU77 [183], JU76 [184], KR99 [185], LO70 [186], SC97 [187], SC01 [188], SC10 [189], SA65 [190], SH79 [191], SU07 [192], TL62 [193], WR67 [194], WC60 [195], WO68 [196], YO80 [197], ZE88 [198].

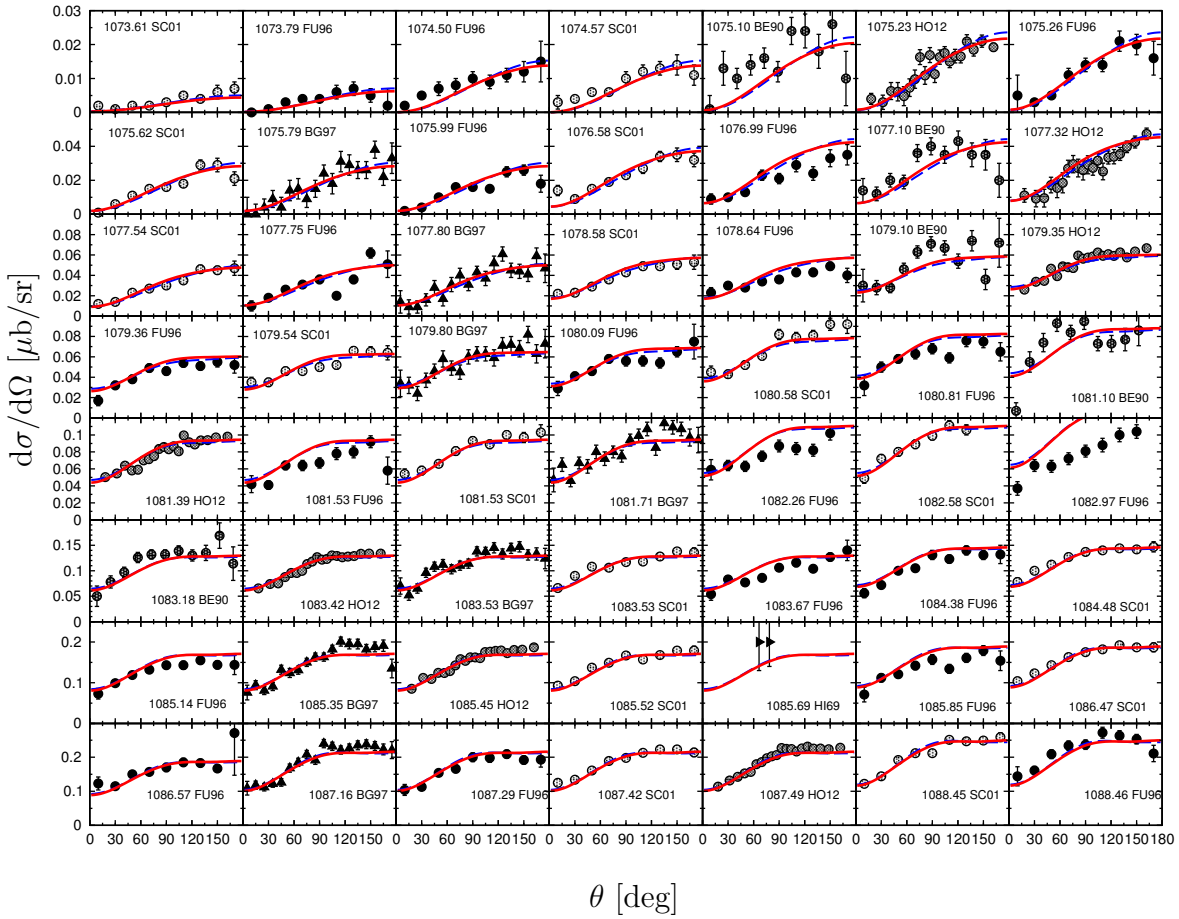

Figure A.1: Differential cross section of the reaction $\gamma p \to \pi^0 p$.

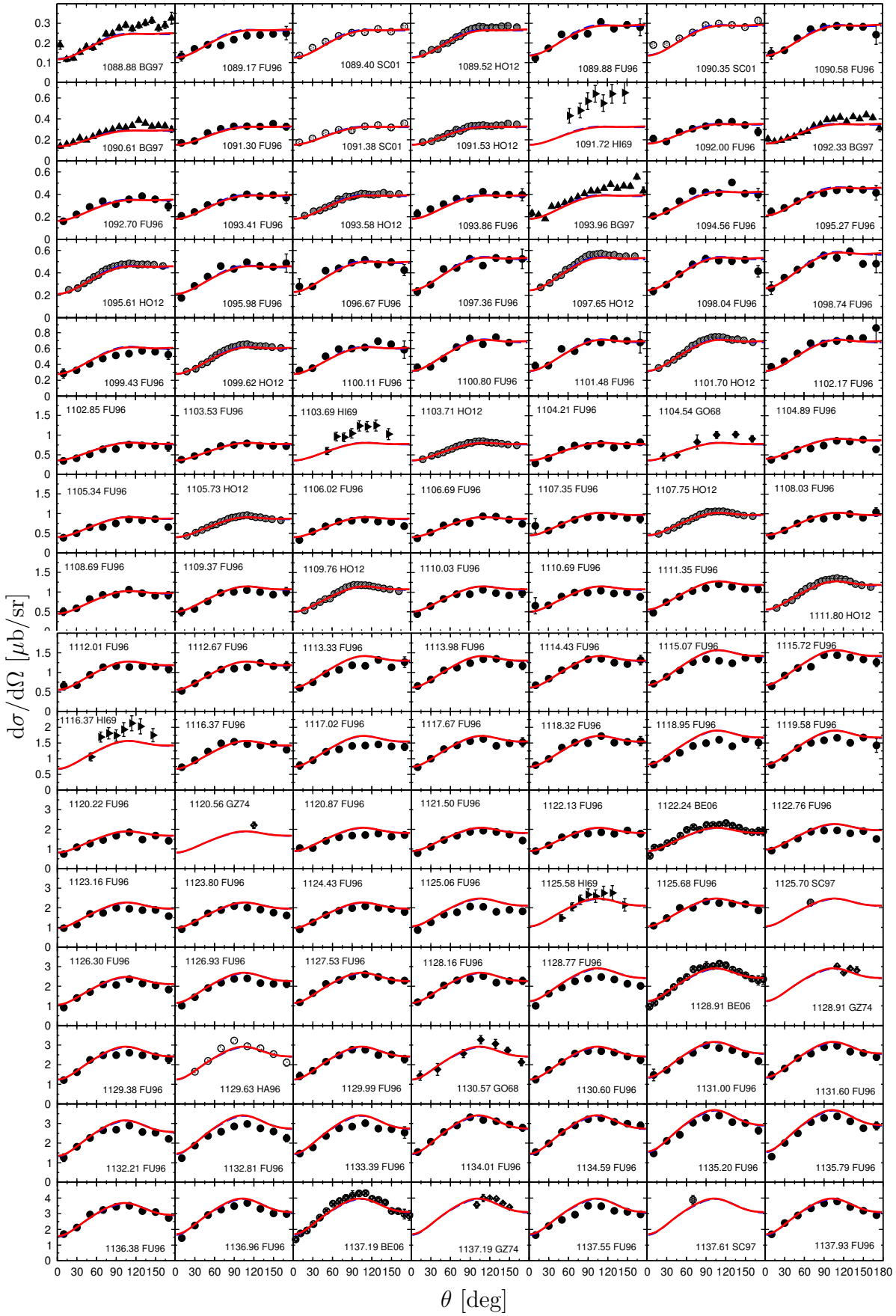

Figure A.2: Differential cross section of the reaction $\gamma p \to \pi^0 p$.

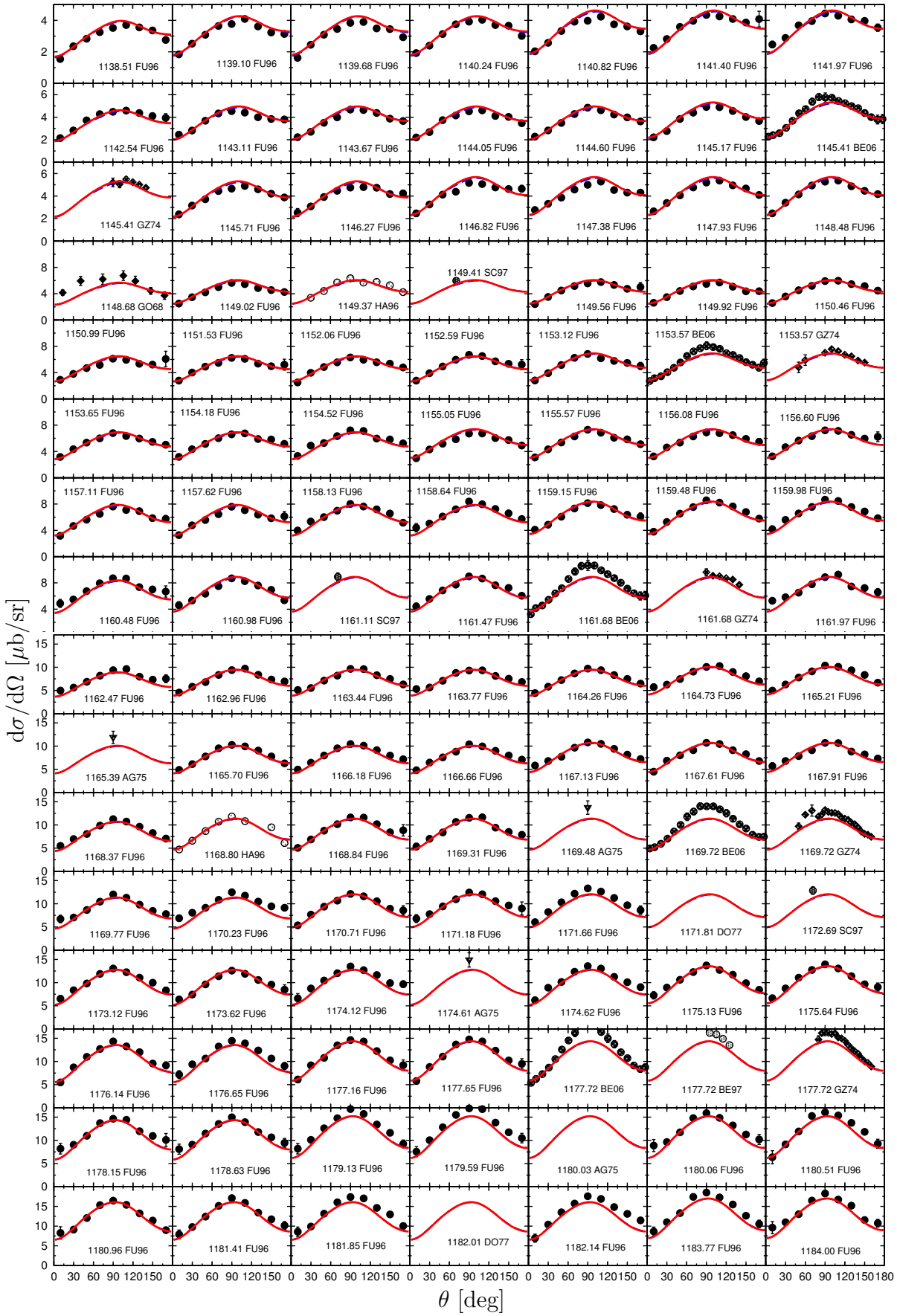

Figure A.3: Differential cross section of the reaction $\gamma p \to \pi^0 p$.

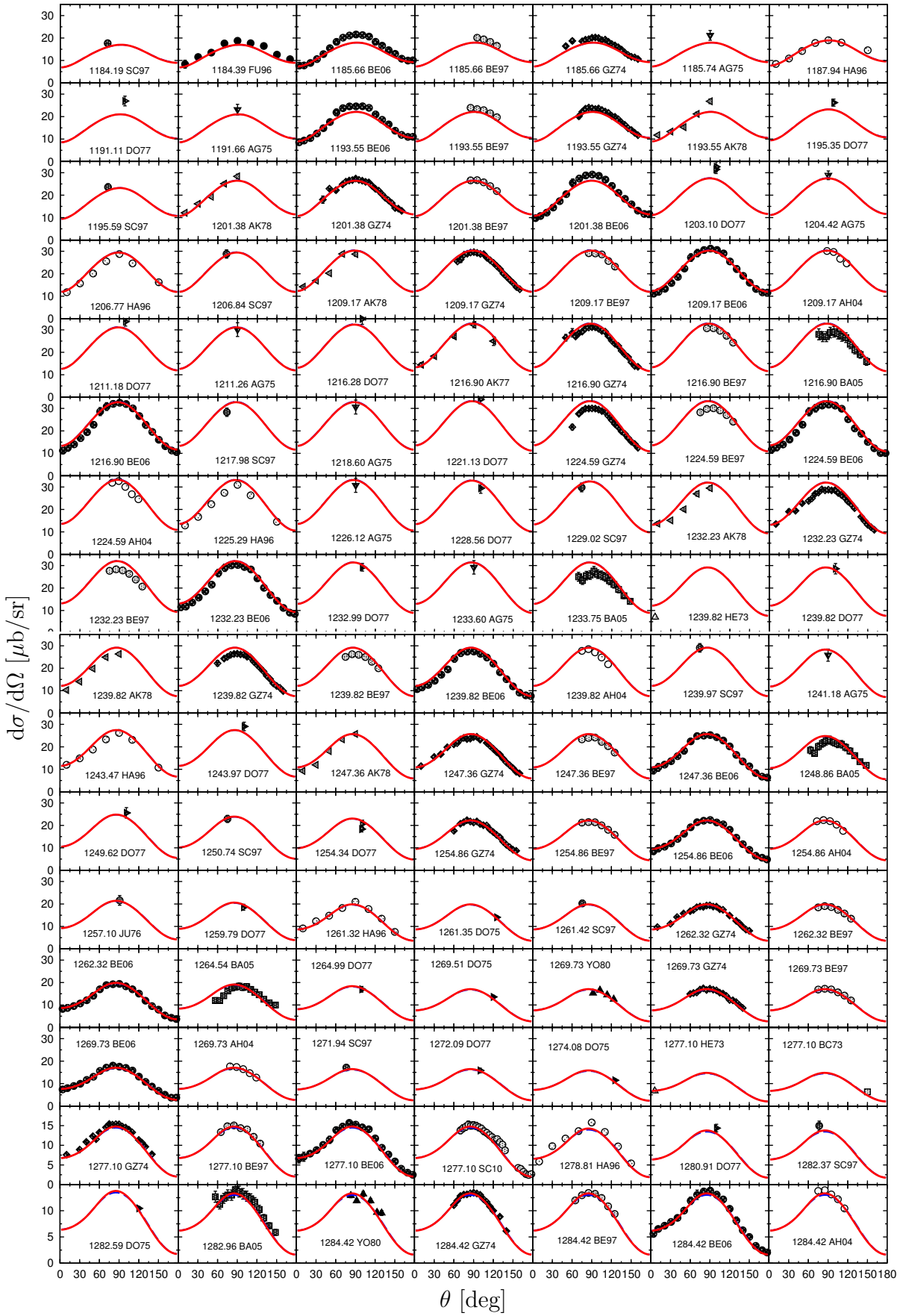

Figure A.4: Differential cross section of the reaction $\gamma p \to \pi^0 p$.

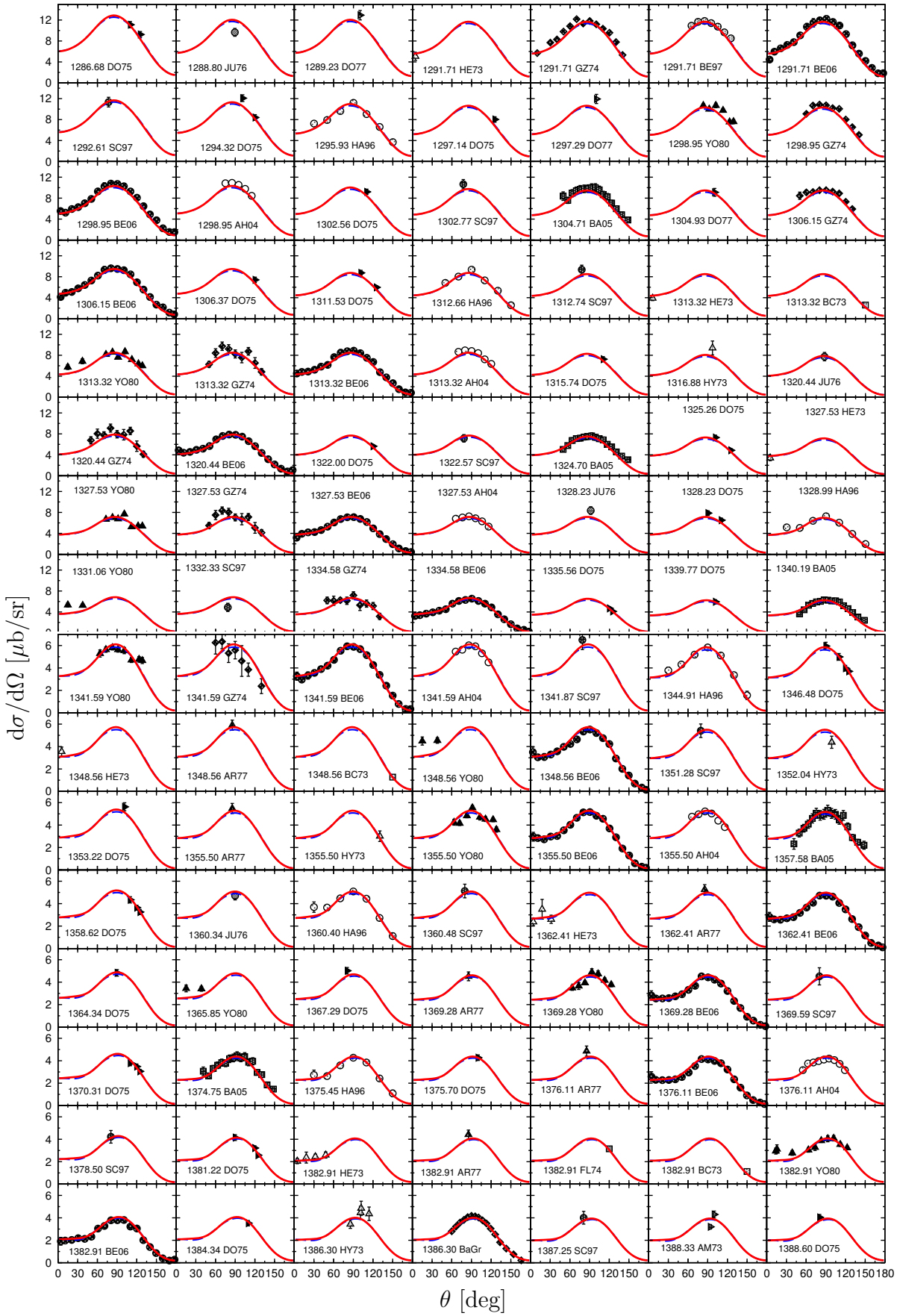

Figure A.5: Differential cross section of the reaction $\gamma p \to \pi^0 p$.

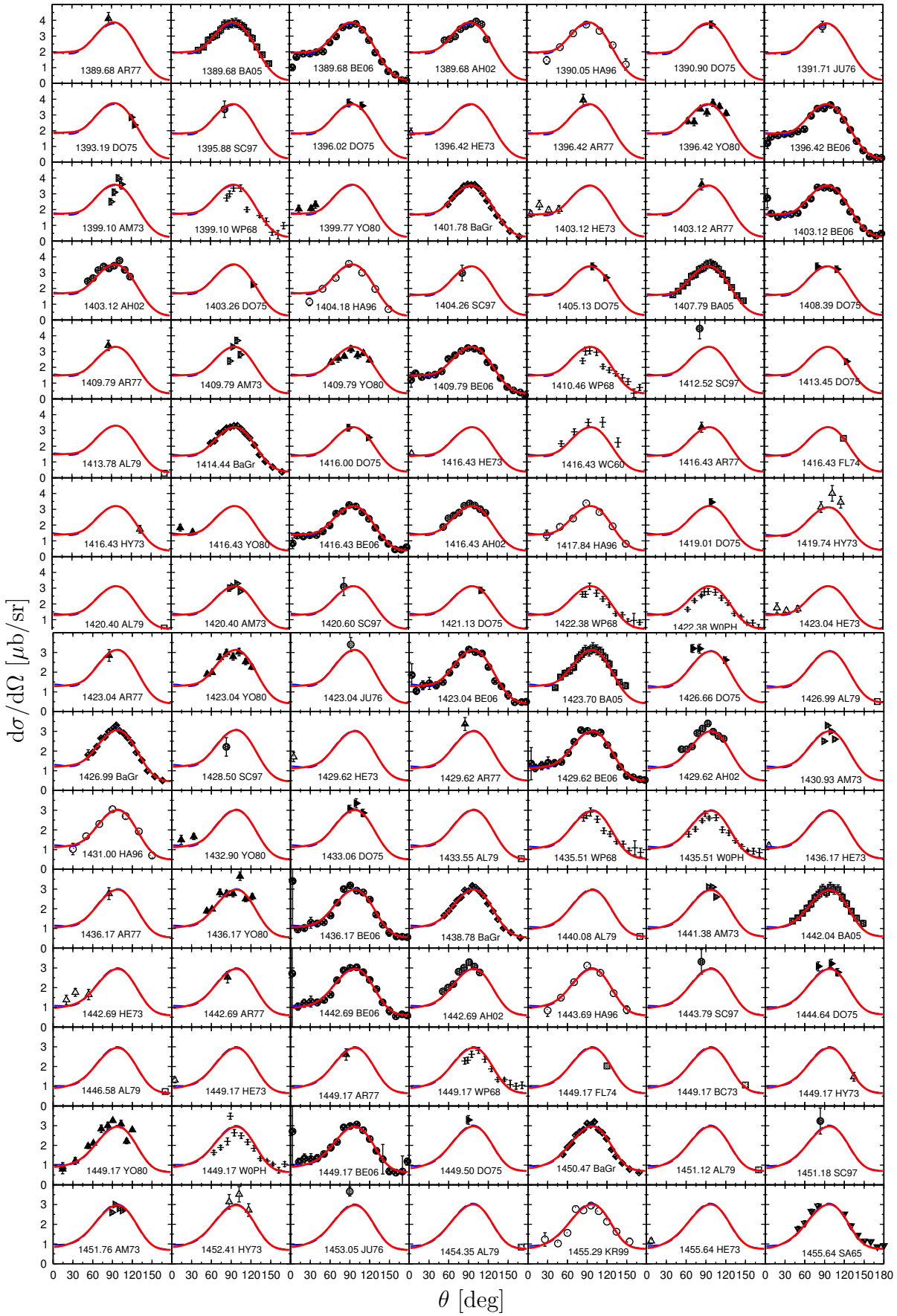

Figure A.6: Differential cross section of the reaction $\gamma p \to \pi^0 p$.

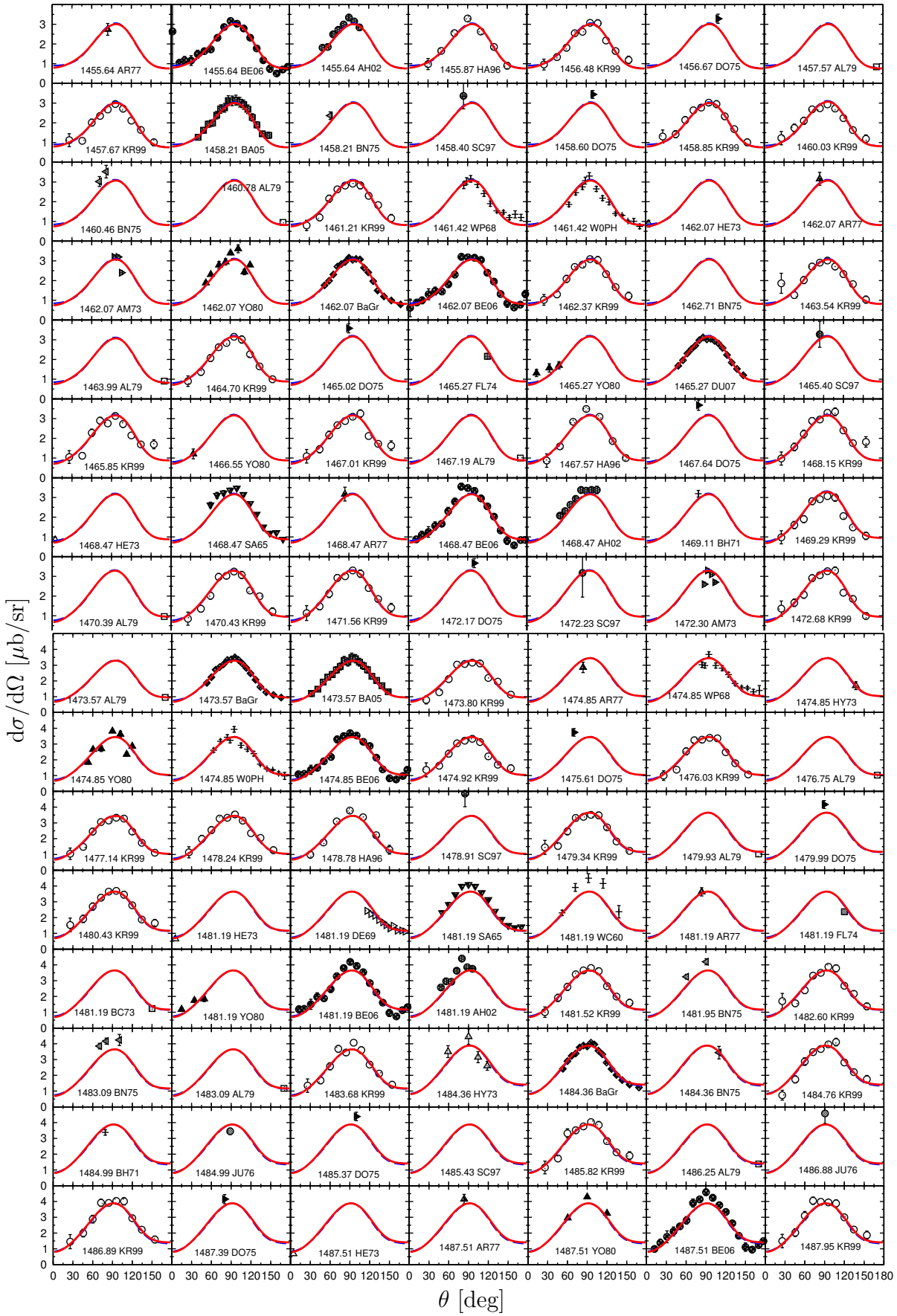

Figure A.7: Differential cross section of the reaction $\gamma p \to \pi^0 p$.

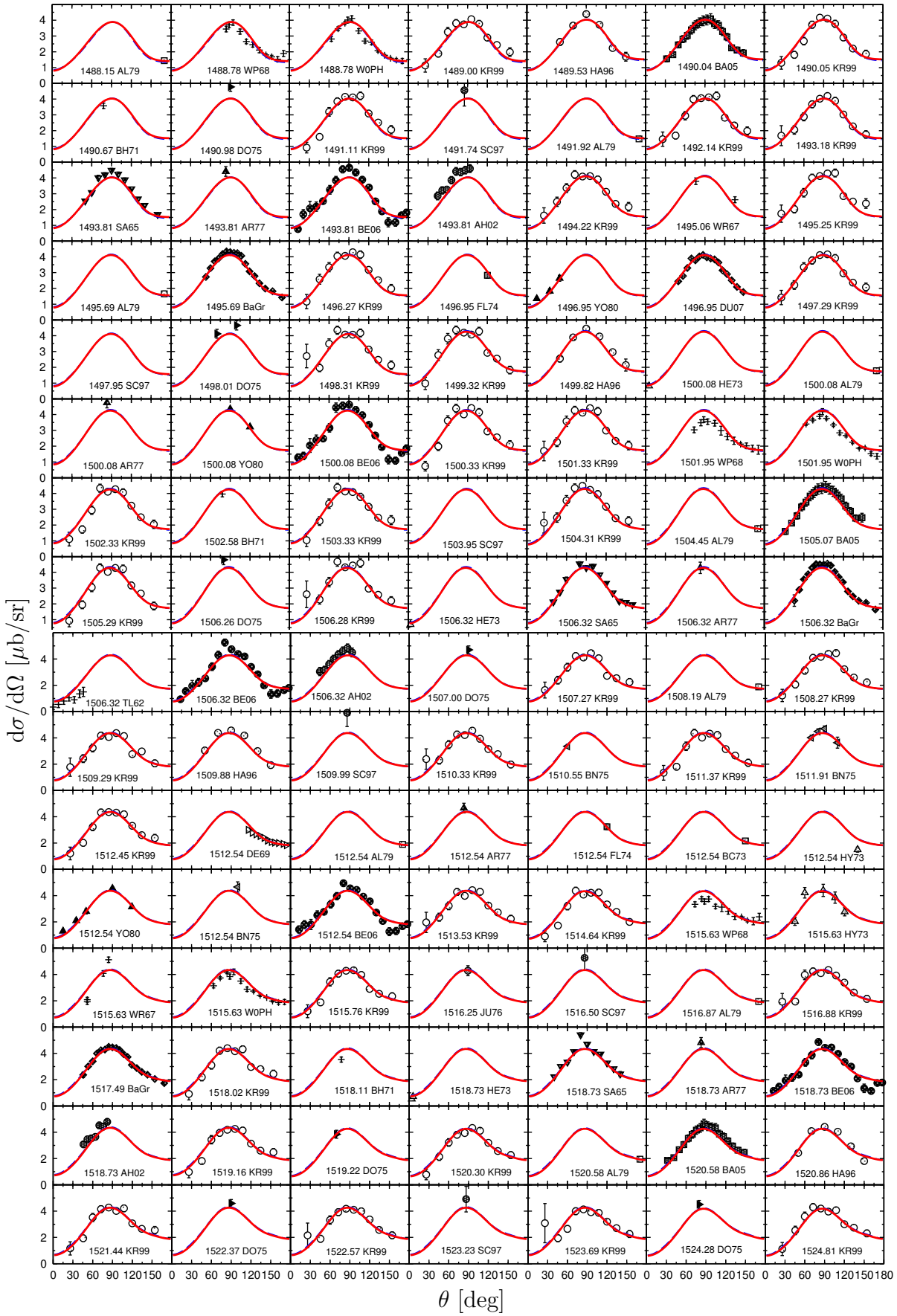

Figure A.8: Differential cross section of the reaction $\gamma p \to \pi^0 p$.

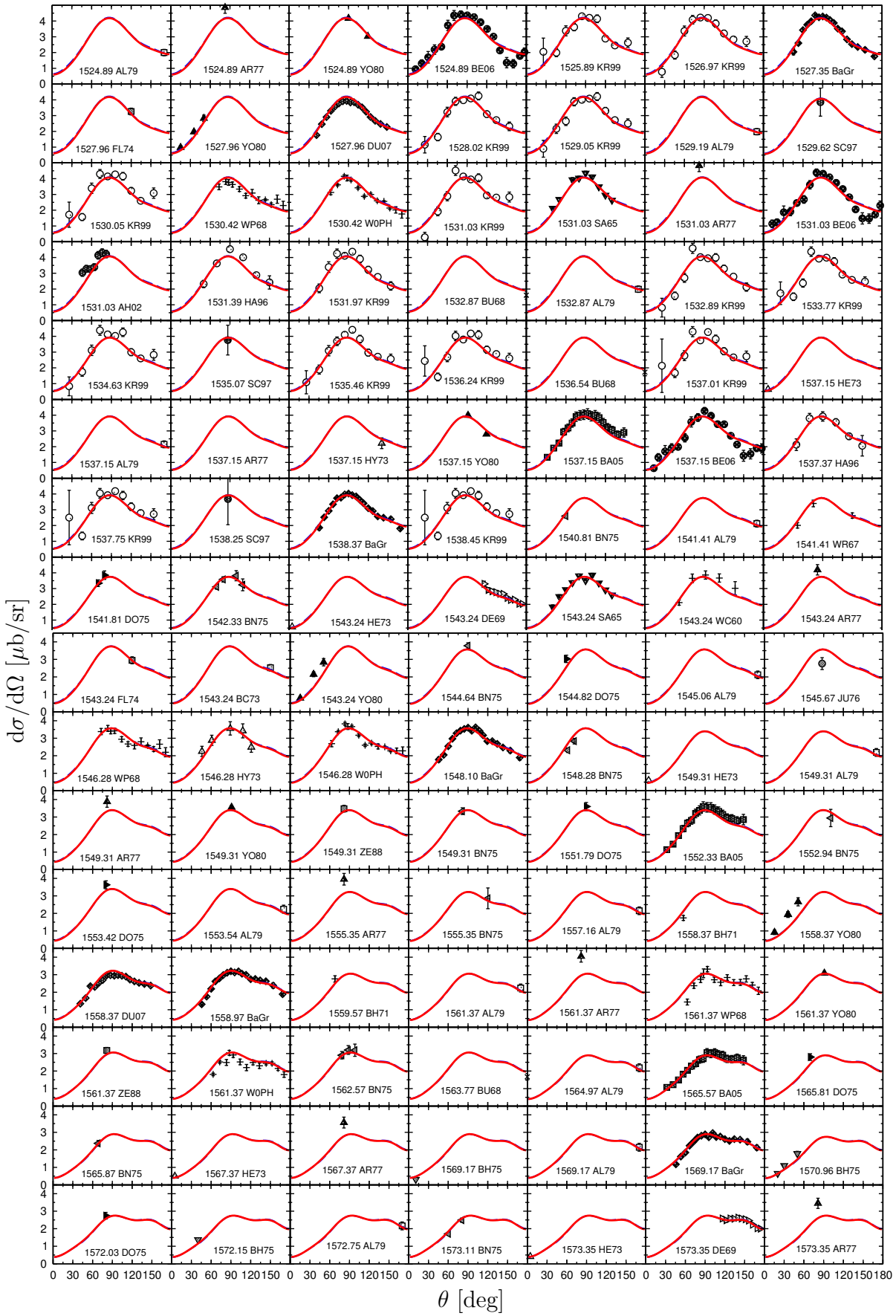

Figure A.9: Differential cross section of the reaction $\gamma p \to \pi^0 p$.

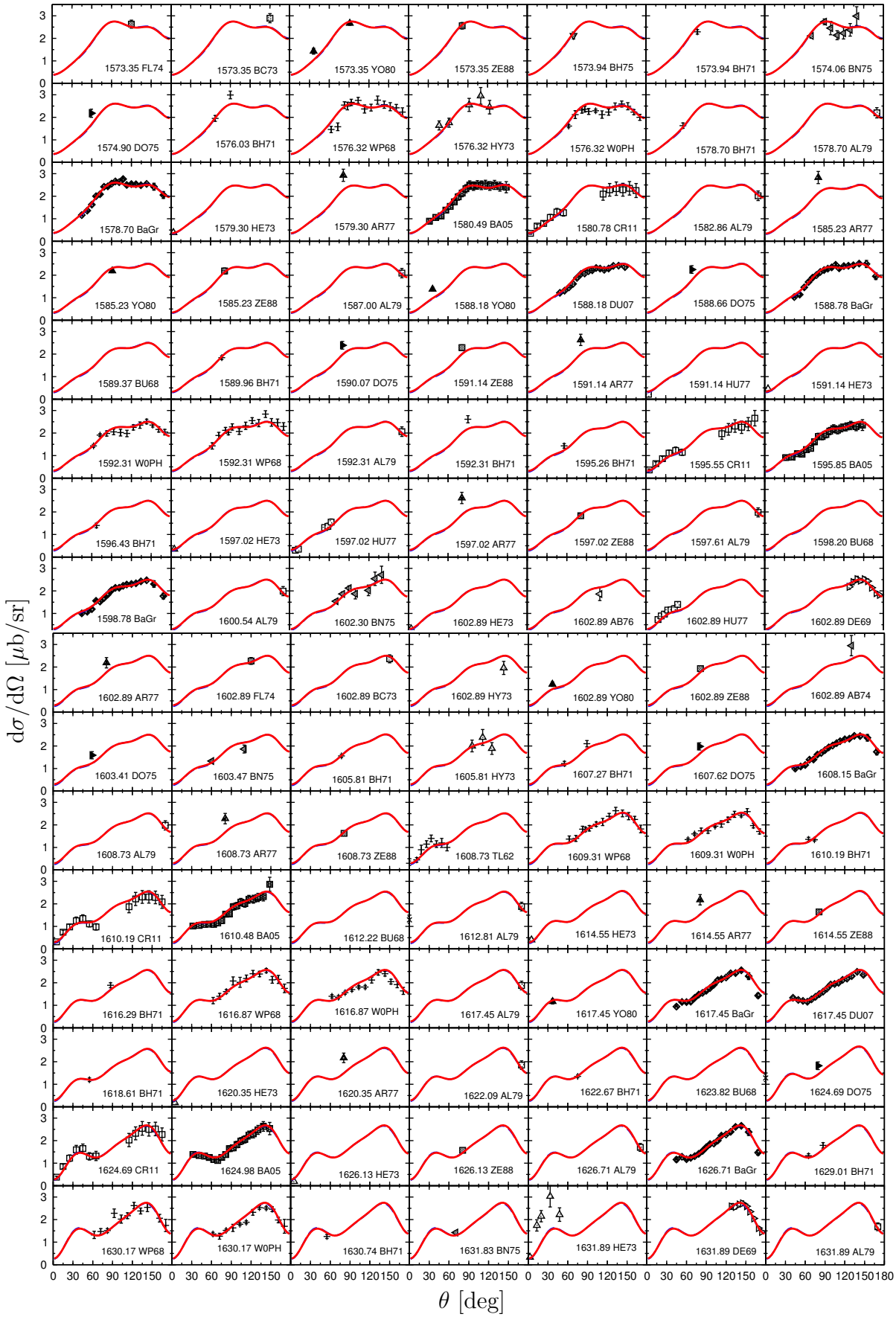

Figure A.10: Differential cross section of the reaction $\gamma p \to \pi^0 p$.

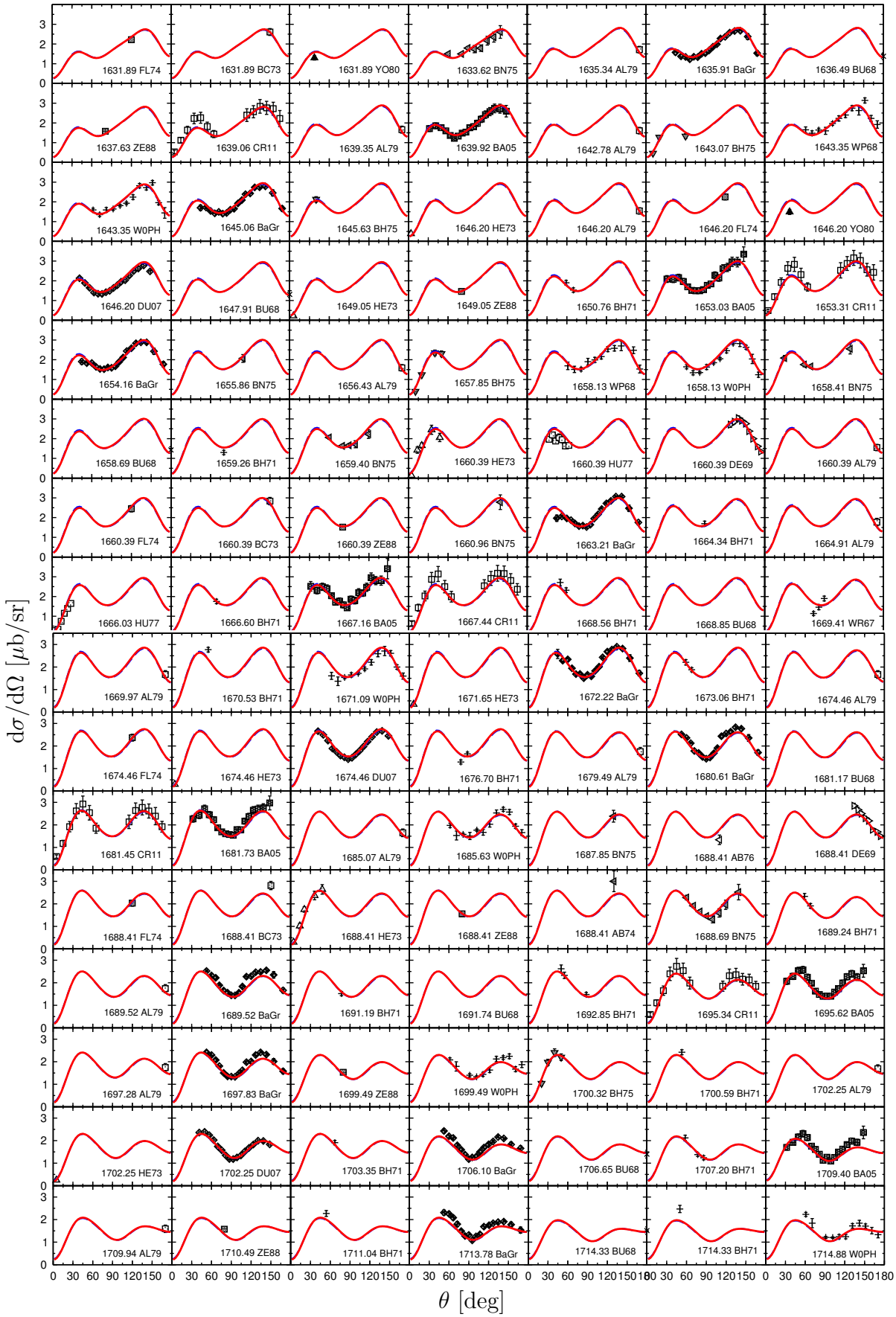

Figure A.11: Differential cross section of the reaction $\gamma p \to \pi^0 p$.

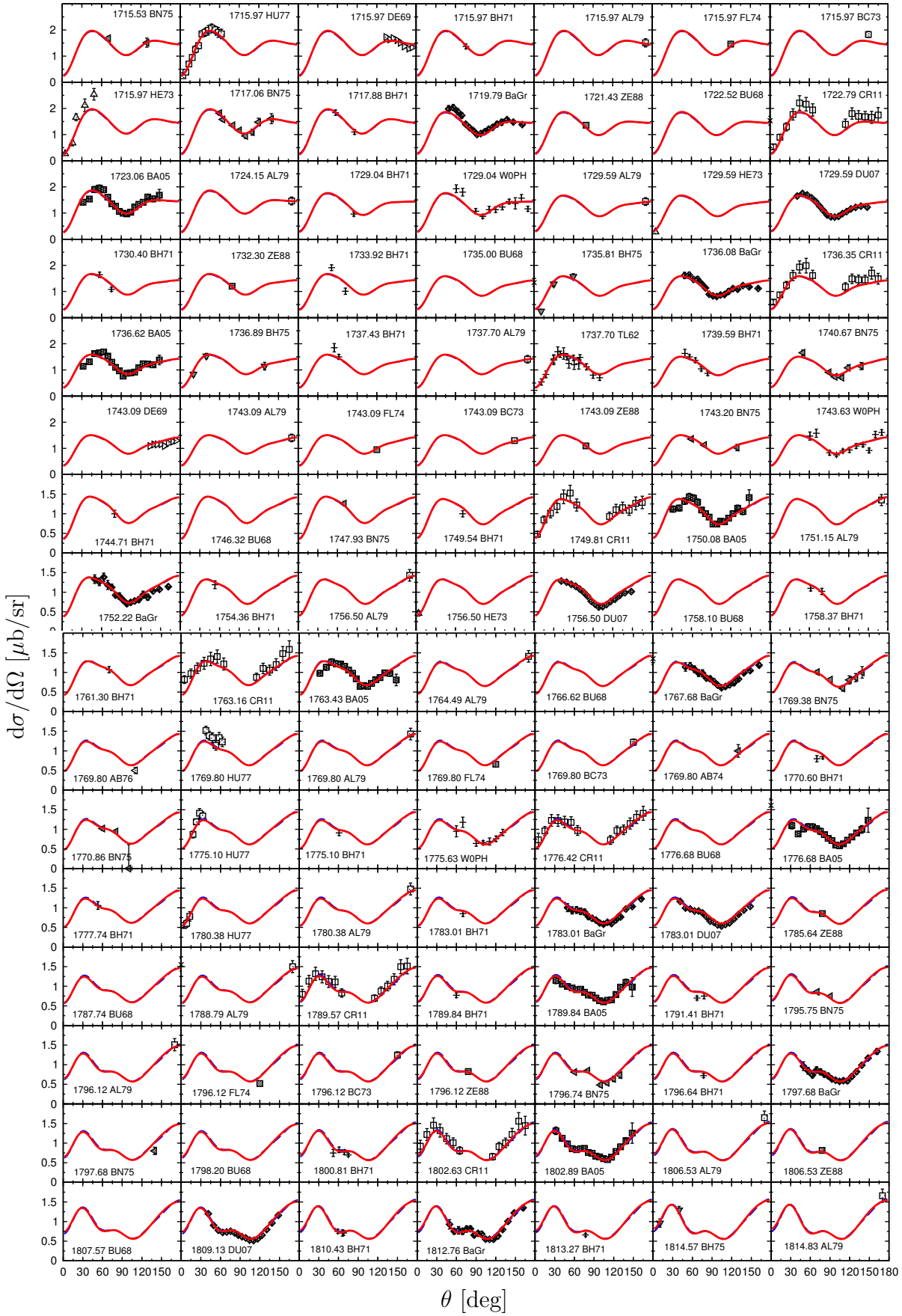

Figure A.12: Differential cross section of the reaction $\gamma p \to \pi^0 p$.

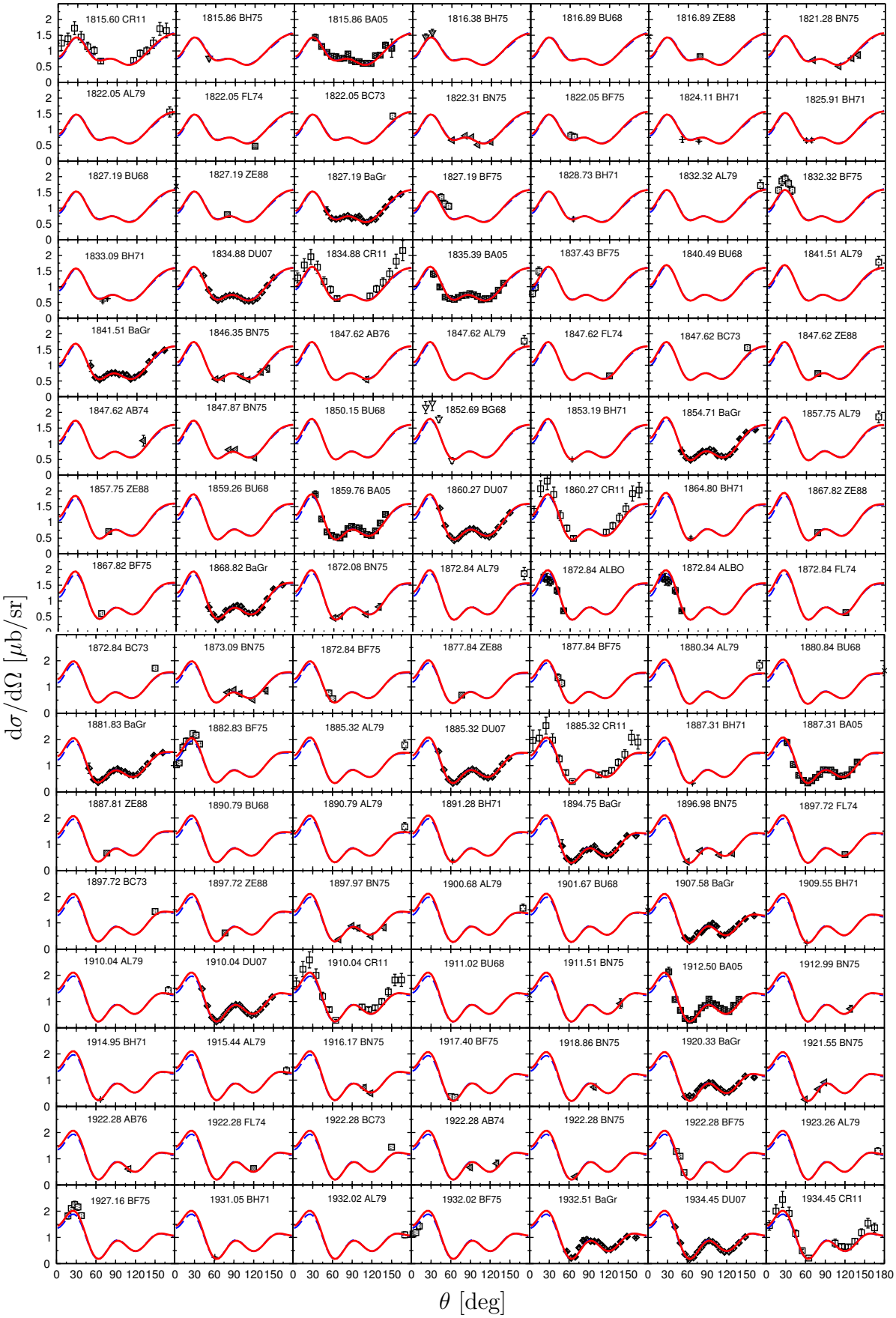

Figure A.13: Differential cross section of the reaction $\gamma p \to \pi^0 p$.

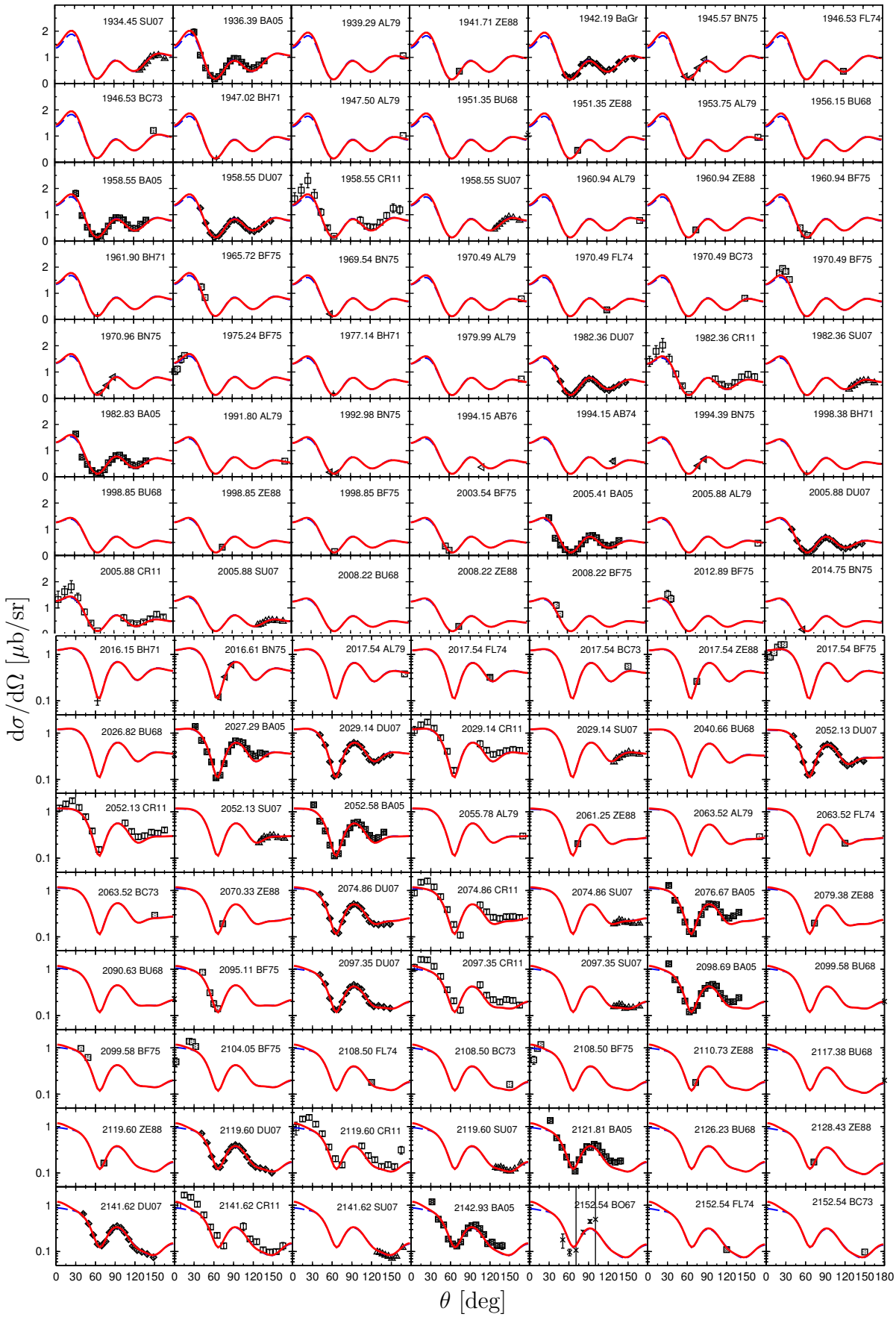

Figure A.14: Differential cross section of the reaction $\gamma p \to \pi^0 p$.

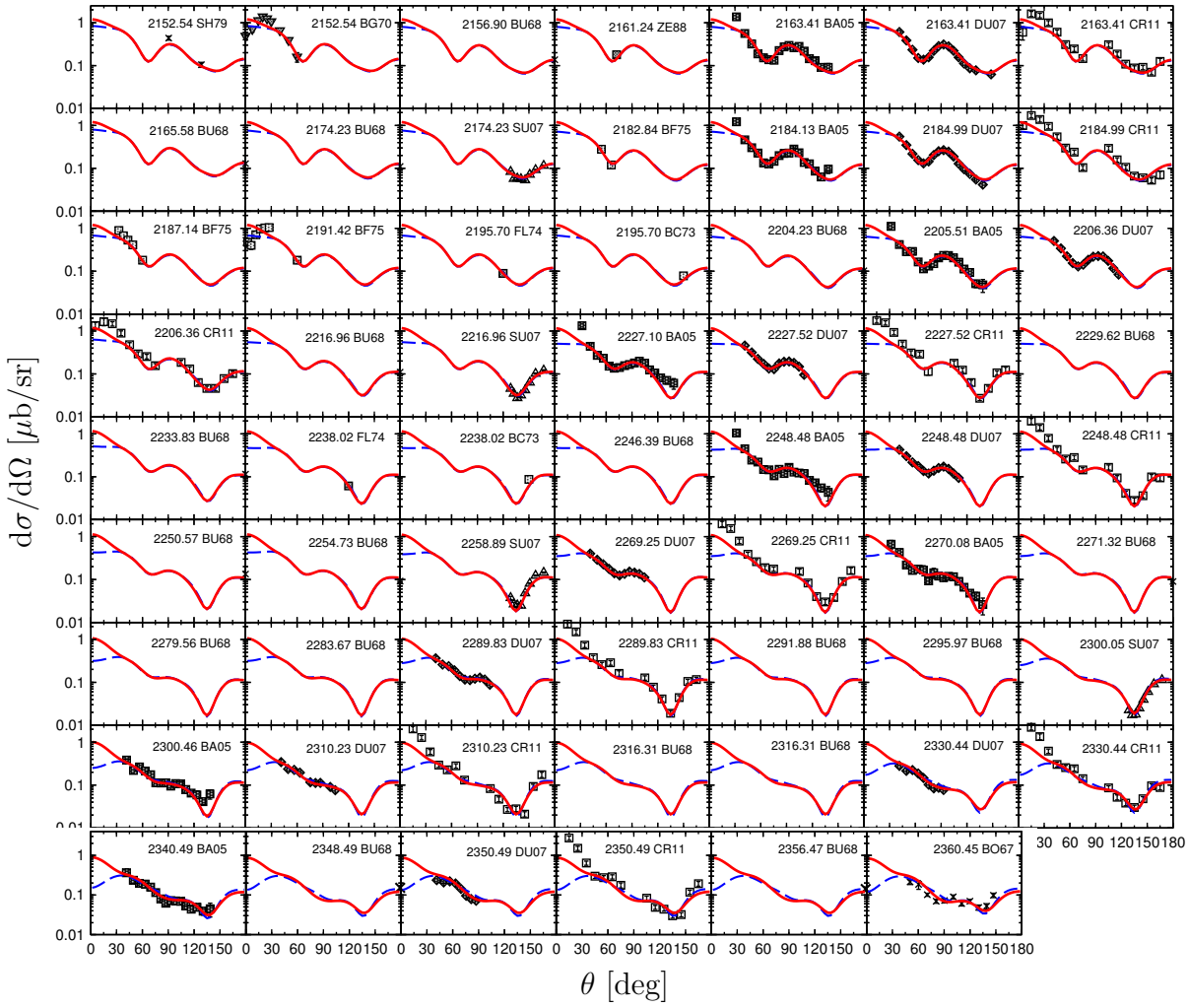

Figure A.15: Differential cross section of the reaction $\gamma p \to \pi^0 p$.

A.1.2 $\gamma p \to \pi^+ n$

Data shown in the figures of this section can be found under the following references:

AB74 [147], AH04 [151], AH06 [199], AK71 [200], AL83 [201], AR77 [157], AV70 [202], BE00 [203], BO71 [204], BR95 [205], BR00 [206], BT68 [207], BU66 [208], BU67 [209], BU94 [210], BY61 [211], DA01 [212], DO67 [213], DU80 [214], DU09 [215], EC67 [216], EK72 [217], FA84 [218], FI70 [219], FI72 [220], FI96 [221], FU71 [222], FU77 [223], HE88 [224], KI62 [225], KN63 [226], KO99 [227], LI64 [228], WA62 [229], ZE88 [198], ZH05 [230].

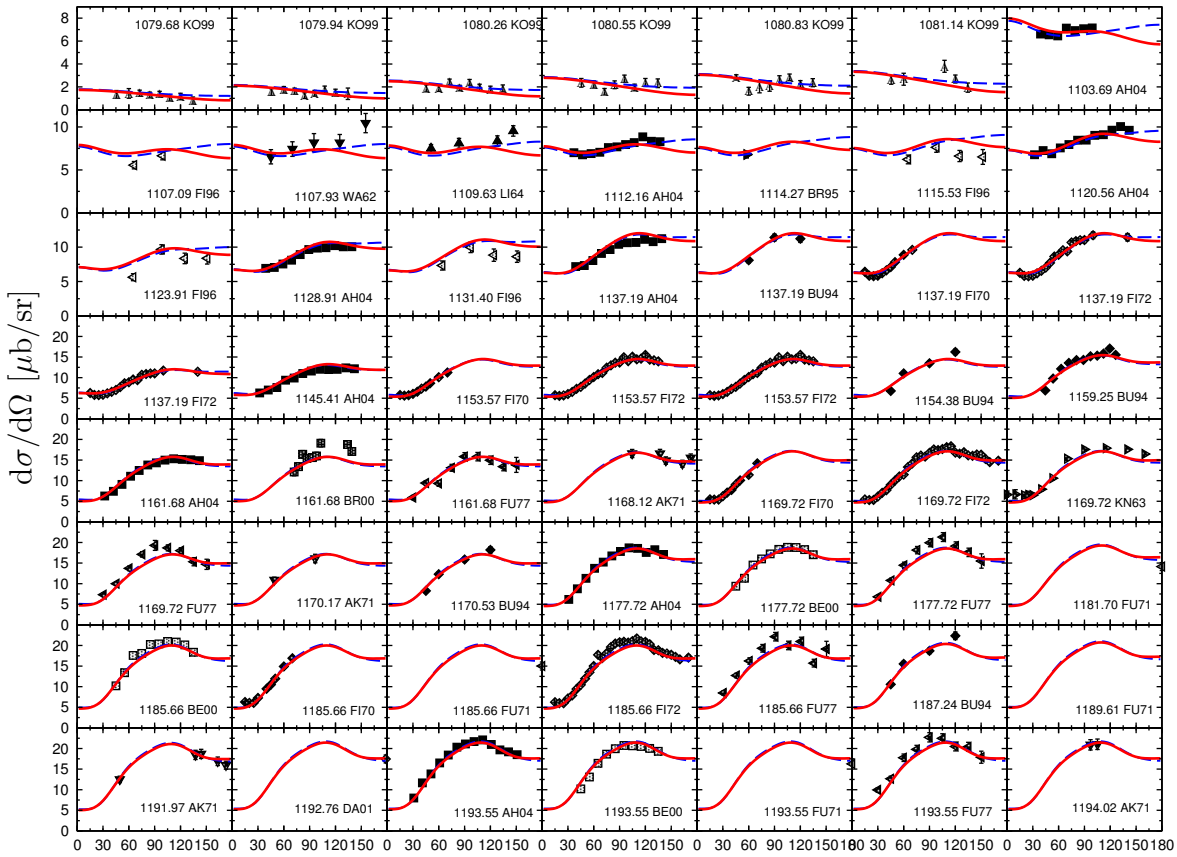

Figure A.16: Differential cross section of the reaction $\gamma p \to \pi^+ n$.

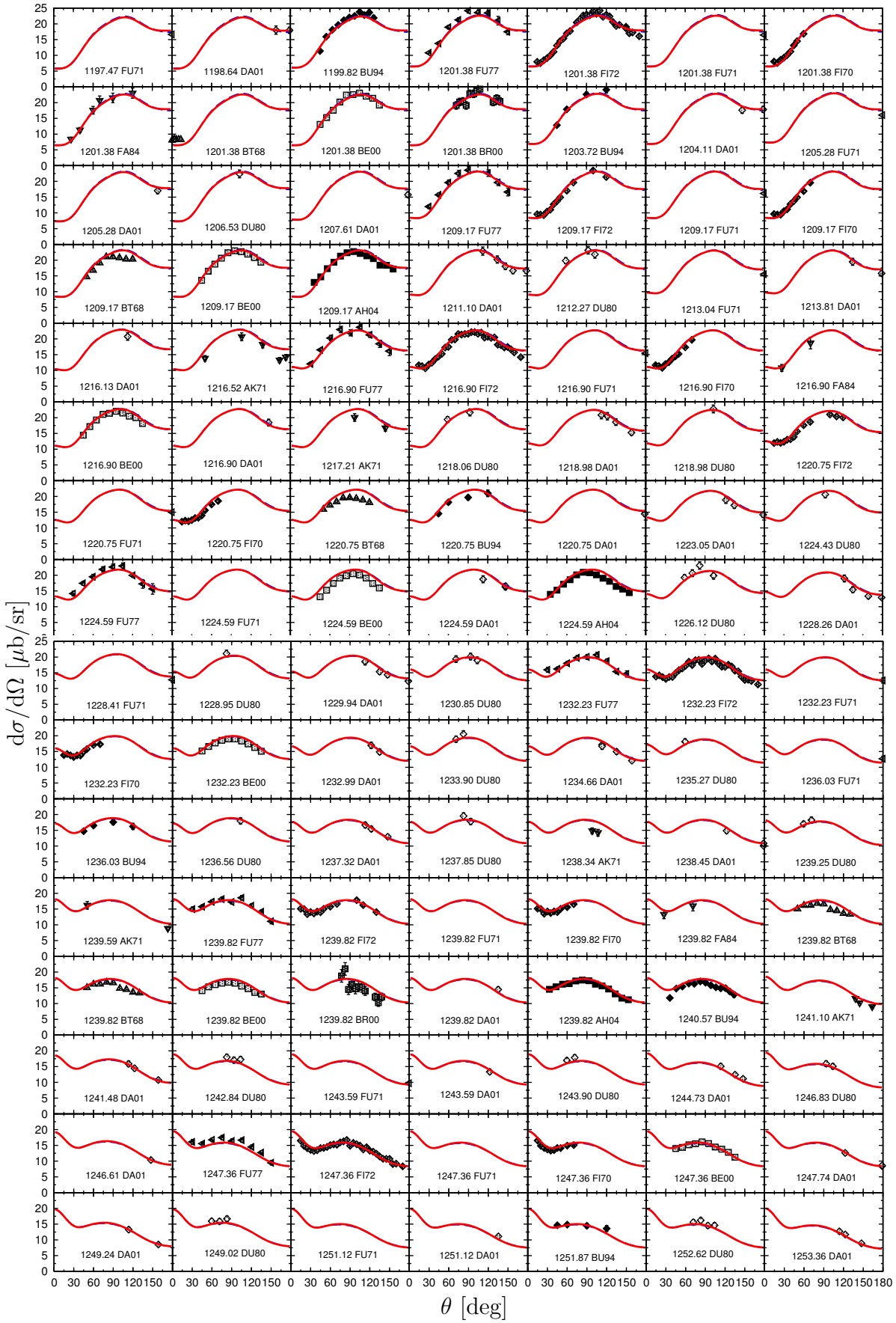

Figure A.17: Differential cross section of the reaction $\gamma p \to \pi^+ n$.

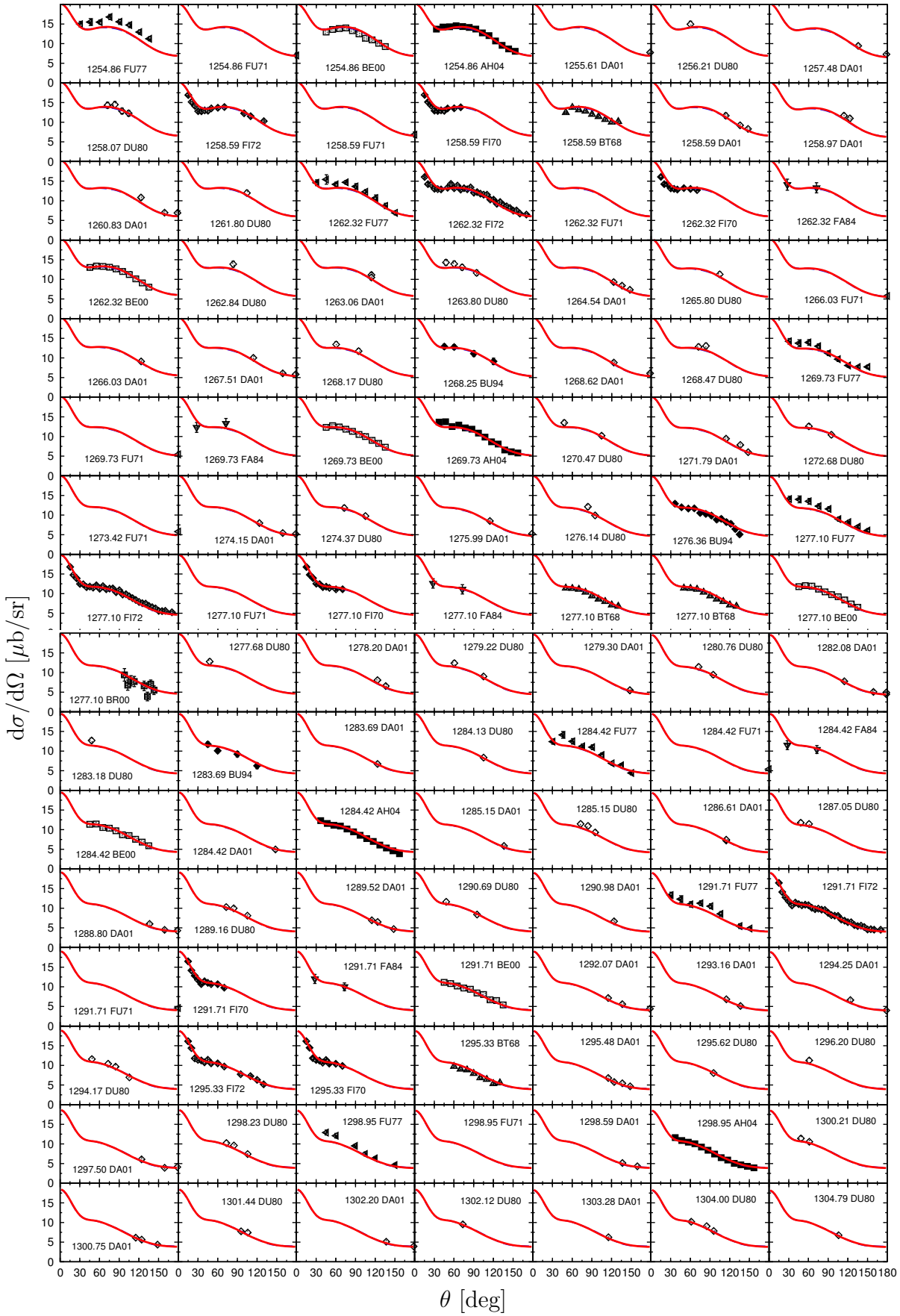

Figure A.18: Differential cross section of the reaction $\gamma p \to \pi^+ n$.

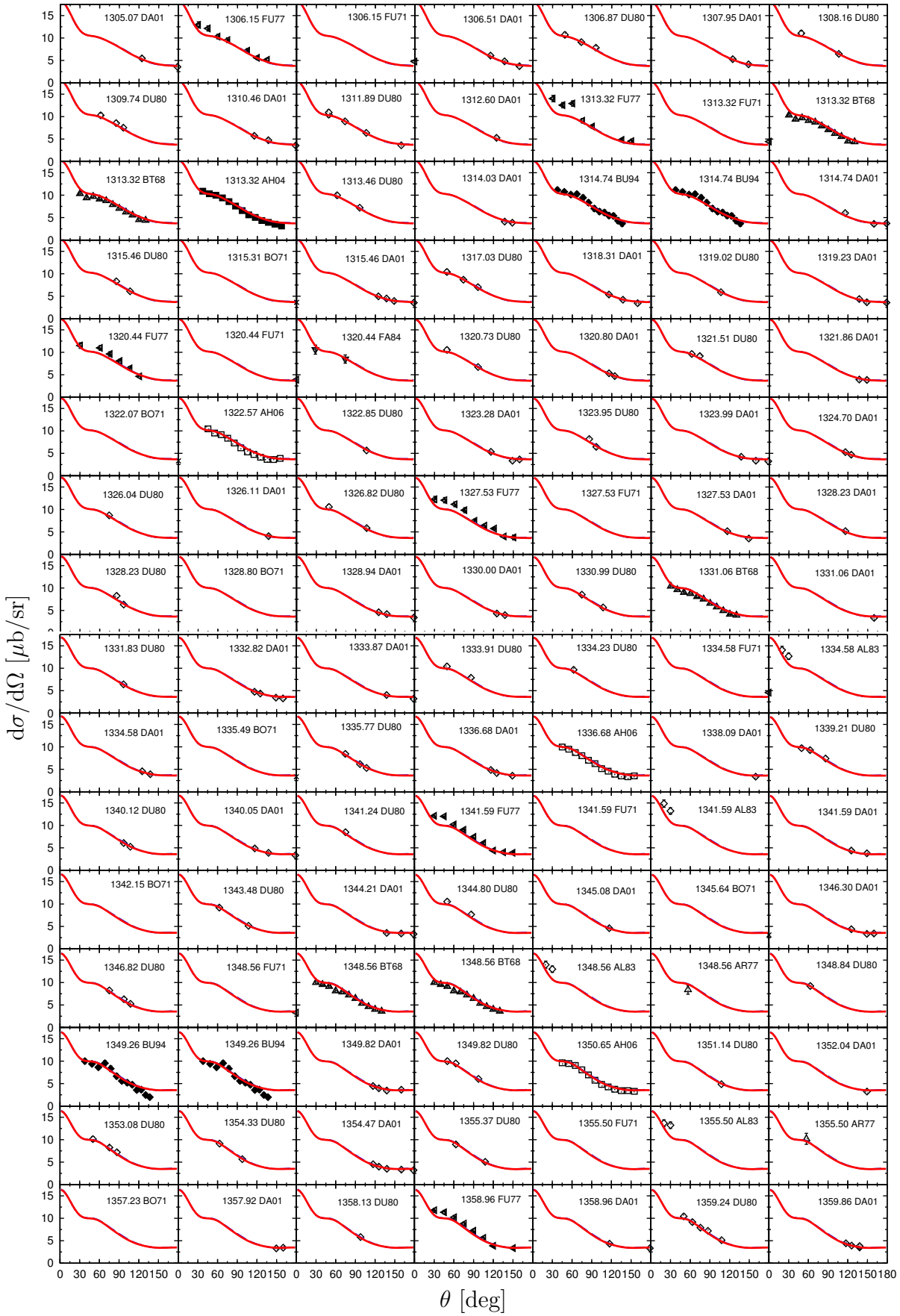

Figure A.19: Differential cross section of the reaction $\gamma p \to \pi^+ n$.

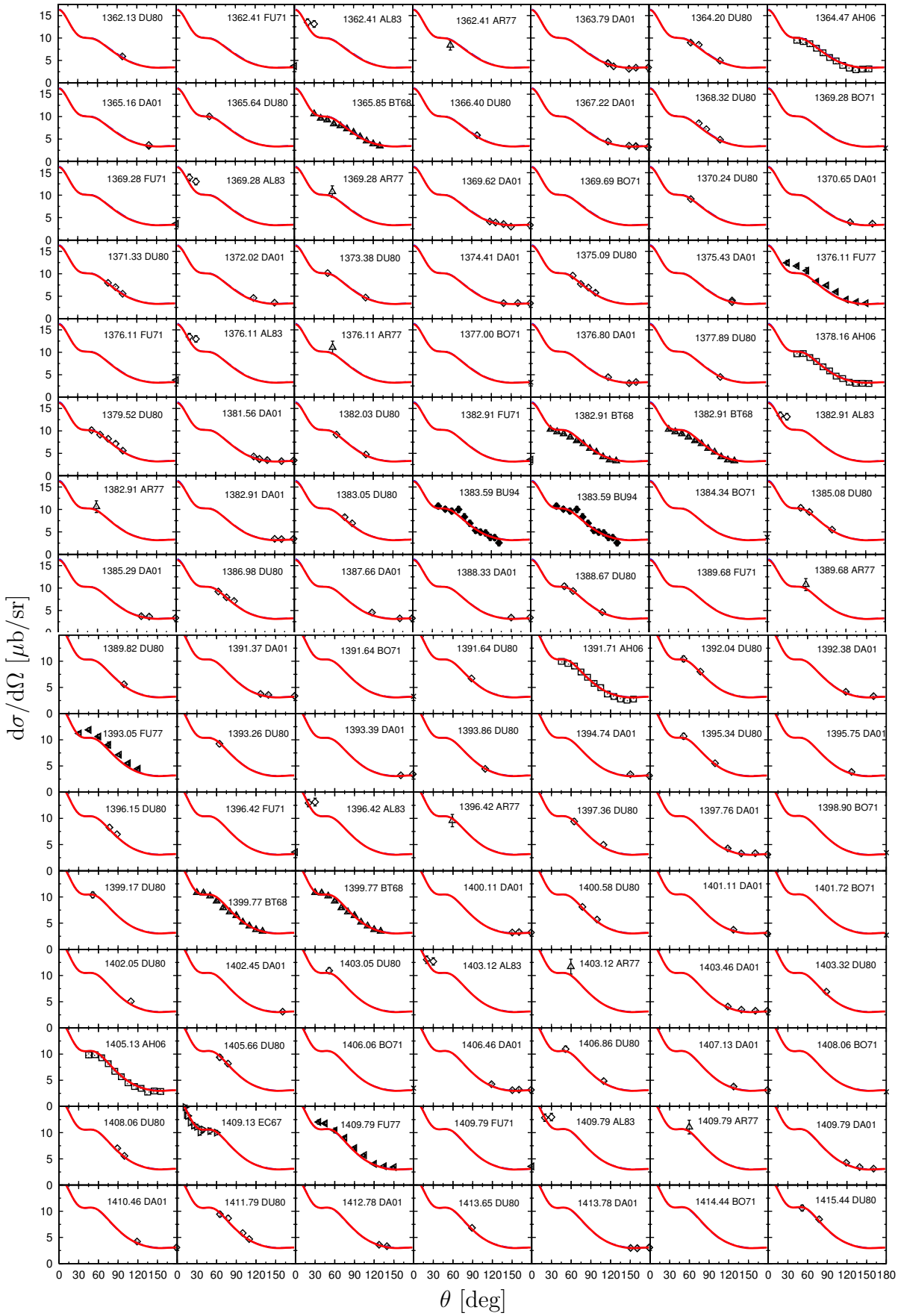

Figure A.20: Differential cross section of the reaction $\gamma p \to \pi^+ n$.

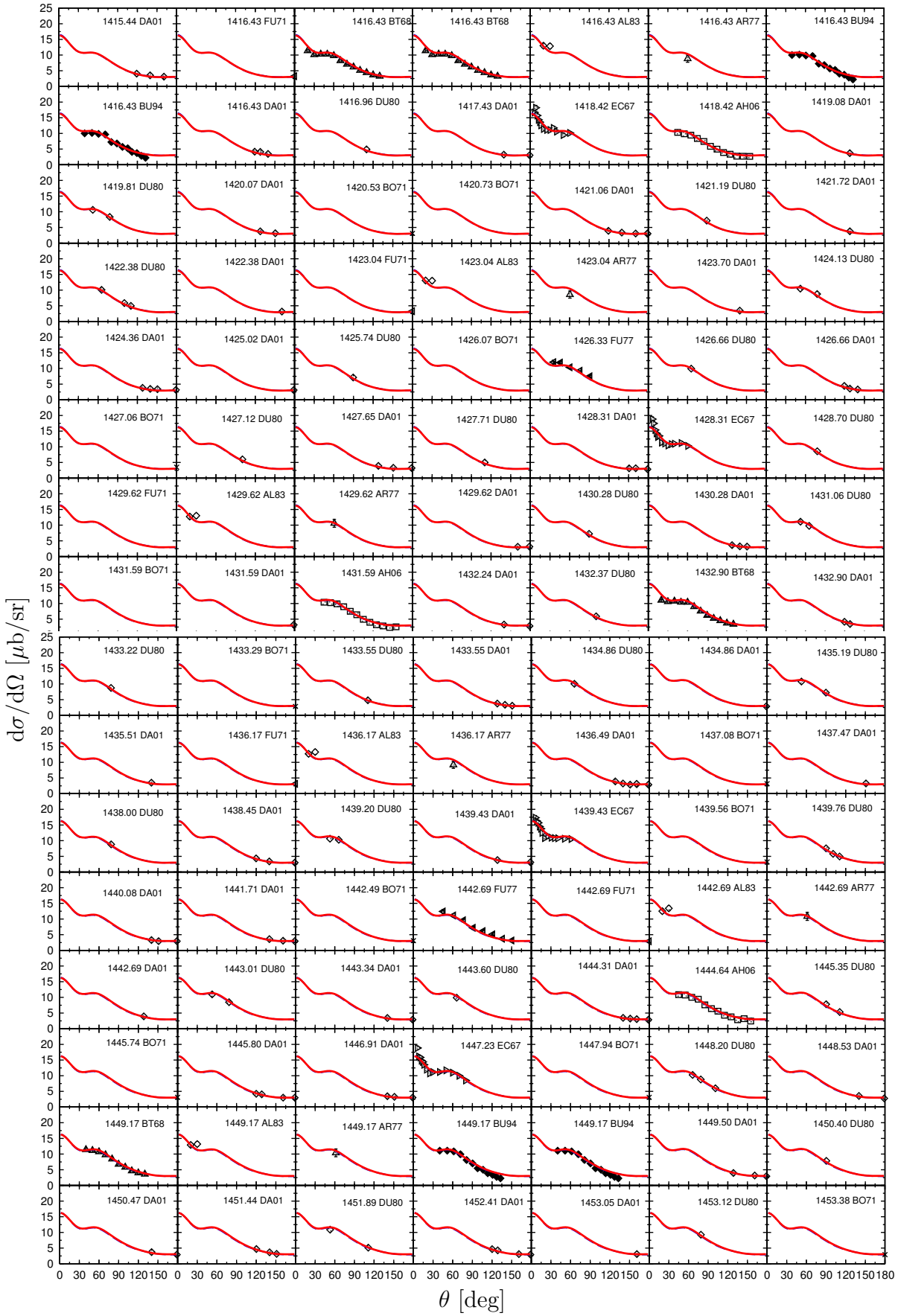

Figure A.21: Differential cross section of the reaction $\gamma p \to \pi^+ n$.

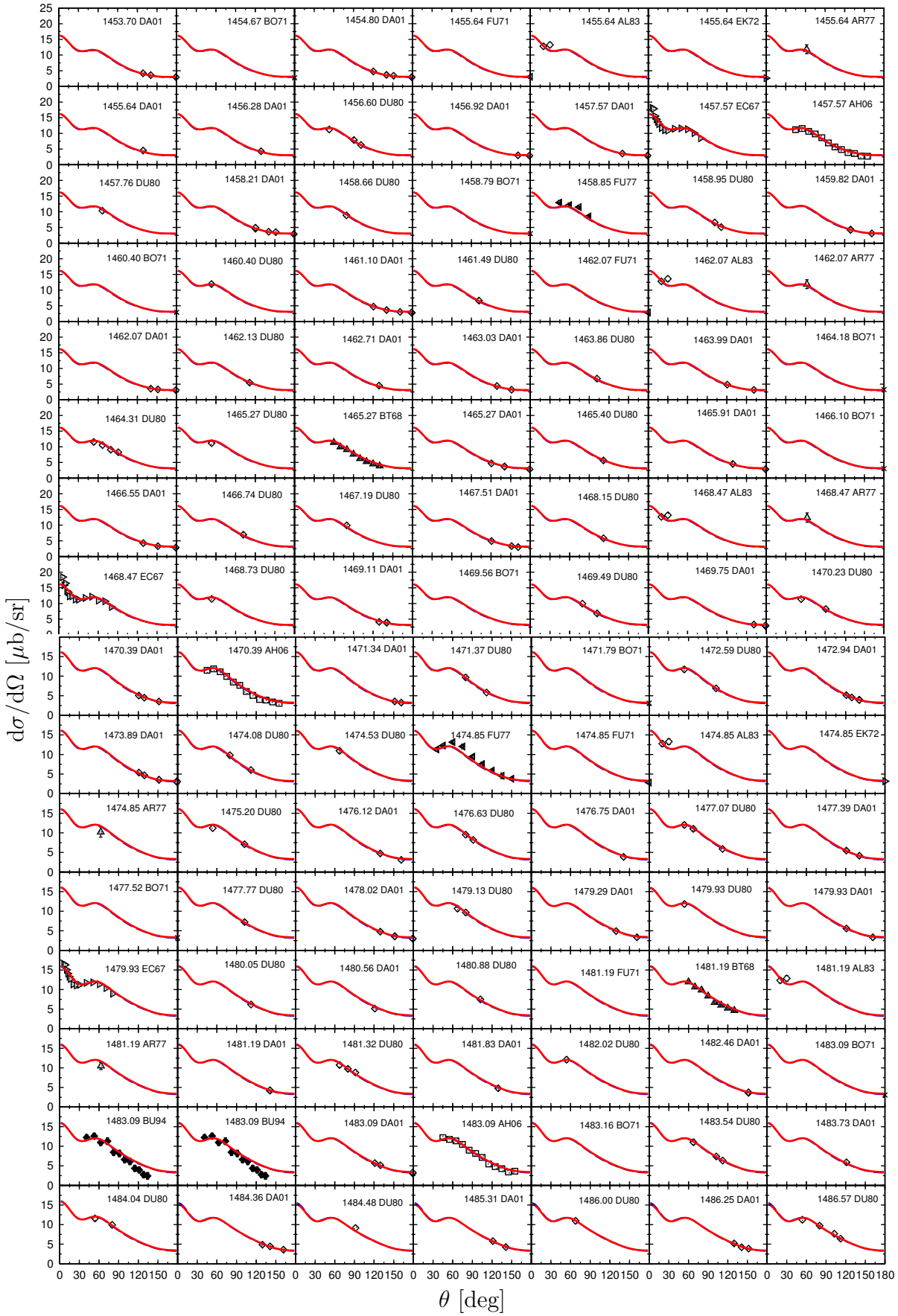

Figure A.22: Differential cross section of the reaction $\gamma p \to \pi^+ n$.

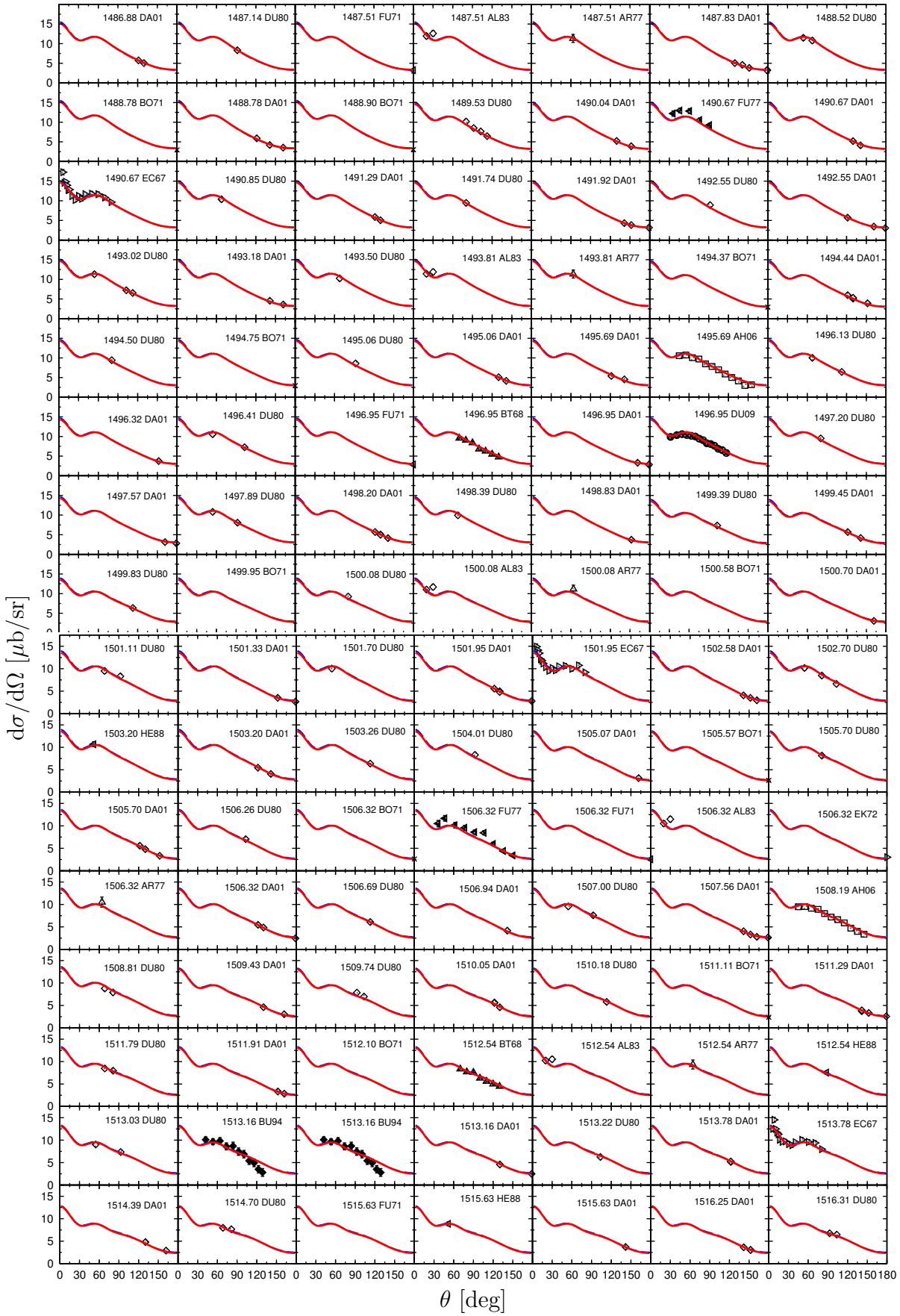

Figure A.23: Differential cross section of the reaction $\gamma p \to \pi^+ n$.

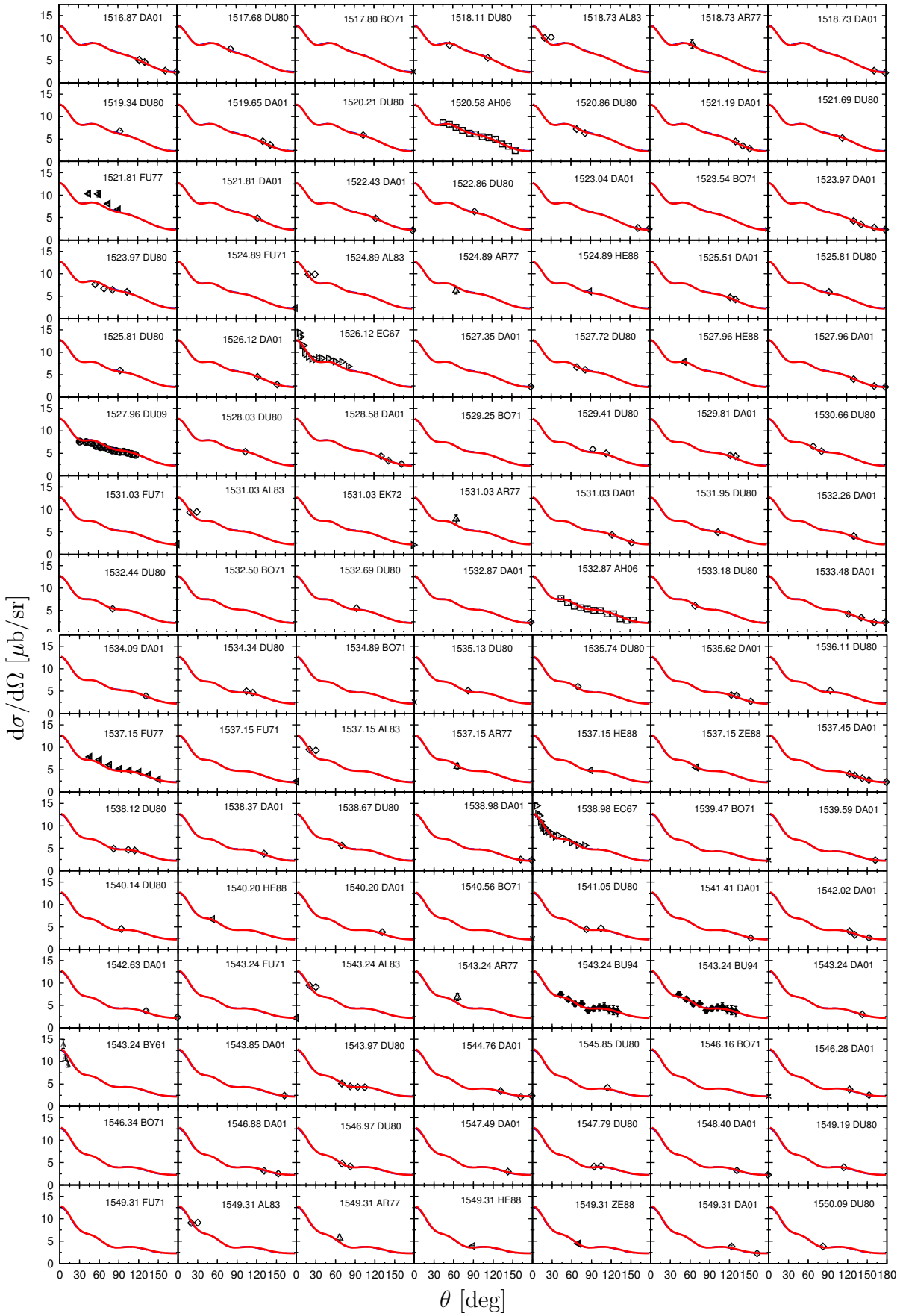

Figure A.24: Differential cross section of the reaction $\gamma p \to \pi^+ n$.

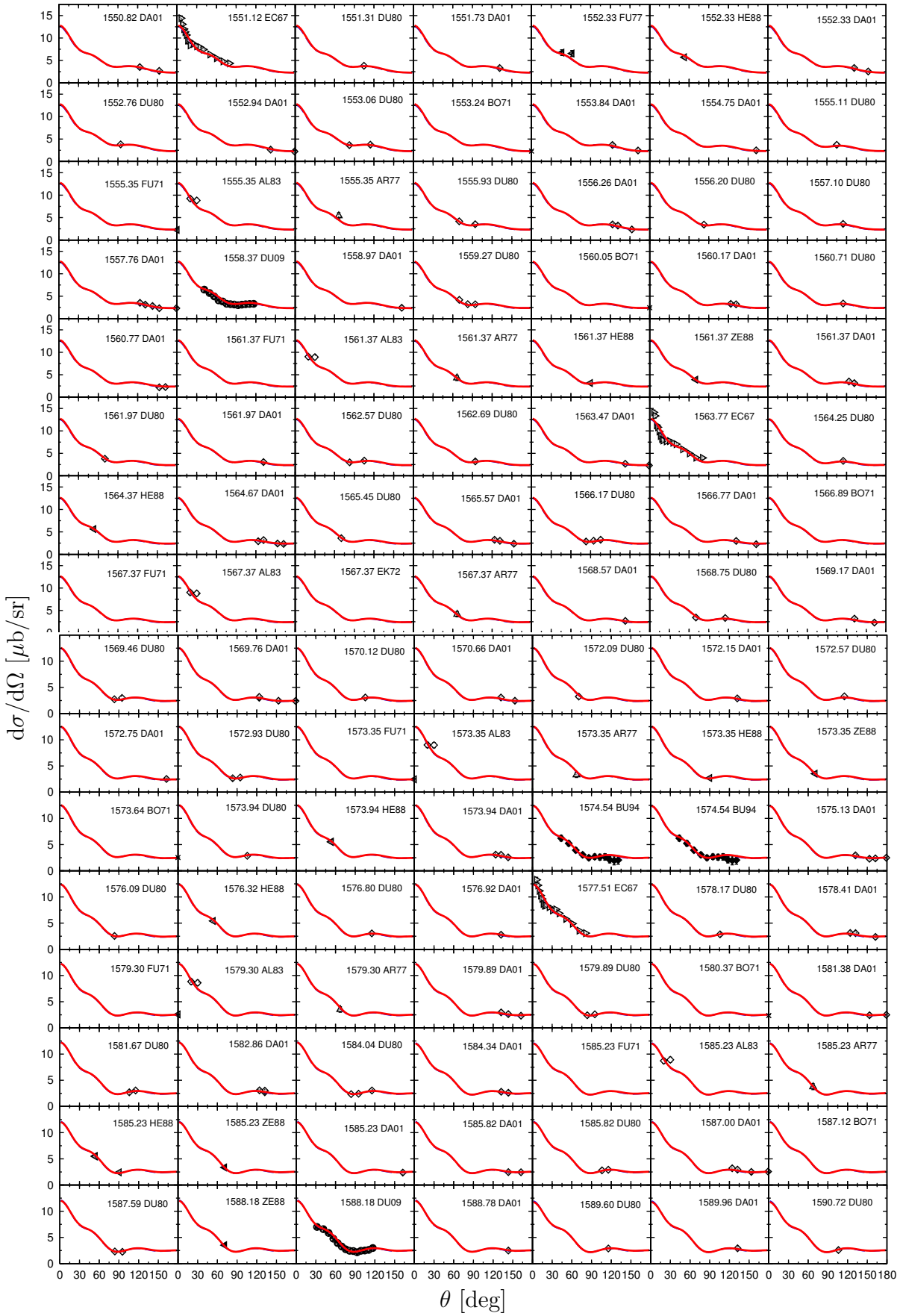

Figure A.25: Differential cross section of the reaction $\gamma p \to \pi^+ n$.

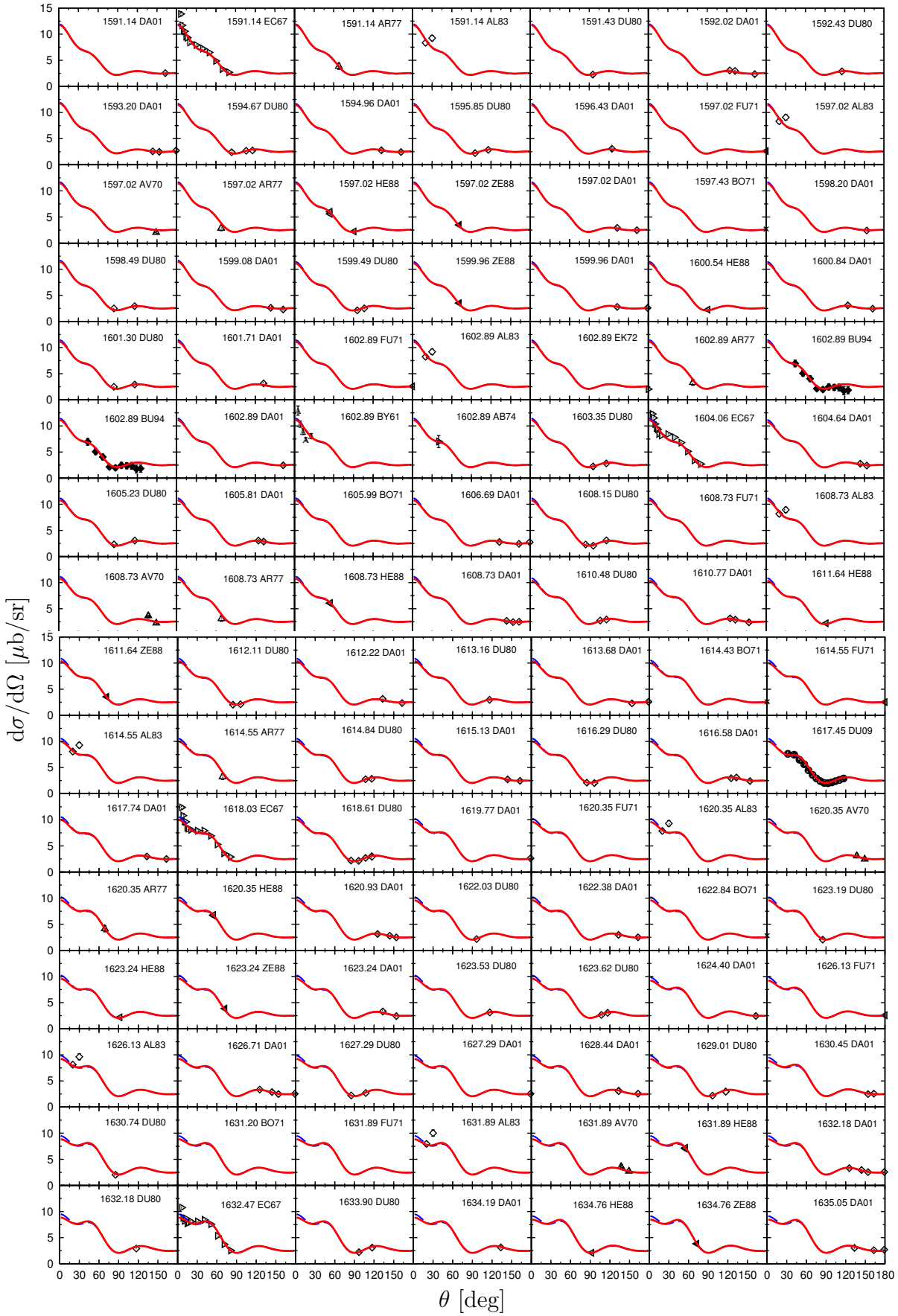

Figure A.26: Differential cross section of the reaction $\gamma p \to \pi^+ n$.

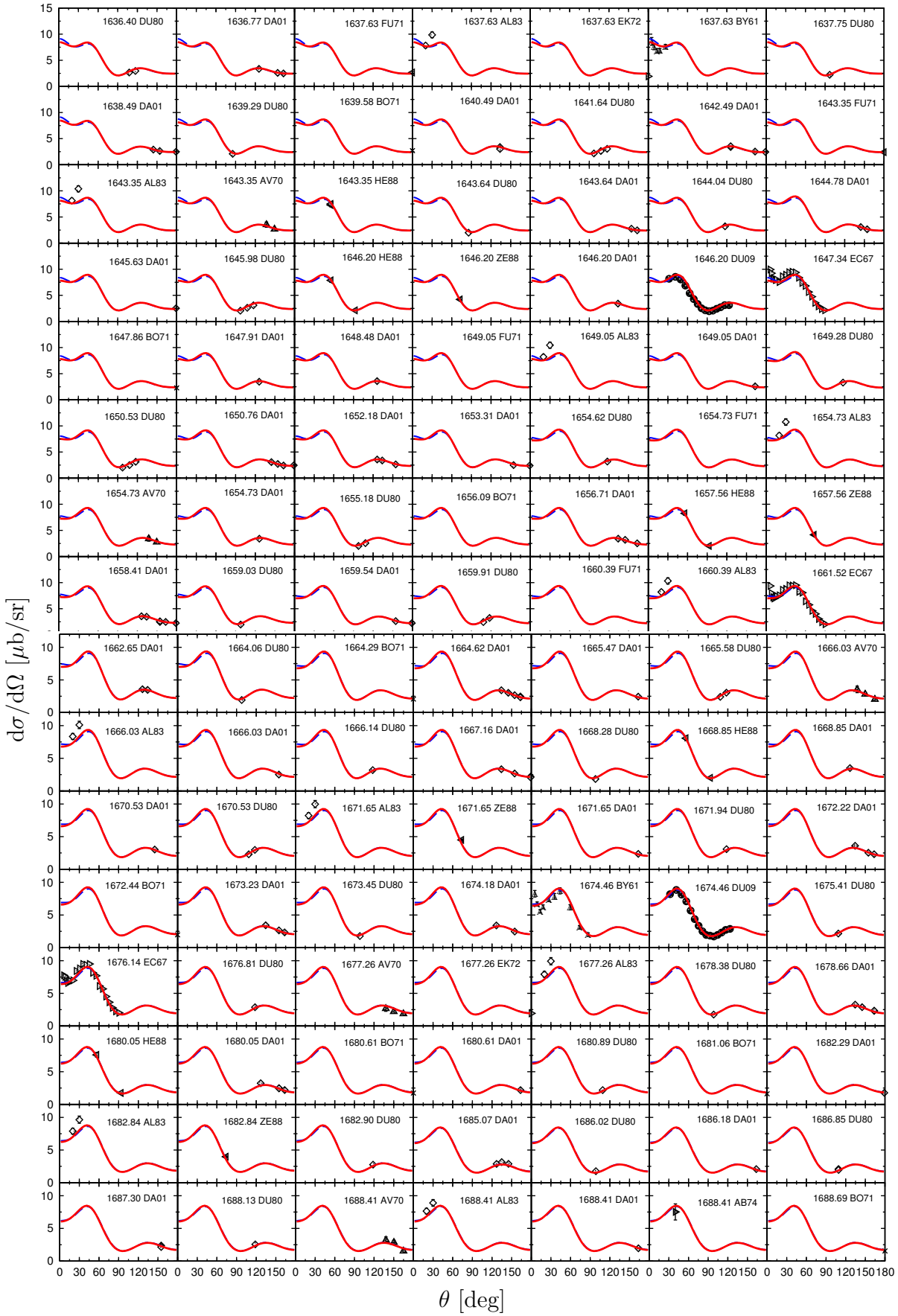

Figure A.27: Differential cross section of the reaction $\gamma p \to \pi^+ n$.

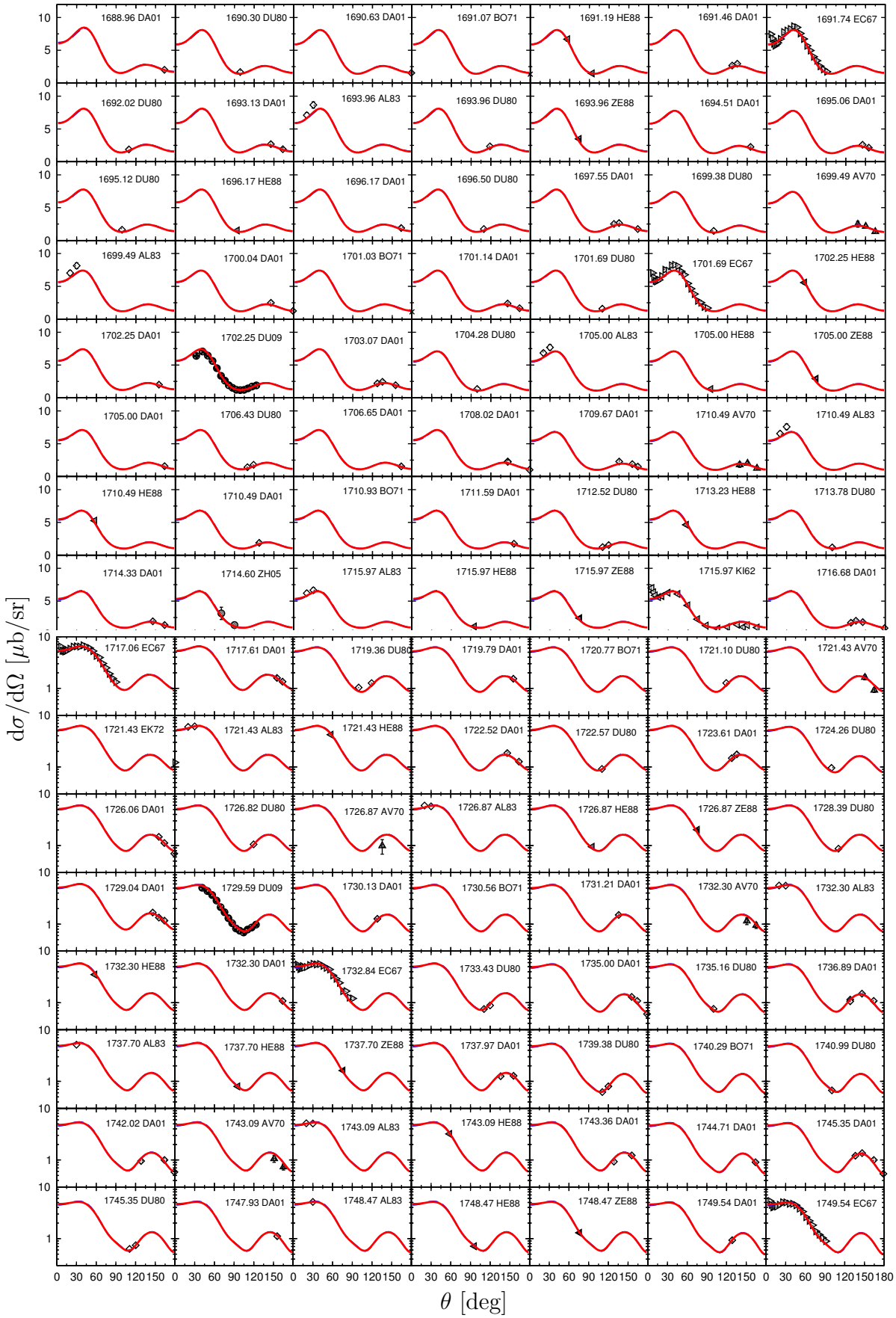

Figure A.28: Differential cross section of the reaction $\gamma p \to \pi^+ n$.

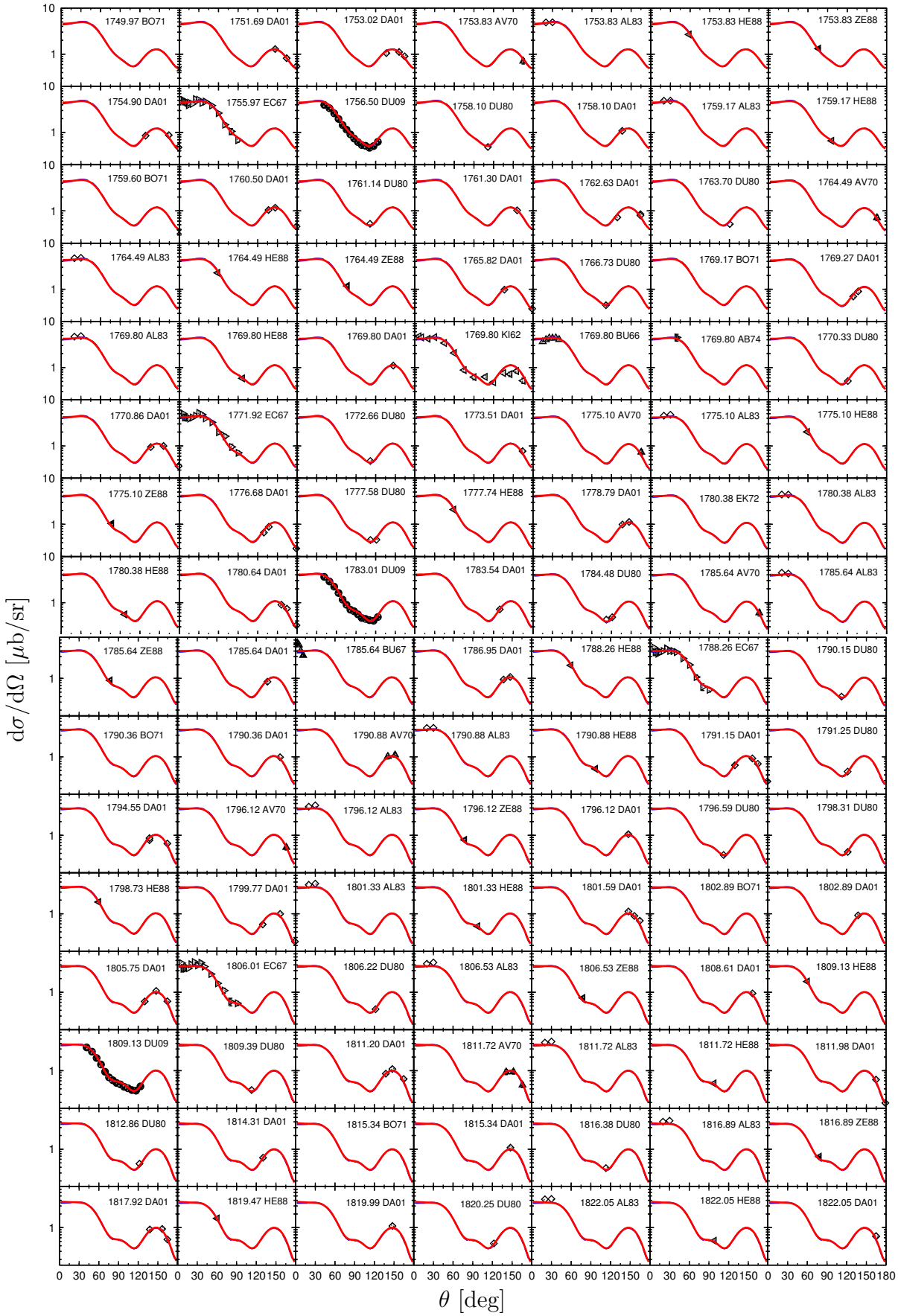

Figure A.29: Differential cross section of the reaction $\gamma p \to \pi^+ n$.

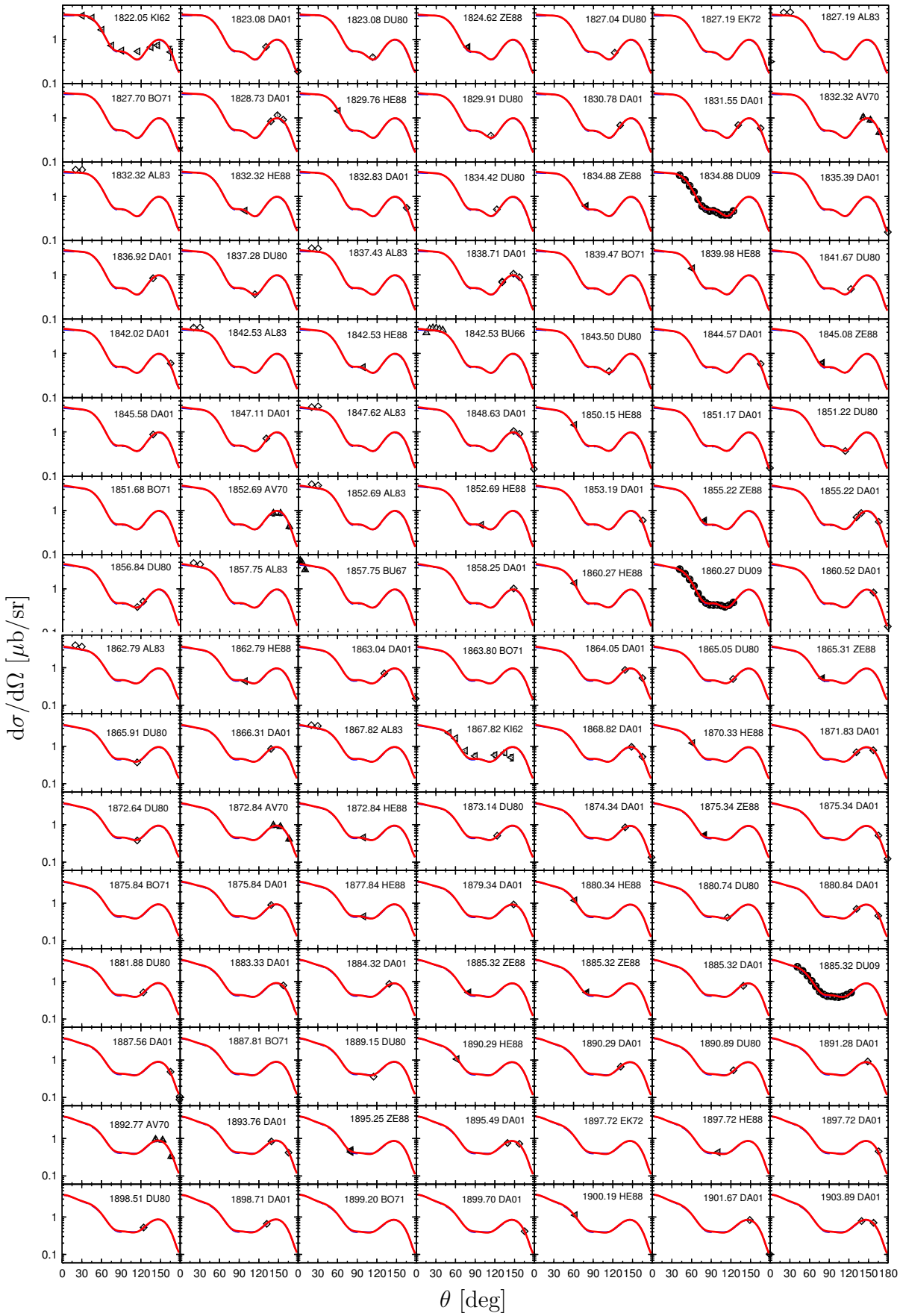

Figure A.30: Differential cross section of the reaction $\gamma p \to \pi^+ n$.

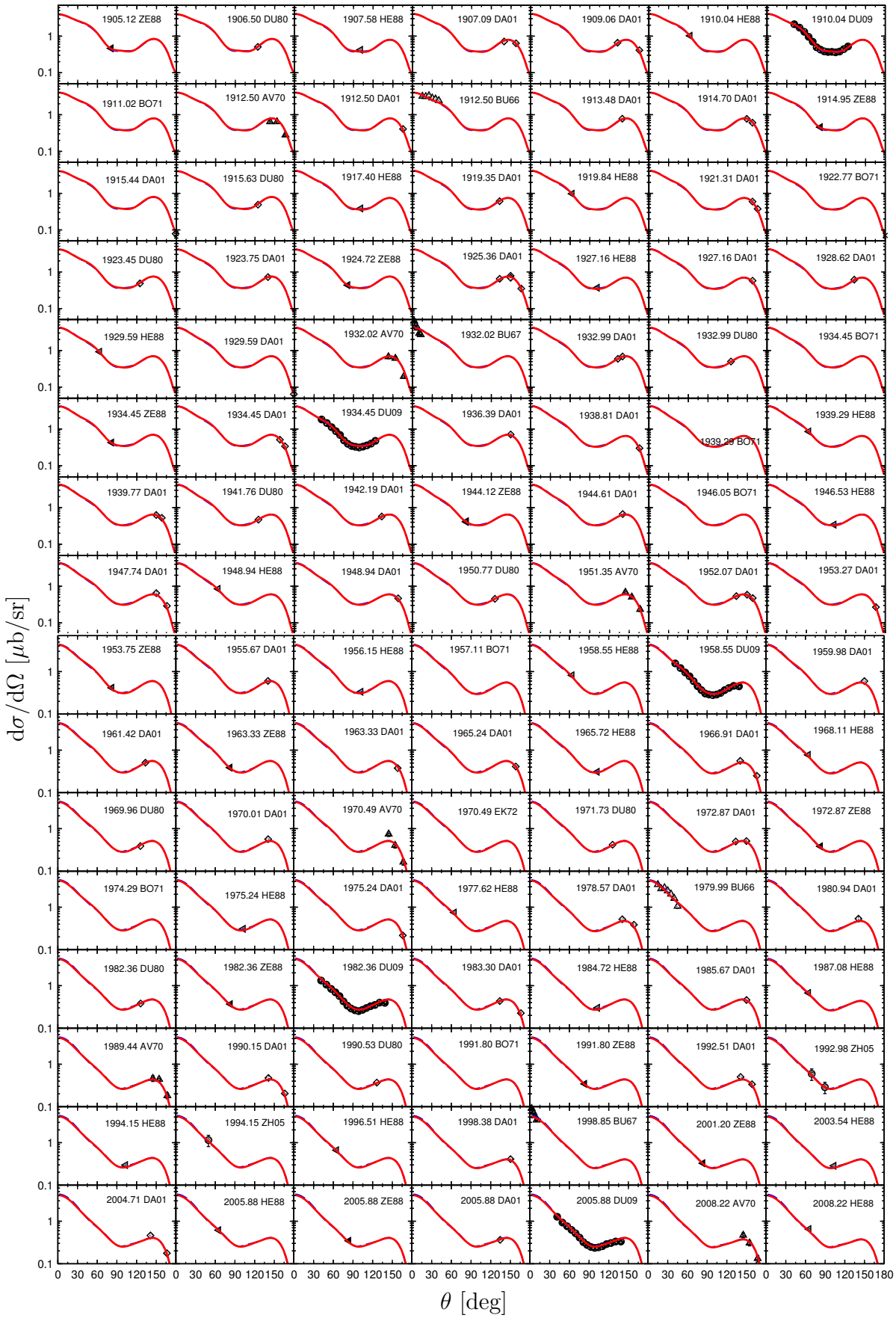

Figure A.31: Differential cross section of the reaction $\gamma p \to \pi^+ n$.

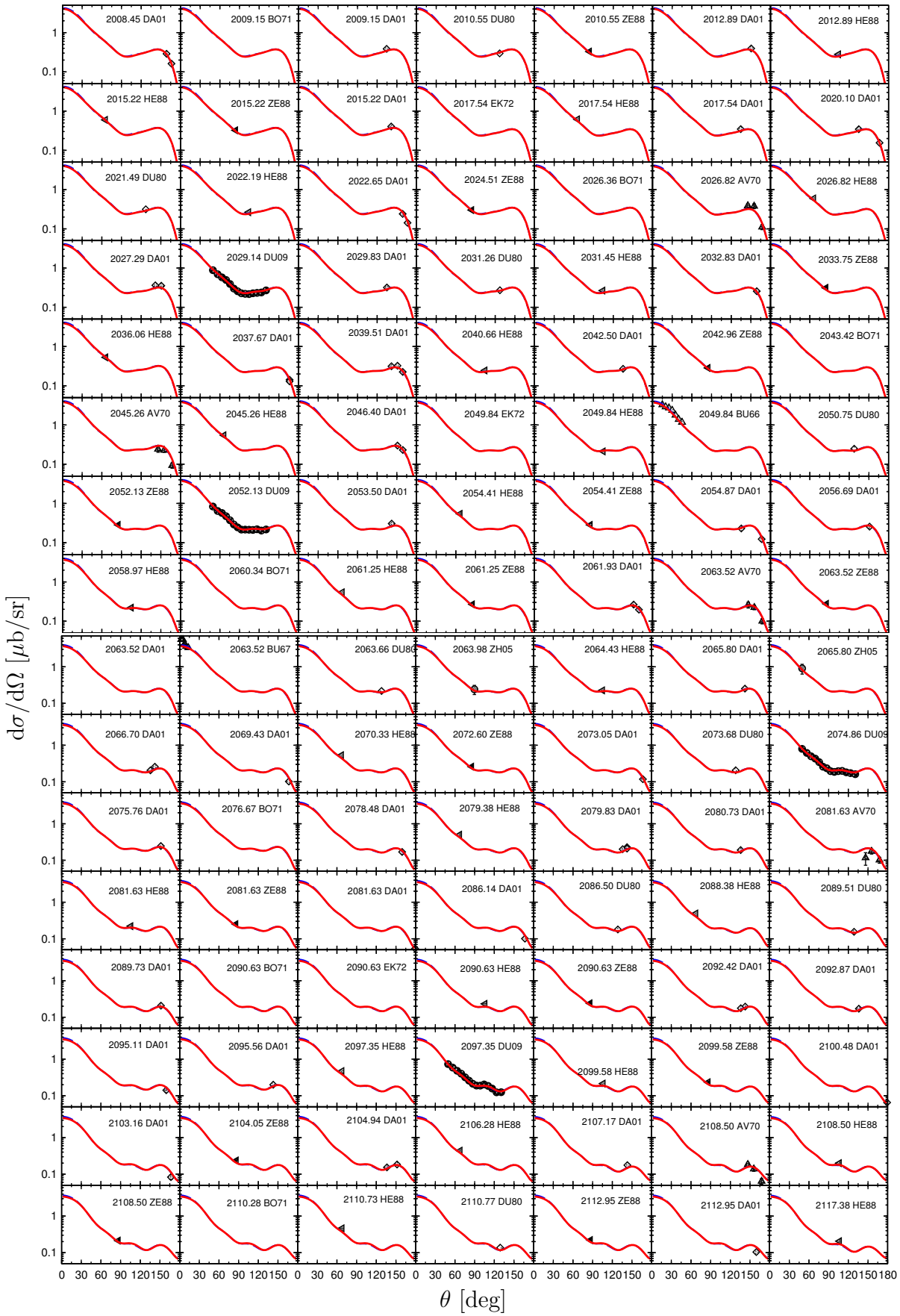

Figure A.32: Differential cross section of the reaction $\gamma p \to \pi^+ n$.

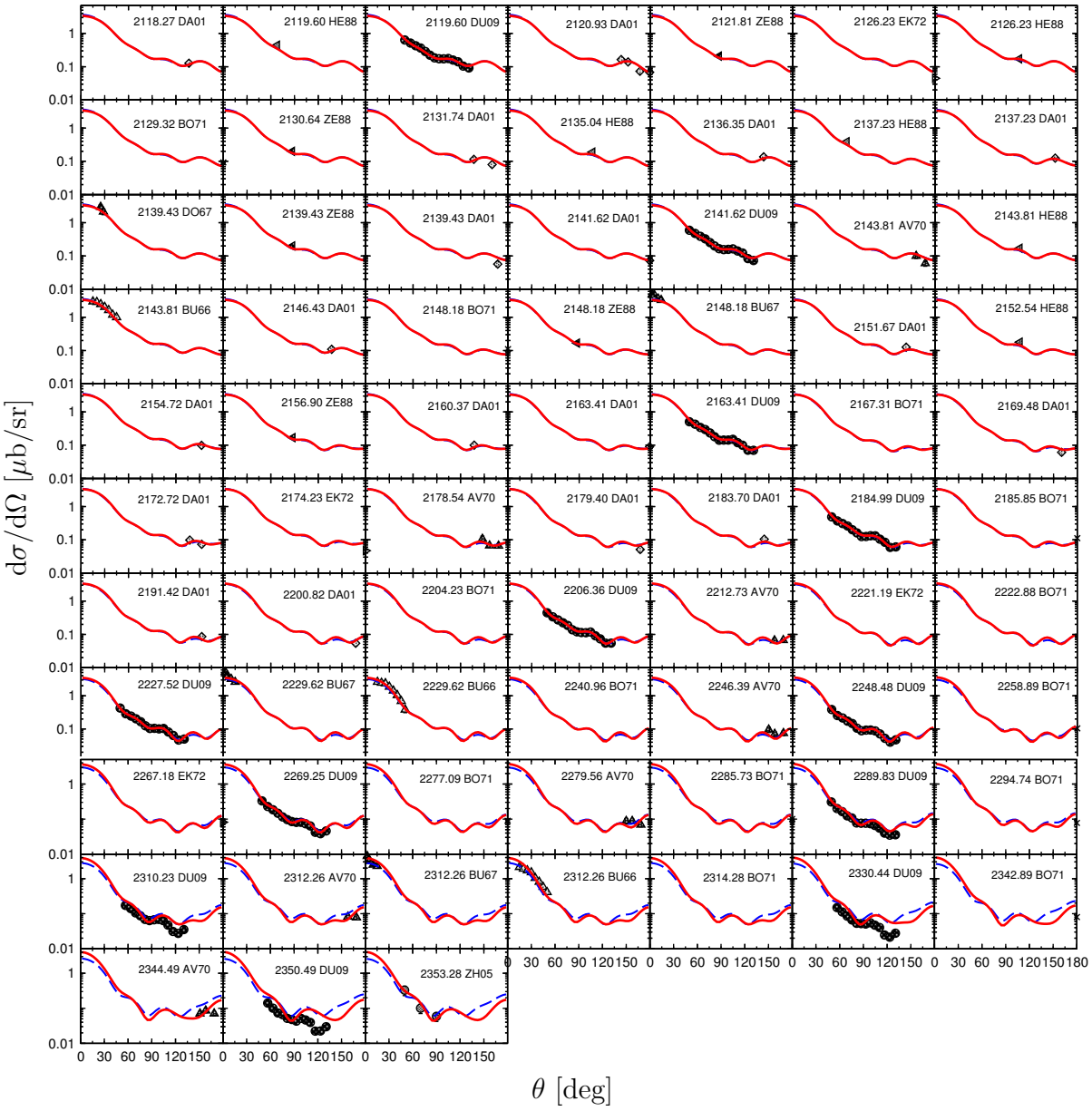

Figure A.33: Differential cross section of the reaction $\gamma p \to \pi^+ n$.

A.2 Beam asymmetry

A.2.1 $\gamma p \to \pi^0 p$

Data shown in the figures of this section can be found under the following references:

AB74 [147], AD01 [231], AG89 [232], AS72 [233], AT86 [234], AV77 [235], AV79 [236], AV83 [238], AV84 [239], BaGr [158], BE97 [161], BE06 [162], BJ69 [240], BL83 [241], BL92 [242], BL01 [243], BP70 [244], BS76 [245], BS79 [246], DR64 [247], EL09 [248], GB74 [249], GBXX [251], GB77 [252], GB78 [253], HO12 [181], KE74 [254], SC01 [188], SP10 [255], SU07 [192].

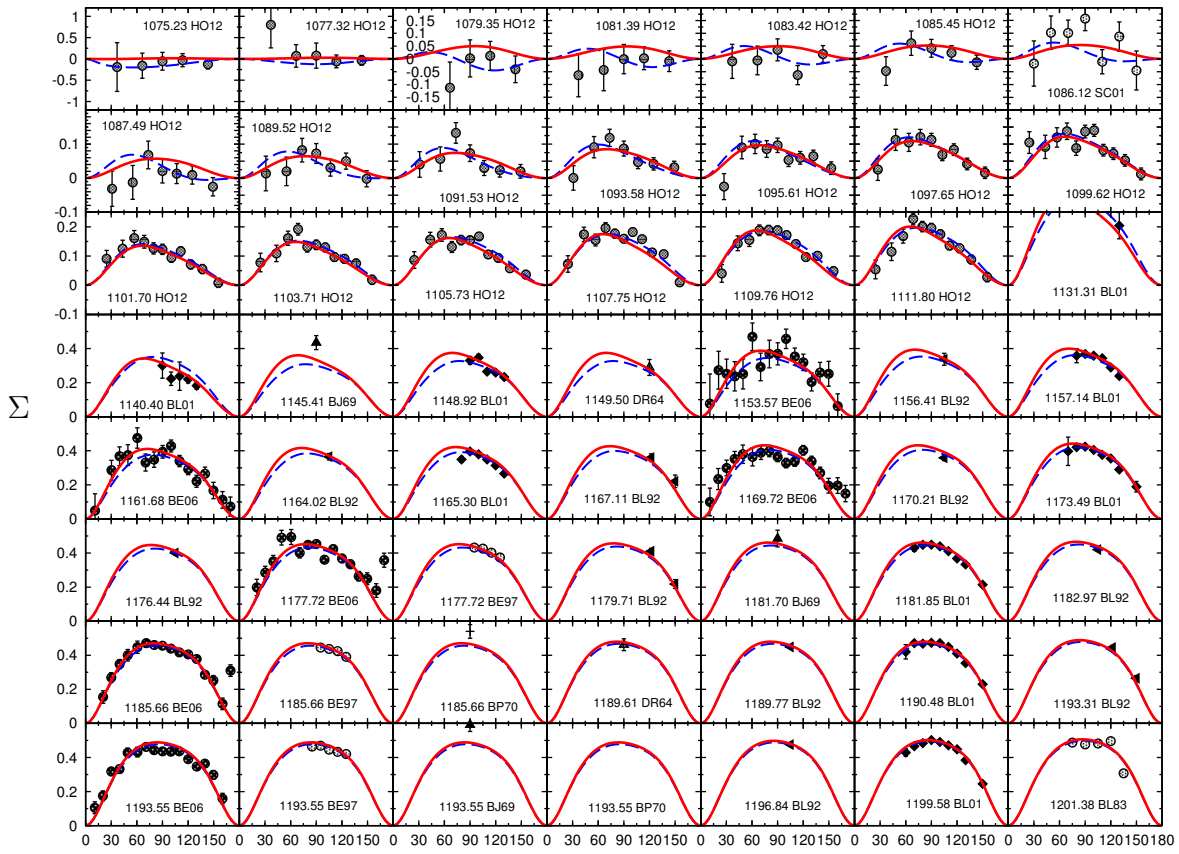

Figure A.34: Beam asymmetry of the reaction $\gamma p \to \pi^0 p$.

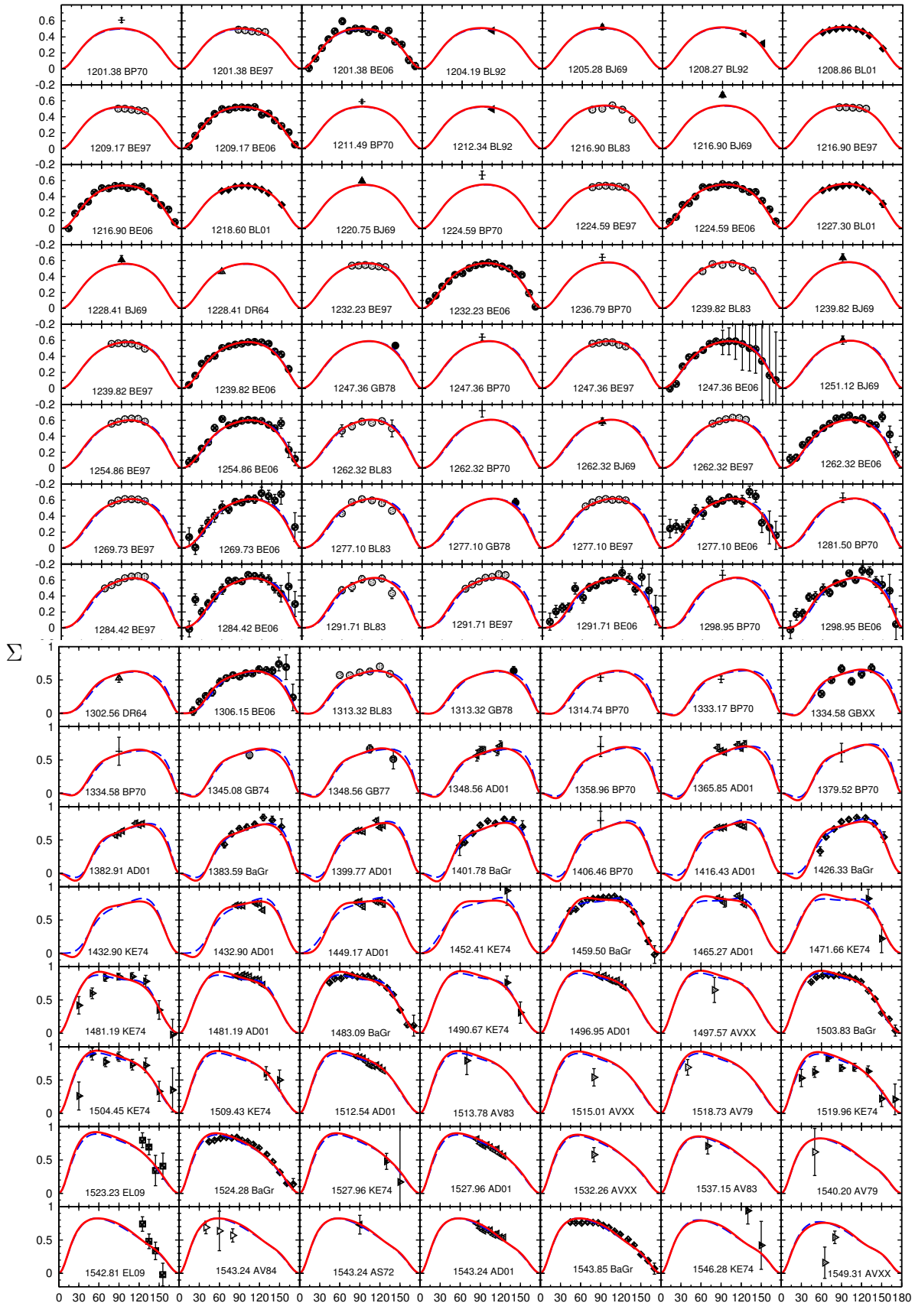

Figure A.35: Beam asymmetry of the reaction $\gamma p \to \pi^0 p$.

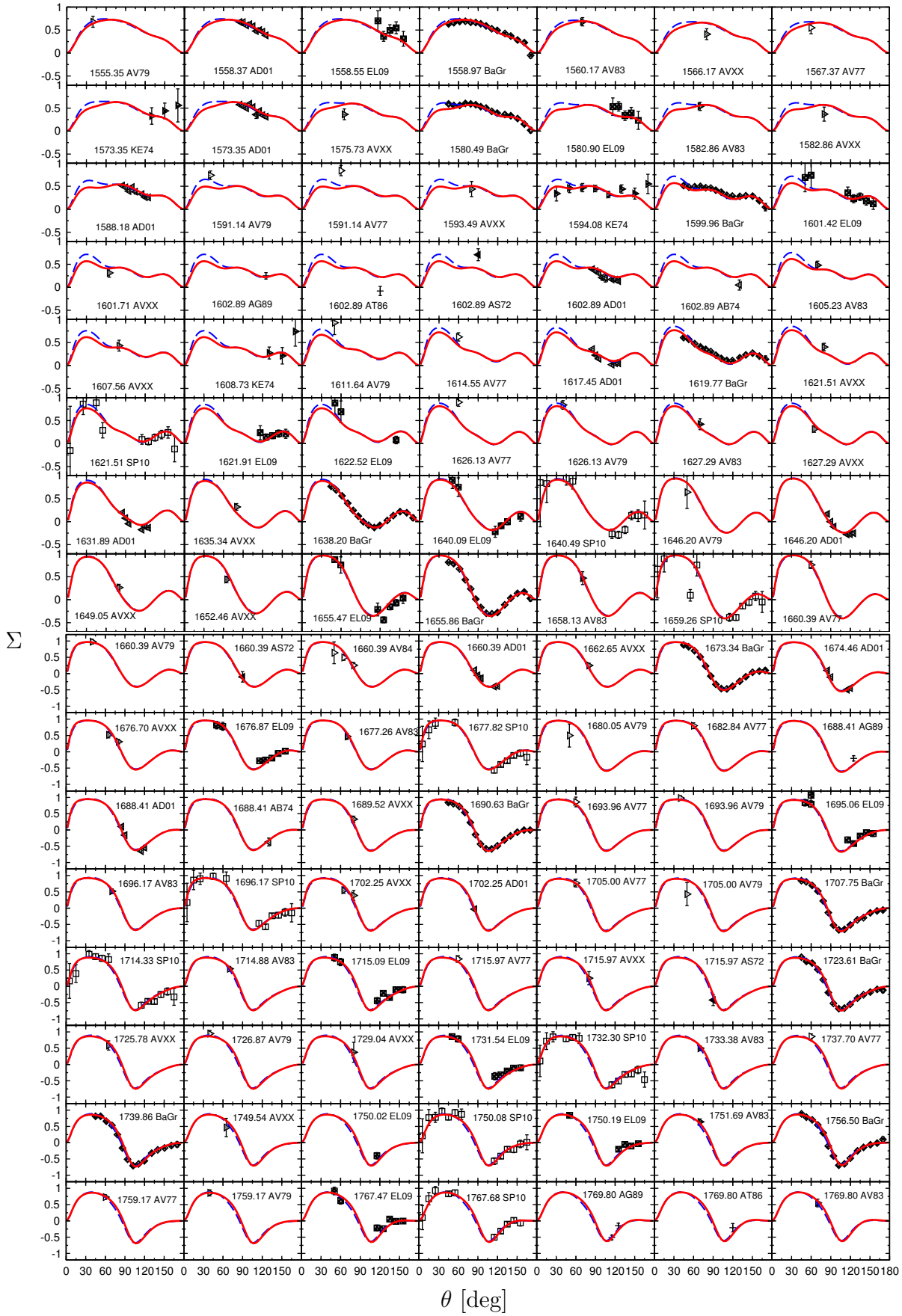

Figure A.36: Beam asymmetry of the reaction $\gamma p \to \pi^0 p$.

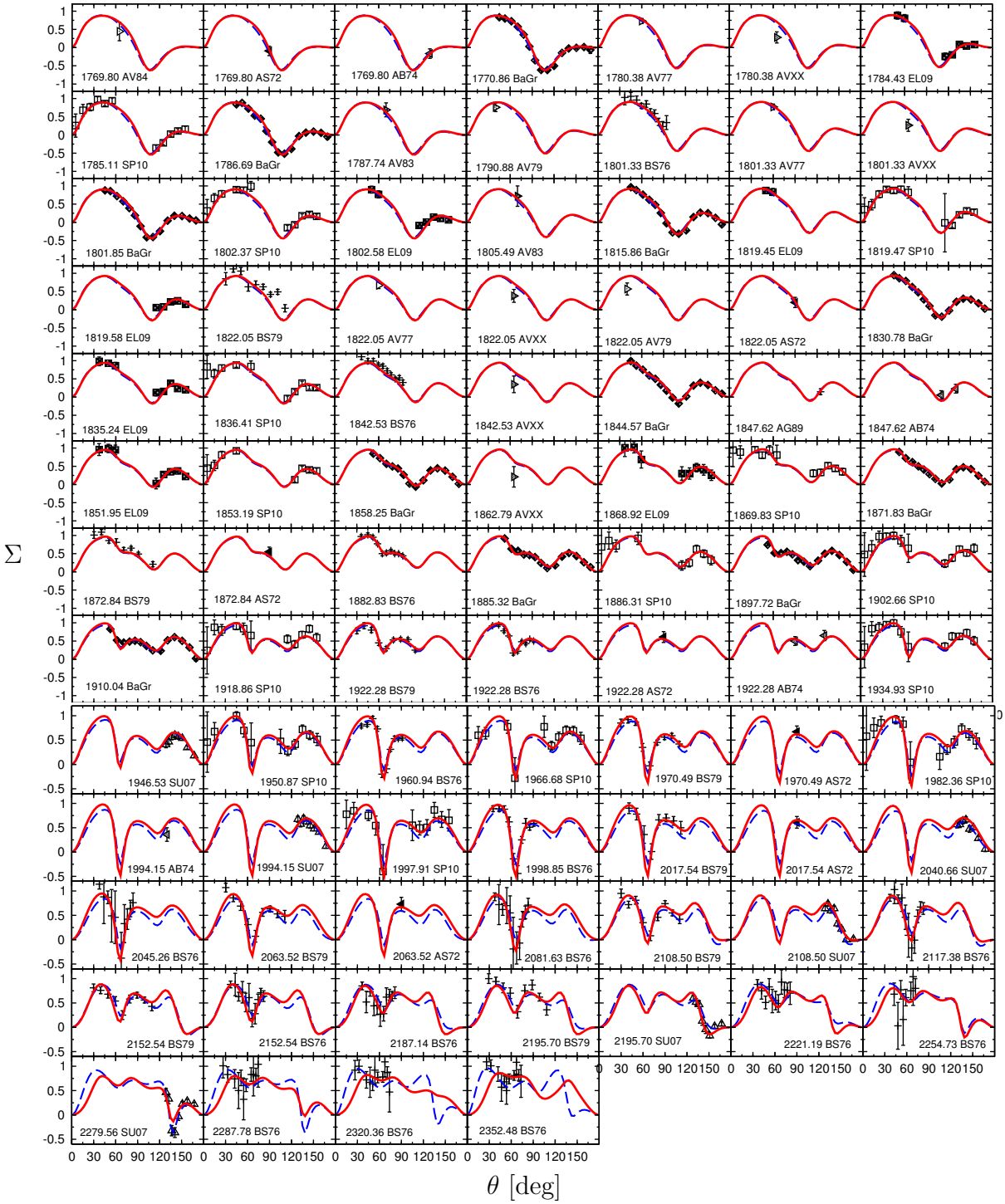

Figure A.37: Beam asymmetry of the reaction $\gamma p \to \pi^0 p$.

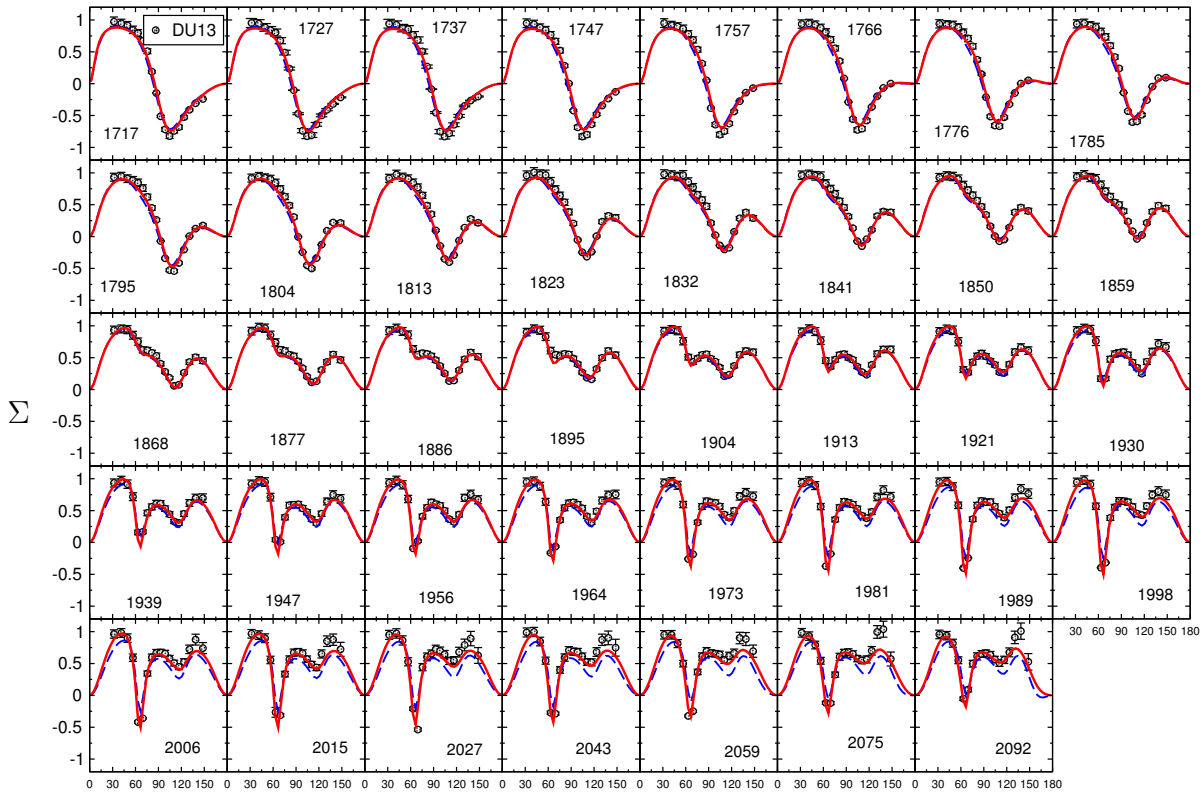

Figure A.38: Beam asymmetry of the reaction $\gamma p \to \pi^0 p$. Data: Ref. [139].

A.2.2 $\gamma p \to \pi^+ n$

Data shown in the figures of this section can be found under the following references:

AB74 [147], AB80 [256], AJ00 [257], AS72 [233], BA02 [258], BE00 [203], BL01 [243], BS79 [259], DU13 [139], GE69 [260], GE81 [261], GE89 [262], GN76 [263], HM80 [264], KE74 [254], KU71 [265], LU66 [266], SM63 [267], TA60 [268], ZA75 [269].

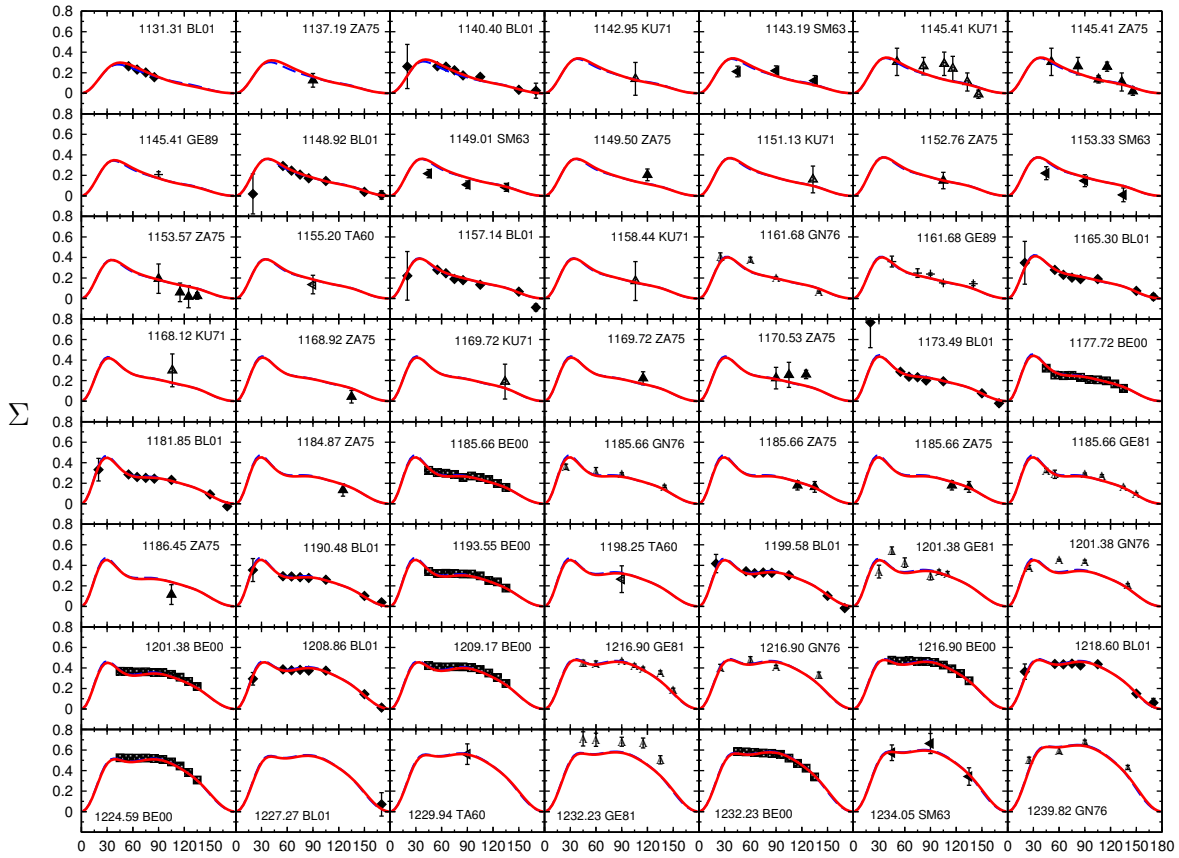

Figure A.39: Beam asymmetry of the reaction $\gamma p \to \pi^+ n$.

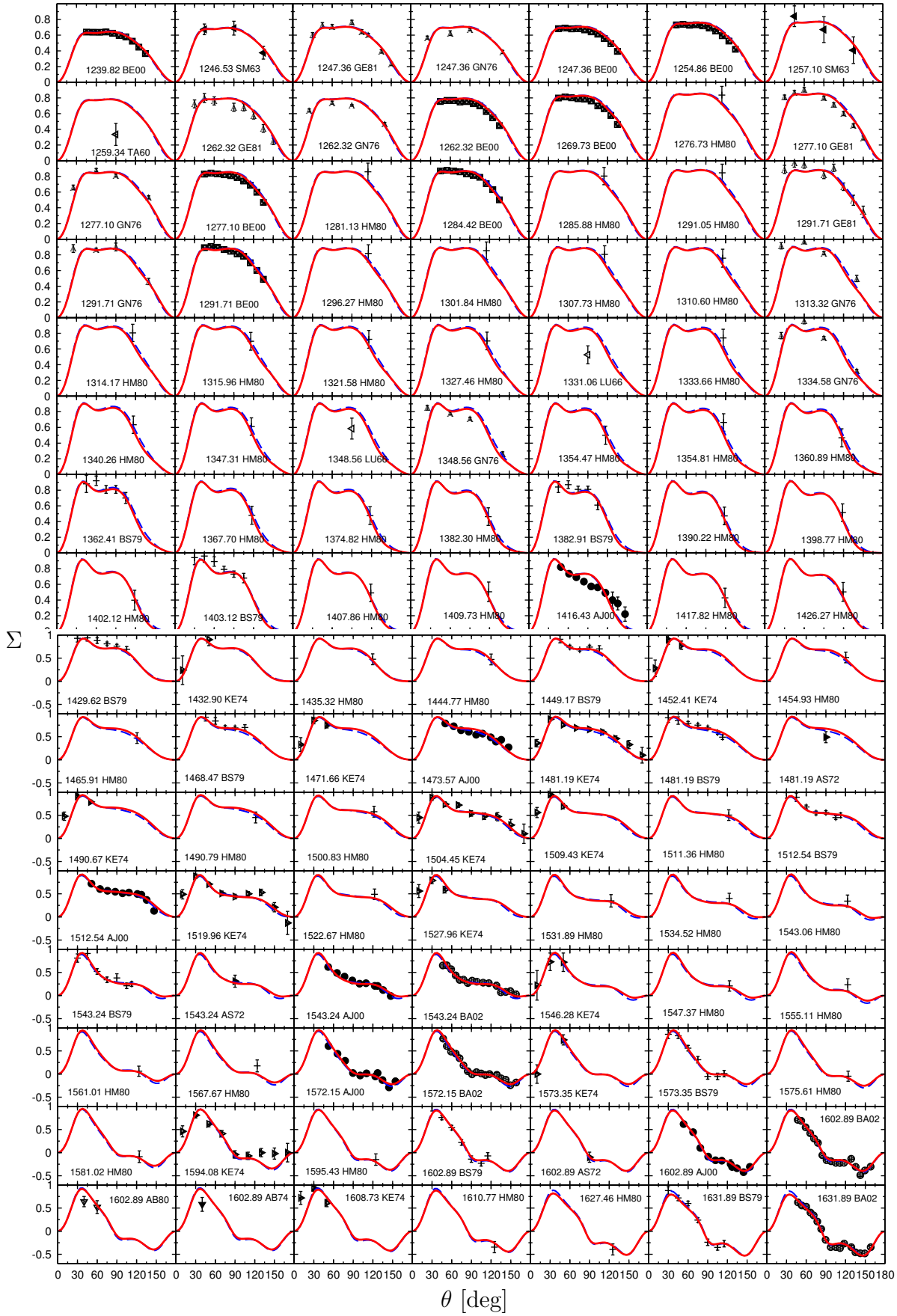

Figure A.40: Beam asymmetry of the reaction $\gamma p \to \pi^+ n$.

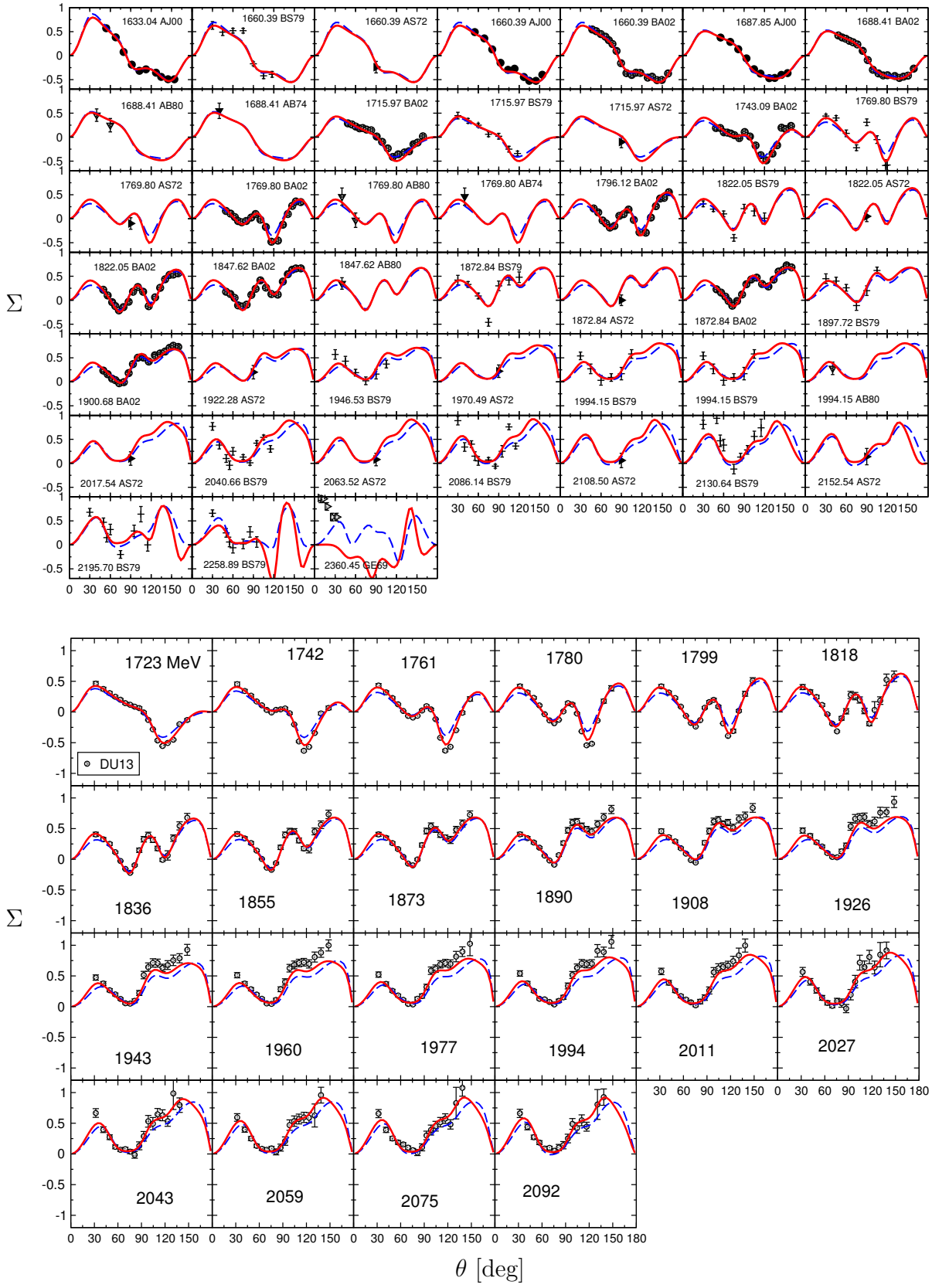

Figure A.41: Beam asymmetry of the reaction $\gamma p \to \pi^+ n$.

A.3 Target asymmetry

A.3.1 $\gamma p \to \pi^0 p$

Data shown in the figures of this section can be found under the following references:

AG89 [232], AT86 [234], BH77 [270], BL83 [241], BO98 [271], BS79 [246], FE76 [272], FK77 [273], GB74 [249], GB77 [252], GB78 [253], HH77 [274].

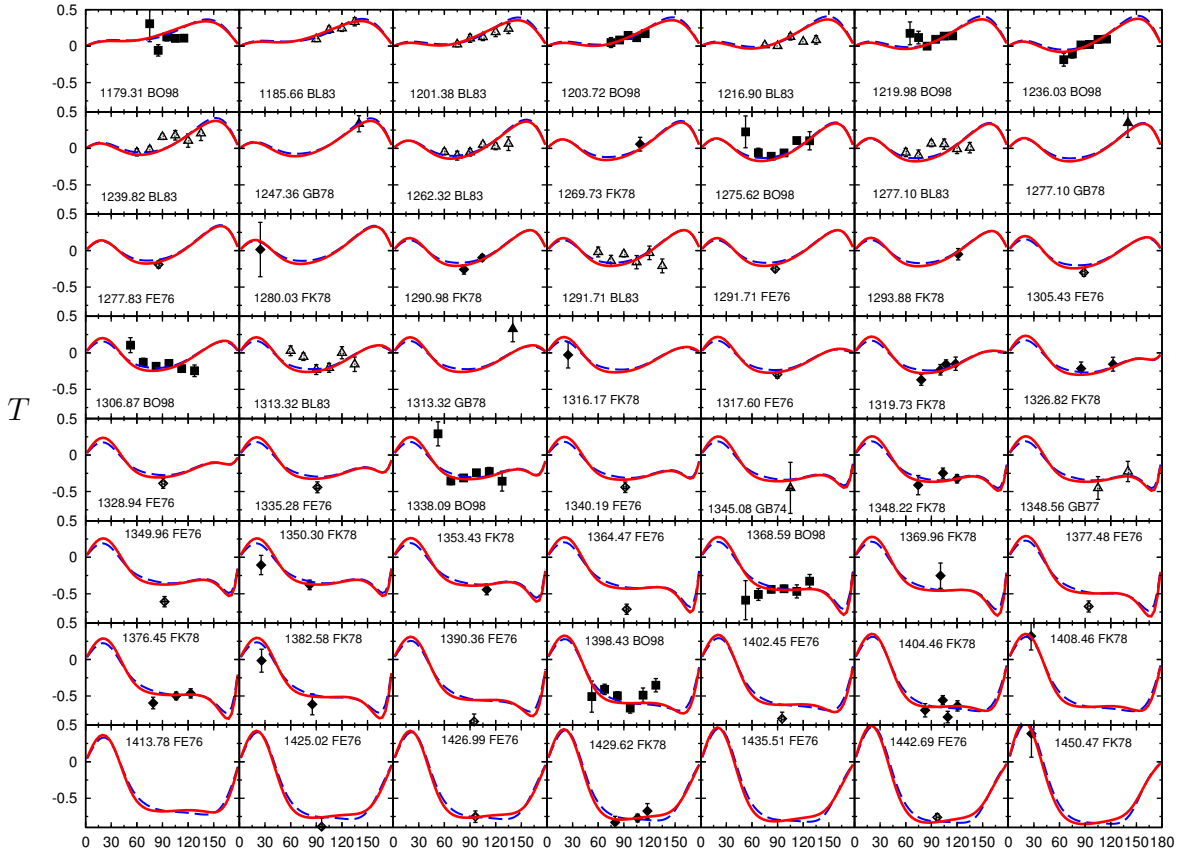

Figure A.42: Target asymmetry of the reaction $\gamma p \to \pi^0 p$.

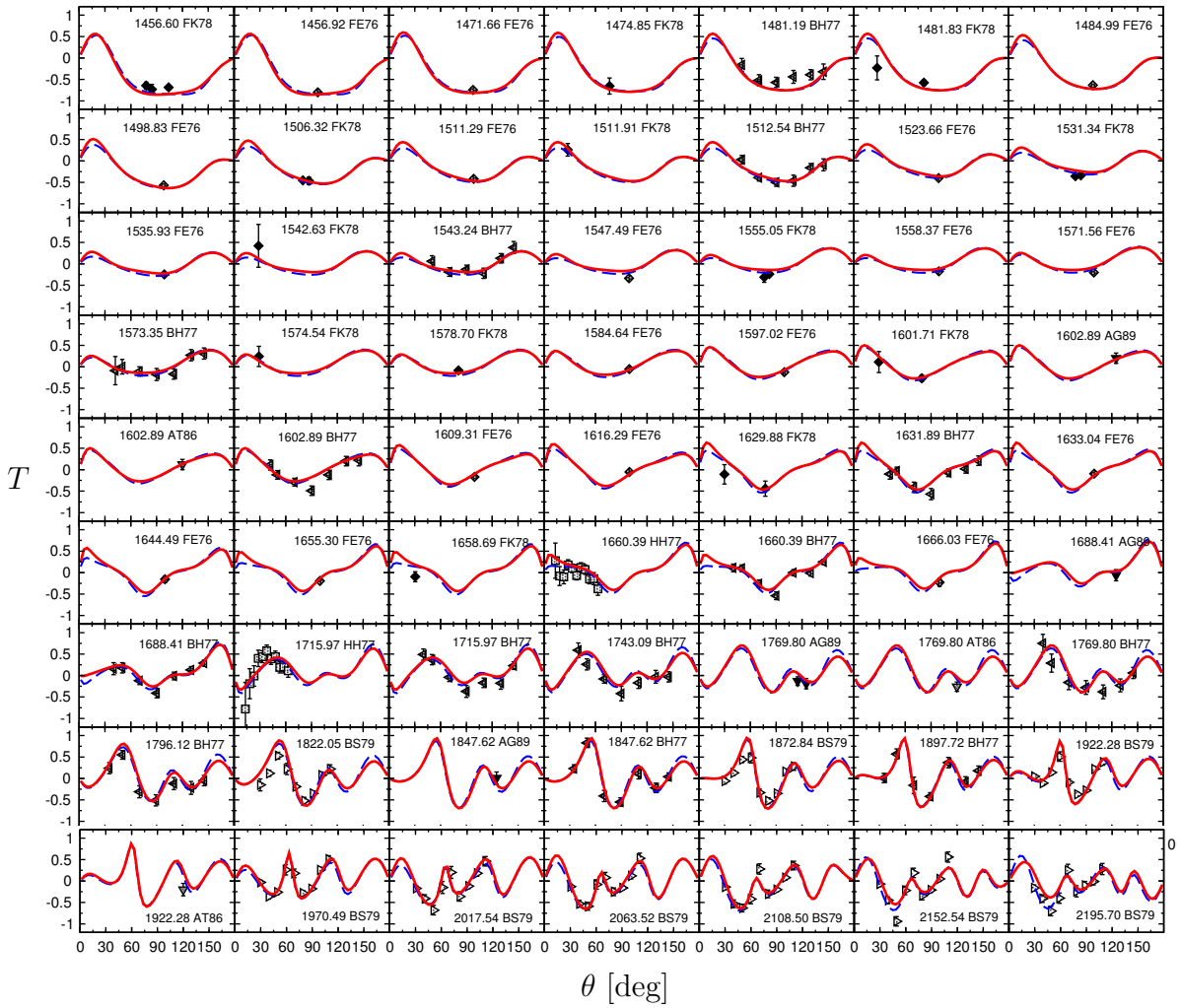

Figure A.43: Target asymmetry of the reaction $\gamma p \to \pi^0 p$.

A.3.2 $\gamma p \to \pi^+ n$

Data shown in the figures of this section can be found under the following references:

AA72 [275], AL73 [276], AL75 [277], AL76 [278], AL77 [279], BS79 [259], DU96 [280], FE76 [281], FJ82 [282], FK77 [283], GE80 [284], GE81 [261], GE89 [262], GZ75 [285].

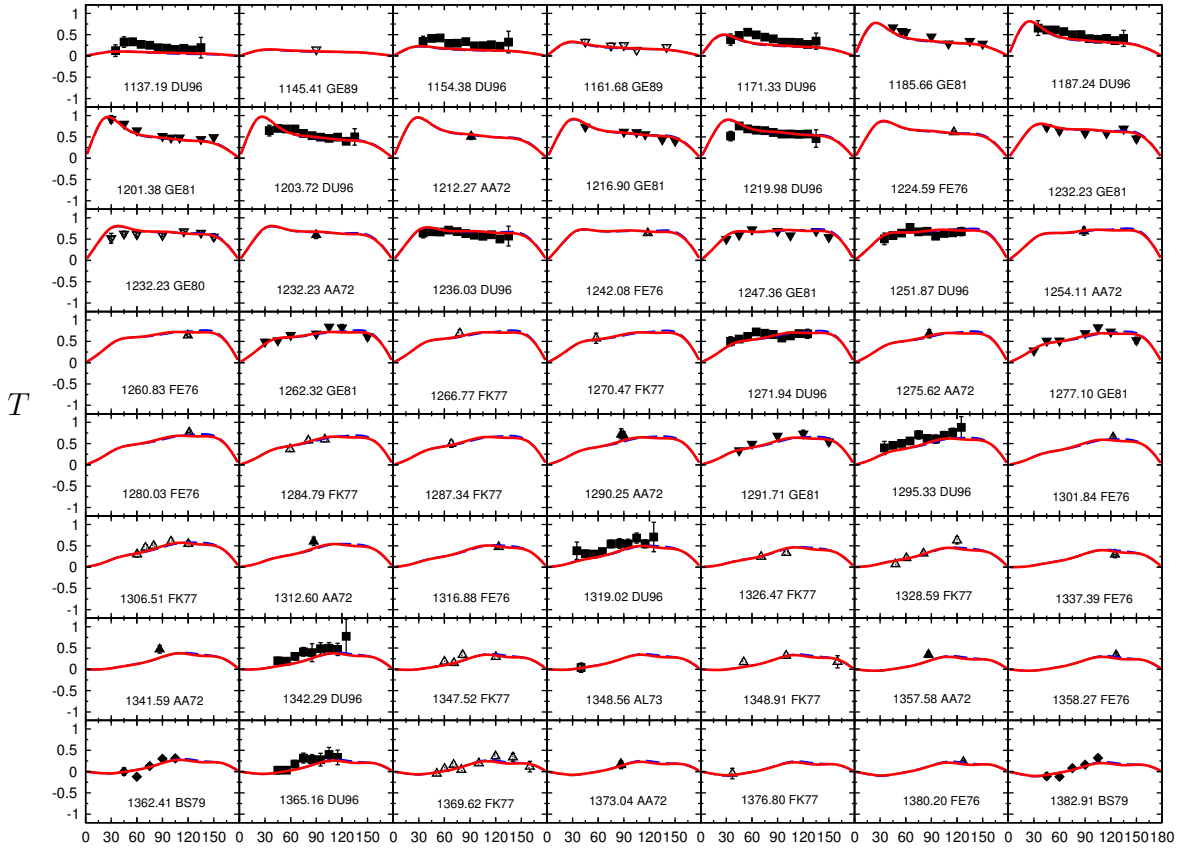

Figure A.44: Target asymmetry of the reaction $\gamma p \to \pi^+ n$.

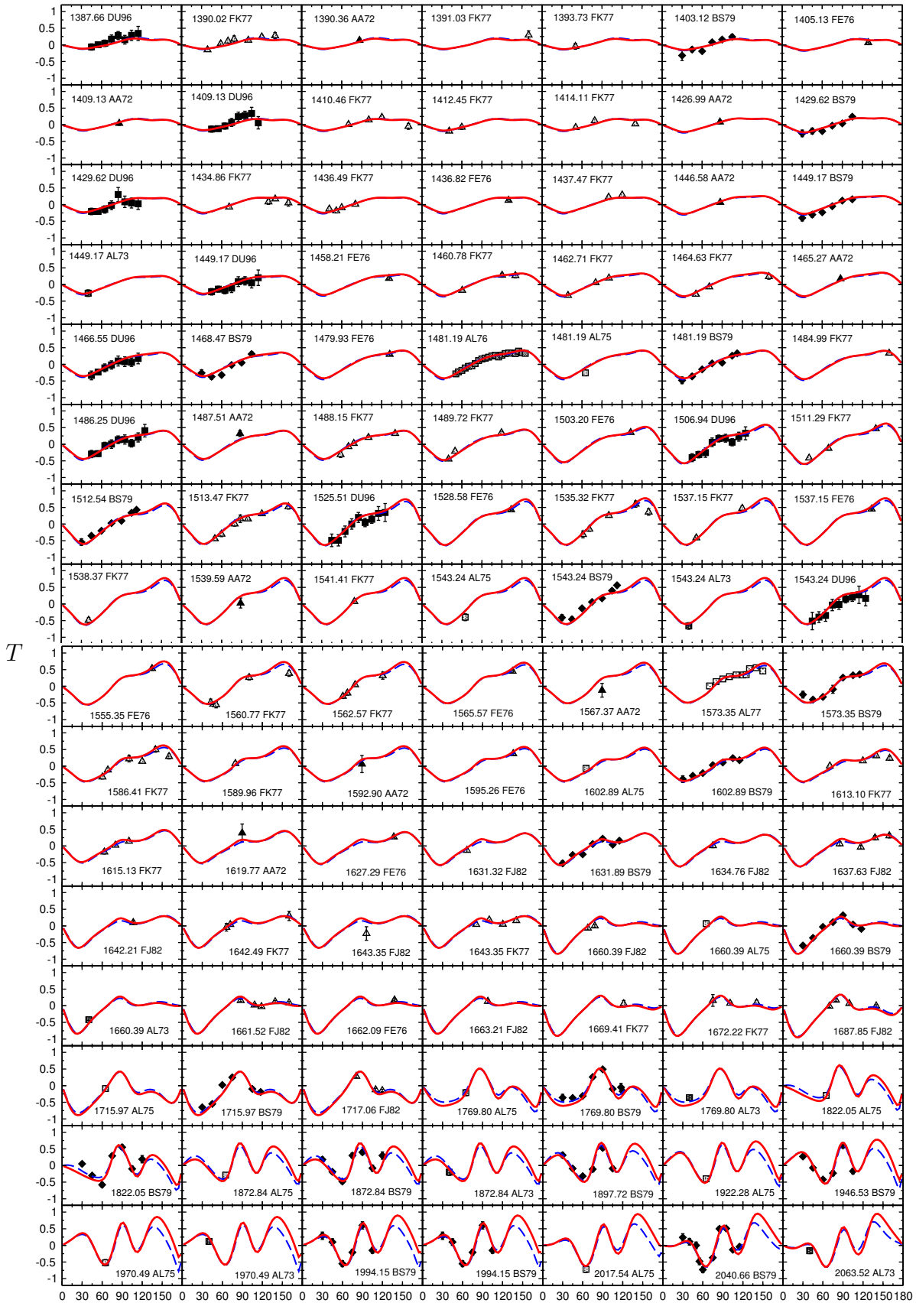

Figure A.45: Target asymmetry of the reaction $\gamma p \to \pi^+ n$.

A.4 Recoil polarization

A.4.1 $\gamma p \to \pi^0 p$

Data shown in the figures of this section can be found under the following references:

AG89 [232], AL66 [286], ALBO [287], AL68 [288], AT86 [234], AV83 [289], AV87 [290], AV88 [291], AV91 [292], BB62 [293], BD67 [294], BL83 [241], BM69 [295], BM70 [296], BM76 [297], BMXX [298], BS79 [246], BV80 [299], BV82 [300], BV83 [301], BVXX [302], BV85 [303], BV86 [304], BV87 [305], DC74 [306], DC76 [307], GC73 [308], GB74 [249], GB75 [250], GB77 [252], GB78 [253], HK68 [309], KA80 [310], KB72 [311], LU12 [142], ML65 [312], PR72 [313], QU61 [314], TN73 [315], TR72 [316], WI02 [141], ZY78 [317].

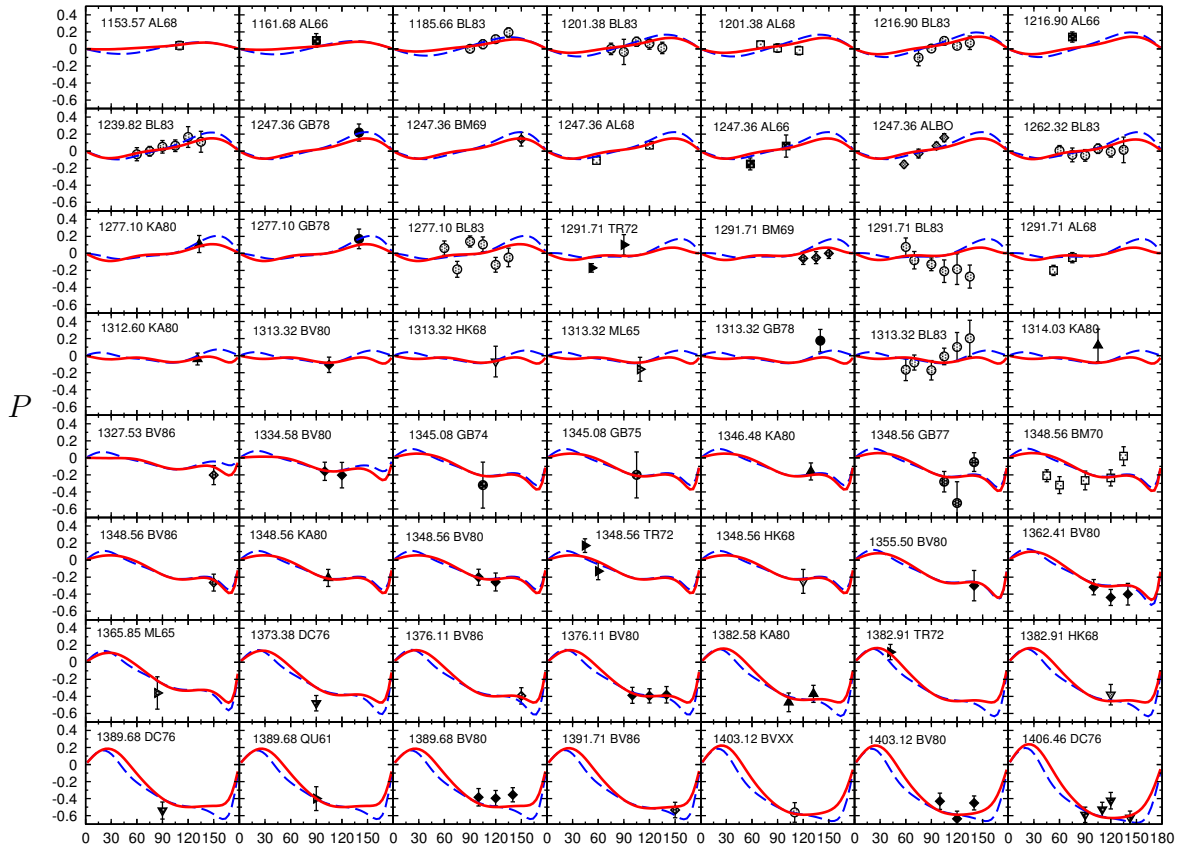

Figure A.46: Recoil polarization of the reaction $\gamma p \to \pi^0 p$.

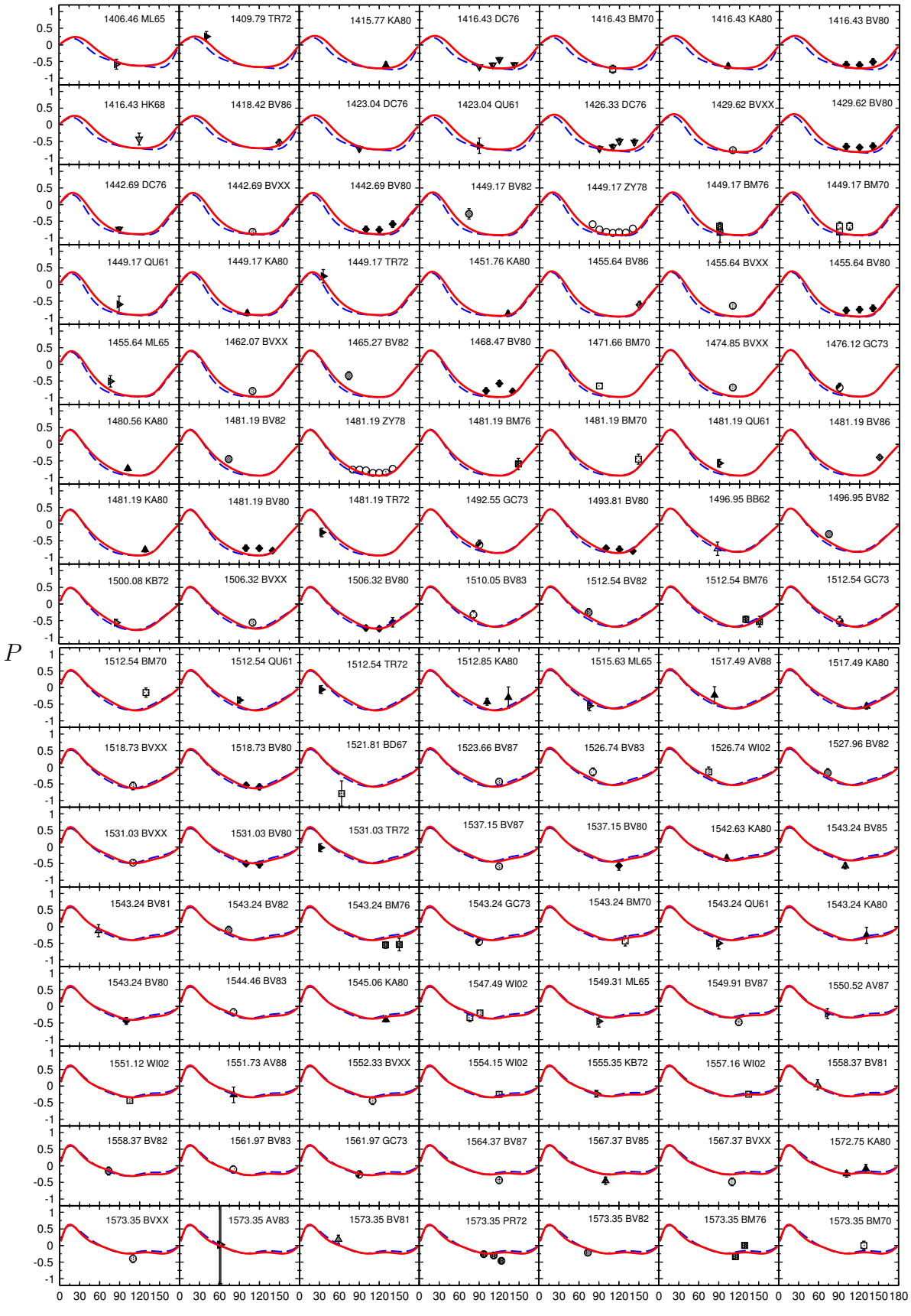

Figure A.47: Recoil polarization of the reaction $\gamma p \to \pi^0 p$.

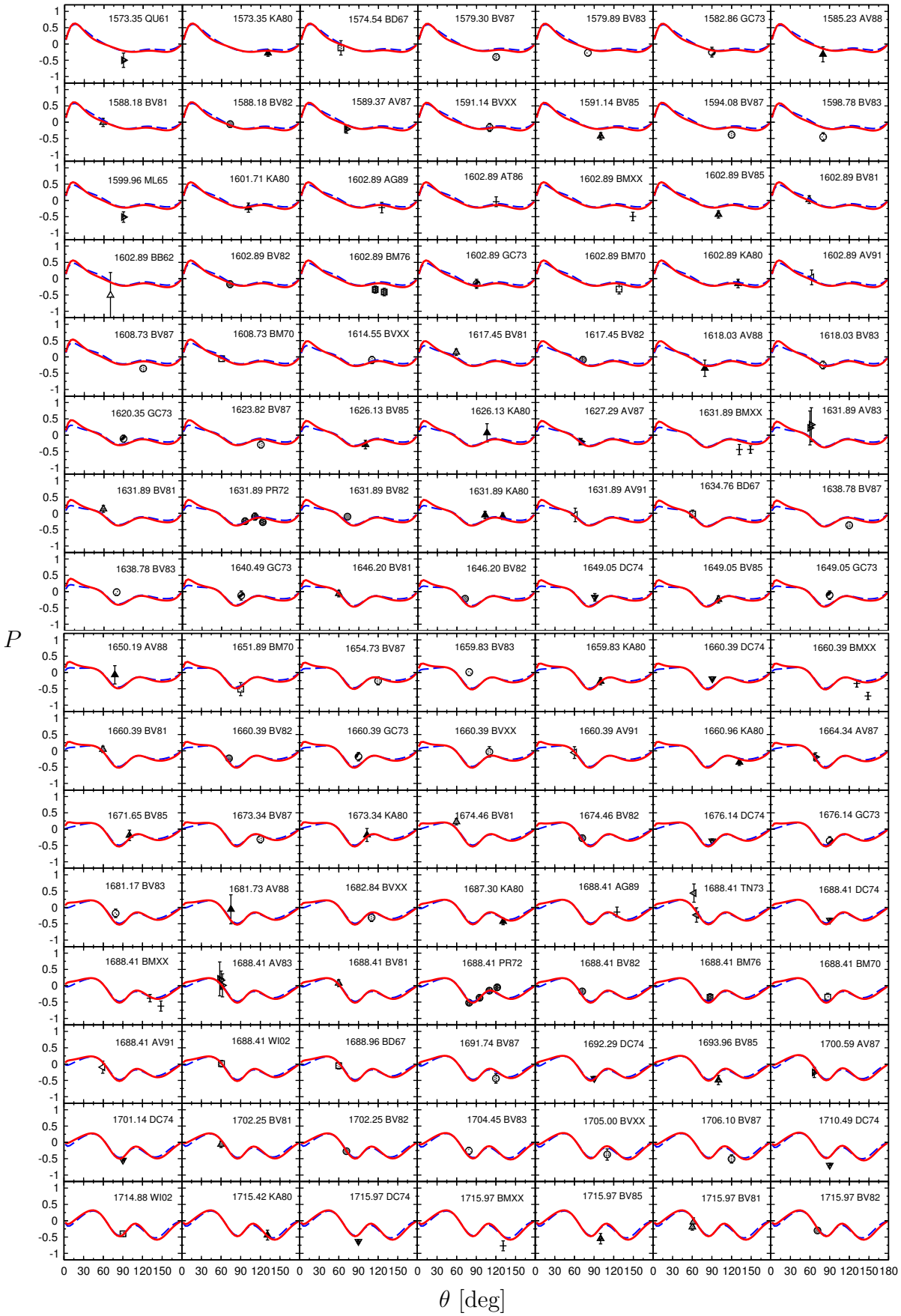

Figure A.48: Recoil polarization of the reaction $\gamma p \to \pi^0 p$.

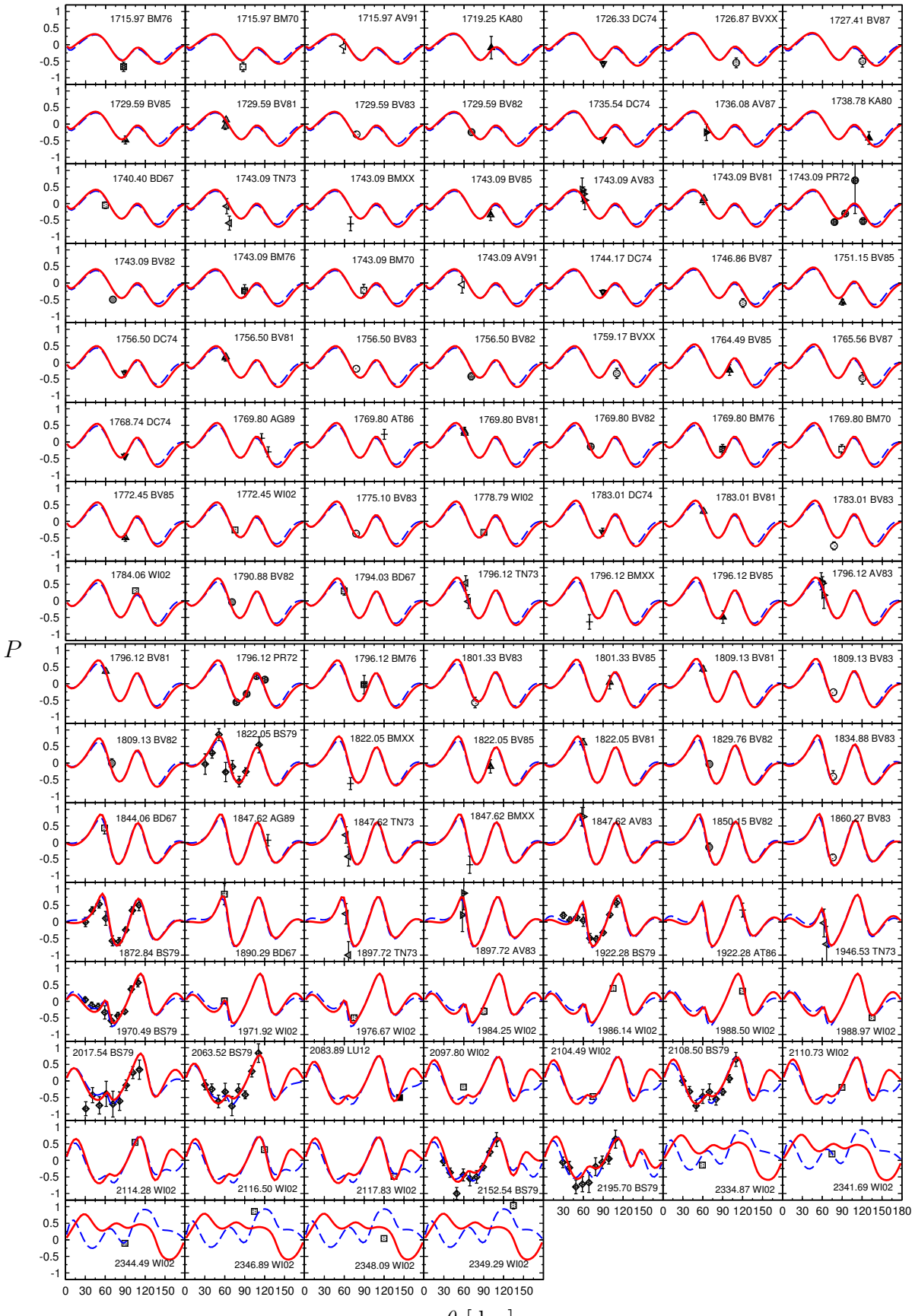

Figure A.49: Recoil polarization of the reaction $\gamma p \to \pi^0 p$.

A.4.2 $\gamma p \to \pi^+ n$

Data shown in the figures of this section can be found under the following references:

AL68 [318], BS79 [259], EG81 [319], GE81 [261], GE89 [262], HA71 [320], WL72 [321].

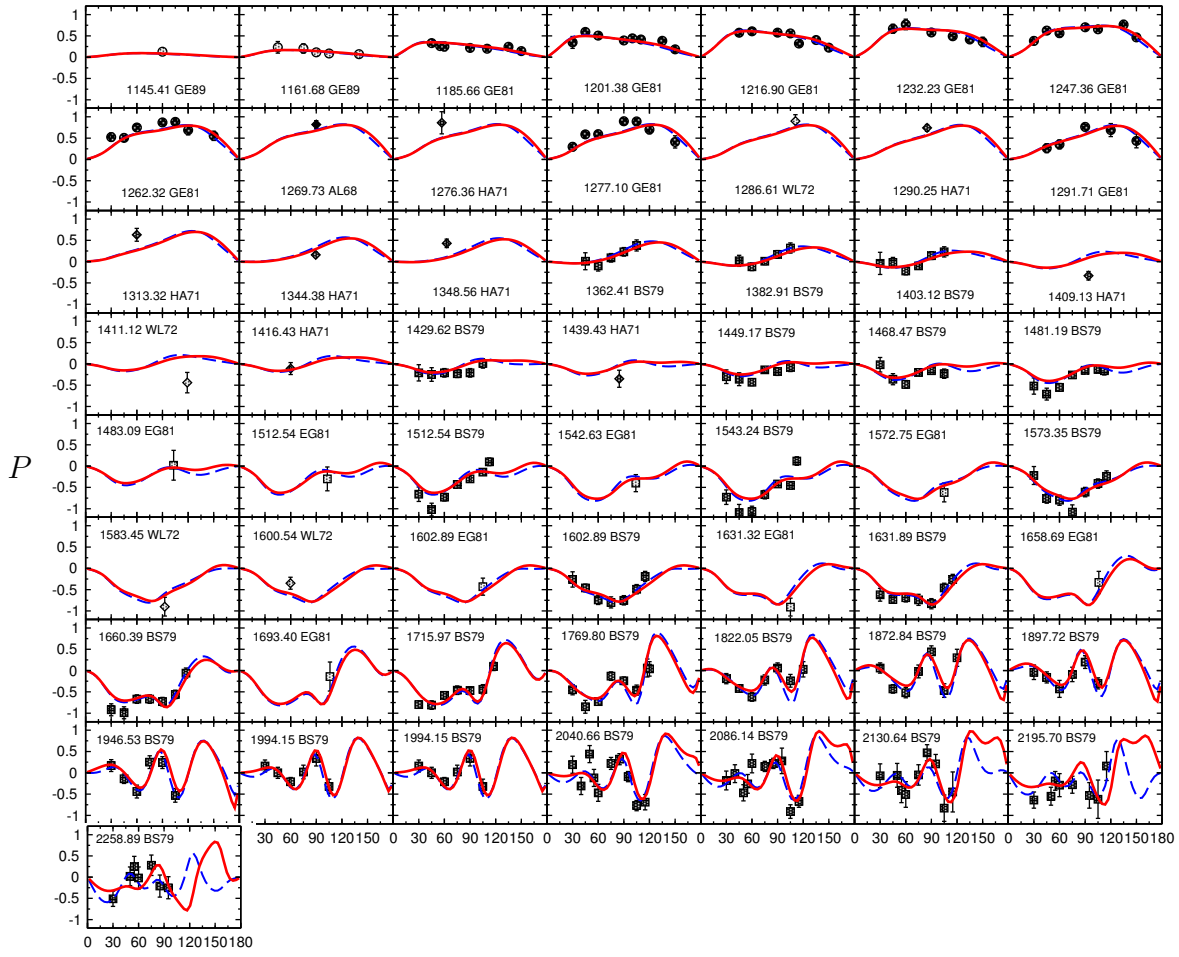

Figure A.50: Recoil polarization of the reaction $\gamma p \to \pi^+ n$.

Appendix B

Transformation of the hadronic scattering amplitude

B.1 Partial Wave Decomposition

To reduce the three-dimensional scattering equation to one dimension we perform a partial wave decomposition. In a first step, Eq. (1.17) is rewritten to take the form

$$\begin{aligned}\langle\lambda_3\lambda_4\vec{p}\,''|T|\lambda_1\lambda_2\vec{p}\,'\rangle &= \langle\lambda_3\lambda_4\vec{p}\,''|V|\lambda_1\lambda_2\vec{p}\,'\rangle + \\ &\sum_{\gamma_1,\gamma_2}\int dp^3\langle\lambda_3\lambda_4\vec{p}\,''|V|\gamma_1\gamma_2\vec{p}\rangle G(p)\langle\gamma_1\gamma_2\vec{p}|T|\lambda_1\lambda_1\vec{p}\,'\rangle\,. \quad \text{(B.1)}\end{aligned}$$

Here, λ_1 and λ_2 (λ_3 and λ_4, γ_1 and γ_2) denote the helicities of the incoming (outgoing, intermediate) particles 1 and 2. Since the helicity operator and the angular momentum commute, we can expand the states $|\lambda_1\lambda_2\vec{p}\rangle$ in terms of the eigenstates of the total angular momentum J [322]:

$$\langle\lambda''\vec{p}\,''|T|\lambda'\vec{p}\,'\rangle = \frac{1}{4\pi}\sum_J(2J+1)D^J_{\lambda'\lambda''}(\Omega_{p''p'},0)^*\langle\lambda''\vec{p}\,''|T^J|\lambda'\vec{p}\,'\rangle \quad \text{(B.2)}$$

with $\lambda' := \lambda_1 - \lambda_2$ and $\lambda'' := \lambda_3 - \lambda_4$. $\Omega_{p''p'}$ is the solid angle of $\vec{p}\,'$ and $\vec{p}\,''$.
The $D^J_{\lambda''\lambda'}(\Omega_{p''p'},0)$ are the matrix elements of the (finite) rotation operator

$$\mathcal{D}^J(\alpha\beta\gamma) = e^{-i\alpha J_z}e^{-i\beta J_y}e^{-i\gamma J_z} \quad \text{(B.3)}$$

$$D^J_{\lambda'\lambda''}(\alpha\beta\gamma) = \langle J\lambda''|\mathcal{D}^J(\alpha\beta\gamma)|J\lambda'\rangle = e^{-i\alpha J_z}d^J_{\lambda'\lambda''}(\beta)e^{-i\gamma J_z} \quad \text{(B.4)}$$

and the $d^J_{\lambda'\lambda''}(\beta)$ are the reduced rotation matrices or Wigner (small) d-functions. The explicit expressions for the $d^J_{\lambda'\lambda''}$ up to $J = 9/2$ can be found in Appendix B.1.1.

Applying the expansion of Eq. (B.2), the scattering equation reads

$$\begin{aligned}\frac{1}{4\pi}\sum_J \quad & (2J+1)D^J_{\lambda'\lambda''}(\Omega_{p''p'},0)^*\langle\lambda''\vec{p}\,''|T^J|\lambda'\vec{p}\,'\rangle = \langle\lambda_3\lambda_4\vec{p}\,''|V^{J'}|\lambda_1\lambda_2\vec{p}\,'\rangle + \\ + \quad & \frac{1}{4\pi}\sum_{\gamma_1,\gamma_2}\sum_{J',J''}\int dp^3(2J'+1)(2J''+1)D^{J'}_{\gamma_1\lambda''}(\Omega_{p''p},0)^*D^{J''}_{\lambda'\gamma_2}(\Omega_{pp'},0)^* \\ \times \quad & \langle\lambda_3\lambda_4\vec{p}\,''|V^{J'}|\gamma_1\gamma_2\vec{p}\rangle G(p)\langle\gamma_1\gamma_2\vec{p}|T^{J''}|\lambda_1\lambda_1\vec{p}\,'\rangle \end{aligned} \tag{B.5}$$

Substituting $\int dp^3$ with $\int dpd\Omega_{pp'}p^2$ restricts the angular dependence to $D^{J'}_{\lambda'\lambda''}$. Using the following relations [323], the integration over $d\Omega_{pp'}$ can be carried out straightforward

$$D^J_{\lambda\lambda'}(\Omega_{p'p},0) = \left(D^J_{\lambda'\lambda}(\Omega_{pp'},0)\right)^* \tag{B.6}$$

$$D^J_{\lambda\lambda'}(\Omega_1\Omega_2,0) = \sum_\gamma D^J_{\lambda\gamma}(\Omega_1,0)D^J_{\gamma\lambda'}(\Omega_2,0) \tag{B.7}$$

$$\int d\Omega\left(D^J_{\lambda\lambda'}(\Omega,0)\right)^* D^{J'}_{\gamma\gamma'}(\Omega,0) = \frac{4\pi}{2J+1}\delta_{J'J}\delta_{\lambda\gamma}\delta_{\lambda'\gamma'}. \tag{B.8}$$

We obtain

$$\int d\Omega_{qk}D^{J'}_{\gamma\lambda'}(\Omega_{k'q},0)^*D^{J''}_{\lambda\gamma}(\Omega_{qk},0)^* = D^{J'}_{\lambda\lambda'}(\Omega_{k'k},0)^*\frac{4\pi}{2J'+1}\delta_{J'J''}. \tag{B.9}$$

Inserting Eq. (B.9) into Eq. (B.5) the sum over J'' vanishes. In a final step we exploit the fact that the Wigner rotation matrices form a complete set of orthogonal functions and we arrive by comparison of coefficients at a one-dimensional integral equation for every J:

$$\begin{aligned}\langle\lambda_3\lambda_4\vec{p}\,''|T^J|\lambda_1\lambda_2\vec{p}\,'\rangle = \; & \langle\lambda_3\lambda_4\vec{p}\,''|V^J|\lambda_1\lambda_2\vec{p}\,'\rangle + \\ & \sum_{\gamma_1,\gamma_2}\int dpp^2\langle\lambda_3\lambda_4\vec{p}\,''|V^J|\gamma_1\gamma_2\vec{p}\rangle G(p)\langle\gamma_1\gamma_2\vec{p}|T^J|\lambda_1\lambda_1\vec{p}\,'\rangle.\end{aligned} \tag{B.10}$$

Applying the orthogonality relation

$$\int d(\cos\theta)d^J_{\lambda\lambda'}(\theta)d^{J'}_{\lambda\lambda'}(\theta) = \frac{2}{2J+1}\delta_{JJ'} \tag{B.11}$$

we can invert Eq. (B.10):

$$\langle\lambda'\vec{p}\,''|T^J|\lambda\vec{p}\,'\rangle = 2\pi\int d(\cos\theta)d^J_{\lambda\lambda'}\langle\lambda'\vec{p}\,''|T|\lambda\vec{p}\,'\rangle. \tag{B.12}$$

B.1.1 Small d-Functions

The small d-function are group-theoretical representations of finite rotations:

$$d^J_{m'm}(\theta) = \langle jm'|e^{-i\frac{\theta}{2}J_y}|jm\rangle \tag{B.13}$$

We use the convention of Brink and Satchler [323]

$$\begin{aligned} d^J_{m'm}(\theta) &= \sum_s (-1)^s \frac{[(J+m')!(J-m')!(J+m)!(J-m)!]^{\frac{1}{2}}}{(J+m'-s)!(J-m-s)!s!(s+m-m')!} \\ &\times \left(\cos\frac{\theta}{2}\right)^{2J+m'-m-2s} \left(\sin\frac{\theta}{2}\right)^{2s+m-m'} . \end{aligned} \tag{B.14}$$

Explicitly, the small d-functions up to a total spin of $J = 9/2$ read:

- J=1/2

$$d^{\frac{1}{2}}_{\frac{1}{2}\frac{1}{2}}(\theta) = \cos\frac{\theta}{2}, \qquad d^{\frac{1}{2}}_{\frac{-1}{2}\frac{1}{2}}(\theta) = \sin\frac{\theta}{2}$$

- J=3/2

$$\begin{aligned} d^{\frac{3}{2}}_{\frac{1}{2}\frac{1}{2}}(\theta) &= \cos\frac{\theta}{2}\left(3\cdot\cos^2\frac{\theta}{2} - 2\right) \\ d^{\frac{3}{2}}_{\frac{-1}{2}\frac{1}{2}}(\theta) &= -\sin\frac{\theta}{2}\left(3\cdot\sin^2\frac{\theta}{2} - 2\right) \end{aligned}$$

- J=5/2

$$\begin{aligned} d^{\frac{5}{2}}_{\frac{1}{2}\frac{1}{2}}(\theta) &= \cos\frac{\theta}{2}\left(10\cdot\cos^4\frac{\theta}{2} - 12\cdot\cos^2\frac{\theta}{2} + 3\right) \\ d^{\frac{5}{2}}_{\frac{-1}{2}\frac{1}{2}}(\theta) &= \sin\frac{\theta}{2}\left(10\cdot\sin^4\frac{\theta}{2} - 12\cdot\sin^2\frac{\theta}{2} + 3\right) \end{aligned}$$

- J=7/2

$$\begin{aligned} d^{\frac{7}{2}}_{\frac{1}{2}\frac{1}{2}}(\theta) &= \cos^7\frac{\theta}{2} - 12\cdot\cos^5\frac{\theta}{2}\sin^2\frac{\theta}{2} + 18\cdot\cos^3\frac{\theta}{2}\sin^4\frac{\theta}{2} - 4\cdot\cos\frac{\theta}{2}\sin^6\frac{\theta}{2} \\ d^{\frac{7}{2}}_{\frac{-1}{2}\frac{1}{2}}(\theta) &= -\sin^7\frac{\theta}{2} + 12\cdot\cos^2\frac{\theta}{2}\sin^5\frac{\theta}{2} - 18\cdot\cos^4\frac{\theta}{2}\sin^3\frac{\theta}{2} + 4\cdot\cos^6\frac{\theta}{2}\sin\frac{\theta}{2} \end{aligned}$$

- J=9/2

$$\begin{aligned} d^{\frac{9}{2}}_{\frac{1}{2}\frac{1}{2}}(\theta) &= \cos^9\frac{\theta}{2} - 20\cdot\cos^7\frac{\theta}{2}\sin^2\frac{\theta}{2} + 60\cdot\cos^5\frac{\theta}{2}\sin^4\frac{\theta}{2} - 40\cdot\cos^3\frac{\theta}{2}\sin^6\frac{\theta}{2} + 5\cdot\cos\frac{\theta}{2}\sin^8\frac{\theta}{2} \\ d^{\frac{9}{2}}_{\frac{1}{2}\frac{-1}{2}}(\theta) &= 5\cos^8\frac{\theta}{2}\cdot\sin\frac{\theta}{2} - 40\cdot\cos^6\frac{\theta}{2}\cdot\sin^3\frac{\theta}{2} + 60\cos^4\frac{\theta}{2}\cdot\sin^5\frac{\theta}{2} - 20\cos^2\frac{\theta}{2}\cdot\sin^7\frac{\theta}{2} + \sin^9\frac{\theta}{2} \end{aligned}$$

B.2 Transformation from helicity to JLS-Basis

In the following we explain the transformation of partial-wave amplitudes from helicity to JLS basis. The different states are no longer distinguished by their helicities λ but by the orbital angular momentum L and their spin S.
For a state with total spin J and its z-projections M the transformation has the form

$$|JM\lambda_1\lambda_2\rangle = \sum_{LS}\langle JMLS|JM\lambda_1\lambda_2\rangle|JMLS\rangle\,, \tag{B.15}$$

where λ_1 and λ_2 are the helicities of the two particles in the state. In Eq. (B.15) and the following the momentum index p is suppressed.
The transformation matrix $U^{J,LS}_{\lambda_1\lambda_2} := \langle JMLS|JM\lambda_1\lambda_2\rangle$ can be calculated via [322]

$$\langle JMLS|JM\lambda_1\lambda_2\rangle = \left(\frac{2L+1}{2J+1}\right)^{\frac{1}{2}}\langle L0S\lambda|J\lambda\rangle\langle S_1\lambda_1 S_2\lambda_2|S\lambda\rangle\,. \tag{B.16}$$

$\langle L0S\lambda|J\lambda\rangle$ and $\langle S_1\lambda_1 S_2\lambda_2|S\lambda\rangle$ are Clebsch-Gordan coefficients and $\lambda = \lambda_1 - \lambda_2$. Explicit expressions for $U^{J,LS}_{\lambda_1\lambda_2}$ for the different two-body states used in this study are listed below. Applying the transformation to the potential V (T analogous) we get

$$\langle L'S'|V^J|LS\rangle = \sum_{\lambda_1\lambda_2\lambda_3\lambda_4}\langle JML'S'|JM\lambda_3\lambda_4\rangle\langle\lambda_3\lambda_4|V^J|\lambda_1\lambda_2\rangle\langle JM\lambda_1\lambda_2|JMLS\rangle \tag{B.17}$$

or in matrix notation

$$V^{J,L'S'}_{LS} = U^{J,L'S'}_{\lambda_3\lambda_4}V^{J,\lambda_3\lambda 4}_{\lambda 1\lambda 2}\left(U^{J,LS}_{\lambda_1\lambda_2}\right)^{\dagger}\,. \tag{B.18}$$

This leads to the scattering equation in the JLS basis Eq. (1.18)

$$\begin{aligned}\langle L'S'p'|T^J|LSp\rangle &= \langle L'S'p'|V^J|LSp\rangle + \\ &\sum_{L''S''}\int dq\, q^2\langle L'S'p'|V^J|L''S''q\rangle\, G(q)\,\langle L''S''q|T^J|LSp\rangle\,.\end{aligned} \tag{B.19}$$

Coefficients of the transformation matrix $U^{J,LS}_{\lambda_1\lambda_2}$:

- $S_1 = \frac{1}{2}$, $S_2 = 0$ (channels πN, σN, ηN, $K\Lambda$ and $K\Sigma$)

$$\begin{pmatrix}|JM, L = J+\frac{1}{2}, S = \frac{1}{2}\rangle\\ |JM, L = J-\frac{1}{2}, S = \frac{1}{2}\rangle\end{pmatrix} = \underbrace{\begin{pmatrix}d^1_+ & -d^1_+\\ d^1_- & d^1_-\end{pmatrix}}_{U^{J,LS}_{\lambda_1\lambda_2}(\frac{1}{2}\times 0)}\begin{pmatrix}|JM, \lambda_1 = \frac{1}{2}, \lambda_2 = 0\rangle\\ |JM, \lambda_1 = -\frac{1}{2}, \lambda_2 = 0\rangle\end{pmatrix} \tag{B.20}$$

  with $d^1_+ = -\frac{1}{\sqrt{2}}$ and $d^1_- = \frac{1}{\sqrt{2}}$.

- $S_1 = \frac{3}{2}$, $S_2 = 0$ ($\pi\Delta$ channel)

$$\begin{pmatrix} |JM, L = J + \frac{1}{2}, S = \frac{3}{2}\rangle \\ |JM, L = J - \frac{1}{2}, S = \frac{3}{2}\rangle \\ |JM, L = J + \frac{3}{2}, S = \frac{3}{2}\rangle \\ |JM, L = J - \frac{3}{2}, S = \frac{1}{2}\rangle \end{pmatrix} = \underbrace{\begin{pmatrix} e^1_+ & e^1_+ & e^2_+ & e^2_+ \\ e^1_- & -e^1_- & e^2_- & -e^2_- \\ f^1_+ & -f^1_+ & f^2_+ & -f^2_+ \\ f^1_- & f^1_- & f^2_- & f^2_- \end{pmatrix}}_{U^{J,LS}_{\lambda_1\lambda_2}(\frac{3}{2}\times 0)} \times \begin{pmatrix} |JM, \lambda_1 = \frac{1}{2}, \lambda_2 = 0\rangle \\ |JM, \lambda_1 = -\frac{1}{2}, \lambda_2 = 0\rangle \\ |JM, \lambda_1 = \frac{3}{2}, \lambda_2 = -1\rangle \\ |JM, \lambda_1 = -\frac{3}{2}, \lambda_2 = 1\rangle \end{pmatrix} \tag{B.21}$$

The coefficients of $U^{J,LS}_{\lambda_1\lambda_2}(\frac{3}{2} \times 0)$ are given in table D.1.

	Index +	Index -
e^1	$-\frac{1}{2\sqrt{2}}\sqrt{\frac{2J+3}{2J}}$	$-\frac{1}{2\sqrt{2}}\sqrt{\frac{2J-1}{2J+1}}$
e^2	$\sqrt{\frac{3}{8}}\sqrt{\frac{2J-1}{2J}}$	$-\sqrt{\frac{3}{8}}\sqrt{\frac{2J+3}{2J+2}}$
f^1	$\sqrt{\frac{3}{8}}\sqrt{\frac{2J+3}{2J+2}}$	$\sqrt{\frac{3}{8}}\sqrt{\frac{2J-1}{2J}}$
f^2	$-\frac{1}{2\sqrt{2}}\sqrt{\frac{2J-1}{2J+2}}$	$\frac{1}{2\sqrt{2}}\sqrt{\frac{2J+3}{2J}}$

Table B.1: Coefficients of $U^{J,LS}_{\lambda_1\lambda_2}(\frac{3}{2} \times 0)$

- $S_1 = \frac{1}{2}$, $S_2 = 1$ (ρN channel)

$$\begin{pmatrix} |JM, L = J + \frac{1}{2}, S = \frac{1}{2}\rangle \\ |JM, L = J - \frac{1}{2}, S = \frac{1}{2}\rangle \\ |JM, L = J + \frac{3}{2}, S = \frac{3}{2}\rangle \\ |JM, L = J - \frac{3}{2}, S = \frac{3}{2}\rangle \\ |JM, L = J + \frac{1}{2}, S = \frac{3}{2}\rangle \\ |JM, L = J - \frac{1}{2}, S = \frac{3}{2}\rangle \end{pmatrix} = \underbrace{\begin{pmatrix} a^2_+ & a^2_+ & a^1_+ & a^1_+ & 0 & 0 \\ a^2_- & -a^2_- & a^1_- & -a^1_- & 0 & 0 \\ b^3_+ & -b^3_+ & b^2_+ & -b^2_+ & b^1_+ & -b^1_+ \\ b^3_- & b^3_- & b^2_- & b^2_- & b^1_- & b^1_- \\ c^3_+ & c^3_+ & c^2_+ & c^2_+ & c^1_+ & c^1_+ \\ c^3_- & -c^3_- & c^2_- & -c^2_- & c^1_- & -c^1_- \end{pmatrix}}_{U^{J,LS}_{\lambda_1\lambda_2}(\frac{1}{2}\times 1)} \times \begin{pmatrix} |JM, \lambda_1 = \frac{1}{2}, \lambda_2 = 0\rangle \\ |JM, \lambda_1 = -\frac{1}{2}, \lambda_2 = 0\rangle \\ |JM, \lambda_1 = -\frac{1}{2}, \lambda_2 = -1\rangle \\ |JM, \lambda_1 = \frac{1}{2}, \lambda_2 = 1\rangle \\ |JM, \lambda_1 = \frac{1}{2}, \lambda_2 = -1\rangle \\ |JM, \lambda_1 = -\frac{1}{2}, \lambda_2 = 1\rangle \end{pmatrix} \tag{B.22}$$

The coefficients of $U^{J,LS}_{\lambda_1\lambda_2}(\frac{1}{2}\times 1)$ can be found in table D.2

	Index +	Index -
a^1	$\frac{1}{\sqrt{3}}$	$-\frac{1}{\sqrt{3}}$
a^2	$-\frac{1}{\sqrt{6}}$	$\frac{1}{\sqrt{6}}$
b^1	$-\frac{1}{2\sqrt{2}}\sqrt{\frac{2J-1}{2J+2}}$	$\frac{1}{2\sqrt{2}}\sqrt{\frac{2J+3}{2J}}$
b^2	$\frac{1}{2\sqrt{2}}\sqrt{\frac{2J+3}{2J+2}}$	$\frac{1}{2\sqrt{2}}\sqrt{\frac{2J-1}{2J}}$
b^3	$-\frac{1}{2}\sqrt{\frac{2J+3}{2J+2}}$	$\frac{1}{2}\sqrt{\frac{2J-1}{2J}}$
c^1	$\sqrt{\frac{3}{8}}\sqrt{\frac{2J-1}{2J}}$	$-\sqrt{\frac{3}{8}}\sqrt{\frac{2J+3}{2J+2}}$
c^2	$\frac{1}{2\sqrt{6}}\sqrt{\frac{2J+3}{2J}}$	$-\frac{1}{2\sqrt{6}}\sqrt{\frac{2J-1}{2J+2}}$
c^3	$\frac{1}{2\sqrt{3}}\sqrt{\frac{2J+3}{2J}}$	$-\frac{1}{2\sqrt{6}}\sqrt{\frac{2J-1}{2J+2}}$

Table B.2: Coefficients of $U^{J,LS}_{\lambda_1\lambda_2}(\frac{3}{2}\times 0)$

B.2.1 Parity conservation

The number of independed elements in the scattering amplitude is reduced if parity conservation holds [322].
Limitations depending on the total spin J of the system reduce the number of different L that contribute to a given J. From

$$|J-S| \leq L \leq J+S \tag{B.23}$$

follows that $L = J \pm 1/2$ in case of πN, σN, ηN, $K\Lambda$, $K\Sigma$ and $L = J \pm 1/2$, $|J \pm 3/2|$ for $\pi\Delta$, ρN.
The total parity of a two-particle system is defined as

$$\eta_P = \eta_1\eta_2(-1)^L. \tag{B.24}$$

Here η_1 and η_2 are the intrinsic parities of the particles 1 and 2 and $\eta_1\eta_2 = 1$ for all channels except for σN, where $\eta_1\eta_2 = -1$.

Parity conservation then leads to the following selection rules for the allowed transitions:

$$\begin{aligned} L_{\eta N} &= L_{\pi N}, \\ L_{K\Lambda} &= L_{\pi N}, \\ L_{K\Sigma} &= L_{\pi N}, \\ |L_{\sigma N} - L_{\pi N}| &= 1, \\ |L_{\rho N} - L_{\pi N}| &= 0 \,\text{or}\, 2, \\ |L_{\pi\Delta} - L_{\pi N}| &= 0 \text{ or } 2. \end{aligned} \tag{B.25}$$

See also Table 11 in Chap. 3.

Appendix C

Bare resonance vertices

In this section we list explicit expressions for the partial wave projected bare resonance vertices $\gamma^{a,c}$ in Eq. (2), Sec. 3.2 of Chap. 3

$$\gamma^a = v\, F(k) IR \sqrt{\frac{E+m_B}{E\omega}}\ , \tag{C.1}$$

where v is the partial wave projected vertex function listed below, $k = |\vec{k}|$ is the center of mass (c.m.) meson-baryon momentum and the isospin factors IR can be found in Tab. C.1. E and ω denote the baryon and meson on-shell c.m. energy

$$E = \sqrt{\vec{p_i}^{\,2} + m_B^2} \quad \text{and} \quad \omega = \sqrt{\vec{p_i}^{\,2} + m_m^2} \tag{C.2}$$

with the baryon and meson masses m_B and m_m, respectively. The resonance form factor $F(k)$ have the form

$$F(k) \;=\; \left(\frac{\Lambda^4 + m_R^4}{\Lambda^4 + (E(k)+\omega(k))^4}\right)^n \tag{C.3}$$

with m_R being the nominal mass of the resonance. $E(k)$ and $\omega(k)$ are the energies of the incoming or outgoing baryon and meson with center of mass (off-shell) momentum k. For $J \leq 3/2$ we use $n = 1$ for all channels except $\pi\Delta$ ($n = 2$). In case of $J \geq 5/2$ we have $n = 2$ for all channels except $\pi\Delta$ ($n = 3$). The cut-off parameters Λ were set to 2 GeV for all resonances.

Resonances with a total spin $J \geq 5/2$ are not derived from Lagrangians but are constructed to obey the correct dependence on the orbital angular momentum L (centrifugal barrier). Parity considerations give the following relations to bare vertices with $J \leq 3/2$:

$$
\begin{aligned}
(\gamma^{a,c})_{\frac{5}{2}^-} &= \frac{k}{m_b}\,(\gamma^{a,c})_{\frac{3}{2}^+} & (\gamma^{a,c})_{\frac{5}{2}^+} &= \frac{k}{m_b}\,(\gamma^{a,c})_{\frac{3}{2}^-} \\
(\gamma^{a,c})_{\frac{7}{2}^+} &= \frac{k^2}{m_b^2}\,(\gamma^{a,c})_{\frac{3}{2}^+} & (\gamma^{a,c})_{\frac{7}{2}^-} &= \frac{k^2}{m_b^2}\,(\gamma^{a,c})_{\frac{3}{2}^-} \\
(\gamma^{a,c})_{\frac{9}{2}^-} &= \frac{k^3}{m_b^3}\,(\gamma^{a,c})_{\frac{3}{2}^+} & (\gamma^{a,c})_{\frac{9}{2}^+} &= \frac{k^3}{m_b^3}\,(\gamma^{a,c})_{\frac{3}{2}^-}
\end{aligned}
\tag{C.4}
$$

Explicit expressions for resonance vertex functions:

- S_{11} (S_{31})
  - $N\pi$
$$v = -\,i\,\frac{f}{m_\pi}\,\frac{1}{\sqrt{8}\,\pi}\,(\omega_\pi + E_N - m_N)$$
  - $N\eta$
$$v = -\,i\,\frac{f}{m_\pi}\,\frac{1}{\sqrt{8}\,\pi}\,(\omega_\eta + E_N - m_N)$$
  - $N\rho$ (L=0, S=1/2)
$$v = -\,f\,\frac{1}{\sqrt{24}\,\pi}\,\frac{1}{m_\rho}\,(\omega_\rho + E_N - m_N + 2\,m_\rho)$$
  - $N\rho$ (L=2, S=3/2)
$$v = -\,f\,\frac{1}{\sqrt{12}\,\pi}\,\frac{1}{m_\rho}\,(\omega_\rho + E_N - m_N - m_\rho)$$
  - $\Delta\pi$
$$v = -\,i\,\frac{f}{m_\pi}\,\frac{1}{\sqrt{12}\,\pi}\,\frac{E_\Delta + \omega_\pi}{m_\Delta}\,(E_\Delta - m_\Delta)$$
  - ΛK
$$v = -if\,\frac{1}{\sqrt{8}\pi}\left(\omega_K + \frac{\vec{k}^2}{E_\Lambda + m_\Lambda}\right)$$
  - ΣK
$$v = -if\,\frac{1}{\sqrt{8}\pi}\left(\omega_K + \frac{\vec{k}^2}{E_\Sigma + m_\Sigma}\right)$$
- P_{11} (P_{31})

- $N\pi$

$$v = i\,\frac{f}{m_\pi}\,\frac{1}{\sqrt{8}\,\pi}\,k\,\left(1+\frac{\omega_\pi}{E_N+m_N}\right)$$

- $N\eta$

$$v = i\,\frac{f}{m_\pi}\,\frac{1}{\sqrt{8}\,\pi}\,k\,\left(1+\frac{\omega_\eta}{E_N+m_N}\right)$$

- $N\rho$ (L=1, S=1/2)

$$v = f\,\frac{1}{\sqrt{24}\,\pi}\,\frac{k}{m_\rho}\,\left(1+\frac{\omega_\rho}{E_N+m_N}-\frac{2\,m_\rho}{E_N+m_N}\right)$$

- $N\rho$ (L=1, S=3/2)

$$v = f\,\frac{1}{\sqrt{12}\,\pi}\,\frac{k}{m_\rho}\,\left(1+\frac{\omega_\rho}{E_N+m_N}+\frac{m_\rho}{E_N+m_N}\right)$$

- $\Delta\pi$

$$v = i\,\frac{f}{m_\pi}\,\frac{1}{\sqrt{12}\,\pi}\,\frac{k}{m_\Delta}\,\left(E_\Delta+\omega_\pi\right)$$

- ΛK

$$v = if\frac{1}{\sqrt{8}\pi}\,k\,\left(1+\frac{\omega_K}{E_\Lambda+m_\Lambda}\right)$$

- ΣK

$$v = if\frac{1}{\sqrt{8}\pi}k\,\left(1+\frac{\omega_K}{E_\Sigma+m_\Sigma}\right)$$

- P_{13} (P_{33})
  - $N\pi$

$$v = \,i\,\frac{f}{m_\pi}\,\frac{1}{\sqrt{24}\,\pi}\,k$$

  - $N\eta$

$$v = \,i\,\frac{f}{m_\pi}\,\frac{1}{\sqrt{24}\,\pi}\,k$$

  - $N\rho$ (L=1, S=1/2)

$$v = \frac{f}{m_\rho}\,\frac{1}{\sqrt{72}\,\pi}\,\frac{k}{E_N+m_N}\,\left(E_N+m_N-\omega_\rho-m_\rho\right)$$

– $N\rho$ (L=1, S=3/2)

$$v = \frac{f}{m_\rho}\,\frac{1}{\sqrt{360}\,\pi}\,\frac{k}{E_N + m_N}\,(5\,E_N + 5\,m_N + 4\,\omega_\rho + m_\rho)$$

– $N\rho$ (L=3, S=3/2)

$$v = \frac{f}{m_\rho}\,\frac{1}{\sqrt{40}\,\pi}\,\frac{k}{E_N + m_N}\,(\omega_\rho - m_\rho)$$

– $\Delta\pi$ (L=1)

$$v = i\,\frac{f}{m_\pi}\,\frac{1}{\sqrt{360}\,\pi}\,\frac{k}{m_\Delta}\,(E_\Delta + 4\,m_\Delta)\,\left(1 + \frac{\omega_\pi}{E_\Delta + m_\Delta}\right)$$

– $\Delta\pi$ (L=3)

$$v = -\,i\,\frac{f}{m_\pi}\,\frac{1}{\sqrt{40}\,\pi}\,\frac{k}{m_\Delta}\,(E_\Delta - m_\Delta)\,\left(1 + \frac{\omega_\pi}{E_\Delta + m_\Delta}\right)$$

– ΛK

$$v = i f\,k\,\frac{1}{\sqrt{24\pi}}$$

– ΣK

$$v = i f\,k\,\frac{1}{\sqrt{24}\,\pi}$$

- D_{13} (D_{33})

– $N\pi$

$$v = \frac{f}{m_\pi^2}\,\frac{1}{\sqrt{24}\,\pi}\,k^2\,\left(1 + \frac{\omega_\pi}{E_N + m_N}\right)$$

– $N\eta$

$$v = \frac{f}{m_\pi^2}\,\frac{1}{\sqrt{24}\,\pi}\,\left(1 + \frac{\omega_\eta}{E_N + m_N}\right)$$

– $N\rho$ (L=0, S=3/2)

$$v = -\,i\,\frac{f}{m_\rho}\,\frac{1}{\sqrt{72}\,\pi}\,(2\omega_\rho + m_\rho + E_N - m_N)$$

– $N\rho$ (L=2, S=1/2)

$$v = -\,i\,\frac{f}{m_\rho}\,\frac{1}{\sqrt{72}\,\pi}\,(\omega_\rho - m_\rho - E_N + m_N)$$

	$N\pi$	$N\eta$	$N\rho$	$\Delta\pi$	ΛK	ΣK
$I=\frac{1}{2}$	$\sqrt{3}$	1	$\sqrt{3}$	$-\sqrt{2}$	1	$-\sqrt{3}$
$I=\frac{3}{2}$	1	0	1	$\sqrt{\frac{5}{3}}$	0	-1

Table C.1: Isospin factors IR for resonances vertices.

– $N\rho$ (L=2, S=3/2)

$$v = -\,i\,\frac{f}{m_\rho}\,\frac{1}{\sqrt{72}\,\pi}\,(\omega_\rho - m_\rho + 2E_N - 2m_N)$$

– $\Delta\pi$ (L=0)

$$v = \frac{f}{m_\pi}\,\frac{1}{\sqrt{72}\,\pi}\,\frac{1}{m_\Delta}\left(\omega_\pi + \frac{\vec{k}^2}{E_\Delta + m_\Delta}\right)(E_\Delta + 2\,m_\Delta)$$

– $\Delta\pi$ (L=2)

$$v = -\,\frac{f}{m_\pi}\,\frac{1}{\sqrt{72}\,\pi}\,\frac{1}{m_\Delta}\left(\omega_\pi + \frac{\vec{k}^2}{E_\Delta + m_\Delta}\right)(E_\Delta - m_\Delta)$$

– ΛK

$$v = f\,k^2\,\frac{1}{\sqrt{24}\,\pi}\left(1 + \frac{\omega_K}{E_\Lambda + m_\Lambda}\right)$$

– ΣK

$$v = f\,k^2\,\frac{1}{\sqrt{24}\,\pi}\left(1 + \frac{\omega_K}{E_\Sigma + m_\Sigma}\right)$$

The bare couplings f are free parameters and fitted to data. Explicit values, also for the bare resonance masses m_b, can be found in Tables 9 and 10 of Chap. 3.

Vertex	$\mathcal{L}_{int}$	Vertex	$\mathcal{L}_{int}$
$N^*(S_{11})N\pi$	$\frac{f_{N^*N\pi}}{m_\pi}\bar{\Psi}_{N^*}\gamma^\mu\vec{\tau}\partial_\mu\vec{\pi}\Psi$ + h.c.	$N^*(D_{13})\Lambda K$	$\frac{f}{m_\pi^2}\bar{\Psi}_{N^*}\gamma^5\gamma^\nu\partial_\nu\partial_\mu\phi_K\Psi_\Lambda$ + h.c.
$N^*(S_{11})N\eta$	$\frac{f_{N^*N\eta}}{m_\pi}\bar{\Psi}_{N^*}\gamma^\mu\partial_\mu\eta\Psi$ + h.c.	$\Delta^*(S_{31})N\pi$	$\frac{f_{\Delta^*N\pi}}{m_\pi}\bar{\Delta}^*\gamma^\mu\vec{S}^\dagger\Psi\partial_\mu\vec{\pi}$ + h.c.
$N^*(S_{11})N\rho$	$g_{N^*N\rho}\bar{\Psi}_{N^*}\gamma^5\gamma^\mu\vec{\tau}\vec{\rho}_\mu\Psi$ + h.c.	$\Delta^*(S_{31})N\rho$	$g\bar{\Psi}_{\Delta^*}\vec{S}^\dagger\gamma^5(\gamma^\mu-\frac{\kappa}{2m_0}\sigma^{\mu\nu}\partial_\nu)\vec{\rho}_\mu\Psi$
$N^*(S_{11})\Delta\pi$	$-\frac{f_{N^*\Delta\pi}}{m_\pi}\bar{\Psi}_{N^*}\gamma^5\vec{S}\Delta^\mu\partial_\mu\vec{\pi}\Psi$ + h.c.	$\Delta^*(S_{31})\Delta\pi$	$-\frac{f_{\Delta^*\Delta\pi}}{m_\pi}\bar{\Delta}^*\gamma^5\vec{T}\Delta^\mu\partial_\mu\vec{\pi}$ + h.c.
$N^*(S_{11})\Sigma K$	$\frac{f_{N^*\Sigma K}}{m_\pi}\bar{\Psi}_{N^*}\gamma^\mu\vec{\tau}\partial_\mu\phi_K\Psi_\Sigma$ + h.c.	$\Delta^*(S_{31})\Sigma K$	$\frac{f_{\Delta^*\Sigma K}}{m_\pi}\bar{\Delta}^*\gamma^\mu\vec{S}^\dagger\partial_\mu\phi_K\Psi_\Sigma$ + h.c.
$N^*(S_{11})\Lambda K$	$\frac{f_{N^*\Lambda K}}{m_\pi}\bar{\Psi}_{N^*}\gamma^\mu\partial_\mu\phi_K\Psi_\Lambda$ + h.c.	$\Delta^*(P_{31})N\pi$	$-\frac{f_{\Delta^*N\pi}}{m_\pi}\bar{\Delta}^*\gamma^5\gamma^\mu\vec{S}^\dagger\Psi\partial_\mu\vec{\pi}$ + h.c.
$N^*(P_{13})N\pi$	$\frac{f_{N^*N\pi}}{m_\pi}\bar{\Psi}^\mu_{N^*}\vec{\tau}\Psi\partial_\mu\vec{\pi}$ + h.c.	$\Delta^*(P_{31})N\rho$	$-g\bar{\Psi}_{\Delta^*}(\gamma^\nu-\frac{\kappa}{2m_0}\sigma^{\mu\nu}\partial_\nu)\vec{\rho}_\mu\Psi$
$N^*(P_{13})N\eta$	$\frac{f_{N^*N\eta}}{m_\pi}\bar{\Psi}^\mu_{N^*}\Psi\partial_\mu\eta$ + h.c.	$\Delta^*(P_{31})\Delta\pi$	$-\frac{f_{\Delta^*\Delta\pi}}{m_\pi}\bar{\Delta}^*\vec{T}\Delta^\mu\partial_\mu\vec{\pi}$ + h.c.
$N^*(P_{13})\Delta\pi$	$\frac{f_{N^*\Delta\pi}}{m_\pi}\bar{\Psi}^\mu_{N^*}\gamma^5\gamma^\mu\vec{S}\Delta_\mu\partial_\nu\vec{\pi}$ + h.c.	$\Delta^*(P_{31})\Sigma K$	$\frac{f_{\Delta^*\Sigma K}}{m_\pi}\bar{\Delta}^*\vec{S}^\dagger\gamma^5\gamma^\mu\partial_\mu\phi_K\Psi_\Sigma$ + h.c.
$N^*(P_{13})\Sigma K$	$\frac{f_{N^*\Sigma K}}{m_\pi}\bar{\Psi}_{N^*}\vec{\tau}\partial_\mu\phi_K\Psi_\Sigma$ + h.c.	$\Delta^*(P_{33})N\pi$	$\frac{f_{\Delta^*N\pi}}{m_\pi}\bar{\Delta}^*_\mu\vec{S}^\dagger\psi\partial^\mu\vec{\pi}$ + h.c.,
$N^*(P_{13})\Lambda K$	$\frac{f_{N^*\Lambda K}}{m_\pi}\bar{\Psi}_{N^*}\partial_\mu\phi_K\Psi_\Lambda$ + h.c.	$\Delta^*(P_{33})N\rho$	$-i\frac{f_{\Delta^*N\rho}}{m_\rho}\bar{\Delta}^*_\mu\gamma^5\gamma_\nu\vec{S}^\dagger\vec{\rho}^{\mu\nu}\Psi$ + h.c.
$N^*(D_{13})N\pi$	$\frac{f_{N^*N\pi}}{m_\pi^2}\bar{\Psi}\gamma^5\gamma^\nu\vec{\tau}\bar{\Psi}^\mu_{N^*}\partial_\nu\partial_\mu\vec{\pi}$ + h.c.	$\Delta^*(P_{33})\Sigma K$	$\frac{f_{\Delta^*\Sigma K}}{m_\pi}\bar{\Psi}_{\Delta^*}\vec{S}^\dagger\gamma^\mu\partial_\mu\phi_K\Psi_\Sigma$ + h.c.
$N^*(D_{13})N\eta$	$\frac{f_{N^*N\eta}}{m_\pi^2}\bar{\Psi}\gamma^5\gamma^\nu\bar{\Psi}^\mu_{N^*}\partial_\nu\partial_\mu\eta$ + h.c.	$\Delta^*(D_{33})N\pi$	$\frac{f_{\Delta^*N\pi}}{m_\pi^2}\bar{\Psi}\gamma^5\gamma_\nu\vec{S}^\dagger\Delta^*_\mu\partial^\nu\partial^\mu\vec{\pi}$ + h.c.
$N^*(D_{13})\Delta\pi$	$i\frac{f_{N^*\Delta\pi}}{m_\pi}\bar{\Psi}^\nu_{N^*}\vec{S}\gamma^\mu\Delta_\nu\partial_\mu\vec{\pi}$ + h.c.	$\Delta^*(D_{33})\Delta\pi$	$i\frac{f_{\Delta^*\Delta\pi}}{m_\pi}\bar{\Delta}^*_\nu\vec{T}\gamma^\mu\Delta^\nu\partial_\mu\vec{\pi}$ + h.c.
$N^*(D_{13})N\rho$	$\frac{f_{N^*N\rho}}{m_\rho}\bar{\Psi}^\nu_{N^*}\gamma^\nu\vec{\tau}\vec{\rho}_{\mu\nu}\Psi$ + h.c.	$\Delta^*(D_{33})N\rho$	$\frac{f_{\Delta^*N\rho}}{m_\rho}\bar{\Delta}^*_\mu\gamma_\nu\vec{S}^\dagger\vec{\rho}^{\mu\nu}\Psi$ + h.c.
$N^*(D_{13})\Sigma K$	$\frac{f}{m_\pi^2}\bar{\Psi}_{N^*}\vec{\tau}\gamma^5\gamma^\nu\partial_\nu\partial_\mu\phi_K\Psi_\Sigma$ + h.c.	$\Delta^*(D_{33})\Sigma K$	$\frac{f_{\Delta^*\Sigma K}}{m_\pi^2}\bar{\Psi}_\Sigma\gamma^5\gamma_\nu\vec{S}^\dagger\Delta^*_\mu\partial^\nu\partial^\mu\phi_K$ + h.c.

Table C.2: Effective Lagrangians for s-channel diagrams.

Bibliography

[1] D. Rönchen, M. Döring, F. Huang, H. Haberzettl, J. Haidenbauer, C. Hanhart, S. Krewald and U.-G. Meißner *et al.*, Eur. Phys. J. A **49**, 44 (2013).

[2] D. Rönchen, M. Döring, F. Huang, H. Haberzettl, J. Haidenbauer, C. Hanhart, S. Krewald and U.-G. Meißner, arXiv:1401.0634 [nucl-th].

[3] A. Bondar *et al.* [Belle Collaboration], Phys. Rev. Lett. **108**, 122001 (2012).

[4] I. Adachi *et al.* [Belle Collaboration], arXiv:1209.6450 [hep-ex].

[5] I. Adachi *et al.* [Belle Collaboration], arXiv:1207.4345 [hep-ex].

[6] N. Brambilla, S. Eidelman, B. K. Heltsley, R. Vogt, G. T. Bodwin, E. Eichten, A. D. Frawley and A. B. Meyer *et al.*, Eur. Phys. J. C **71**, 1534 (2011).

[7] E. D. Bloom, D. H. Coward, H. C. DeStaebler, J. Drees, G. Miller, L. W. Mo, R. E. Taylor and M. Breidenbach *et al.*, Phys. Rev. Lett. **23**, 930 (1969).

[8] R. E. Taylor, Rev. Mod. Phys. **63**, 573 (1991).

[9] J. S. Poucher, M. Breidenbach, W. R. Ditzler, J. I. Friedman, H. W. Kendall, E. D. Bloom, R. L. Cottrell and D. H. Coward *et al.*, Phys. Rev. Lett. **32**, 118 (1974).

[10] J. D. Bjorken, Phys. Rev. **179**, 1547 (1969).

[11] H. Fritzsch, M. Gell-Mann and H. Leutwyler, Phys. Lett. B **47**, 365 (1973).

[12] N. G. Kozlenko, V. V. Abaev, V. S. Bekrenev, S. P. Kruglov, A. A. Koulbardis, I. V. Lopatin, A. B. Starostin and B. Draper *et al.*, Phys. Atom. Nucl. **66**, 110 (2003) [Yad. Fiz. **66**, 112 (2003)].

[13] S. Prakhov, B. M. K. Nefkens, C. E. Allgower, R. A. Arndt, V. Bekrenev, W. J. Briscoe, M. Clajus and J. R. Comfort *et al.*, Phys. Rev. C **72**, 015203 (2005).

[14] D. E. Bayadilov, Y. .A. Beloglazov, A. B. Gridnev, N. G. Kozlenko, S. P. Kruglov, A. A. Kulbardis, I. V. Lopatin and D. V. Novinsky *et al.*, Eur. Phys. J. A **35**, 287 (2008).

[15] I. G. Alekseev *et al.* [EPECUR Collaboration], arXiv:1204.6433 [hep-ex].

[16] K. Shirotori, T. N. Takahashi, S. Adachi, M. Agnello, S. Ajimura, K. Aoki, H. C. Bhang and B. Bassalleck *et al.*, Phys. Rev. Lett. **109**, 132002 (2012).

[17] E. Klempt and J. -M. Richard, Rev. Mod. Phys. **82**, 1095 (2010).

[18] M. Gell-Mann, Phys. Rev. **125**, 1067 (1962).

[19] G. Zweig, Report No. CERN-TH-401 (1964)

[20] V. E. Barnes, P. L. Connolly, D. J. Crennell, B. B. Culwick, W. C. Delaney, W. B. Fowler, P. E. Hagerty and E. L. Hart *et al.*, Phys. Rev. Lett. **12**, 204 (1964).

[21] N. Isgur and G. Karl, Phys. Rev. D **18**, 4187 (1978).

[22] S. Capstick and N. Isgur, Phys. Rev. D **34**, 2809 (1986).

[23] T. Melde, W. Plessas and B. Sengl, Phys. Rev. D **77**, 114002 (2008).

[24] U. Löring, K. Kretzschmar, B. C. Metsch and H. R. Petry, Eur. Phys. J. A **10**, 309 (2001); U. Löring, B. C. Metsch and H. R. Petry, Eur. Phys. J. A **10**, 395 (2001); U. Löring, B. C. Metsch and H. R. Petry, Eur. Phys. J. A **10**, 447 (2001).

[25] M. Ronniger and B. C. Metsch, Eur. Phys. J. A **47**, 162 (2011); M. Ronniger and B. C. Metsch, Eur. Phys. J. A **49**, 8 (2013).

[26] R. Koniuk and N. Isgur, Phys. Rev. Lett. **44**, 845 (1980).

[27] S. Weinberg, Physica A **96**, 327 (1979).

[28] W. Heisenberg and H. Euler, Z. Phys. **98**, 714 (1936).

[29] C. Vafa and E. Witten, Nucl. Phys. B **234**, 173 (1984).

[30] J. Goldstone, Nuovo Cim. **19**, 154 (1961).

[31] J. Goldstone, A. Salam and S. Weinberg, Phys. Rev. **127**, 965 (1962).

[32] S. R. Coleman, J. Wess and B. Zumino, Phys. Rev. **177**, 2239 (1969).

[33] C. G. Callan, Jr., S. R. Coleman, J. Wess and B. Zumino, Phys. Rev. **177**, 2247 (1969).

[34] J. Gasser and H. Leutwyler, Annals Phys. **158**, 142 (1984).

[35] J. Gasser and H. Leutwyler, Nucl. Phys. B **250**, 465 (1985).

[36] U.-G. Meißner, Rept. Prog. Phys. **56**, 903 (1993).

[37] V. Bernard and U.-G. Meißner, Ann. Rev. Nucl. Part. Sci. **57**, 33 (2007).

[38] V. Bernard, Prog. Part. Nucl. Phys. **60**, 82 (2008).

[39] J. Gasser, M. E. Sainio and A. Svarc, Nucl. Phys. B **307**, 779 (1988).

[40] E. E. Jenkins and A. V. Manohar, Phys. Lett. B **255**, 558 (1991).

[41] V. Bernard, N. Kaiser, J. Kambor and U.-G. Meißner, Nucl. Phys. B **388**, 315 (1992).

[42] B. Borasoy and U.-G. Meißner, Annals Phys. **254**, 192 (1997).

[43] T. Becher and H. Leutwyler, Eur. Phys. J. C **9**, 643 (1999)

[44] U.-G. Meißner, Int. J. Mod. Phys. E **1**, 561 (1992).

[45] V. Bernard, N. Kaiser and U.-G. Meißner, Int. J. Mod. Phys. E **4**, 193 (1995).

[46] N. Kaiser, P. B. Siegel and W. Weise, Phys. Lett. B **362**, 23 (1995).

[47] U.-G. Meißner and J. A. Oller, Nucl. Phys. A **673**, 311 (2000).

[48] J. A. Oller and U.-G. Meißner, Phys. Lett. B **500**, 263 (2001).

[49] M. Döring and K. Nakayama, Phys. Lett. B **683**, 145 (2010).

[50] A. Gasparyan and M. F. M. Lutz, Nucl. Phys. A **848**, 126 (2010).

[51] M. Mai, P. C. Bruns and U.-G. Meißner, Phys. Rev. D **86**, 094033 (2012).

[52] N. Fettes, U.-G. Meißner and S. Steininger, Nucl. Phys. A **640**, 199 (1998).

[53] N. Fettes and U.-G. Meißner, Nucl. Phys. A **693**, 693 (2001).

[54] K. G. Wilson, Phys. Rev. D **10**, 2445 (1974).

[55] S. Dürr, Z. Fodor, J. Frison, C. Hoelbling, R. Hoffmann, S. D. Katz, S. Krieg and T. Kurth *et al.*, Science **322**, 1224 (2008).

[56] J. J. Dudek, R. G. Edwards, M. J. Peardon, D. G. Richards and C. E. Thomas, Phys. Rev. Lett. **103**, 262001 (2009).

[57] G. P. Engel *et al.* [BGR [Bern-Graz-Regensburg] Collaboration], Phys. Rev. D **82**, 034505 (2010).

[58] J. Bulava, R. G. Edwards, E. Engelson, B. Joo, H-W. Lin, C. Morningstar, D. G. Richards and S. J. Wallace, Phys. Rev. D **82**, 014507 (2010).

[59] C. B. Lang and V. Verduci, Phys. Rev. D **87**, no. 5, 054502 (2013).

[60] G. P. Engel, C. B. Lang, D. Mohler and A. Schäfer, Phys. Rev. D **87**, 074504 (2013).

[61] C. Alexandrou, J. W. Negele, M. Petschlies, A. Strelchenko and A. Tsapalis, Phys. Rev. D **88**, 031501 (2013).

[62] R. G. Edwards, N. Mathur, D. G. Richards and S. J. Wallace, Phys. Rev. D **87**, 054506 (2013).

[63] M. Döring, M. Mai and U.-G. Meißner, Phys. Lett. B **722**, 185 (2013).

[64] R. E. Cutkosky, C. P. Forsyth, R. E. Hendrick and R. L. Kelly, Phys. Rev. D **20**, 2839 (1979).

[65] G. Höhler, F. Kaiser, R. Koch and E. Pietarinen, Physics Data **12-1**, 1 (1979).

[66] G. Höhler, *Pion Nucleon Scattering*, edited by H. Schopper, Landolt Börnstein, New Series, Group 9b, Vol. I (Springer, New York, 1983).

[67] G. Höhler, πN Newsletter **9**, 1 (1993).

[68] R. A. Arndt, I. I. Strakovsky, R. L. Workman and M. M. Pavan, Phys. Rev. C **52**, 2120 (1995) [nucl-th/9505040].

[69] R. A. Arndt, W. J. Briscoe, I. I. Strakovsky and R. L. Workman, Phys. Rev. C **74**, 045205 (2006).

[70] R. L. Workman, R. A. Arndt and M. W. Paris, Phys. Rev. C **79**, 038201 (2009).

[71] R. L. Workman, M. W. Paris, W. J. Briscoe and I. I. Strakovsky, Phys. Rev. C **86**, 015202 (2012).

[72] A. V. Anisovich, E. Klempt, V. A. Nikonov, A. V. Sarantsev and U. Thoma, Eur. Phys. J. A **47**, 153 (2011).

[73] A. V. Anisovich, R. Beck, E. Klempt, V. A. Nikonov, A. V. Sarantsev and U. Thoma, Eur. Phys. J. A **48**, 15 (2012)

[74] A. V. Anisovich, R. Beck, E. Klempt, V. A. Nikonov, A. V. Sarantsev and U. Thoma, Eur. Phys. J. A **48**, 88 (2012)

[75] A. V. Anisovich, R. Beck, E. Klempt, V. A. Nikonov, A. V. Sarantsev, U. Thoma and Y. Wunderlich, Eur. Phys. J. A **49**, 121 (2013)

[76] D. Drechsel, S. S. Kamalov and L. Tiator, Eur. Phys. J. A **34**, 69 (2007).

[77] L. Tiator, D. Drechsel, S. S. Kamalov and M. Vanderhaeghen, Eur. Phys. J. ST **198**, 141 (2011).

[78] G. Penner and U. Mosel, Phys. Rev. C **66**, 055212 (2002).

[79] R. Shyam, O. Scholten and H. Lenske, Phys. Rev. C **81**, 015204 (2010) [arXiv:0911.3351 [hep-ph]].

[80] X. Cao, V. Shklyar and H. Lenske, Phys. Rev. C **88**, 055204 (2013).

[81] V. Shklyar, H. Lenske and U. Mosel, Phys. Rev. C **87**, 015201 (2013).

[82] R. Arndt, W. Briscoe, I. Strakovsky and R. Workman, Eur. Phys. J. A **35**, 311 (2008).

[83] M. G. Fuda and H. Alharbi, Phys. Rev. C **68**, 064002 (2003).

[84] V. Pascalutsa and J. A. Tjon, Phys. Rev. C **70**, 035209 (2004).

[85] C. Fernandez-Ramirez, E. Moya de Guerra and J. M. Udias, Annals Phys. **321**, 1408 (2006).

[86] A. Matsuyama, T. Sato and T. -S. H. Lee, Phys. Rept. **439**, 193 (2007).

[87] B. Julia-Diaz, T. -S. H. Lee, A. Matsuyama and T. Sato, Phys. Rev. C **76**, 065201 (2007).

[88] B. Julia-Diaz, T. -S. H. Lee, A. Matsuyama, T. Sato and L. C. Smith, Phys. Rev. C **77**, 045205 (2008).

[89] M. W. Paris, Phys. Rev. C **79**, 025208 (2009).

[90] N. Suzuki, T. Sato and T. -S. H. Lee, Phys. Rev. C **82**, 045206 (2010).

[91] L. Tiator, S. S. Kamalov, S. Ceci, G. Y. Chen, D. Drechsel, A. Svarc and S. N. Yang, Phys. Rev. C **82**, 055203 (2010).

[92] H. Kamano, S. X. Nakamura, T. -S. H. Lee and T. Sato, Phys. Rev. C **88**, 035209 (2013).

[93] C. Schütz, J. W. Durso, K. Holinde and J. Speth, Phys. Rev. C **49**, 2671 (1994).

[94] C. Schutz, K. Holinde, J. Speth, B. C. Pearce and J. W. Durso, Phys. Rev. C **51**, 1374 (1995).

[95] C. Schütz, J. Haidenbauer, J. Speth and J. W. Durso, Phys. Rev. C **57**, 1464 (1998).

[96] O. Krehl, C. Hanhart, S. Krewald and J. Speth, Phys. Rev. C **62**, 025207 (2000).

[97] O. Krehl, C. Hanhart, S. Krewald and J. Speth, Phys. Rev. C **60**, 055206 (1999).

[98] A. M. Gasparyan, J. Haidenbauer, C. Hanhart and J. Speth, Phys. Rev. C **68**, 045207 (2003).

[99] M. Döring, C. Hanhart, F. Huang, S. Krewald, U.-G. Meißner and D. Rönchen, Nucl. Phys. A **851**, 58 (2011).

[100] M. Döring, C. Hanhart, F. Huang, S. Krewald and U.-G. Meißner, Nucl. Phys. A **829**, 170 (2009).

[101] M. Döring, C. Hanhart, F. Huang, S. Krewald and U.-G. Meißner, Phys. Lett. B **681**, 26 (2009).

[102] R. Blankenbecler and R. Sugar, Phys. Rev. **142**, 1051 (1966).

[103] S. S. Schweber, *An Introduction to relativistic Quantum Field Theory* (Harper and Row, New York, 1962).

[104] D. Schütte, Nucl. Phys. A **221**, 450 (1974).

[105] K. Kotthoff, K. Holinde, R. Machleidt and D. Schütte, Nucl. Phys. A **242**, 429 (1975).

[106] R. Machleidt, K. Holinde and C. Elster, Phys. Rept. **149**, 1 (1987).

[107] M. I. Haftel and F. Tabakin, Nucl. Phys. A **158**, 1 (1970).

[108] M. Döring and K. Nakayama, Eur. Phys. J. A **43**, 83 (2010).

[109] U.-G. Meißner, Phys. Rept. **161**, 213 (1988).

[110] B. Borasoy and U.-G. Meißner, Int. J. Mod. Phys. A **11**, 5183 (1996).

[111] J. Wess and B. Zumino, Phys. Rev. **163**, 1727 (1967).

[112] S. Ceci, M. Döring, C. Hanhart, S. Krewald, U.-G. Meißner and A. Svarc, Phys. Rev. C **84**, 015205 (2011).

[113] J. Beringer *et al.* [Particle Data Group Collaboration], Phys. Rev. D **86**, 010001 (2012).

[114] F. Huang, M. Döring, H. Haberzettl, J. Haidenbauer, C. Hanhart, S. Krewald, U.-G. Meißner and K. Nakayama, Phys. Rev. C **85**, 054003 (2012).

[115] H. Haberzettl, Phys. Rev. C **56**, 2041 (1997).

[116] H. Haberzettl, K. Nakayama, S. Krewald, Phys. Rev. **C74** , 045202 (2006).

[117] H. Haberzettl, F. Huang and K. Nakayama, Phys. Rev. C **83**, 065502 (2011).

[118] G. F. Chew, M. L. Goldberger, F. E. Low and Y. Nambu, Phys. Rev. **106**, 1345 (1957).

[119] K. Nakayama and W. G. Love, Phys. Rev. C **72**, 034603 (2005).

[120] I. S. Barker, A. Donnachie and J. K. Storrow, Nucl. Phys. B **95**, 347 (1975).

[121] G. Keaton and R. Workman, Phys. Rev. C **53**, 1434 (1996).

[122] W.-T. Chiang and F. Tabakin, Phys. Rev. C **55**, 2054 (1997).

[123] M. H. Sikora, D. P. Watts, D. I. Glazier, P. Aguar-Bartolome, L. K. Akasoy, J. R. M. Annand, H. J. Arends and K. Bantawa *et al.*, arXiv:1309.7897 [nucl-ex].

[124] D. G. Ireland, Phys. Rev. C **82**, 025204 (2010).

[125] R. L. Workman, M. W. Paris, W. J. Briscoe, L. Tiator, S. Schumann, M. Ostrick and S. S. Kamalov, Eur. Phys. J. A **47**, 143 (2011).

[126] A. M. Sandorfi, S. Hoblit, H. Kamano and T. -S. H. Lee, J. Phys. G **38**, 053001 (2011).

[127] T. Vrancx, J. Ryckebusch, T. Van Cuyck and P. Vancraeyveld, Phys. Rev. C **87**, 055205 (2013).

[128] A. S. Omelaenko, Sov. J. Nucl. Phys. **34**, 406 (1981).

[129] Y. Wunderlich, R. Beck and L. Tiator, arXiv:1312.0245 [nucl-th].

[130] A. M. Sandorfi, B. Dey, A. Sarantsev, L. Tiator, and R. Workmann, AIP Conf. Proc. **1432**, 219 (2012); (see, arXiv:1108.5411v2 for a revised version).

[131] C. G. Callan, Jr. and D. J. Gross, Phys. Rev. Lett. **22**, 156 (1969).

[132] J. C. Doyle, F. S. Crawford and J. A. Anderson, Phys. Rev. **165**, 1483 (1968).

[133] R. D. Baker, R. M. Brown, A. G. Clark, J. K. Davies, J. De Pagter, W. M. Evans, R. J. Gray and E. S. Groves *et al.*, Nucl. Phys. B **156**, 93 (1979).

[134] K. W. Bell, J. A. Blissett, T. A. Broome, H. M. Daley, J. C. Hart, A. L. Lintern, R. Maybury and A. G. Parham *et al.*, Nucl. Phys. B **222**, 389 (1983).

[135] V. Credé *et al.* [CBELSA/TAPS Collaboration], Phys. Rev. C **84**, 055203 (2011).

[136] O. Bartholomy *et al.* [CB-ELSA Collaboration], Phys. Rev. Lett. **94**, 012003 (2005).

[137] M. Dugger, B. G. Ritchie, J. P. Ball, P. Collins, E. Pasyuk, R. A. Arndt, W. J. Briscoe, I. I. Strakovsky *et al.*, Phys. Rev. C **76**, 025211 (2007)

[138] G. Buschhorn, P. Heide, U. Kotz, R. A. Lewis, P. Schmuser and H. J. Skronn, Phys. Rev. Lett. **20**, 230 (1968).

[139] M. Dugger, B. G. Ritchie, P. Collins, E. Pasyuk, W. J. Briscoe, I. I. Strakovsky, R. L. Workman, Y. Azimov *et al.*, arXiv:1308.4028 [nucl-ex].

[140] M. Gottschall *et al.* [CBELSA/TAPS Collaboration], arXiv:1312.2187 [nucl-ex].

[141] K. Wijesooriya, A. Afanasev, M. Amarian, K. Aniol, S. Becher, K. Benslama, L. Bimbot, P. Bosted *et al.*, Phys. Rev. C **66**, 034614 (2002).

[142] W. Luo *et al.* [GEp-III and GEp2γ Collaborations], Phys. Rev. Lett. **108**, 222004 (2012).

[143] M. Döring, J. Haidenbauer, U.-G. Meißner and A. Rusetsky, Eur. Phys. J. A **47**, 163 (2011).

[144] M. Döring, U.-G. Meißner, E. Oset and A. Rusetsky, Eur. Phys. J. A **47**, 139 (2011).

[145] M. Döring and U.-G. Meißner, JHEP **1201**, 009 (2012).

[146] M. Döring, U.-G. Meißner, E. Oset and A. Rusetsky, Eur. Phys. J. A **48**, 114 (2012).

[147] L. O. Abrahamian, R. O. Avakian, A. O. Aganyants, F. D. Adamian, A. A. Armaganian, L. G. Arutunian, N. A. Demekhina and G. M. Elbakian *et al.*, Phys. Lett. B **48**, 463 (1974).

[148] L. O. Abrahamian, Jetp Lett. **23** (1976)

[149] P. Argan, Nucl. Phys. A **237**, 447 (1975).

[150] J. Ahrens *et al.* [GDH and A2 Collaborations], Phys. Rev. Lett. **88**, 232002 (2002)

[151] J. Ahrens *et al.* [GDH and A2 Collaboration], Eur. Phys. J. A **21**, 323 (2004).

[152] B. M. Aleksandrov, Sov. J. Nucl. Phys. **25**, 43 (1977).

[153] B. M. Aleksandrov, Sov. J. Nucl. Phys. **28**, 344 (1978).

[154] K. H. Althoff, M. Gies, O. Kaul, K. Konigsmann, D. Menze, W. Meyer, T. Miczaika and W. Pfeil *et al.*, Z. Phys. C **1**, 327 (1979).

[155] K. H. Althoff, M. Gies, O. Kaul, K. Konigsmann, D. Menze, W. Meyer, T. Miczaika and E. Roderburg *et al.*, Z. Phys. C **1**, 257 (1979).

[156] S. Almehed, Conf. Bonn (1973)

[157] I. Arai, H. Fujii, S. Homma, Y. Hoshi, H. Ikeda, T. Ishii, A. Itano and K. Maruyama *et al.*, J. Phys. Soc. Jap. **43**, 363 (1977).

[158] O. Bartalini *et al.* [GRAAL Collaboration], Eur. Phys. J. A **26**, 399 (2005).

[159] H. Becks, P. Feller, D. Menze, U. Opara, W. Schulz and W. J. Schwille, Nucl. Phys. B **60**, 267 (1973).

[160] R. Beck, F. Kalleicher, B. Schoch, J. Vogt, G. Koch, H. Ströher, V. Metag, J. C. McGeorge *et al.*, Phys. Rev. Lett. **65**, 1841 (1990).

[161] R. Beck, H. P. Krahn, J. Ahrens, H. J. Arends, G. Audit, A. Braghieri, N. d'Hose and S. J. Hall *et al.*, Phys. Rev. Lett. **78**, 606 (1997).

[162] R. Beck, Eur. Phys. J. A **28S1**, 173 (2006).

[163] M. Braunschweig *et al.*, Phys. Lett. B **26**, 405 (1968)

[164] M. Braunschweig, W. Braunschweig, D. Husmann, K. Luebelsmeyer and D. Schmitz, Nucl. Phys. B **20**, 191 (1970).

[165] J. C. Bergstrom, R. Igarashi and J. M. Vogt, Phys. Rev. C **55**, 2016 (1997).

[166] P. S. L. Booth, Daresbury Nuclear Physics Laboratory, Preprint Volume 95 (1971).

[167] P. S. L. Booth, L. J. Carroll, J. R. Holt, J. N. Jackson, W. H. Range, K. A. Sprakes and J. R. Wormald, Nucl. Phys. B **84**, 437 (1975).

[168] J. S. Barton, P. S. L. Booth, L. J. Carroll, J. R. Holt, J. N. Jackson, G. Moscati and J. R. Wormald, Nucl. Phys. B **84**, 449 (1975).

[169] W. Brefeld, D. Husmann, W. Jansen, B. Lohr, K. Reichmann and H. Schilling, Nucl. Phys. B **100**, 93 (1975).

[170] G. C. Bolon, C. Garelick, S. Homma, R. Lewis, W. Lobar, D. Luckey, L. S. Osborne and R. Schwitters *et al.*, Phys. Rev. Lett. **18**, 926 (1967).

[171] B. Delcourt, J. Lefrancois, G. Parrour, J. P. Perez-Y-Jorba and G. Sauvage, Phys. Lett. B **29**, 70 (1969).

[172] P. Dougan, Z. Phys. A **274**, 73 (1975).

[173] P. Dougan, V. Ramsay and W. Stiefler, Z. Phys. A **280**, 341 (1977).

[174] P. Feller, H. Herr, E. Hilger, V. Kadansky, D. Menze, T. Miczaika, U. Opara and W. J. Schwille, Phys. Lett. B **49**, 197 (1974).

[175] M. Fuchs, J. Ahrens, G. Anton, R. Averbeck, R. Beck, A. M. Bernstein, A. R. Gabler, F. Härter *et al.*, Phys. Lett. B **368**, 20 (1996).

[176] H. Genzel, E. Hilger, G. Knop, H. Kemen and R. Wedemeyer, Z. Phys. **268**, 43 (1974).

[177] B. B. Govorkov, Sov. J. Nucl. Phys. **26**, 370 (1968).

[178] F. Härter, Ph.D thesis, Mainz (1996).

[179] Y. Hemmi, Y. Inagaki, T. Inagaki, A. Maki, K. Miyake, T. Nakamura, Tamura and J. Tsukamoto *et al.*, Phys. Lett. B **43**, 79 (1973).

[180] W. Hitzeroth, Nuovo Cim. A **60**, 467 (1969).

[181] D. Hornidge *et al.* [A2 and CB-TAPS Collaboration], Phys. Rev. Lett. **111**, 062004 (2013).

[182] Y. Hemmi, T. Inagaki, R. Kikuchi, A. Maki, K. Miyake, T. Nakamura, A. Sasaki and N. Tamura *et al.*, Nucl. Phys. B **55**, 333 (1973).

[183] D. Husmann, W. Jansen, B. Lohr and H. Schilling, Nucl. Phys. B **126**, 436 (1977).

[184] M. Jung, J. Kattein, P. Leu, K.-D. de Marne, W. Rosenstock and R. Wedemeyer, BONN-HE-76-15 (1976).

[185] B. Krusche, M. Fuchs, V. Metag, M. Robig-Landau, H. Stroher, R. Beck, F. Harter and S. J. Hall *et al.*, Eur. Phys. J. A **6**, 309 (1999).

[186] B. Lohr, BONN-PI1-98 (1970).

[187] M. Schneider, Ph.D thesis, Mainz (1994).

[188] A. Schmidt, P. Achenbach, J. Ahrens, H. J. Arends, R. Beck, A. M. Bernstein, V. Hejny, M. Kotulla *et al.*, Phys. Rev. Lett. **87**, 232501 (2001) [Erratum-ibid. **110**, 039903 (2013)].

[189] S. Schumann, B. Boillat, E. J. Downie, P. Aguar-Bartolome, J. Ahrens, J. R. M. Annand, H. J. Arends and R. Beck *et al.*, Eur. Phys. J. A **43**, 269 (2010).

[190] D. Staebler, Phys. Rev. B **140**, 336 (1965).

[191] M. A. Shupe, R. H. Milburn, D. J. Quinn, J. P. Rutherfoord, A. R. Stottlemyer, S. S. Hertzbach, R. RKofler and F. D. Lomanno *et al.*, Phys. Rev. D **19**, 1921 (1979).

[192] M. Sumihama, J. K. Ahn, H. Akimune, Y. Asano, W. C. Chang, S. Date, H. Ejiri, H. Fujimura *et al.*, Phys. Lett. B **657**, 32 (2007).

[193] R. M. Talman, C. R. Clinesmith, R. Gomez and A. V. Tollestrup, Phys. Rev. Lett. **9**, 177 (1962).

[194] C. Ward, B. Kenton and C. York, Phys. Rev. **159**, 1176 (1967).

[195] R. M. Worlock, Phys. Rev. **117**, 537 (1960).

[196] F. Wolverton, Ph.D thesis, California Institute of Technology (1968).

[197] M. Yoshioka, A. Noda, M. Daigo, Y. Hemmi, R. Kikuchi, M. Minowa, K. Miyake and T. Nakamura *et al.*, Nucl. Phys. B **168**, 222 (1980).

[198] P. Zenz, Ph.D. thesis, Bonn, BONN-IR-88-12 (1988).

[199] J. Ahrens, S. Altieri, J. R. M. Annand, H. -J. Arends, R. Beck, C. Bradtke, A. Braghieri, N. d'Hose *et al.*, Phys. Rev. C **74**, 045204 (2006).

[200] Y. Aleksandrov, Sov. J. Nucl. Phys. **12**, 416 (1971).

[201] K. H. Althoff, G. Anton, B. Bock, D. Bour, W. Ferber, H. W. Gelhausen, T. Jahnen and O. Kaul *et al.*, Z. Phys. C **18**, 199 (1983).

[202] R. A. Alvarez, G. Cooperstein, K. Kalata, R. C. Lanza and D. Luckey, Phys. Rev. D **1**, 1946 (1970).

[203] R. Beck, H. P. Krahn, J. Ahrens, J. R. M. Annand, H. J. Arends, G. Audit, A. Braghieri, N. d'Hose *et al.*, Phys. Rev. C **61**, 035204 (2000).

[204] B. Bouquet, B. D' Almagne, P. T. Eschstruth, M. Croissiaux, E. F. Erickson, R. Morand, J. P. Pahin, P. Kitching *et al.*, Phys. Rev. Lett. **27**, 1244 (1971).

[205] H. B. van den Brink, H. P. Blok, H. T. Chung, H. Choi, T. Gresko, E. L. Hallin, W. H. A. Hesselink, T. Kobayashi *et al.*, Nucl. Phys. A **587**, 657 (1995).

[206] D. Branford, J. A. MacKenzie, F. X. Lee, J. Ahrens, J. R. M. Annand, R. Beck, G. E. Cross, T. Davinson *et al.*, Phys. Rev. C **61**, 014603 (2000).

[207] C. Betourne, J. C. Bizot, J. P. Perez-y-Jorba, D. Treille and W. Schmidt, Phys. Rev. **172**, 1343 (1968).

[208] G. Buschhorn, J. Carroll, R. D. Eandi, P. Heide, R. Hubner, W. Kern, U. Kotz, P. Schmuser *et al.*, Phys. Rev. Lett. **17**, 1027 (1966).

[209] G. Buschhorn, J. Carroll, R. D. Eandi, P. Heide, R. Hubner, W. Kern, U. Kotz, P. Schmuser *et al.*, Phys. Rev. Lett. **18**, 571 (1967).

[210] K. Büchler, K. H. Althoff, G. Anton, J. Arends, W. Beulertz, M. Breuer, P. Detemple, H. Dutz *et al.*, Nucl. Phys. A **570**, 580 (1994).

[211] J. H. Boyden, Ph.D thesis (1961).

[212] H. W. Dannhausen, E. J. Durwen, H. M. Fischer, M. Leneke, W. Niehaus and F. Takasaki, Eur. Phys. J. A **11**, 441 (2001).

[213] J. P. Dowd, D. O. Caldwell, K. Heinloth and T. R. Sherwood, Phys. Rev. Lett. **18**, 414 (1967).

[214] E. J. Durwen, PRP IR-80-7 (1980).

[215] M. Dugger *et al.* [CLAS Collaboration], Phys. Rev. C **79**, 065206 (2009).

[216] S. D. Ecklund and R. L. Walker, Phys. Rev. **159**, 1195 (1967).

[217] K. Ekstrand, A. Browman, L. Hand and M. E. Nordberg, Phys. Rev. D **6**, 1 (1972).

[218] J. L. Faure, P. Argan, G. Audit, A. Bloch, N. de Botton, L. Ghedira, J. M. Laget and A. Magnon *et al.*, Nucl. Phys. A **424**, 383 (1984).

[219] G. Fischer, H. Fischer, M. Heuel, G. Von Holtey, G. Knop and J. Stumpfig, Nucl. Phys. B **16**, 119 (1970).

[220] G. Fischer, G. Von Holtey, G. Knop and J. Stuempfig, Z. Phys. **253**, 38 (1972).

[221] K. G. Fissum, H. S. Caplan, E. L. Hallin, D. M. Skopik, J. M. Vogt, M. Frodyma, D. P. Rosenzweig, D. W. Storm *et al.*, Phys. Rev. C **53**, 1278 (1996).

[222] T. Fujii, H. Okuno, S. Orito, H. Sasaki, T. Nozaki, F. Takasaki, Takikawa, K. Amako *et al.*, Phys. Rev. Lett. **26**, 1672 (1971).

[223] T. Fujii, T. Kondo, F. Takasaki, S. Yamada, S. Homma, K. Huke, S. Kato, H. Okuno *et al.*, Nucl. Phys. B **120**, 395 (1977).

[224] W. Heise, Ph.D thesis, Bonn, BONN-IR-88-06 (1988).

[225] J. R. Kilner, Ph.D. thesis (1962).

[226] E. A. Knapp, R. W. Kenney and V. Perez-Mendez, Phys. Rev. **114**, 605 (1959).

[227] E. Korkmaz, N. R. Kolb, D. A. Hutcheon, G. V. O'Rielly, J. C. Bergstrom, G. Feldman, D. Jordan and A. K. Opper *et al.*, Phys. Rev. Lett. **83**, 3609 (1999).

[228] D. W. G. S. Leith, R. Little and E. M. Lawson, Phys. Lett. **8**, 355 (1964).

[229] J. K. Walker and J. P. Burq, Phys. Rev. Lett. **8**, 37 (1962).

[230] L. Y. Zhu *et al.* [Jefferson Lab Hall A and Jefferson Lab E94-104 Collaborations], Phys. Rev. C **71**, 044603 (2005).

[231] F. V. Adamian, A. Y. Bunyatyan, G. S. Frangulian, P. I. Galumian, V. H. Grabsky, A. V. Airapetian, H. H. Hakopian, V. K. Hoktanian *et al.*, Phys. Rev. C **63**, 054606 (2001).

[232] N. M. Agababyan *et al.*, Sov. J. Nucl. Phys. **50**, 834 (1989).

[233] J. Alspector, D. Fox, D. Luckey, C. Nelson, L. S. Osborne, G. Tarnopolsky, Z. Bar-Yam and J. De Pagter *et al.*, Phys. Rev. Lett. **28**, 1403 (1972).

[234] M. M. Asaturyan *et al.*, JETP Lett. **44**, 341 (1986).

[235] R. O. Avakyan *et al.*, Sov. J. Nucl. Phys. **26**, 537 (1977).

[236] R. O. Avakyan *et al.*, Sov. J. Nucl. Phys. **29**, 625 (1979).

[237] R. O. Avakyan, PRP EPI-674-6 (1983).

[238] R. O. Avakyan *et al.*, Sov. J. Nucl. Phys. **38**, 721 (1983).

[239] R. O. Avakyan *et al.*, Sov. J. Nucl. Phys. **40**, 588 (1984).

[240] G. Barbiellini, G. Bologna, G. Capon, G. De Zorzi, F. L. Fabbri, G. P. Murtas, G. Diambrini and G. Sette *et al.*, Phys. Rev. **184**, 1402 (1969).

[241] A. A. Belyaev, V. A. Getman, V. G. Gorbenko, V. A. Gushchin, A. Y. .Derkach, Y. V. Zhebrovsky, I. M. Karnaukhov, L. Y. .Kolesnikov *et al.*, Nucl. Phys. B **213**, 201 (1983).

[242] G. Blanpied *et al.* [LEGS Collaboration], Phys. Rev. Lett. **69**, 1880 (1992).

[243] G. Blanpied, M. Blecher, A. Caracappa, R. Deininger, C. Djalali, G. Giordano, K. Hicks, S. Hoblit *et al.*, Phys. Rev. C **64**, 025203 (2001).

[244] G. Bologna, Laboratori Nazionali Frascati, LNF-70 39 (1970).

[245] P. J. Bussey, C. Raine, J. G. Rutherglen, P. S. L. Booth, L. J. Carroll, P. R. Daniel, C. J. Hardwick and J. R. Holt *et al.*, Nucl. Phys. B **104**, 253 (1976).

[246] P. J. Bussey, C. Raine, J. G. Rutherglen, P. S. L. Booth, L. J. Carroll, G. R. Court, P. R. Daniel, A. W. Edwards *et al.*, Nucl. Phys. B **154**, 492 (1979).

[247] D. J. Drickey and R. F. Mozley, Phys. Rev. **136**, B543 (1964).

[248] D. Elsner *et al.* [CBELSA and TAPS Collaborations], Eur. Phys. J. A **39**, 373 (2009).

[249] V. G. Gorbenko *et al.*, JETP Lett. **19**, 340 (1974).

[250] V. G. Gorbenko *et al.*, JETP Lett. **22**, 186 (1975).

[251] V. G. Gorbenko *et al.*, VANT2, 36 (1977).

[252] V. G. Gorbenko *et al.*, Sov. J. Nucl. Phys. **26**, 167 (1977).

[253] V. G. Gorbenko, A. I. Derebchinskii, Y. V. Zhebrovskii, A. A. Zybalov, O. G. Konovaloo, V. I. Nikiforov, A. L. Rubashkin, P. V. Sorokin and A. E. Tenishev, Sov. J. Nucl. Phys. **27**, 638 (1978).

[254] G. Knies, H. Oberlack, A. Rittenberg, A. H. Rosenfeld, M. Bogdanski and G. Smadja, Phys. Rev. D **10**, 2778 (1974).

[255] N. Sparks *et al.* [CBELSA/TAPS Collaboration], Phys. Rev. C **81**, 065210 (2010).

[256] L. O. Abrahamian *et al.*, Sov. J. Nucl. Phys. **32**, 66 (1980).

[257] J. Ajaka *et al.* [GRAAL Collaboration], Phys. Lett. B **475**, 372 (2000).

[258] O. Bartalini *et al.* [GRAAL and GW-SAID Group Collaborations], Phys. Lett. B **544**, 113 (2002).

[259] P. J. Bussey, C. Raine, J. G. Rutherglen, P. S. L. Booth, L. J. Carroll, G. R. Court, P. R. Daniel and A. W. Edwards *et al.*, Nucl. Phys. B **154**, 205 (1979).

[260] C. Geweniger, P. Heide, U. Koetz, R. A. Lewis, P. Schmueser, H. J. Skronn, H. Wahl and K. Wegener, Phys. Lett. B **29**, 41 (1969).

[261] V. A. Getman, V. G. Gorbenko, A. Y. .Derkach, Y. .V. Zhebrovsky, I. M. Karnaukhov, L. Y. .Kolesnikov, A. A. Lukhanin and A. L. Rubashkin *et al.*, Nucl. Phys. B **188**, 397 (1981).

[262] V. A. Getman *et al.*, Journal of Kharkov Physical Technical Institute, Voprosu Atomnoi Nauki i Techniki **8**, 3 (1989).

[263] V. B. Ganenko *et al.*, Sov. J. Nucl. Phys. **23**, 52 (1976).

[264] P. Hampe, Ph.D thesis, Bonn, BONN-IR-80-1 (1980).

[265] V. M. Kuznetsov, O. I. Stukov, E. V. Repenko and B. N. Kalinin, Lett. Nuovo Cim. **1S2**, 233 (1971) [Lett. Nuovo Cim. **1**, 233 (1971)].

[266] F. F. Liu and S. Vitale, Phys. Rev. **144**, 1093 (1966).

[267] R. C. Smith and R. F. Mozley, Phys. Rev. **130**, 2429 (1963).

[268] R. E. Taylor and R. F. Mozley, Phys. Rev. **117**, 835 (1960).

[269] V. N. Zabaev *et al.*, Sov. J. Nucl. Phys. **21**, 286 (1975).

[270] P. S. L. Booth, L. J. Carroll, G. R. Court, P. R. Daniel, R. Gamet, C. J. Hardwick, P. J. Hayman, J. R. Holt *et al.*, Nucl. Phys. B **121**, 45 (1977).

[271] A. Bock, G. Anton, W. Beulertz, C. Bradtke, H. Dutz, R. Gehring, S. Goertz, K. Helbing *et al.*, Phys. Rev. Lett. **81**, 534 (1998).

[272] P. Feller, M. Fukushima, N. Horikawa, R. Kajikawa, K. Mori, T. Nakanishi, T. Ohshima and C. O. Pak *et al.*, Nucl. Phys. B **110**, 397 (1976).

[273] M. Fukushima, N. Horikawa, R. Kajikawa, H. Kobayakawa, K. Mori, T. Nakanishi, C. O. Pak, S. Suzuki *et al.*, Nucl. Phys. B **136**, 189 (1978).

[274] H. Herr, D. Husmann, W. Jansen, V. Kadansky, B. Lohr, W. Meyer, H. Schilling and T. Yamaki, Nucl. Phys. B **125**, 157 (1977).

[275] S. Arai, S. Fukui, N. Horikawa, R. Kajikawa, T. Kasuga, H. Kobayakawa, A. Masaike and T. Matsuda *et al.*, Nucl. Phys. B **48**, 397 (1972).

[276] K. H. Althoff, P. Feller, H. Herr, W. Hoffmann, V. Kadansky, D. Menze, U. Opara and F. J. Schittko *et al.*, Nucl. Phys. B **53**, 9 (1973).

[277] K. H. Althoff, R. Conrad, H. Herr, E. Hilger, V. Kadansky, O. Kaul, D. Menze and W. Meyer *et al.*, Phys. Lett. B **59**, 93 (1975).

[278] K. H. Althoff, R. Conrad, M. Gies, H. Herr, V. Kadansky, O. Kaul, K. Konigsmann and G. Lenzen *et al.*, Phys. Lett. B **63**, 107 (1976).

[279] K. H. Althoff, M. Gies, H. Herr, V. Kadansky, O. Kaul, K. Konigsmann, D. Menze and W. Meyer *et al.*, Nucl. Phys. B **131**, 1 (1977).

[280] H. Dutz, D. Krämer, B. Zucht, K. H. Althoff, G. Anton, J. Arends, W. Beulertz, A. Bock *et al.*, Nucl. Phys. A **601**, 319 (1996).

[281] P. Feller, M. Fukushima, N. Horikawa, R. Kajikawa, K. Mori, T. Nakanishi, T. Ohshima and C. O. Pak *et al.*, Phys. Lett. **52B**, 105 (1974) [Nucl. Phys. B **102**, 207 (1976)].

[282] K. Fujii, H. Hayashii, S. Iwata, R. Kajikawa, A. Miyamoto, T. Nakanishi, Y. Ohashi, S. Okumi *et al.*, Nucl. Phys. B **197**, 365 (1982).

[283] M. Fukushima, N. Horikawa, R. Kajikawa, H. Kobayakawa, K. Mori, T. Nakanishi, C. O. Pak and S. Suzuki *et al.*, Nucl. Phys. B **130**, 486 (1977).

[284] V. A. Getman *et al.*, Sov. J. Nucl. Phys. **31**, 480 (1980).

[285] H. Genzel, P. Heide, J. Knutel, H. Lierl, K. -H. Mess, M. -J. Schachter, P. Schmueser and B. Sonne *et al.*, Nucl. Phys. B **92**, 196 (1975).

[286] K. H. Althoff, K. Kramp, H. Matthay and H. Piel, Z. Phys. **194**, 135 (1966).

[287] K. H. Althoff, K. Kramp, H. Matthay and H. Piel, Z. Phys. **194**, 144 (1966).

[288] K. H. Althoff, D. Finken, N. Minatti, H. Piel, D. Trines and M. Unger, Phys. Lett. B **26**, 677 (1968).

[289] R. O. Avakyan *et al.*, Sov. J. Nucl. Phys. **37**, 199 (1983).

[290] R. O. Avakyan *et al.*, Sov. J. Nucl. Phys. **46**, 853 (1987).

[291] R. O. Avakyan *et al.*, Sov. J. Nucl. Phys. **48**, 1030 (1988).

[292] R. O. Avakyan *et al.*, Sov. J. Nucl. Phys. **53**, 448 (1991).

[293] L. Bertanza, I. Mannelli, S. Santucci, G. V. Silvestrini and V. Z. Peterson, Nuovo Cim. **24**, no. 4, 734 (1962).

[294] E. D. Bloom, C. A. Heusch, C. Y. Prescott and L. S. Rochester, Phys. Rev. Lett. **19**, 671 (1967).

[295] P. Blüm, Conf. Dares (1969).

[296] P. Blüm, BONN-PI1-105 70 (1970).

[297] P. Blüm, P. Brinckmann, R. Brockmann, P. Lutter, W. Mohr and R. Sauerwein, Z. Phys. A **277**, 311 (1976).

[298] P. Blüm, R. Brockmann and W. Mohr, Z. Phys. A **278**, 275 (1976).

[299] A. S. Bratashevsky, V. G. Gorbenko, A. I. Derebchinsky, A. Y. Derkach, Y. V. Zhebrovsky, A. A. Zybalov, I. M. Karnaukhov and L. Y. Kolesnikov *et al.*, Nucl. Phys. B **166**, 525 (1980).

[300] A. S. Bratashevsky *et al.*, Sov. J. Nucl. Phys. **35**, 33 (1982).

[301] A. S. Bratashevsky *et al.*, Sov. J. Nucl. Phys. **38**, 233 (1983).

[302] A. S. Bratashevsky *et al.*, Sov. J. Nucl. Phys. **42**, 417 (1985).

[303] A. S. Bratashevsky *et al.*, Sov. J. Nucl. Phys. **41**, 960 (1985).

[304] A. S. Bratashevsky, A. A. Zybalov, S. P. Karasev, O. G. Konovalov, A. S. Omelaenko, P. V. Sorokin, Y. .O. Storozhenko and A. E. Tenishev, Ukr. Fiz. Zh. (Russ. Ed.) **31**, 1306 (1986).

[305] A. S. Bratashevsky *et al.*, Sov. J. Nucl. Phys. **46**, 635 (1987).

[306] A. I. Derebchinsky *et al.*, JETP **39**, 30 (1974).

[307] A. I. Derebchinsky *et al.*, JETP **43**, 218 (1976).

[308] N. V. Goncharov *et al.*, JETP **37**, 205 (1973).

[309] S. Kayakawa *et al.*, J. Phys. Soc. Jap. **25**, 307 (1968).

[310] S. Kato, T. Miyachi, K. Sugano, K. Toshioka, K. Ukai, M. Chiba, K. Egawa, T. Ishii *et al.*, Nucl. Phys. B **168**, 1 (1980).

[311] S. Kabe, T. Fujii, T. Kamei, R. Yamada, T. Yamagata, S. Kato, I. Kita and T. Kiyoshima, Nucl. Phys. B **50**, 17 (1972).

[312] J. O. Maloy, V. Z. Peterson, G. A. Salandin, F. Waldner, A. Manfredini, J. I. Friedman and H. Kendall, Phys. Rev. **139**, B733 (1965).

[313] M. N. Prentice, R. Railton, J. G. Rutherglen, K. M. Smith, G. R. Brookes, P. J. Bussey, F. H. Combley, G. H. Eaton *et al.*, Nucl. Phys. B **41**, 353 (1972).

[314] R. Querzoli, G. Salvini and A. Silverman, Nuovo Cim. **19**, no. 1, 53 (1961).

[315] N. Tanaka, M. M. Castro, R. H. Milburn, W. B. Richards, J. P. Rutherfoord, B. F. Stearns, M. Deutsch, P. M. Patel *et al.*, Phys. Rev. D **8**, 1 (1973).

[316] D. Trines, BONN-PI1-160 72 (1972).

[317] A. A. Zybalov *et al.*, Sov. J. Nucl. Phys. **28**, 52 (1978).

[318] K. H. Althoff, Phys. Lett. B **26**, 640 (1968).

[319] K. Egawa, T. Ishii, M. Daigo, S. Kato, T. Miyachi, K. Sugano, K. Ukai and M. Chiba *et al.*, Nucl. Phys. B **188**, 11 (1981).

[320] U. Hahn, BONN-PI1-143 71 (1971).

[321] W. Wallraff, BONN-PIB1-162 72 (1972).

[322] M. Jacob and G. C. Wick, *Quantum Collision Theory* (North Holland, Amsterdam, 1975).

[323] D. Brink and G. Sachtler, *Angular Momentum* (Oxford Library of the Physical Siences, Oxford, 1968).

Danksagung

Ich möchte mich sehr herzlich bei Herrn Prof. Siegfried Krewald und Herrn Prof. Ulf-G. Meißner für die Ermöglichung meiner Doktorarbeit und die Unterstützung während meiner Promotion bedanken. Großer Dank geht natürlich an Prof. Döring für die super Betreuung und jeder Zeit vorhandene Hilfe. Auch den Mitgliedern der Jülich-Athens-Washington-Collaboration danke ich besonders für die tolle Zusammenarbeit. A special thanks goes to Prof. Kanzo Nakayama and Prof. Fei Huang for making my stay at the University of Georgia, Athens possible. I had a wonderful time! In dem Zusammenhang danke ich auch dem Deutschen Akademischen Austauschdienst für die finanzielle Unterstützung im Rahmen eines Doktorandenstipendiums.
Allen Mitarbeitern und Kollegen des Instituts für Kernphysik am Forschungszentrum Jülich und des Helmholtz-Instituts für Strahlen- und Kernphysik der Universität Bonn möchte ich für die große Hilfsbereitschaft bei wissenschaftlichen oder verwaltungstechnischen Problemen und nicht zuletzt für die freundliche und entspannte Arbeitsatmosphäre danken.
Schließlich möchte ich mich natürlich auch bei meinen Eltern, Geschwistern und vor allem bei Christoph für ihre Unterstützung bedanken.